WEARABLE EXOSKELETON SYSTEMS BASED-ON PNEUMATIC SOFT ACTUATORS AND CONTROLLED BY PARALLEL PROCESSING

Hassanin Shaker Husein Al-Fahaam

Autonomous Systems and Robotics Centre
School of Computing, Science & Engineering
University of Salford, Salford, UK

Submitted in Partial Fulfilment of the Requirements of the Degree of Doctor of Philosophy

2019

PUBLICATIONS

1- Al-Fahaam, H., Davis, S., & Nefti-Meziani, S. (2016). Power Assistive and Rehabilitation Wearable Robot based on Pneumatic Soft Actuators. Paper presented at the Methods and Models in Automation and Robotics (MMAR), 2016 21th ieee International Conference in Międzyzdroje, Poland.

2- Al-Fahaam, H., Davis, S., & Nefti-Meziani, S. (2016). Wrist rehabilitation exoskeleton robot based on pneumatic soft actuators. Paper presented at the International Conference for Students on Applied Engineering (ISCAE), , Newcastle upon Tyne, UK.

3- Al-Fahaam, H., Davis, S. and Nefti-Meziani, S., 2018. The design and mathematical modelling of novel extensor bending pneumatic artificial muscles (EBPAMs) for soft exoskeletons. Robotics and Autonomous Systems, 99, pp.63-74.

4- Hassanin, A.F., Steve, D. and Samia, N.M., 2017, September. A novel, soft, bending actuator for use in power assist and rehabilitation exoskeletons. In 2017 IEEE/RSJ International Conference on Intelligent Robots and Systems (IROS) (pp. 533-538). IEEE.

5- Al-Fahaam, H., Nefti-Meziani, S., Theodoridis, T. and Davis, S., 2018. The Design and Mathematical Model of a Novel Variable Stiffness Extensor-Contractor Pneumatic Artificial Muscle. Soft robotics, 5(5), pp.576-591.

6- Al-Fahaam, H., Davis, S., Nefti-Meziani, S. and Theodoridis, T., 2018. Novel soft bending actuator-based power augmentation hand exoskeleton controlled by human intention. Intelligent Service Robotics, 11, pp.247-268.

7- Al-Fahaam, H., Davis, S. and Nefti-Meziani, S., 2018, September. Power Augmentation and Rehabilitation Exoskeleton Robot based on Variable Stiffness Soft Actuators. In 8th Joint Workshop on New Technologies For Computer/Robot Assisted Surgery (CRAS 2018). Joint Workshop on New Technologies For Computer/Robot Assisted Surgery.

CONTENTS

LIST OF FIGURES

LIST OF TABLES

ABBREVIATIONS

ABPAM	All Directional Bending Pneumatic Muscle Actuator
BBPAM	Bidirectional Bending Pneumatic Muscle Actuator
BF	Big Fill
BV	Big Vent
CM	Carpometacarpal
CPU	Central Processing Unit
CVA	Cerebrovascular Accidents
DC	Direct Current
DEA	Dielectric-Elastomer Actuators
DIP	Distal Interphalangeal
DOF	Degree Of Freedom
EBPAM	Extensor Bending Pneumatic Artificial Muscle
ECPAM	Extensor-Contractor Pneumatic Artificial Muscle
EMG	Electromyography
EPAM	Extensor Pneumatic Artificial Muscle
FEM	Finite Element Model
FPGA	Field-Programmable Gate Array
FSM	Finite State Machine
IP	Interphalangeal
IPMC	Ionic Polymer-Metal Composite
M1	Muscle Number One
M2	Muscle Number Two
M3	Muscle Number Three
MAX	Maximum amplitude
MP	Metacarpophalangeal
NB	Negative Big
NiTi	Nickel-titanium
NS	Negative Small

OCC	On-Chip Controller
PAM	Pneumatic Artificial Muscle
PB	Positive Big
PD	Proportional Derivative
PI	Proportional Integral
PID	Proportional Integral Derivative
PIP	Proximal Interphalangeal
PMA	Pneumatic Muscle Actuator
PMDPM	Parallel Manipulator Driven by Pneumatic Muscle
PPAM	Pleated Pneumatic Artificial Muscle
PS	Positive Small
PWM	Pulse Width Modulation
RMS	Root Mean Square
SCI	Spinal Cord Injuries
SD	Standard deviation
SF	Small Fill
SMA	Shape-Memory Alloy
SNR	Signal-to-Noise Ratio
SV	Small Vent
VHDL	High-Level Hardware Description Language
Z	Zero
ZF	Zero Fill
ZV	Zero Vent

PARAMETERS AND VARIABLES

L_o	Muscle Length Without Pressurization [m]
L_n	Muscle Length Under Pressure [m]
ΔL	Change In Length [m]
L	Muscle Length [m]
D	Muscle Diameter [m]
θ	Braid Angle [deg.]
b	Sleeve Strand Length [m]
n	Sleeve Strands Number
D_c	Curved Muscle Diameter [m]
α	Bend Angle Of The Muscle [deg.]
r_o	Inner Radius Of Bending Muscle [m]
r_n	Outer Radius Of Bending Muscle [m]
L_c	The Bending Actuator Length [m]
θ_{max}	The Maximum Braid Angle [deg.]
W_{in}	The Input Work [J]
P'	Internal Absolute Air Pressure [Pa]
P_o	Environment Pressure [Pa]
P	Relative Differential Air Pressure [Pa]
S_i	Actuator Inner Surface [m^2]
dl_i	Inner Surface Displacement Vector [m]
d_{s_i}	The Area Vector [m^2]
dV_c	Actuator Volume Change [m^3]
V	Volume [m^3]
V_c	Curved Actuator Volume [m^3]

W_{out}	Output Work [J]
F	Force [N]
P_r	Radially Expand Lost Pressure [Pa]
P_a	Actual Pressure [Pa]
K_r	Linearized Radial Actuator Elasticity [$\frac{\mathrm{KPa}}{\mathrm{m}}$]
D_o	Actual Bending Muscle Diameter [m]
t_s	Sleeve Thickness [m]
t_b	Bladder Thickness [m]
t_a	Total Muscle Border Thickness [m]
D_a	Muscle Actual Diameter [m]
V_a	Bending Muscle Actual Volume [m^3]
h	Height [m]
r	Radius Of The Lower Base [m]
R	Radius Of The Upper Base [m]
V_l	Deformation Volume [m^3]
L_l	Deformation Length [m]
d	Actuator End Cap Diameter [m]
V_t	Total Volume [m^3]
L_t	Total Length [m]

ACKNOWLEDGEMENTS

Undertaking this PhD has been a truly life-changing experience for me and it would not have been possible without the support and guidance that I received from many people.

I would like to thank the Ministry of Higher Education in my country, Iraq, as well as the University of Basrah, especially my department of Computer Engineering, who have initiated, administrated and sponsored my study throughout this scholarship.

I wish to express my sincere thanks to my supervisor, Dr. Steven T. Davis, for his constructive feedback, guidance and the freedom given to me in research matters. Furthermore, I would like to convey my gratitude to the director of the Autonomous Systems and Robotics Centre at the School of Computing, Science and Engineering, Prof. Samia Nefti-Meziani, for her support and kindness.

Last but not least, I would like to express my deepest gratitude to my family and friends. This dissertation would not have been possible without their warm love, continued patience, and endless support.

ABSTRACT

Human assistance innovation is essential in an increasingly aging society and one technology that may be applicable is exoskeletons. However, traditional rigid exoskeletons have many drawbacks. This research includes the design and implementation of upper-limb power assist and rehabilitation exoskeletons based on pneumatic soft actuators.

A novel extensor-contractor pneumatic muscle has been designed and constructed. This new actuator has bidirectional action, allowing it to both extend and contract, as well as create force in both directions. A mathematical model has been developed for the new novel actuator which depicts the output force of the actuator. Another new design has been used to create a novel bending pneumatic muscle, based on an extending McKibben muscle and modelled mathematically according to its geometric parameters. This novel bending muscle design has been used to create two versions of power augmentation gloves. These exoskeletons are controlled by adaptive controllers using human intention. For finger rehabilitation a glove has been developed to bend the fingers (full bending) by using our novel bending muscles. Inspired by the zero position (straight fingers) problem for post-stroke patients, a new controllable stiffness bending actuator has been developed with a novel prototype. To control this new rehabilitation exoskeleton, online and offline controller systems have been designed for the hand exoskeleton and the results have been assessed experimentally. Another new design of variable stiffness actuator, which controls the bending segment, has been developed to create a new version of hand exoskeletons in order to achieve more rehabilitation movements in the same single glove. For Forearm rehabilitation, a rehabilitation exoskeleton has been developed for pronation and supination movements by using the novel extensor-contractor pneumatic muscle. For the Elbow rehabilitation an elbow rehabilitation exoskeleton was designed which relies on novel two-directional bending actuators with online and offline feedback controllers. Lastly for upper-limb joint is the wrist, we designed a novel all-directional bending actuator by using the moulding bladder to develop the wrist rehabilitation exoskeleton by a single all-directional bending muscle. Finally, a totally portable, power assistive and rehabilitative prototype has been developed using a parallel processing intelligent control chip.

Chapter 1

Introduction

1.1 Overview

Human upper-limb robotic apparatuses can be broadly catergorised into two types: prosthesis and orthosis. Prosthesis is an artificial body part, such as a hand or leg, that disabled people can wear to replace a missing body part in order to help them in their daily activities. Orthosis is an orthopaedic device that can be utilised to straighten alignment, provide support to disabled individuals, or to provide a functionality improvement for movable human body segments. In addition, orthosis devices are outside the human body and provide a suitable external force to support the desired movement of the human limb without considering individual joint movements of the limb. The most recent kind of orthosis is the wearable robot, which is generally worn by the person. The joints and connections of the wearable robot have lineal harmonisation with the individual joints and limbs, respectively. Moreover, the robot axes are aligned with the anatomic axes of the human limb. Wearable robots have been extensively researched in the fields related to rehabilitation, assistance robots, human force augmentation, impairment evaluation, and impedance exercises. Power assistive and rehabilitation robots have significantly increased in number to assist physically weak, elderly individuals and disabled people who have neurological damage, in order to improve their quality of life and independence. The exoskeleton plays a significant role in providing comfort and safety for the wearer. The physical human–robot interaction includes various aspects, such as transmission of power, actuation, uniqueness, the degree of freedom (DOF), dexterity, compliance and kinematic concatenation. A power assistive and/or rehabilitation exoskeleton must be safe because it

is in direct contact with patients and elderly individuals. It also needs to be a lightweight device so that it can be portable and can be used at home without any clinical assistance. In addition, it should be small and soft so as to be flexible in daily independent use. All of these features are found in the pneumatic soft muscles used to build exoskeletons and therefore many researchers depend on these soft actuators to manufacture power assistive and/or rehabilitation wearable robots. Upper-limbs are the most common examples of neurological weakness or damage because the worker's hand is in direct contact with machines and repetitive movements at work cause neurological damage, which then produces a reduction in ability to control upper-limb muscles.

1.2 Research Motivation

In the future, with the increasing numbers of elderly people and the decreasing birth-rate, there might not be sufficient working individuals in the different fields, such as for medical well-being, cultivation and industry. In particular, the expansion of the elderly population and the shortfall of caregivers will be an interesting challenge. To manage this issue, it may be necessary to develop a device or robot to provide assistance to elderly individuals, disabled persons, nurses, manual workers, caregivers, and so on. Human assistive technology has now become a major concern and researchers in mechatronics and robotics have become more interested in the relationship between the machine and the human. Furthermore, rehabilitation and physical therapy are proven successful methods for regaining the ability to control body motion for individuals with physical injuries, neurological damage and different kinds of disabilities. The most widely recognised are hand disabilities, because the manual worker's hand is in direct contact with machines and repeated motions at work can cause neurological damage which then produces a reduction in capability to control hand muscles. All of these reasons have inspired and motivated research into upper-limb power assistance and/or rehabilitation robots to solve these problems.

1.3 Aims and Objectives

This research aims to develop power assistive and/or rehabilitation exoskeletons based on pneumatic artificial muscles for human upper-limb segments (hands, fingers, wrist joints and elbow joints). These exoskeletons, with novel actuators, mathematical models and robust controllers, will be lightweight, soft, small, portable, fit for any adult (a

single device suitable for any person to wear), with high output force but safe for human interaction.

To achieve these targets the following objectives are set:

1- Develop a novel Extensor-Contractor pneumatic artificial muscle.
2- Develop a kinematic analysis for the novel Extensor-Contractor actuator.
3- Develop a mathematical model for the novel Extensor-Contractor actuator output force.
4- Design a novel soft bending actuator based on the extensor McKibben muscle.
5- Develop a kinematic analysis for the novel bending actuator.
6- Develop a mathematical model for the novel bending actuator output force and enhance this mathematical model to decrease the error between the model and the experimental results.
7- Construct a power assistive glove to provide augmentation force for the fingers which is controlled by human intention; this glove could be used for elderly or partially disabled individuals or for force augmentation for manual workers with heavy work.
8- Design and construct a novel, fully soft (materials and actuation) rehabilitation exoskeleton glove, fit for any adult and capable of assisting all hand rehabilitation motions.
9- Develop and build a novel soft wearable robot for wrist power assistive rehabilitation purposes; this device should be portable and capable of performing all wrist movements including Flexion/Extension, Radial/Ulnar deviation and circular movements.
10- Design and construct a novel soft wearable device for elbow and forearm power assistive rehabilitation; this device should have the ability to assist the elbow Flexion/Extension movements and forearm pronation and supination movements.
11- Design and implement a totally portable rehabilitation system based on parallel processing controllers on-chip, with a small and lightweight air compressor as an air pressure supply for the pneumatic rehabilitation system.
12- Critically evaluate the suitability of the soft exoskeleton system for safe human interaction.

1.4 Methodology

The methodology that will be adopted in order to complete the present project will involve the following steps: (Figure 1.1 shows the research methodology and its key steps).

1- Reviewing previous research: previous research which is related to power assistive and/or rehabilitation devices and soft actuators or any relevant field has been reviewed to understand the project area and construct a clear understanding about the whole design system. This review has also provided us with good knowledge on the different areas of research in the soft wearable robot systems.
2- Identifying the research problem: the first step in the research was identifying the research problem by reviewing previous work and specifying the drawbacks in the previous exoskeleton systems.
3- Describing the available solutions and validating those that are essential for improving the performance of the wearable system.
4- Designing and constructing novel soft actuators.
5- Developing a kinematic analysis and mathematical model for these actuators.
6- Developing a novel soft exoskeleton design for each upper-limb segment.
7- Developing a suitable controller system for each exoskeleton part.
8- Evaluating and validating the proposed designs: the proposed design will be evaluated by implementing an experimental evaluation of the system to assess its effectiveness.
9- Ongoing modification of the design system based on the evaluation, to improve the system performance and to optimise its design.
10- Finalising conclusions, publishing results and submitting a PhD thesis for examination.

1.5 List of Contributions

1- Design and construct a novel extensor-contractor pneumatic artificial muscle (ECPAM).
    - This new actuator has bidirectional action allowing it to both extend and contract, as well as create force in both directions, with controllable stiffness at a specific length and fixed stiffness with variable lengths.

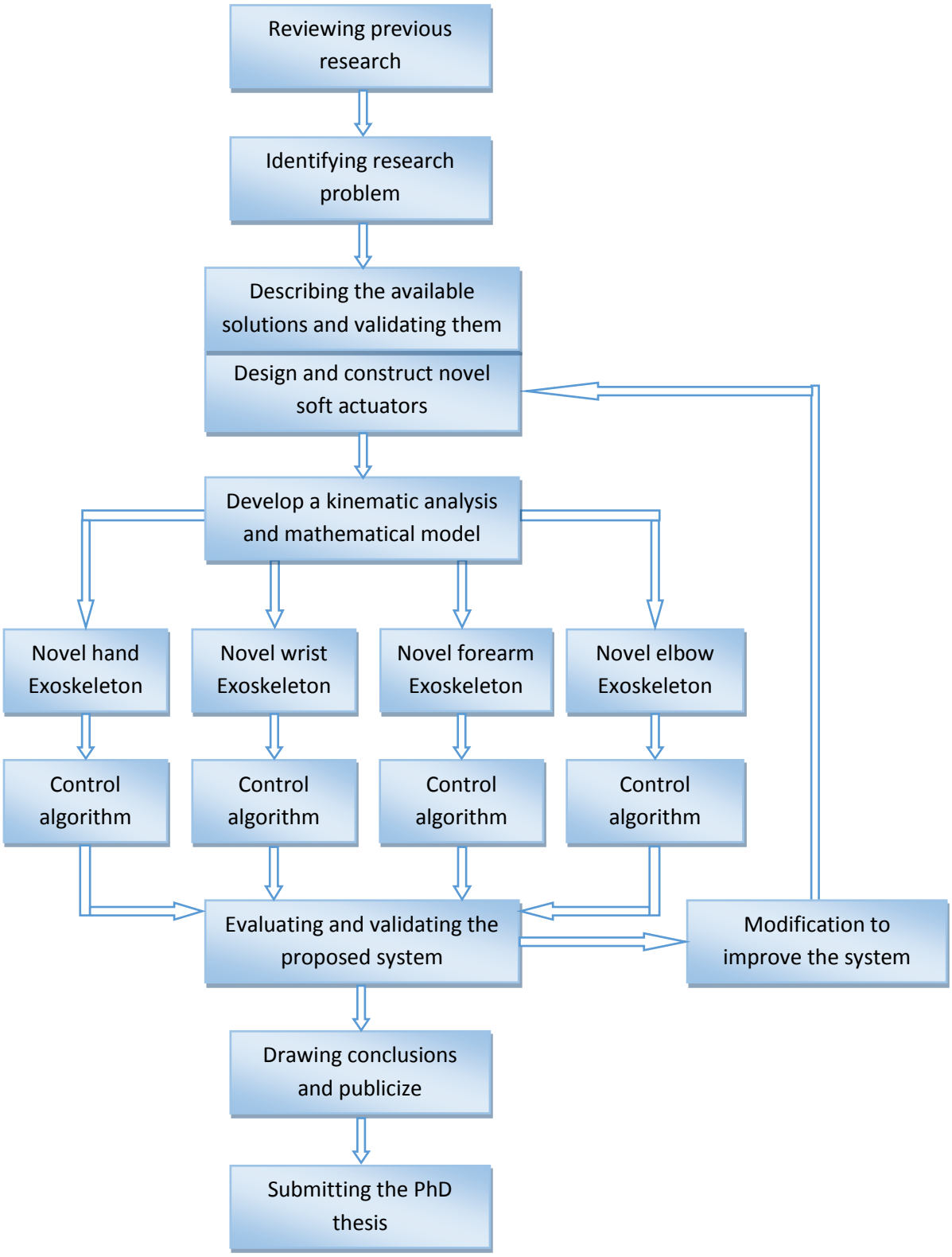

Figure 1.1: Stages of Research Methodology.

- A mathematical model has been developed for the new novel ECPAM which describes the actuator output force.
- A stiffness position controller has been developed to control the stiffness of the actuator (ECPAM) at specific lengths. Verification was conducted using the controller and the average stiffness and position errors were found to be less than 5%.

2- Design and construct novel extender bending pneumatic artificial muscles (EBPAMs).
   - Create kinematics analysis for EBPAM depending on its geometrical parameters.
   - Develop a novel axial output force mathematical model for EBPAMs, with an average percentage error of 15.81% between experimental results and our mathematical model.
   - Enhance our mathematical model based on the loss of radial expansion pressure of the proposed actuators in order to obtain an average percentage error reduction of 45.21% for our last model in previous point.
   - Enhance our last mathematical model based on actual muscle diameter in order to have an average percentage error reduction of 29.81% for our last model in previous point.
   - Enhance our last mathematical model based on the total muscle actual volume in order to have an average percentage error reduction of 22.64% for our last model in previous point.
3- A new design for a power assistive glove for partially disabled individuals with a novel solution for release movement problems after assistive has occurred.
4- A new design for a power augmentation glove for partially disabled or healthy individuals with a novel hybrid, cascaded position/force intelligent control system, based on human intention.
5- A fingers rehabilitation glove has been developed to bend the fingers by using our novel bending muscles.
   - To solve the zero position (straight fingers) problem for post-stroke patients, a new controllable stiffness bending actuator has been developed with a novel prototype.

- Online and offline controller systems have been designed for the hand exoskeleton and the results have been assessed experimentally.

6- New designs of variable stiffness actuators to control the bending segment have been developed to create a new version of hand exoskeletons in order to achieve more rehabilitation movements in the same single glove, such as hook and table fists.

7- A forearm rehabilitation exoskeleton has been developed for pronation and supination movements.

8- The elbow rehabilitation exoskeleton is designed based on our novel bending actuators with online and offline feedback controllers.

9- A novel two-directional bending actuator has been developed based on moulding a bladder from elastic liquid materials. This bending actuator has been used to enhance the elbow exoskeleton so as to make it capable of performing the rehabilitation exercises vertically and horizontally with a controllable stiffness.

10- A wrist exoskeleton has been developed in order to perform the wrist rehabilitation movements.

11- The novel all-directional bending actuator has been developed based on the moulding bladder technique. This actuator is used to develop a new version of the wrist rehabilitation exoskeleton.

12- Design and implementation of a totally portable rehabilitation system based on parallel processing controllers on-chip.

1.6 Organisation of the thesis

This thesis is organised into nine chapters so as to present the different aspects of the research that has been undertaken to complete the goals described above.

Chapter 1: Introduction : - This chapter presents a general overview of the power assistive and rehabilitation exoskeleton. It then illustrates the research motivation, aims and objective for this PhD research. It also explains the research methodology and lists the thesis' contributions.

Chapter 2: Upper-Limb Power-Assistive and/or Rehabilitation Robots : - This chapter presents a review of previous research in the power assistance and rehabilitation area.

Chapter 3: Soft Actuators : - This chapter presents background information on soft actuators, especially traditional PAMs, and discusses their numerous advantages over other actuation technologies. Furthermore, current applications of PAM actuators are briefly considered, along with the modelling efforts that have been used thus far to predict the behaviour of these devices. Given the current state of PAM technology and its analysis, motivation is established to develop novel PAM actuators for new applications.

Chapter 4: The Design and Mathematical Model of a Novel Variable Stiffness Extensor-Contractor Pneumatic Artificial Muscle (ECPAM) : - This chapter presents the design of a novel Extensor-Contractor Pneumatic Artificial Muscle (ECPAM). Furthermore, it contains the kinematics analysis of ECPAM with a mathematical model for these actuators.

Chapter 5: The Design and Mathematical Modelling of Novel Extensor-Bending Pneumatic Artificial Muscles (EBPAMs) : - This chapter presents the design of novel Extensor Bending Pneumatic Artificial Muscles (EBPAMs) for soft exoskeletons. Additionally, this chapter describes the design of the kinematic analysis and mathematical model for these actuators.

Chapter 6: Power Assistive and Augmentation Wearable Robot Based on Soft Actuators : - This chapter presents the design of soft, wearable gloves for power assistance and augmentation based on pneumatic soft actuators.

Chapter 7: Upper-Limb Rehabilitation Exoskeletons : - This chapter presents the design and construction of hand, forearm and wrist rehabilitation devices.

Chapter 8: Parallel Processing based on On-Chip Controllers for a Totally Portable Exoskeleton : - This chapter presents the design and implementation of a totally portable rehabilitation system based on parallel processing controllers on-chip.

Chapter 9: Conclusion and Future Work: - This chapter concludes the entire research and presents a plan for future work.

Chapter 2

Upper-Limb Power-Assistive and/or Rehabilitation Robots

2.1 Introduction

Robots are increasingly relied upon to promote efficient and enhanced living in modern day society. It can lead to a major improvement in quality of life if a robot assists and supports physically disabled and elderly individuals in their daily lives; for example, in social participation, rehabilitation, nursing, agriculture, medical welfare and so on. Furthermore, it is an increasing challenge to overcome the scarcity of caregivers for people in need of care. Elderly and disabled individuals need to be able to live independently if they so desire. In addition, rehabilitation and physical therapy are effective ways of regaining the ability to control body movement for people with neurological damage, physical injuries and other causes of disability. The most common are hand disabilities because the worker's hand is in direct contact with machines and repetitive movements at work cause neurological damage which then produces a decrease in the ability to control hand muscles. All the above reasons have inspired the invention of numerous kinds of power assistance and rehabilitation robots to solve these problems.

This chapter describes the human upper-limb anatomy by demonstrating the joints and movements of each segment in the upper-limb. A classification has been made for the power assistive and/or rehabilitation devices depending on their actuation type, such as electric actuations, hydraulic actuations and soft actuation. In each class we did a literature

review of previous research, drew conclusions from the literature review and discussed the pros and cons of previous research and what the challenges were in this field.

2.2 Upper-Limb Anatomy

The human upper-limb consists of three parts: hand, forearm and upper-arm (see Figure 2.1 a). The human hand consists of two segments: finger joints and wrist joints (see Figure 2.1 b); each finger has three joints.

Figure 2.1 c shows shoulder and elbow segments. The shoulder segment has three bones: the humerus, scapula and clavicle. The humerus is the longest bone in the upper-limb of humans, extending from the shoulder to the elbow. The scapula, or shoulder blade, consists of two flat triangular bones, each forming the back part of a shoulder in humans. The clavicle, or collarbone, consists of two slender bones, each articulating with the sternum and a scapula and forming the anterior part of a shoulder. The elbow is the bend or joint of the human arm between the upper arm and forearm. The wrist is the carpus or lower part of the forearm where it joins the hand.

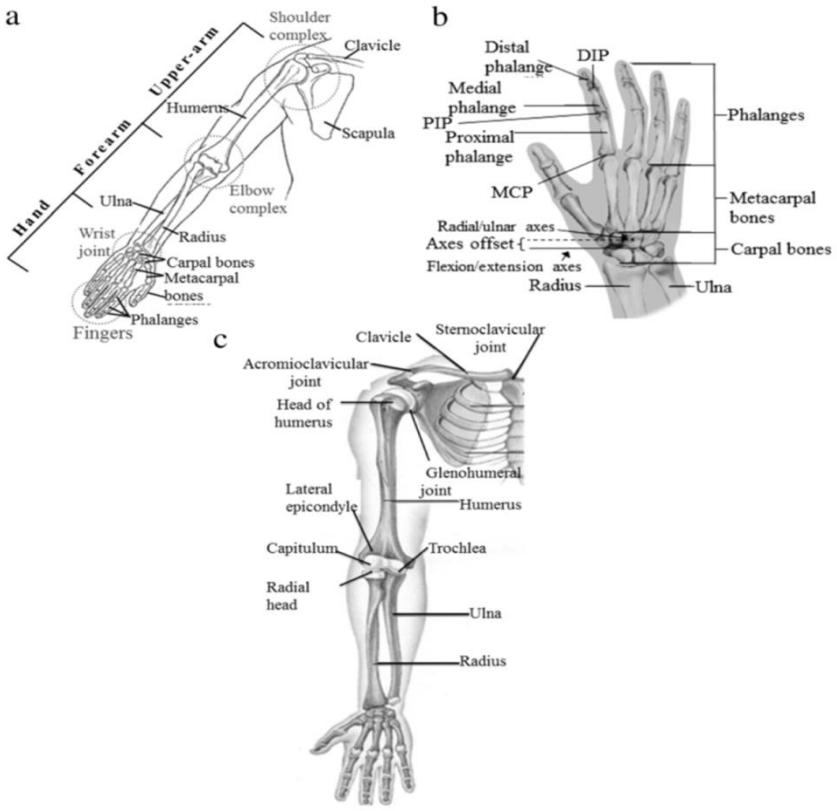

Figure 2.1: Human upper-limb anatomy (R. Gopura, D. Bandara, K. Kiguchi, & G. Mann, 2016a).

2.2.1 Human Shoulder Joint Motion

The shoulder complex is the largest joint of the upper-limb and has three DOF movements, as shown in Figure 2.2. Generally, there are three shoulder joint movements: flexion (forward and upward movement of the humerus on the glenoid in the sagittal plane)/extension (upward movement of the humerus on the glenoid in the sagittal plane towards the rear of the body) (see Figure 2.2 a), abduction (elevation of the humerus on the glenoid in the frontal (coronal) plane)/adduction (movement of the humerus on the glenoid in a medial direction, usually accompanied with some degree of shoulder flexion) (see Figure 2.2 b) and internal rotation (rotation of the humerus on the glenoid in a medial direction)/external rotation (rotation of the humerus on the glenoid in a lateral direction) (see Figure 2.2 c).

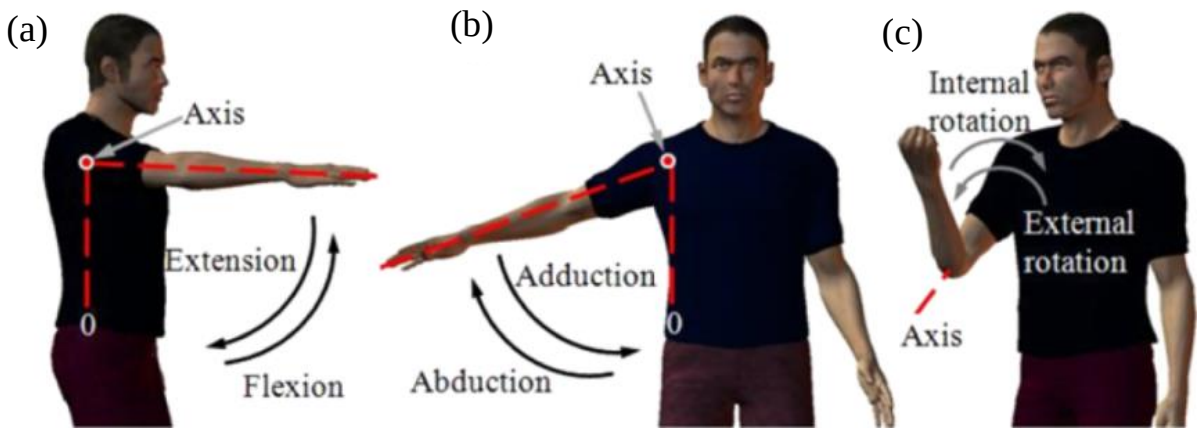

Figure 2.2: Shoulder joint movements (R. Gopura, D. Bandara, K. Kiguchi, & G. K. Mann, 2016b).

2.2.2 Human Elbow Joint Motion

The elbow is the middle joint of the arm between the wrist and the shoulder joints and has two DOFs, as shown in Figure 2.3. Generally, the elbow joint has two movements: flexion/extension (see Figure 2.3 a) and supination/pronation (see Figure 2.3 b).

2.2.3 Human Wrist Joint Motion

The wrist is the last joint before the fingers and the first after the elbow joint. It has two DOF movements, as shown in Figure 2.4. Generally, the wrist joint has two

movements: flexion/extension (see Figure 2.4 a) and radial/ulnar deviation (see Figure 2.4 b).

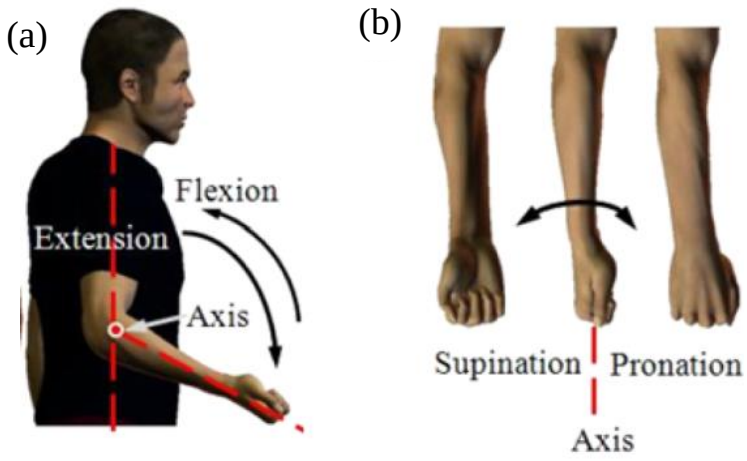

Figure 2.3: Elbow joint movements (Gopura et al., 2016b).

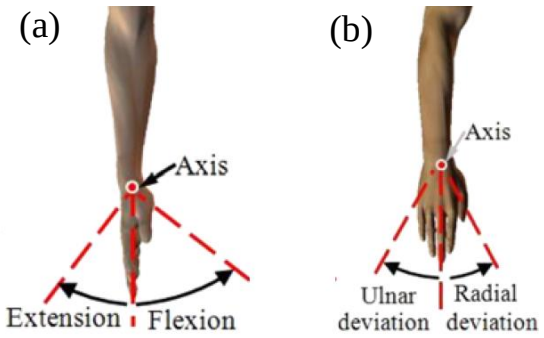

Figure 2.4: Wrist joint movements (Gopura et al., 2016b).

2.2.4 Human Finger Joint Motion

Figure 2.5 shows the human fingers and their joints: index, middle, ring and pinky fingers each contain three joints. The largest joint at the root of the finger is called the MP joint (metacarpophalangeal joint). The middle joint of each finger is the PIP joint (proximal interphalangeal joint). The terminal joint is called the DIP joint (distal interphalangeal joint). The thumb also has three joints: the root joint at the back of the palm is the CM joint (carpometacarpal joint). The middle joint has the same name as the root joints in the fingers: the MP joint. Finally, the IP joint (interphalangeal joint) is the name of the terminal joint of the thumb.

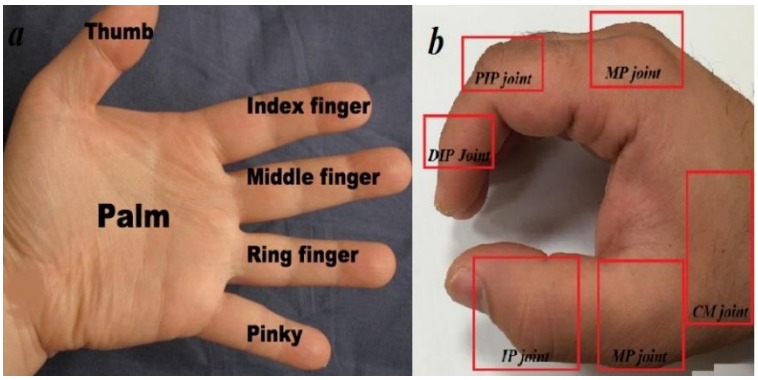

Figure 2.5: The human fingers and their joints.

2.3 Power Assistive and/or Rehabilitation Robots

During the last two decades, power assist and/or rehabilitation robots have been attracting more interest (Rocon & Pons, 2011). There is abundant research in this field and we can classify this research by the type of actuators used. The most common actuator categories are: electric, hydraulic and pneumatic soft actuators.

2.3.1 Power Assistive and/or Rehabilitation Robots using Electric Actuators

Electric actuators are gadgets controlled by engines that transform electrical energy into mechanical torque. Due to no oil is included, electrical actuators are thought to be one of the cleanest and most easily available types of actuators. There are numerous types of electric actuators and their function is dependent on the motor that they use. Electric actuators are commonly used to manufacture wearable robots for power assistance and rehabilitation, and the following research studies are some examples of that:

Frisoli et al. (2005) designed an exoskeleton to support the human shoulder movements and the elbow flexion/extension motions. This exoskeleton has 5 DOFs actuated by 4 DC motor groups and the motor groups' mass is approximately 40% of the whole exoskeleton mass. The prototype has been optimised to solve the problem of high mass and high stiffness in exoskeletons by using lightweight units, such as special carbon fibre mechanical components (see Figure 2.6 a).

Nef, Mihelj, Colombo, and Riener (2006) presented an upper-limb exoskeleton called ARMin. This device provides 6 DOF movements for the rehabilitation patients in the clinic, actuated by 4 DC motors. Force and position sensors have been equipped with

motors to reach the desired force and position for each rehabilitation movement. ARMin has been tested with five patients for more than 30 hours and the test results were extremely successful (see Figure 2.6 b).

Ball, Brown, and Scott (2007) developed a rehabilitation robot for stroke patients called MEDARM. This exoskeleton is capable of providing 6 DOFs for shoulder and elbow joints, actuated by electric motors with cables and belts to improve the power-to-weight ratio of their exoskeleton. MEDARM provides most shoulder movements and one for the elbow joint, and it can independently monitor and control all of its 6 DOFs (see Figure 2.6 c).

Retolaza, Pujana-Arrese, Cenitagoya, Basurko, and Landaluze (2008) presented a power assistive upper-limb exoskeleton device to support the manual worker in the workplace, especially during routine or repetitive movements. Their design was developed to amplify the shoulder and elbow motions with 5 DOFs actuated by a combination of conventional electric motors and pneumatic artificial muscles (see Figure 2.6 d).

Ren, Park, and Zhang Sr (2009) developed a whole upper-limb exoskeleton for fully paralysed stroke patients, especially for the hand and fingers gripping movement. This exoskeleton has 10 DOFs with DC motors to serve the purpose of diagnosis, treatment, training and outcome evaluation. Experimental results proved that this device provides more accurate diagnosis results than the clinician (see Figure 2.6 e).

Rahman, Ouimet, Saad, Kenne, and Archambault (2010) designed a wearable robot for rehabilitation purposes called ExoRob for the human shoulder and elbow joints. ExoRob is an exoskeleton robot that has 2 DOFs to support the internal/external rotation motion for the shoulder joint and the flexion/extension for the elbow joint. The researchers also focused on the mathematical model and the control algorithm of their design. A kinematic model type and nonlinear sliding mode controller were used (see Figure 2.6 f).

Ivanova, Bulavintsev, Ryu, and Poduraev (2011) proposed a 7 DOFs exoskeleton placed on a wheelchair to serve elderly and disabled people. Their design was manufactured to provide assistive movements for shoulder and elbow joints to perform the activities of daily living efficiently. Many tests have been done to examine the mechanism control performance of this prototype; the results were extremely encouraging (see Figure 2.6 g).

Ergin and Patoglu (2012) introduced an exoskeleton device to the rehabilitation exercises for shoulder and elbow segments called ASSISTON-SE. ASSISTON-SE, using independent active control and designed to amplify the force movements of both passive translational movements of the centre of the glenohumeral joint. Implementation details for their prototype have been provided, as well as the results of numerous experiments done for their prototype, to prove the ability of this device to track movements of the shoulder girdle (see Figure 2.6 h).

J. A. Martinez, Ng, Lu, Campagna, and Celik (2013) designed and presented the implementation and specifications of the forearm and wrist rehabilitation device for stroke patients. This device provides 3 DOF movements for the wrist joint and forearm segment to support pronation/supination, flexion/extension, and adduction/abduction joint motions. Using three Maxon DC brush motors for actuation, the design focused on the safety requirements by using mechanical rubber parts and an easily accessible emergency stop switch (see Figure 2.6 i).

Yamamoto et al. (2014) developed a rehabilitation robot for supporting patients when performing their rehabilitation exercises. This design is capable of detecting human intentions and supports any movement of the wrist joint. This device is also small and lightweight so that patients can use it in a clinic or at home. Actuator units receive a biological signal from the muscles to decide which movement the patient needs (see Figure 2.6 j).

Xiang et al. (2015) presented a one DOF wrist and forearm rehabilitation device for stroke patients. This device is capable of providing different training modes and creating a virtual-reality game for the patient to perform during the training. The device had been examined by two stroke patients and one chronic patient with left hemiplegia, and the results were successful. The robot is reconfigurable to each rehabilitation mode and it is portable (see Figure 2.6 k).

S. Chen et al. (2016) presented a rehabilitation robot called NTUH-ARM to rehabilitate the human upper-limb. This robot has 7 DOFs actuated by FAULHABER DC motors to perform most upper-limb rehabilitation exercises. Two 6-axis force/torque sensors have been used to provide a movement capture for the monitor and the controller. This device has been tested clinically by six patients to evaluate the performance of the robot, and the

results were examined by physical therapists, also revealing promising results (see Figure 2.6 l).

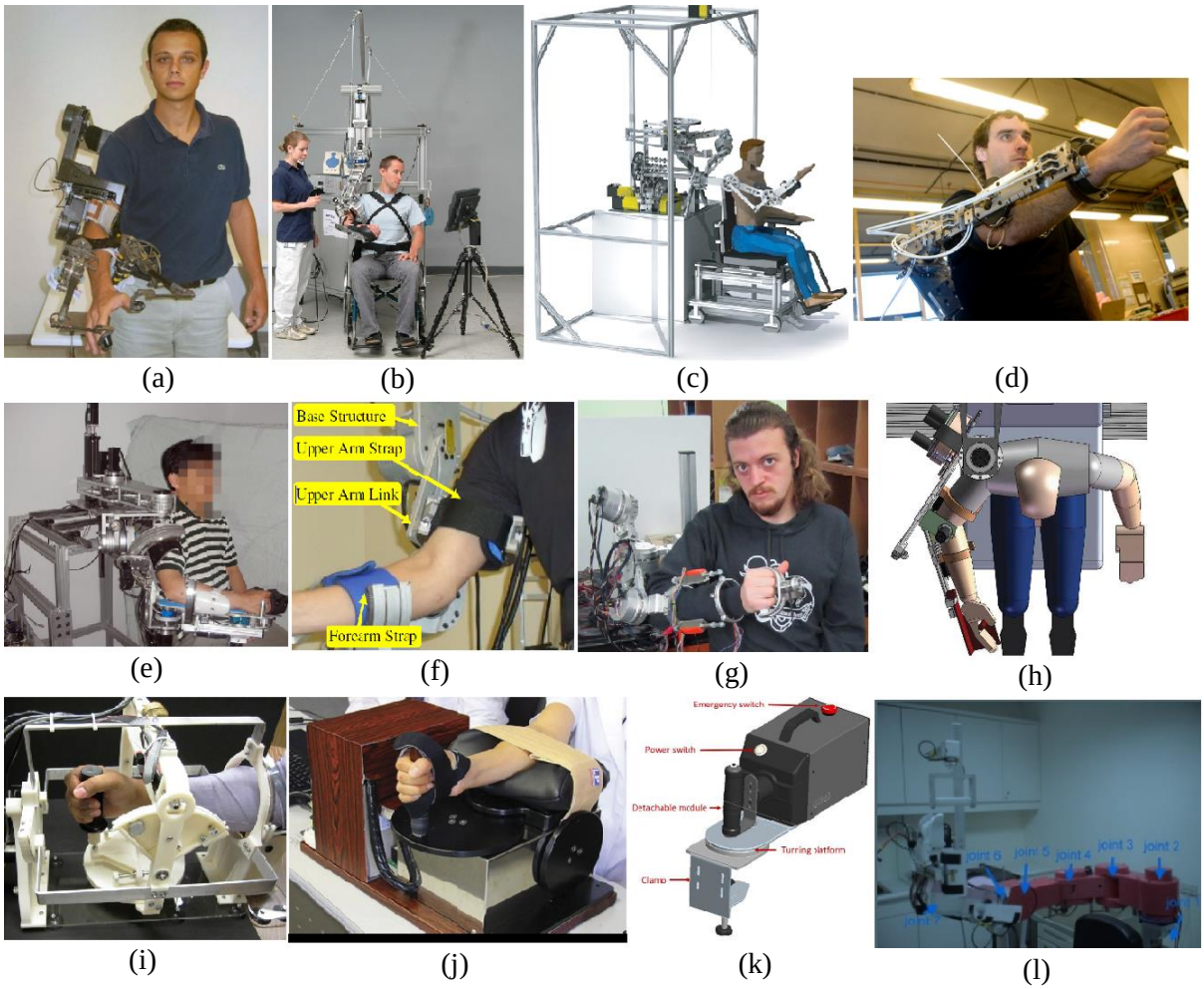

(a) (b) (c) (d)

(e) (f) (g) (h)

(i) (j) (k) (l)

Figure 2.6: Power Assistive and/or Rehabilitation Robots using Electric Actuators: (a) The arm exoskeleton (Frisoli et al., 2005); (b) ARMin exoskeleton (Nef et al., 2006); (c) MEDARM system (Ball et al., 2007); (d) Exoskeleton Prototype IKO (Retolaza et al., 2008); (e) A 8+2 DOF Robot (Ren et al., 2009); (f) Exoskeleton Robot (Rahman et al., 2010); (g) Prototype of The 7-DOF (Ivanova et al., 2011); (h) Solid Model of ASSISTON-SE (Ergin & Patoglu, 2012); (i) Wrist Gimbal (J. A. Martinez et al., 2013); (j) The Prototype Rehabilitative Training Robot (Yamamoto et al., 2014); (k) CAD drawing of The Robot (Xiang et al., 2015); (l) NTUH-ARM (S. Chen et al., 2016).

2.3.2 Power Assistive and/or Rehabilitation Robots using Hydraulic Actuators

Hydraulic actuators consist of a cylinder or liquid engine that uses pressure driven energy to facilitate mechanical operations. The mechanical movement produces an output

involving linear, rotary or oscillatory movement. Because the fluids are approximately incompressible, they take a long time to generate speed and force and, likewise, slow back down. However, they can apply a large force. The hydraulic actuators are widely used to create exoskeletons for power assist and rehabilitation, and the following studies are some examples of that:

Mistry, Mohajerian, and Schaal (2005) proposed an experimental prototype to study the human upper-limb in 3D motion. This prototype has a 7 DOFs hydraulically actuated exoskeleton robot arm to examine the behaviour of human upper-limb motor control. An independent PD servo controller has been used at each joint to create an efficient control structure to fit most human upper-limb movements. Force field experiments have been done to test the effectiveness of this device and the results were promising (see Figure 2.7 a).

Pylatiuk et al. (2009) presented an elbow flexion orthosis device for rehabilitation purposes with one DOF for the elbow joint. The major advantages of this device are that it is lightweight, portable, safe and inexpensive to facilitate a patient's independent usage at home or at a clinic etc. A flexible fluidic actuation system has been used to actuate this prototype. Surface EMG electrodes are used to control elbow flexion and extension movements. The system is also designed to provide the extra elbow flexion force that enables the patient to carry an additional load, such as a glass of water (see Figure 2.7 b).

Vitiello et al. (2013) proposed a powered elbow exoskeleton designed for poststroke physical rehabilitation, ensuring maximum safety and comfort to the patient. They used lightweight mechanical materials to minimise the pressure on the skin. This device has 4 DOFs to drive elbow flexion and extension movements. These DOFs are actuated hydraulically by using two cylinders and tendons to a suitable control for the joint movements under rehabilitation training conditions (see Figure 2.7 c).

Polygerinos, Galloway, Sanan, Herman, and Walsh (2015) designed a power assisted glove for full finger assistance for the activities of daily life. The glove is manufactured in elastomeric and inextensible materials so as to be lightweight and to create soft actuators that conform to the patient's fingers and are able to create enough hand grasp force. A fluidic pressure controller, which depends on human intentions, is used to actuate and control the glove. The patient's intention is detected by monitoring the EMG signals from electrodes placed on the forearm surface of the patient (see Figure 2.7 d).

Otten et al. (2015) developed a hydraulically powered self-aligning upper-limb exoskeleton for identifying the reflex properties of the shoulder and elbow joints in stroke patients. Powerful hydraulic motors are used to actuate this rehabilitation device and to generate high torques and power using lightweight actuators. This exoskeleton is also used for diagnostic purposes to diagnose the level of muscle/neurone damage in the upper-limb (see Figure 2.7 e).

Polygerinos, Wang, Galloway, Wood, and Walsh (2015) presented a soft glove to assist the rehabilitation exercises for functional grasp pathologies. The prototype employs soft actuators consisting of moulded elastomeric chambers with fibre reinforcements that produce suitable curvatures at finger joints under fluid pressurisation. A closed-loop controller is used to regulate the pressure inside the actuators. This device is completely portable with a rechargeable battery (see Figure 2.7 f).

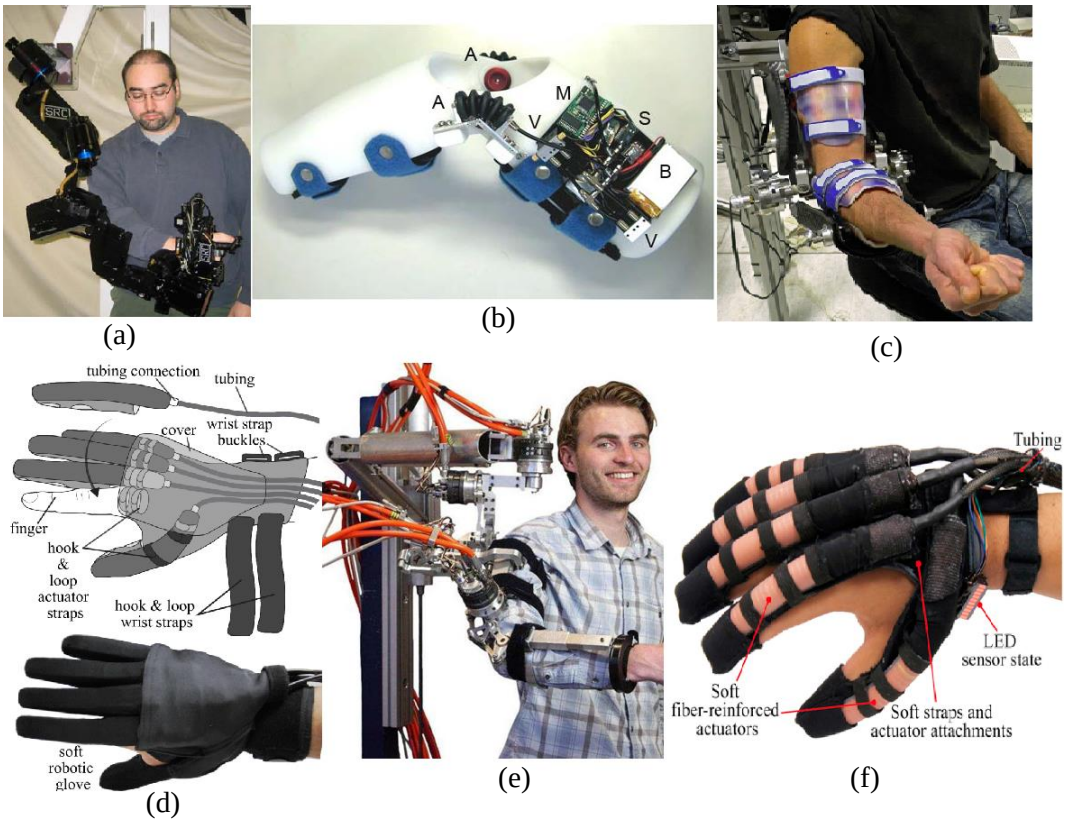

Figure 2.7: Power Assistive and/or Rehabilitation Robots using Hydraulic Actuators: (a) Exoskeleton Robot (Mistry et al., 2005); (b) Components of a Fluidically Driven Elbow Training System Prototype (Pylatiuk et al., 2009); (c) NEUROExos (Vitiello et al., 2013); (d) The fabricated soft robotic glove prototype (Polygerinos, Galloway, et al., 2015); (e) LIMPACT (Otten et al., 2015); (f) The prototyped soft and lightweight robotic hand assistive device (Polygerinos, Wang, et al., 2015).

2.3.3 Power Assistive and/or Rehabilitation Robots using Pneumatic Soft Actuators

Pneumatic soft actuators are actuators motored by air pressure created from soft materials, such as rubber tubes acting as a bladder and braided sleeves. They are the safest actuators for direct human interaction because they are lightweight and contain no rigid parts.

Noritsugu, Yamamoto, Sasaki, and Takaiwa (2004) presented a power assistive wearable glove to assist in making hand-gripping activities easier and safer in day to day life (see Figure 2.8 (a)). McKibben type pneumatic artificial muscles (PAMs) were used, placed on the front of the glove surface, one for each finger and two muscles for the palm (thumb side), one on the back and the other one on the face of the hand. Curved type PAMs are used by reinforcing one side of the muscle then, when pressurised, the muscle will be curved on the reinforced side. This device used the expiration switch (like video games controller switches) as the input signal since the expiration switch is generally easily used by disabled patients. This work was developed by Sasaki, Noritsugu, and Takaiwa (2005a) to manufacture a power assistive device for the wrist joint by also using a PAMs rotary type soft actuator (see Figure 2.8 (b).

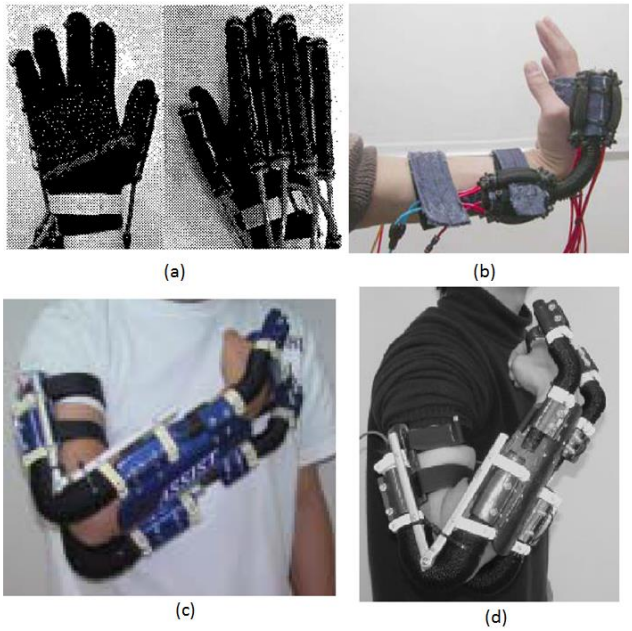

Figure 2.8: Exoskeletons: (a) Power Assist Glove (Noritsugu et al., 2004); (b) Assisting Scene (Sasaki et al., 2005a); (c) Power Assist Splint (Noritsugu, 2005); (d) ASSIST (Sasaki, Noritsugu, & Takaiwa, 2005b).

This type of pneumatic soft actuator consists of a rubber tube, two silicone rubber tubes and polyester bellows, which are reinforced with fibre to produce bending movements. In order to develop this study, Noritsugu (2005) extended the previous wrist assist device into an upper-limb splint to produce assistive power for the wrist and elbow joints (see Figure 2.8 (c)). A power assistive device for the elbow joint was driven by a contraction curved PAM attached to the elbow through a supporter, and the assistive force was controlled by adjusting the pressure inside the muscle. Moreover, a control technique, which takes into account a human aim, is proposed by Sasaki et al. (2005b) (see Figure 2.8 (d)). In the proposed technique, a focal point of pressure, calculated from the contact force between the lower arm and appliance, is utilised as a human aim info signal and the adequacy of the device is assessed utilising EMG.

A new design for power assistive wearable gloves has been developed by Noritsugu, Takaiwa, and Sasaki (2008) using two joint muscles for each finger except the thumb (see Figure 2.9 (a)).

Figure 2.9: (a) Two Joints Power Assisted Glove (Noritsugu et al., 2008); (b) Power-Assist Glove (Toya, Miyagawa, & Kubota, 2011).

Two curved type PAMs with different diameters are connected in series on the back of each finger. The muscle with the smaller diameter is placed on the terminal two joint of the finger and the bigger diameter one on the root joint, with each muscle provided

by a split air supply. The advantage of this technique is its capability of controlling the finger joints separately and to provide more movement types for assistance and rehabilitation. Similar to this, a design with two joints for each finger has been made by Toya et al. (2011), but this device used soft materials moulded to create the bending type artificial muscles (see Figure 2.9 (b)). The controller of this design depends on human intention as the input by using bending sensors attached to the muscles. In addition, the movements are divided into only three modes: power grip, precision grip, and tip pinch; the controller predicts the mode by matching the grasping angles with the stored database.

Another new design of a hand power assistive wearable robot was developed by Kadowaki, Noritsugu, Takaiwa, Sasaki, and Kato (2011) (see Figure 2.10).

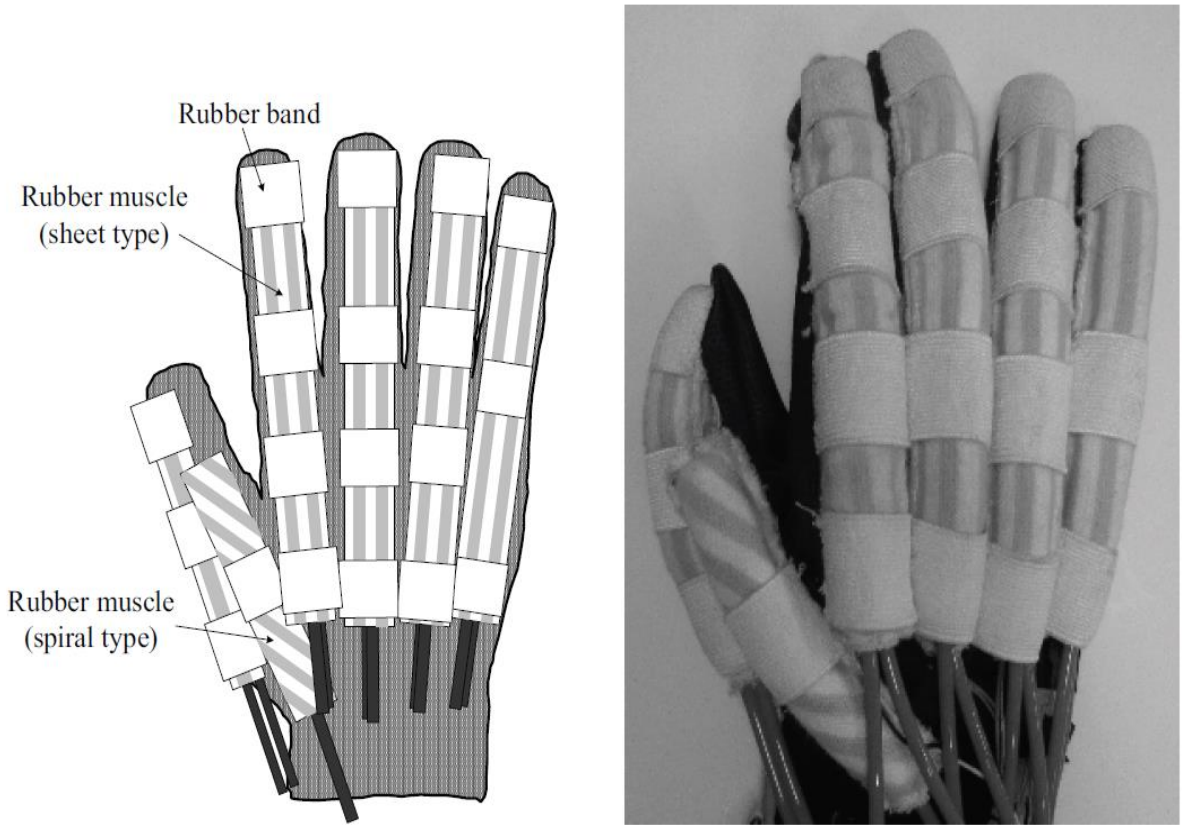

Figure 2.10: Power-assist glove (Kadowaki et al., 2011).

The design of this wearable robot is completely made up of soft materials, inspired by McKibben's muscles. Each muscle has two bladders: a rubber one and one comprising a balloon covered by woven elastic. These muscles are placed on the back of the hand, one for each finger, except that the thumb has two muscles. PI controllers were used to decide the bending angles for the fingers based on a bending sensor attached to each finger joint.

Estimated timing is used to perform the release movement after the gripping movement. They tried to use the EMG signals to control the release movements but they faced a problem due to the similarity between the EMG signals from the fingers and the wrist joint movements. Improvements to the controller algorithm of this robot have been achieved by (Sasaki, Noritsugu, Takaiwa, & Konishi, 2014). A neural network controller is used (Self-Organizing Maps) to recognise the different EMG signals from the wrist and the fingers during a release movement. However, this method assumed that the fingers and the wrist move independently (if the fingers are moving, the wrist is fixed and vice versa).

The power assistive wearable robot is not only for disabled or elderly people, but also for assisting with heavy manual work, such as nursing staff moving disabled patients from/to hospital beds. Kobayashi, Suzuki, Nozaki, and Tsuji (2007) proposed a muscle suit consisting of the upper-limb soft exoskeleton to provide muscular support for a manual worker (see Figure 2.11 (a)).

(a)

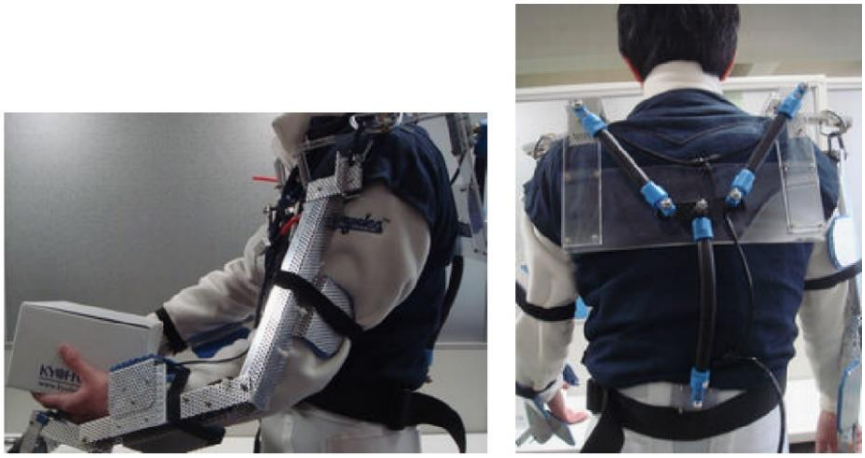

(b)

Figure 2.11: (a) Power Assist System for a Manual Worker by using a Muscle Suit (Kobayashi et al., 2007); (b) The power-assist robot arm (Kadota, Akai, Kawashima, & Kagawa, 2009).

This suit is actuated by PAMs to assist the upper-limbs and the human back, and also to help nurses move disabled patients from/to the wheelchair. Another assistive power suit has been developed by Kadota et al. (2009) (see Figure 2.11 (b)). This suit also consists of a wearable exoskeleton for both upper-limbs and the back in order to support people who carry heavier loads than normal. Bi-articular and singular PAMs have been used to manufacture this suit and a PI controller used as a control method, based on a balloon sensor (inflated balloon with a differential pressure sensor) as a feedback pressure when it has compressed, placed under the elbow muscles. The performance of this device was evaluated by monitoring the EMG signals with and without assistance. Results showed that there was less muscular fatigue with the assistive than without, whilst carrying the same load.

3D printed pneumatic soft actuators also play a part in rehabilitation devices, such as the hand rehabilitation wearable glove proposed by Polygerinos et al. (2013) (see Figure 2.12 (a)).

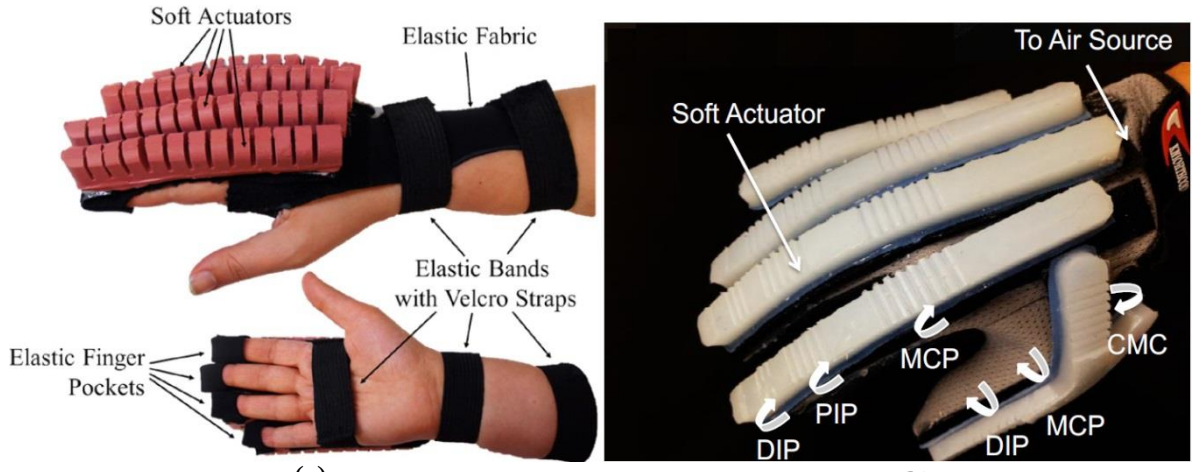

(a) (b)

Figure 2.12: (a) Top and bottom views of the prototype showing the soft actuators and the open palm glove configuration with the velcro straps (Polygerinos et al., 2013); (b) A ExoGlove prototype (Yap, Lim, Nasrallah, Goh, & Yeow, 2015b).

This research reports on the preparatory strides made towards the improvement of a soft exoskeleton glove for hand rehabilitation. The new soft actuators involve elastomeric materials with integrated channels that function as pneumatic networks and are manufactured and geometrically analysed to create bending movements that can safely adjust with the patient's finger movement. The bending curvature and force response of

these actuators are explored utilising a finite element model (FEM) and geometrical analysis before it's created.

Another 3D printed glove was presented by Yap et al. (2015b). This exoskeleton has variable stiffness features to perform most rehabilitation movements (see Figure 2.12 (b)). The variable stiffness is to make the muscle capable of only bending at the finger joints. The flaw in this research is that they have developed a different muscle for each rehabilitation movement. In other words, the patient needs to replace the glove muscles when converting to exercise mode.

2.4 Conclusion

Exoskeleton robots are a blend of human intelligence and machine power. As a result, the device improves the force of the human wearer. During recent decades, specialists have been continually working to increase their understanding and knowledge of robots. Their venture has succeeded practically through recent advances in the fields of mechanical design, electronic engineering, biomedical design and computerised reasoning. Exoskeleton robots are anticipated to play a critical part in the field of rehabilitation, assistive mechanical technology and human force growth. A few upper-limb exoskeleton robots have been created for different purposes with their own particular benefits and faults.

Dependent on the research literature review, this research area has many problems. The soft actuated exoskeleton is the safest device for direct human interaction but the fully soft actuated devices are still a major challenge. There is a noticeable lack of power assistance and rehabilitation research. Moreover, power assistive and rehabilitation devices should fit any adult limb size and should not need to mechanically change from one adult to another. The main problem of power assistive and rehabilitation exoskeletons is the release movements after the assisted movement has occurred as the human intention controller for rehabilitation robots is still a confused issue. Creating fully soft variable stiffness actuators continues to be a big challenge: there are no exoskeletons that can provide a hook movement (e.g. carrying a shopping bag) in power assistive gloves and there are problems in controlling the pneumatic soft actuators because of their nonlinear behaviour. Humans increase their grasping power when an object slips from their hand and there are no exoskeletons that provide a reaction for an object slipping from the hand. There is no design for a fully soft actuated hand rehabilitation device capable of

performing all hand rehabilitation movements due to the complexity of hand movements and the robot's difficulty in performing the complexity of the movements. This is the problem with the series of controllers for the actuators working in parallel. There is no portable, safe, soft, small and lightweight design for a wrist, elbow and forearm, or human shoulder power assistive and rehabilitation device, which is capable of performing all movements.

An exoskeleton power assistive and rehabilitation device must be: i) safe, because it is in direct interaction with humans; ii) lightweight, for easy use and portability, and; iii) small and soft, to be flexible in daily usage. All these properties are found in pneumatic soft actuators and, therefore, many researchers depend on these soft actuators to manufacture power assistive and rehabilitation exoskeletons.

Chapter 3

Soft Actuators

3.1 Introduction

An assortment of creatures and plants perform complicated movements using soft formations without rigid parts. Muscular hydrostats, such as the arms of an octopus and the trunk of an elephant, are almost totally composed of muscles and connective tissue; plant cells are also capable of changing their shape when osmosis is pressurised. Scientists have been inspired by these creatures and plants to design and manufacture robots with artificial soft actuators. Soft actuator structures provide a great degree of freedom; these robots are the safest for human interaction (Noritsugu et al., 2008). Figure 3.1 shows examples of muscular hydrostats and hydroskeletons. These creatures are typically capable of moving without skeletal support (Trivedi, Rahn, Kier, & Walker, 2008).

In this chapter, we review and explain the soft actuators and why they are better in some situations than the rigid actuators. The PAM history is also reviewed in this chapter. In addition, the contraction and operation of PAM are demonstrated. The artificial muscle properties and types from the last 50 years are also reviewed. The mathematical models are a major challenge and we explain that in this chapter by summarising the most important kinds of mathematical models. Finally, the PAM controller's techniques and its applications are also covered.

Figure 3.1: Examples of muscular hydrostats and hydroskeletons (Trivedi et al., 2008).

3.2 Soft Actuator Techniques

This section reviews and discusses on the state of the art of soft actuator techniques. A numerous number of actuators exist, but most of soft robotic applications are based on four soft actuator techniques: Shape-Memory Alloys (SMAs), Ionic Polymer-Metal Composites (IPMCs), Dielectric-Elastomer Actuators (DEAs) and Pneumatic Elastomeric Actuators.

3.2.1 Shape-Memory Alloys (SMAs)

Shape-memory alloys (Jani, Leary, Subic, & Gibson, 2014) actuate by transformation of their crystal structure in response to applied temperature. At low temperature, they have a martensitic structure that changes to an austenite structure at high temperature. When the alloy is deformed at low temperature, the material returns to its original shape upon heating (Figure 3.2). This phenomenon is called the shape memory effect, and can be used as a form of actuation.

SMAs exhibit high stress (e.g., 230 MPa) with substantial strains up to 5 % (Hunter, Lafontaine, Hollerbach, & Hunter, 1991). Nickel-titanium (NiTi) is the most commonly used alloy in this type of actuators (Hodgson, Ming, & Biermann, 1990)).

However, as shown in Figure 3.3 (a), when it is formed into a spring with a wire diameter of 25-500 μm, SMAs can provide compliance and a large actuation strain (e.g., 50 % linear contraction reported (S. Kim et al., 2009)). NiTi alloys are conductive, allowing direct Joule-heating, and they are also biocompatible. The response speed is relatively slow (~10 Hz) due to the thermally-activated phase change, and there is hysteresis across actuation cycles. SMAs can be driven with low voltage, but they require high current and provide low efficiency. The thermos-elastic behaviour of SMAs may also be affected by the external environment. In addition, SMAs have self-sensing capability (Lan & Fan, 2010).

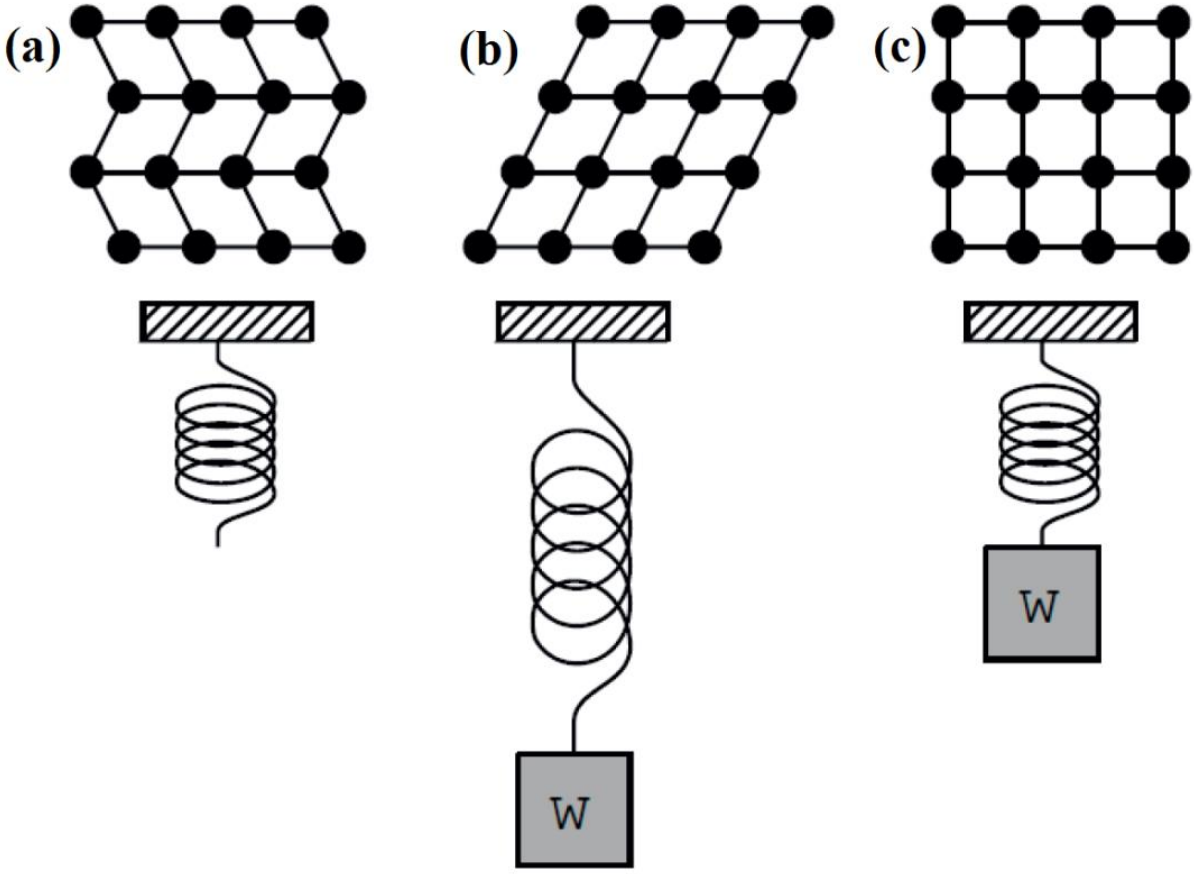

Figure 3.2: Working mechanism of SMAs, adopted from (Schubert, 2011). Top row shows crystal structure of the material at different states. (a) Undeformed SMA spring at low temperature in martensite state. (b) Deformed SMA spring at low temperature in martensite state. (c) SMA spring at high temperature in austenite state.

SMAs have been widely applied in robotic applications. Figure 3.3 (b) shows an inchworm-robot consisting of a mesh tube surrounded by an SMA spring. The compliance of the spring shows a resistance to external shock. Figure 3.3 (c) is a jellyfish robot. SMAs are integrated in the silicone-based bell. The high actuation stress of the actuator enables

jumping (Matsuyama & Hirai, 2007), even from the water's surface (J.-S. Koh et al., 2015). The small size of SMAs allows their implementation in millimetre scale robots (Hoover & Fearing, 2008), low-profile robots (Amir Firouzeh & Paik, 2015), and endoscopes (Ikuta, Tsukamoto, & Hirose, 1988) as well as manipulation devices such as a robotic hand (Price, Jnifene, & Naguib, 2007).

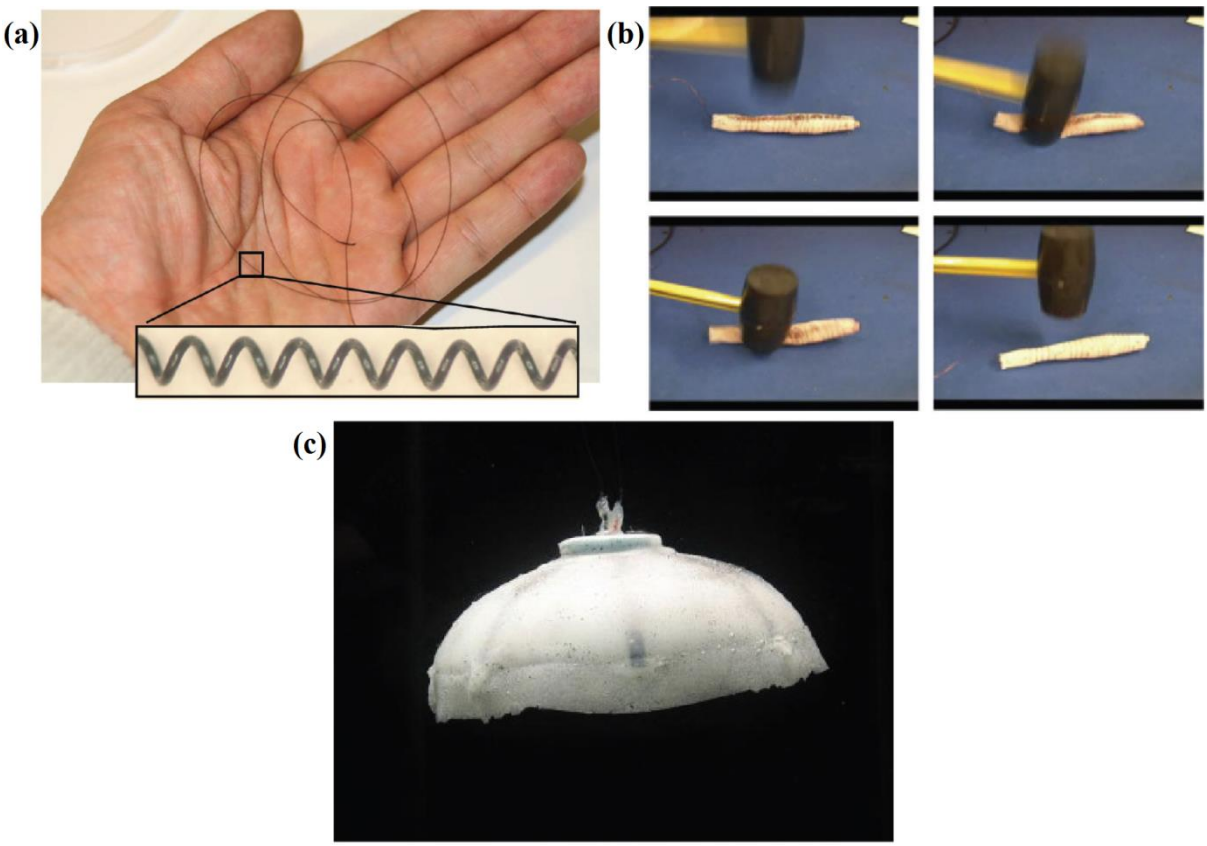

Figure 3.3: SMA actuators; (a) A spring actuator (NiTi) (S. Kim et al., 2009), (b) An inchworm robot (Seok et al., 2013), and (c) A jellyfish robot using SMA (Villanueva, Smith, & Priya, 2011).

And another robotics applications such as an underwater walker (Ayers & Witting, 2007) (Figure 3.4 (a)) to a miniature flying robot (Kovac, Guignard, Nicoud, Zufferey, & Floreano, 2007) (Figure 3.4 (b)). Many bio-inspired robots have been developed. They are simulating the motions of inchworms (Lin, Leisk, & Trimmer, 2011) (Figure 3.4 (c)), microrobotic fish fin (Cho, Hawkes, Quinn, & Wood, 2008) (Figure 3.4 (d)), octopus arm (Laschi et al., 2012) (Figure 3.4 (e)), manta rays (Wang, Wang, Li, & Hang, 2009) (Figure 3.4 (f)), turtles (H.-J. Kim, Song, & Ahn, 2012) (Figure 3.4 (g)), and bat wings (Colorado, Barrientos, Rossi, & Breuer, 2012) (Figure 3.4 (h)).

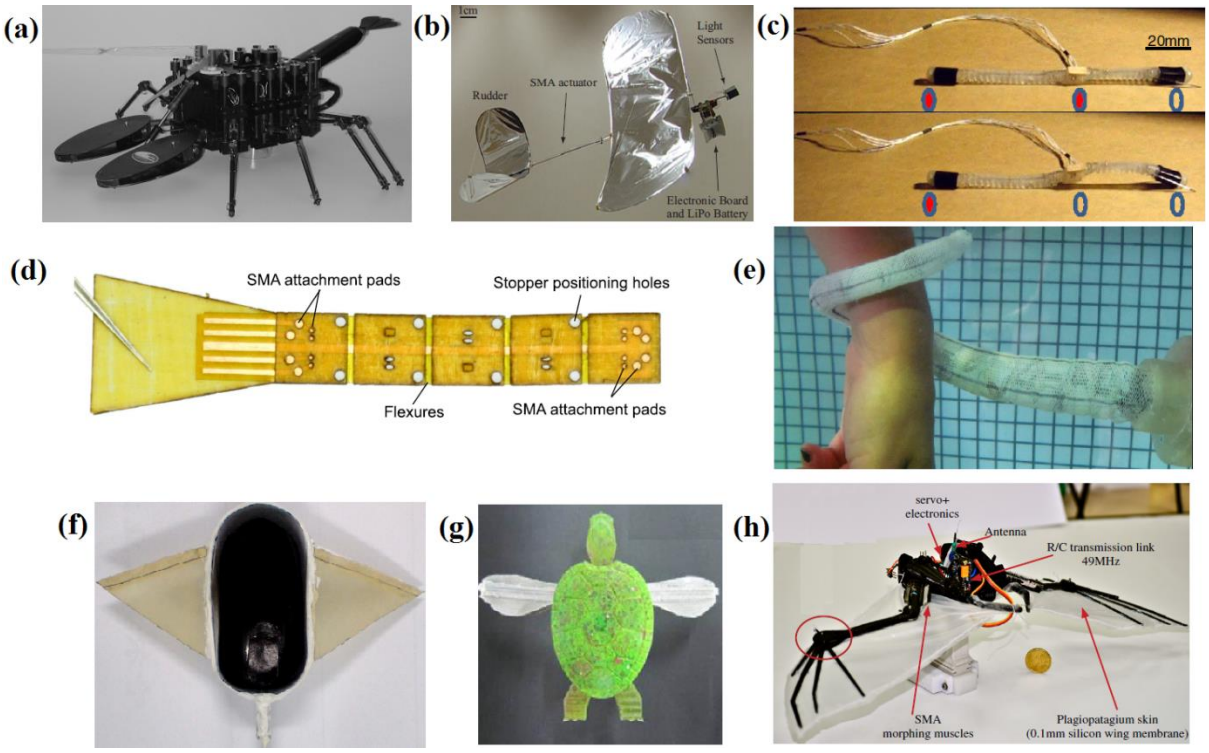

Figure 3.4: SMA robotic applications; (a) Underwater walker (Ayers & Witting, 2007), (b) Miniature flying robot (Kovac et al., 2007), (c) Inchworms (Lin et al., 2011), (d) Microrobotic fish fin (Cho et al., 2008), (e) Octopus arm (Laschi et al., 2012), (f) Manta rays (Wang et al., 2009), (g) Turtles (H.-J. Kim et al., 2012) and (h) Bat wings (Colorado et al., 2012).

3.2.2 Ionic Polymer-Metal Composites (IPMCs)

Ionic polymer-metal composites (Jo, Pugal, Oh, Kim, & Asaka, 2013) consist of an electrolyte-swollen polymer membrane (thickness 100-300 μm) surrounded by two thin metallic layers. Figure 3.5 shows the operation of IPMCs. The polymer is charged negatively and balanced by added mobile cations. When a voltage bias is applied to the electrodes, the cations relocate across the cathode part. The relocation results in swelling the negative part of the membrane, causing a bending movement of the entire structure toward the positive part. Figure 3.6 (a) shows the bending movement of an IPMC actuator.

IPMCs are compliant and are able to provide large bending strokes with low actuation voltages. Encapsulation enhances actuation performance in dry environments (Barramba, Silva, & Branco, 2007). However, their response speed is slow (e.g., an IPMC actuator took 3.5 minutes to achieve ~270 deg of bending angle (Nemat-Nasser & Wu,

2003), Figure 3.6 (b)), and their actuation characteristics exhibit hysteresis. Moreover, the output stress and the efficiency are low. Their slow motion makes them unsuitable to be applied to devices that require fast movements. IPMCs are capable of self-sensing (Punning, Kruusmaa, & Aabloo, 2007) and energy harvesting (Aureli, Prince, Porfiri, & Peterson, 2009). Figure 3.6 (b) shows an untethered fish robot where IPMCs are integrated into the root of the tail. Not confined to aquatic environments, terrestrial IPMC robots have been developed. Examples include worm-like (Arena, Bonomo, Fortuna, Frasca, & Graziani, 2006) and deformable robots (A Firouzeh, Ozmaeian, & Alasty, 2012) that can crawl on the ground, as well as grippers (Jain, Majumder, & Dutta, 2013) and (Khan, Jain, & Naushad, 2015).

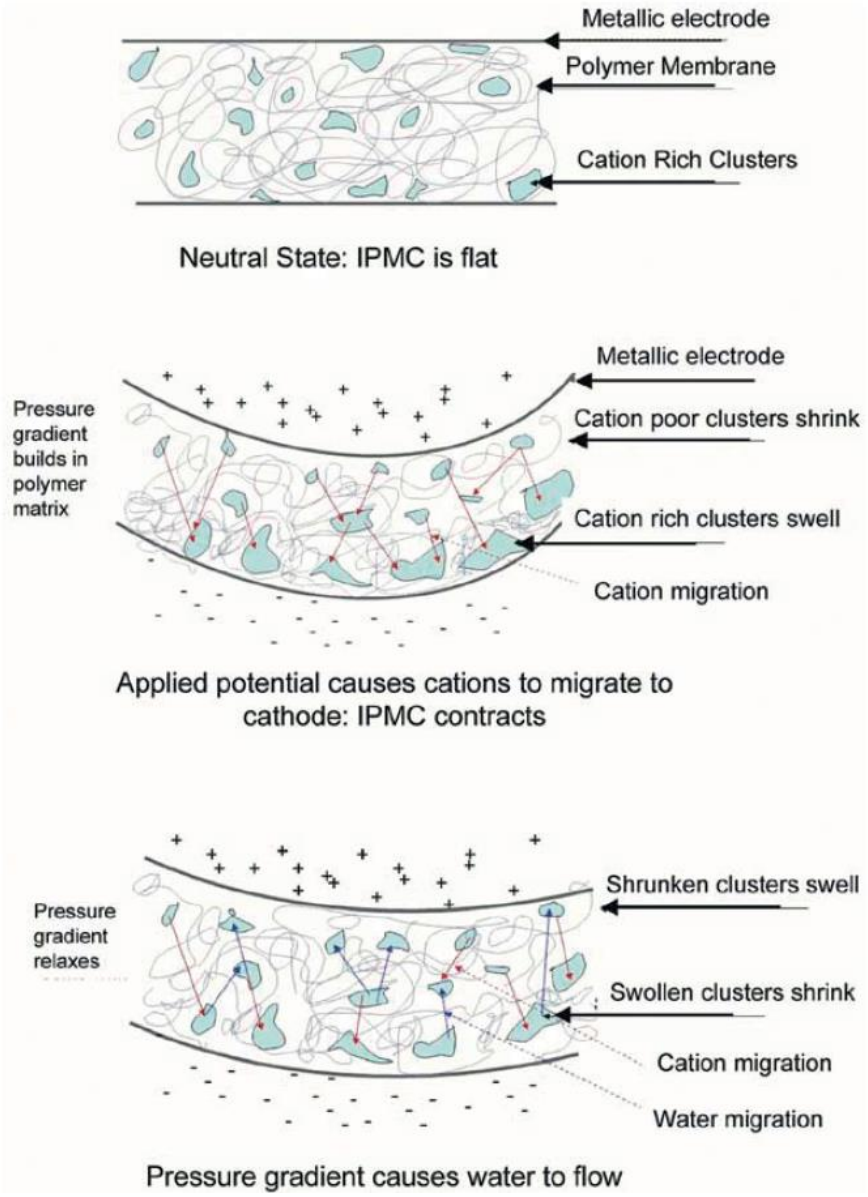

Figure 3.5: Operation of IPMCs (Madden et al., 2004).

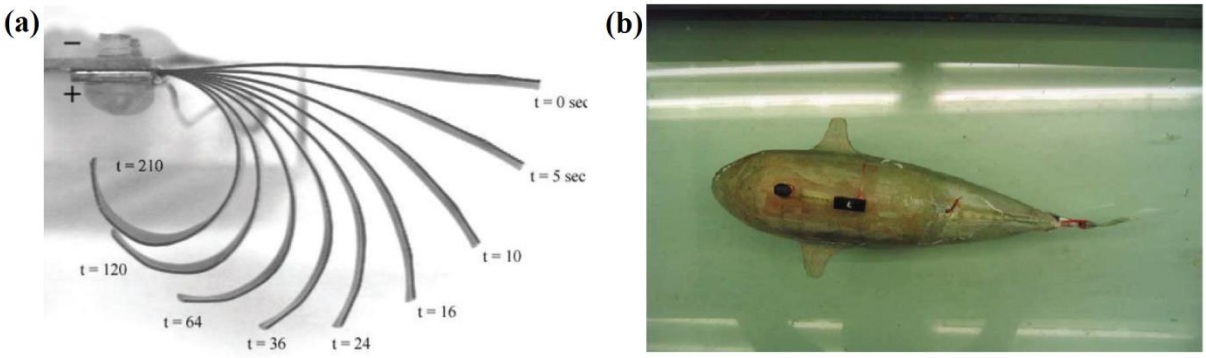

Figure 3.6: IPMC actuators, (a) An IPMC actuator exhibiting bending motion (applied voltage 3 V) (Nemat-Nasser & Wu, 2003) and (b) An untethered fish robot using an IPMC actuator (the actuator is placed in the root of the tail) (Z. Chen, Shatara, & Tan, 2010).

The inherent need of water for IPMCs has accelerated their use in underwater robots. Researchers have demonstrated bio-inspired robots mimicking a sea snake (Kamamichi, Yamakita, Asaka, & Luo, 2006) (Figure 3.7 (a)), manta ray (Z. Chen, Um, & Bart-Smith, 2011) (Figure 3.7 (b)), turtle (Shi et al., 2013) (Figure 3.7 (c)), and jellyfish (Najem, Sarles, Akle, & Leo, 2012) (Figure 3.7 (d)).

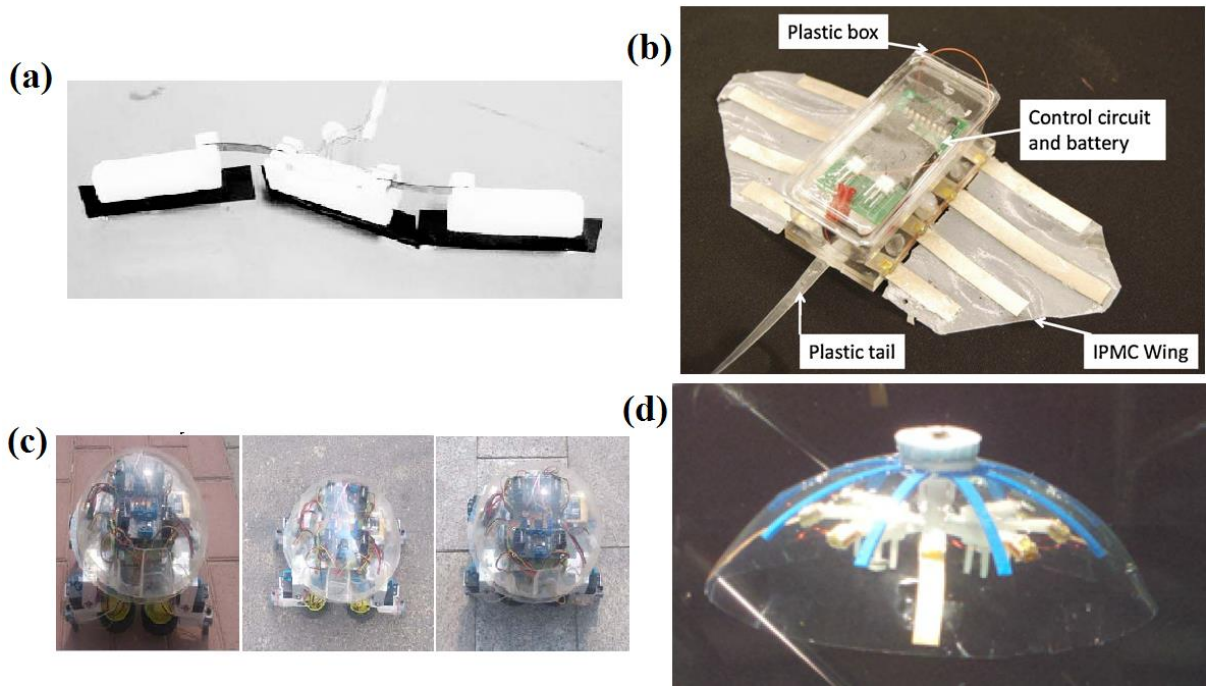

Figure 3.7: IPMC robotic applications; (a) Sea snake (Kamamichi et al., 2006), (b) Manta ray (Z. Chen et al., 2011), (c) Turtle (Shi et al., 2013) and (d) Jellyfish (Najem et al., 2012).

3.2.3 Dielectric-Elastomer Actuators (DEAs)

Dielectric-Elastomer Actuators (DEAs) consists of an elastomer membrane sandwiched between two compliant electrodes. Applying a voltage creates opposing charges on the electrodes. These charges attract each other and squeeze the elastomer membrane, resulting in thickness reduction and area expansion.

DEAs have high compliance (~1 MPa elastic modulus), large actuation strokes (up to 85% of linear strain on a silicone elastomer (Akbari, Rosset, & Shea, 2013)), fast response speeds (response time less than 200 μs (Maffli, Rosset, Ghilardi, Carpi, & Shea, 2015)), and theoretically high electromechanical efficiency (maximum 90% (Carpi, De Rossi, Kornbluh, Pelrine, & Sommer-Larsen, 2011)). In a silicone elastomer, the hysteresis in a cycle is relatively small due to low viscoelasticity (Michel, Zhang, Wissler, Löwe, & Kovacs, 2010). In addition, a silicone elastomer also has a wide thermal tolerance (-100 to 250 ◦C (Madden et al., 2004)). When carefully insulated, DEAs are able to work in an underwater environment (Godaba, Ng, & Zhu, 2014), and are expected to be used in space (Araromi et al., 2015). However, DEAs usually generate low stresses, and a high voltage is necessary for driving them (typically a few kV), which requires the use of DC/DC converters.

DEAs have self-sensing capability (Gisby, Calius, Xie, & Anderson, 2008). Depending on the configuration, they can possess further capabilities, such as, self-healing (Hunt, McKay, & Anderson, 2014), switching (O'Brien, Calius, Inamura, Xie, & Anderson, 2010), energy harvesting and (S. J. A. Koh, Keplinger, Li, Bauer, & Suo, 2011). The simple structure of DEAs has exploited a number of actuator configurations, and a wide range of robotic applications.

Robotic applications based on DEAs have been widely explored. Figure 3.8 (a) is a legged robot consisted of six 2-DOF spring roll actuators (Pei, Rosenthal, Stanford, Prahlad, & Pelrine, 2004). Bending actuation of each leg moves the robot in different directions. For this type of legged robot, employing linear contractile actuators could mimic the movements of animals. Figure 3.8 (b) is a quadruped in which each leg has 2 linear actuators to perform animal-like 2-DOF motion (Nguyen et al., 2014). Biomimetic ground locomotion based on extension or undulation of its body has also been realized in the form of an inchworm (Conn, Hinitt, & Wang, 2014) or snake (Petralia & Wood, 2010).

Figure 3.8 (c) shows an inchworm robot that can extend and contract segments of its body to loco-mote. A similar mechanism can be seen in the snake-like robot shown in Figure 3.8 (d) in which several DEMESs are integrated (Petralia & Wood, 2010).

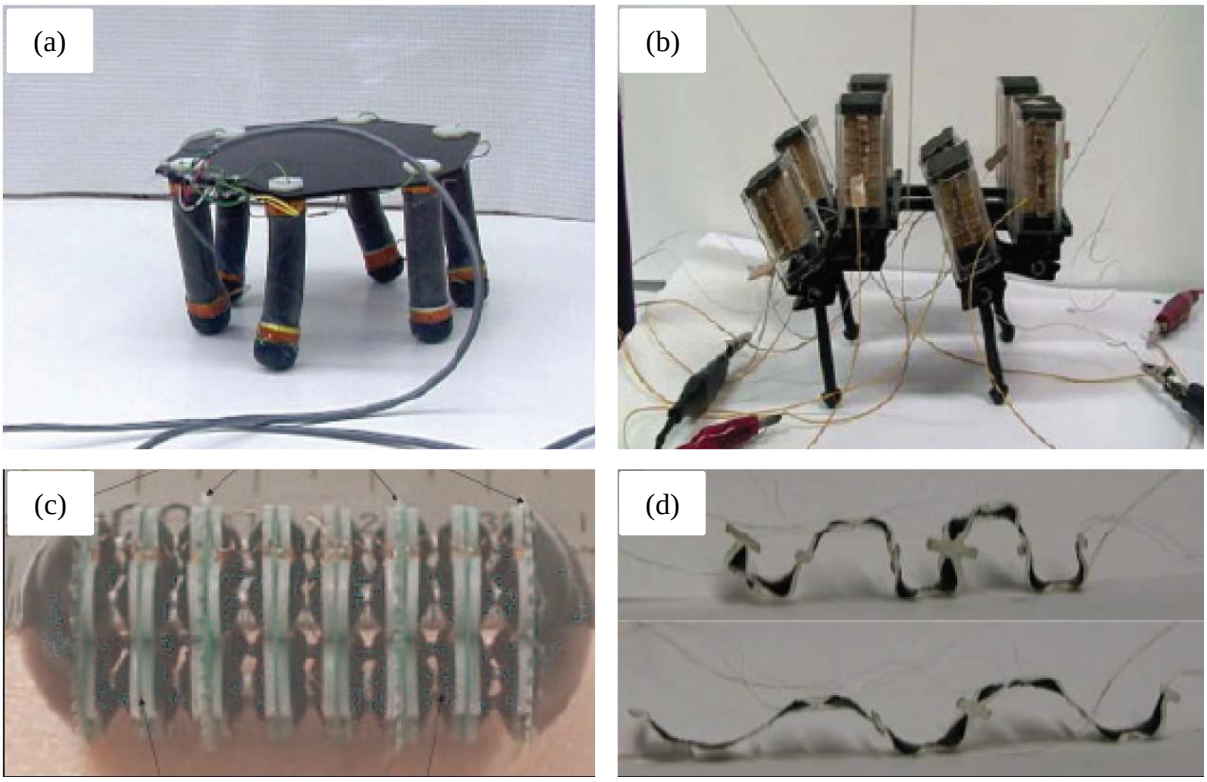

Figure 3.8: Robotic applications based on DEAs; (a) Legged robot using 2-DOF spring roll actuators (Pei et al., 2004), (b) Quadruped using linear contractile actuators (Nguyen et al., 2014), (c) Inchworm robot using modular diaphragm actuators (Jung, Koo, Lee, & Choi, 2007) and (d) Snake-like robot using DEMESs (Petralia & Wood, 2010).

3.2.4 Pneumatic Elastomeric Actuator

This type of actuator has a homogeneous silicone matrix with embedded chambers (PneuNets (Ilievski, Mazzeo, Shepherd, Chen, & Whitesides, 2011)), a paper origami structure (R. V. Martinez, Fish, Chen, & Whitesides, 2012), reinforcing fibres (Galloway, Polygerinos, Walsh, & Wood, 2013), Soft-bodied (Suzumori, Endo, Kanda, Kato, & Suzuki, 2007). Depending on their structural configuration, different actuation behaviours can be achieved, such as bending, contraction, and extension. Figure 3.9 shows the working mechanism of PneuNets actuators. The actuator is often combined with an inextensible, flexible substrate. When pressured with fluid (mostly air), the chambers

inflate, resulting in an anisotropic bending motion. Figure 3.10 shows a real PneuNets actuator exhibiting bending motion (Ilievski et al., 2011).

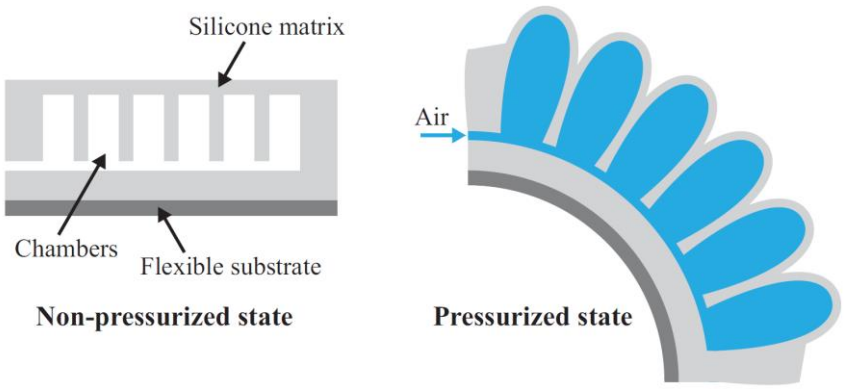

Figure 3.9: Working mechanism of a pneumatic elastomeric actuator (PneuNets). Pressuring the structure inflates the chambers anisotropically, leading to a bending motion (Ilievski et al., 2011).

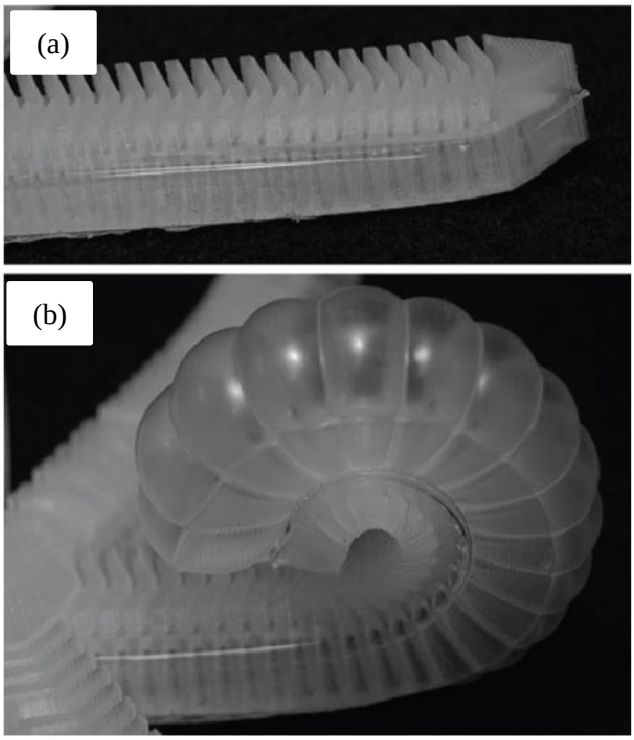

Figure 3.10: A pneumatic elastomeric actuator showing bending motion (Ilievski et al., 2011) (the actuator shown here is the finger of a 9 cm diameter gripper).

Pneumatic elastomeric actuators can be formed with varied geometries and materials, and their actuation characteristics change from one type to another with driving pressure. It is difficult to have representative characteristics for comparison with other soft

actuator technologies. However, pneumatic elastomeric actuators exhibit high compliance (~1MPa elastic modulus) and force (e.g., 7 N at 414 kPa (Galloway, Polygerinos, et al., 2013)), large actuation strokes (e.g., over 200◦ bending angle at 150-350 kPa (Galloway, Polygerinos, et al., 2013)), and fast movements (50 ms to bend circular from a linear shape at 345 kPa (Mosadegh et al., 2014)). The use of elastomers should result in a wide thermal tolerance (-100 to 250◦C in silicone (Madden et al., 2004)). One setback to this actuation technology is the need of compressors, pumps, and air cylinders. They are big, leading to a bulky untethered structure, hindering mobility and the miniaturisation of such robots. Pneumatic elastomeric actuators do not have self-sensing capability as the structure is a homogeneous silicone matrix. However, they can exhibit colour change (camouflage) capability by injecting coloured fluids into embedded channels (Morin et al., 2012). It has been reported that the actuators are resistant to puncture and self-seal when combined with a fibrous material (e.g., Kevlar); however, the mechanism is not yet fully understood (Shepherd, Stokes, Nunes, & Whitesides, 2013).

To date, several robots using pneumatic actuators have been demonstrated (Faudzi et al., 2012). Figure 3.11 is a legged robot that can perform different gait patterns by inflating certain combinations of body parts (Shepherd et al., 2011). Changing the gait pattern enables it to go through narrow gaps. A larger version of this robot has been made untethered, equipped with a compressor and controller (Tolley et al., 2014).

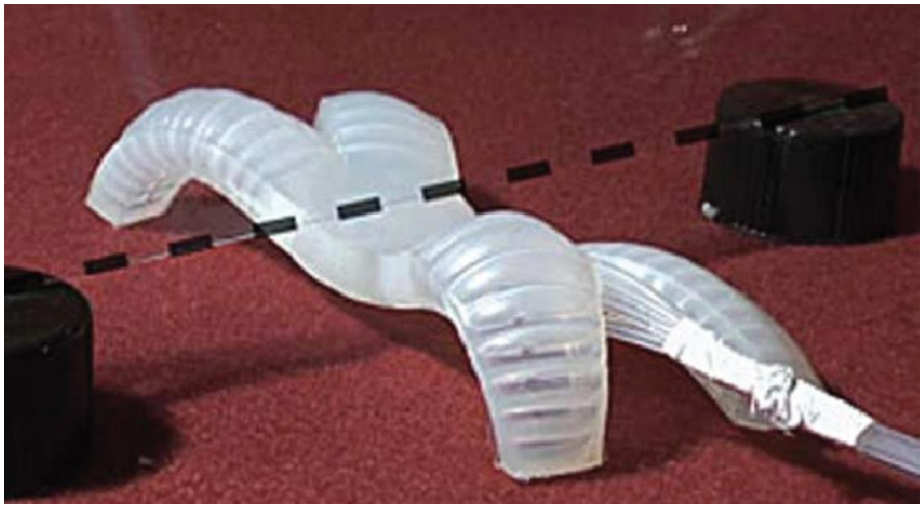

Figure 3.11: A legged robot using a pneumatic elastomeric actuator (Shepherd et al., 2011) (~15 cm long) (the robot is able to crawl through a narrow gap by changing its gait pattern).

There have also been untethered systems such as a rolling robot using a series of pneumatic bending actuators (Onal, Chen, Whitesides, & Rus, 2017), and a bio-inspired fish robot that can perform escape maneuvers in addition to forward swimming (Figure 3.12 (Marchese, Onal, & Rus, 2014)). Meanwhile, manipulation devices have been developed, such as, grippers (Ilievski et al., 2011), a dexterous hand (Deimel & Brock, 2016), a discrete robotic arm (Marchese, Komorowski, Onal, & Rus, 2014), and tentacles (R. V. Martinez et al., 2013).

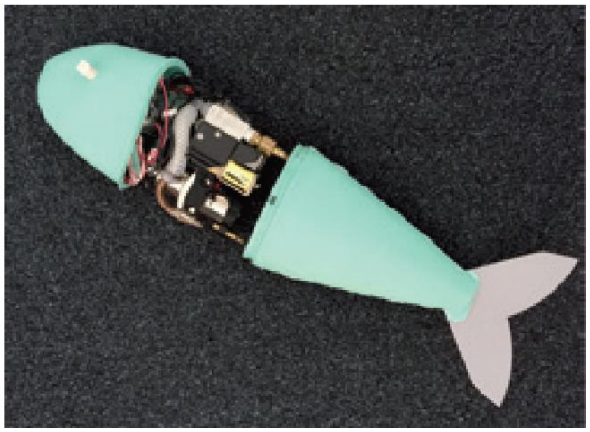

Figure 3.12: An untethered fish robot using pneumatic elastomeric actuators (Marchese, Onal, et al., 2014).

The heights weight to force ratio of pneumatic soft actuator is the pneumatic artificial muscles (Daerden & Lefeber, 2002) (PAMs, also known as McKibben artificial muscles) linearly contract like human muscle when pressurised due to the radial change of an inextensible mesh surrounding a rubber inner bladder (this type of actuators will reviewed in details in the next sections).

3.3 Pneumatic Artificial Muscles

The Pneumatic Muscle Actuator (D. Caldwell, Medrano-Cerda, & Goodwin, 1993), also named the McKibben Pneumatic Artificial Muscle (PAM), Fluidic Actuator or Biomimetic Muscle, is a tube–like actuator that is characterised by a decrease or increase in the muscle length when pressurised (Andrikopoulos, Nikolakopoulos, & Manesis, 2011). The most common soft actuator is the McKibben Muscle, which was invented by the physician Joseph L. McKibben in the 1950s and was used as an orthotic appliance for polio patients (Daerden & Lefeber, 2002).

The first commercial version of PAM was manufactured by a Japanese company named Bridgestone in the 1980s. These muscles are significantly lightweight actuators that feature smooth, fast, and accurate responses and are also capable of producing a high force when fully pressurised (Andrikopoulos et al., 2011).

PAMs are typically designed and manufactured as a latex or rubber tube surrounded by a braid sleeve. Fibre wrapping surrounds the rubber tube for protection, and suitable plastic or metal fittings are attached to both ends. The PAMs convert pneumatic power to a pulling/pushing force and have many benefits, such as a high force to weight ratio, variable installation possibilities, no requirement for additional mechanical parts (e.g. gearboxes), low consumption of compressed air and that they are manufactured from cheap materials. Moving off board heavy rigid motor parts, which make up most of the weight of a robot actuator, with lighter McKibben artificial muscles will produce advantages in industrial and medical robots. The PAM is a pneumatic soft actuator, which shows numerous features found in real muscle.

3.3.1 Construction

According to Chopade, Kauthalkar, and Bhandari (2013), the general design consists of an expandable bladder, such as a rubber tube surrounded by a braided sleeve made of fibre threads, which are attached to both sides. Davis, Tsagarakis, Canderle, and Caldwell (2003) state that the muscles are available in many sizes, producing variable output forces. Furthermore, the range of actuator displacement, and also the lengths of muscles, can be from under 10 cm up to 400 cm, and the range of diameters from under 10 mm up to 70 mm. Figure 3.13 shows the PMA construction.

Figure 3.13: The PMA Construction (Davis et al. (2003)).

3.3.2 Operation

Expansion of the rubber tube bladder against the braided sleeve occurs when pressure is applied. The braided sleeve acts to limit the expansion of the inner tube in order to maintain a cylindrical shape. When the pressure is increased, the volume of the inner tube increases in relation to the applied pressure, the contracting artificial muscle shortens and provides a pulling force to a mechanical load due to the extensor producing a pushing force (the extensor muscle type is the same construction of the contractor type but in this case the braided sleeve is longer than the bladder). "This basic principle is the conversion of the radial stress on the rubber tube into axial stress and during relaxation of the muscle the reverse happens" (Chopade et al., 2013). A thin rubber tube transmits the applied pressure acting on it to the non-stretchable outside braid. Loads can be attached at one end of the PAM and the other end is for the air flow from the valve, as shown in Figure 3.14 (Davis et al., 2003).

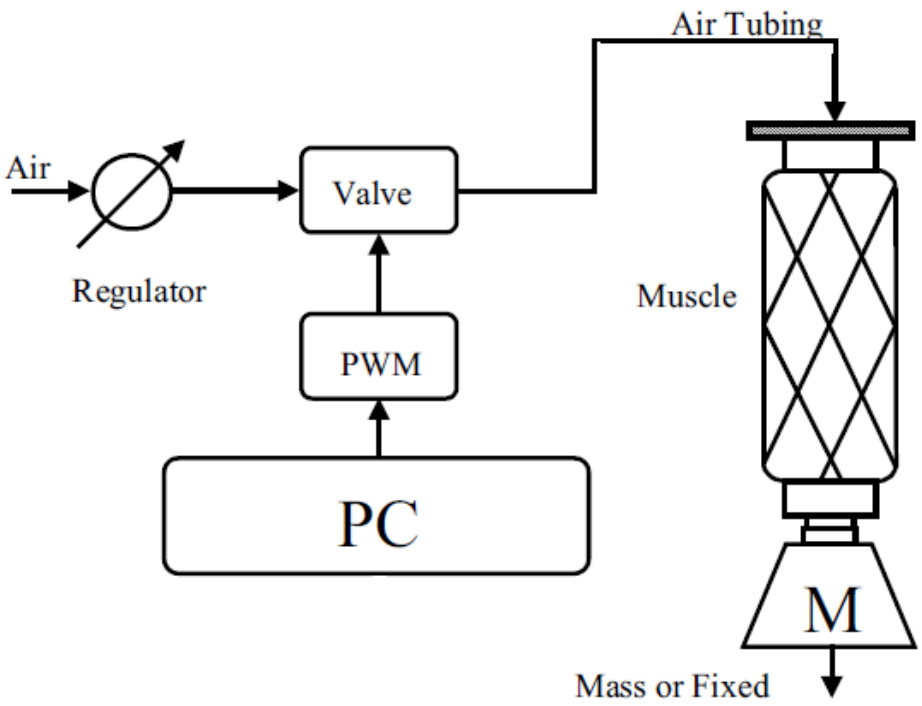

Figure 3.14: Operation of PAM (Davis et al., 2003).

3.4 PAM Properties

Daerden and Lefeber (2002) illustrate the most important properties of PAM as follows:

- ***Static load characteristics***: Under static conditions, the PAM equilibrium length will be determined by the pressure, the external load and the volume to length ratio of that specific muscle.
- ***Compliance***: As a result of air compressibility, every pneumatic actuator demonstrates the compliant behaviour. Regardless of the fact that the pressure is kept at a fixed amount, the muscle demonstrates spring-like behaviour because of the change of force with respect to length.
- ***Antagonistic set-up***: Pneumatic soft actuators are contraction devices and can produce movement in one direction only, like real muscles. To generate bidirectional movements, two muscles are needed, one for each direction. One actuator moves the load in one direction and the other one works as a brake to reach the desired position; changing the muscles' operation produces an opposite movement. Figure 3.15 shows the load motions in rotational or linear directions.

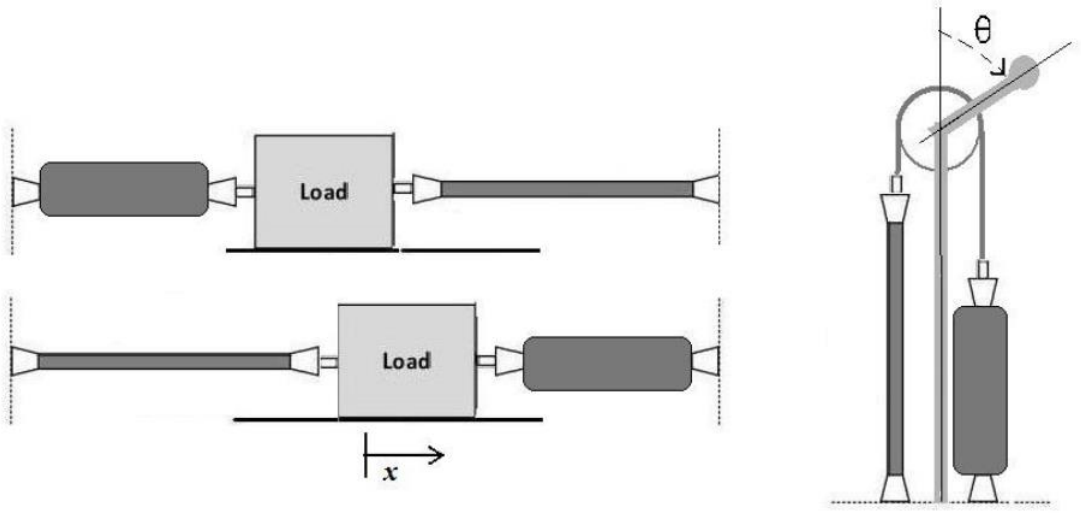

Figure 3.15: Antagonistic set-up (Daerden & Lefeber, 2002).

- ***Skeletal Muscle Resemblance***: PAMs are similar to skeletal muscle in functional behaviour in that both use linear contraction motion with a monotonical relation between decreasing load and the contractile ratio (which does not always happen in real skeletal muscles). To produce bidirectional movement, both require an antagonistic set-up to be able to control the joints efficiently.
- ***Lightweight and strong***: PAMs are extremely lightweight because their components are soft and small. Output force for these actuators is extremely high, up to several thousand newtons.

- ***Ready replacement***: Replacement of a damaged PAM is extremely easy and rapid.
- ***Hazard-free use***: Pneumatic actuators use air pressure, resulting in no pollution, and the soft materials are also safer than rigid units. As a result, pneumatic soft actuators are safest for human interaction.

3.5 Types and Classification

There are numerous types of pneumatic soft actuators used in several applications, such as the medical, agricultural and industrial fields, and especially in direct human interaction machines.

3.5.1 McKibben Muscle

McKibben's muscle is hitherto the most commonly used and published. It is a cylindrical braided muscle that has both its inner bladder tube and its sleeve connected at each end, not only to transfer fibre tension but also to serve as a volume limitation. In general, the materials used are silicone and latex rubber for the bladder and nylon fibres for the sleeve. Figure 3.16 illustrates its structure and operation (Ranjan, Upadhyay, Kumar, & Dhyani, 2012).

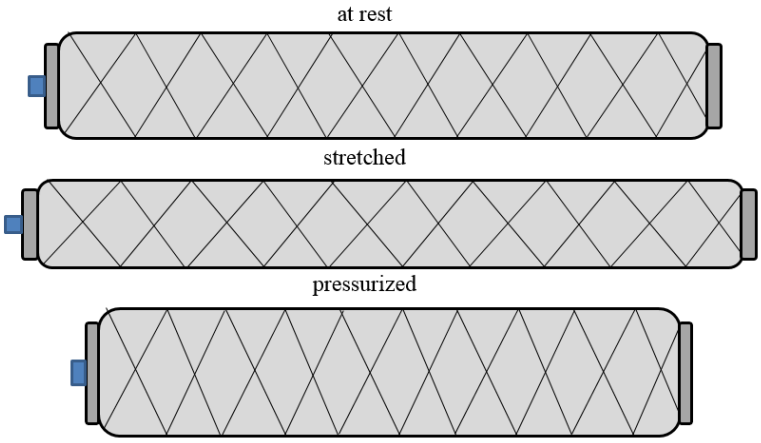

Figure 3.16: McKibben Muscle (Ranjan et al., 2012).

3.5.2 Sleeved Bladder Muscle

The Sleeved Bladder Muscle differs from the McKibben muscle in the design of the inner tube connection; it is not connected with the sleeve at both ends as shown in Figure 3.17 (Beullens, 1989). It is a McKibben-like muscle generally consisting of an inner

tube surrounded by a sleeve directly attached to tendon-like cords; the motion range of a 5–30% contraction ratio depends on the applied pressure and the braid strain angle at rest. The main advantage of this type is that it is extremely easy to construct and to replace the defective bladder.

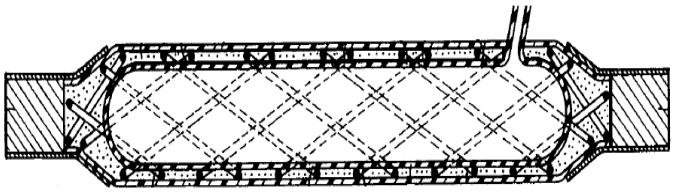

Figure 3.17: Sleeved Bladder Muscle (Beullens, 1989).

3.5.3 Netted Muscles

The netted artificial muscle differs from the braided artificial muscle in the density of the threads in the sleeve surrounding the bladder. The braid in the braided muscles is tightly woven, but in the netted muscle it is a mesh with large holes. As a result, these muscles only need to withstand low pressures. Figure 3.18 shows netted muscle types (Daerden, 1999).

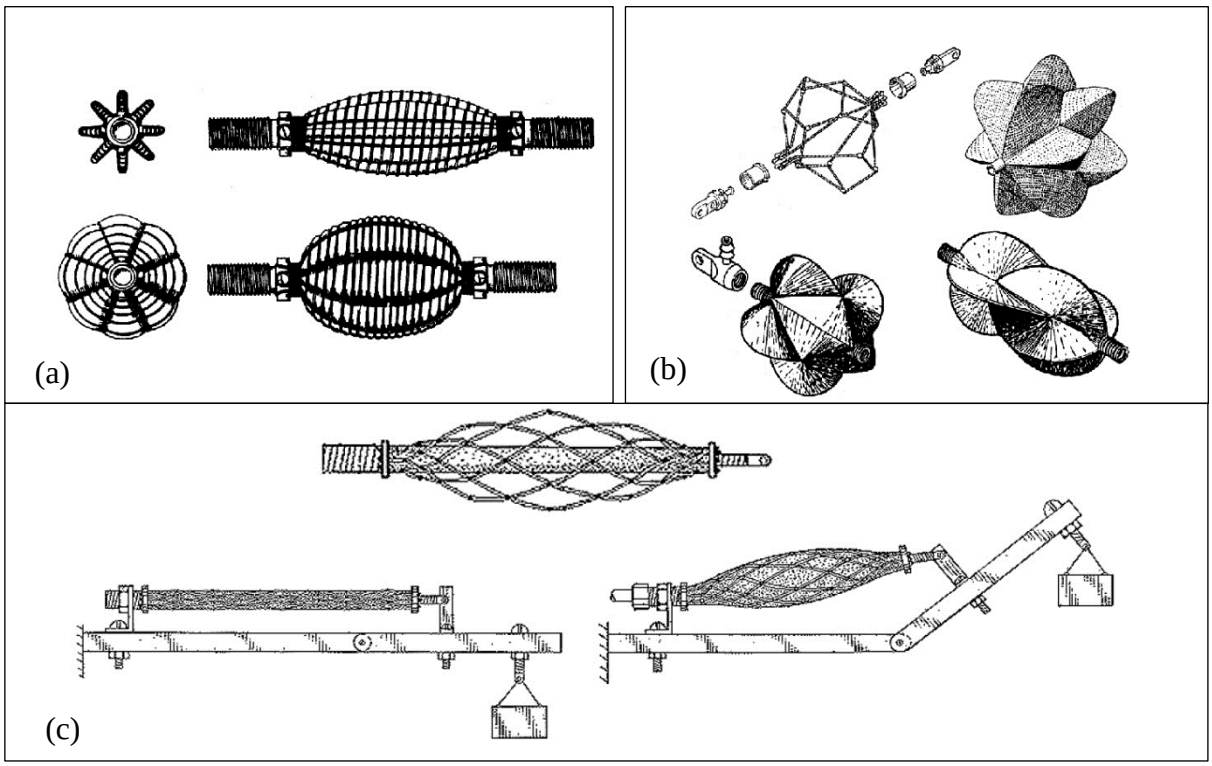

Figure 3.18: Netted muscle types; (a) Yarlott Netted muscles (Yarlott, 1972), (b) ROMAC Netted muscles (Immega, 1986) and (c) Kukolj Netted muscles (Kukolj, 1988).

3.5.4 Pleated PAM

Pleated Pneumatic Artificial Muscle (PPAM) was proposed by Daerden and Lefeber (2001). This type of muscle does not contain a separate inner tube and sleeve bladder but consists of only one membrane with a number of pleats in the axial direction. This means there is no strain in the material when pressurised. Figure 3.19 shows the PPAM design. The operation process is frictionless.

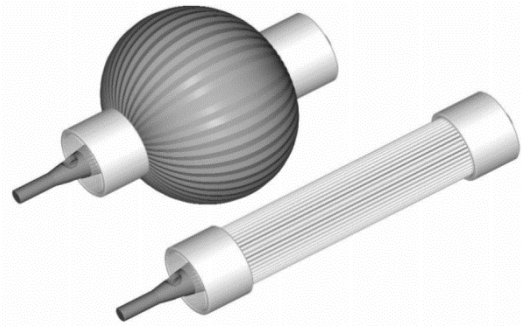

Figure 3.19: Pleated Pneumatic Artificial Muscle (PPAM) (Daerden & Lefeber, 2001).

3.5.5 Parallel Bladders artificial muscles

Davis and Caldwell (2011) proposed a parallel bladders artificial muscle. This type of muscle consists of two or more inner bladders as shown in Figure 3.20. Each bladder can be pressurised separately because each one is connected to a different valve, with all bladders aligned parallel surrounded by one braided sleeve. When only one bladder is pressurised, the muscle bends in relation to the applied pressure and the bending direction will be on the same side of the pressurised bladder.

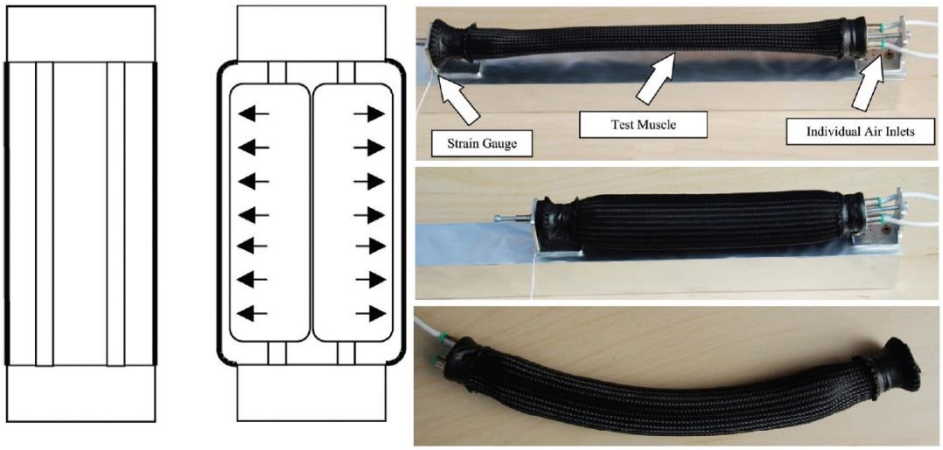

Figure 3.20: Parallel Bladders artificial muscle (Davis & Caldwell, 2011).

3.5.6 Concentric Bladders artificial muscles

This type of artificial muscle is one of the parallel bladders muscles (Davis & Caldwell, 2011). It arranges the bladder tubes one inside the other, as shown in Figure 3.21, and each bladder can be pressurised separately because each one is connected to a different valve. The muscle behaves like a normal PAM when the outer bladder is pressurised; when the inner bladder is pressurised, it also shows ordinary behaviour, but with a slower response and lower output force because of the contrary force from the outer bladder. The major advantage of this type is having a backup bladder when one is defective.

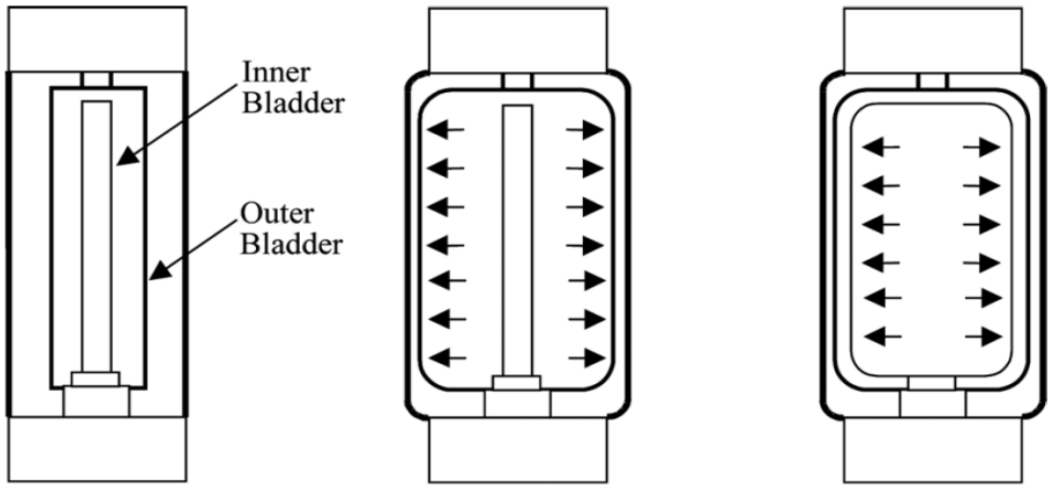

Figure 3.21: Concentric Bladders artificial muscle (Davis & Caldwell, 2011).

3.6 Modelling

Recently, there has been a considerable amount of research into the mathematical modelling of PAMs. The purpose of modelling approaches is to create a mathematical relationship between the length of the PAM and the amount of pressure inside it, and the applied force along its entire axis. These mathematical models depend on variable parameters, such as applied pressure, pulling force, length and the diameter of PAMs, as well as the properties of materials used. All these variables play a considerable role in the dynamic behaviour of the soft actuators. There is strong evidence of non-linear behaviour of PAMs; thus, the major challenge is to build a robust control for this (D. G. Caldwell, Medrano-Cerda, & Goodwin, 1995; Daerden & Lefeber, 2001). A classification of the most common and valuable mathematical models was made by (Kelasidi, Andrikopoulos, Nikolakopoulos, & Manesis, 2012).

3.6.1 Geometrical Model of PMA

The basic mathematical modelling approach was based on the geometric characteristics of PAMs. The models of Chou and Hannaford (1996) and Tondu and Lopez (Tondu & Lopez, 2000) have been widely used. Chou and Hannaford's model was based on static features of the soft actuator; they assumed that the muscle is cylindrical in shape, ignored the extensibility of the threads in the sleeve, ignored the friction force between the sleeve and the bladder and between the threads of the sleeve, and ignored rubber bladder forces. Their model depends on the geometry parameters of the actuator, such as the length *L* of the actuator, the length of the strands used to form the braid *b*, the number of times the strand circles the muscle *n*, and the angle between braided threads and the cylinder long axis θ and the force model in the following equation:

$$F = \frac{\pi D_0^2 P}{4}(3\cos^2\theta - 1) \tag{3.1}$$

Where $D_0 = b/n\pi$, is the muscle diameter when θ equals 90^o and P is the relative pressure. The tension is thus linearly proportional to the pressure, and is a monotonic function of the braid angle ($0^o < \theta < 90^o$). The maximal shortening will be reached when $F = 0$, that is, $\theta = 54.7^o$.

Chou and Hannaford improved their model by adding a new parameter representing the sleeve and bladder thickness to reduce the error, but the error between the mathematical model and the experimental results was still 15-20%. According to Paynter (Paynter, 1996), a stretch in the actuator braided material is caused as a result of increasing muscle volume when input pressure is applied on a fixed muscle length.

Davis et al. (Davis et al., 2003) proved Paynter's theory through practical experiments; the results of these experiments showed around a 5% increase in the length of the thread across the test range, and this increase depended on the applied pressure and the muscle length. The extension of the braid must be calculated to derive a valid mathematical model. Based on Doumit, Fahim, and Munro (Doumit, Fahim, & Munro, 2009), more realistic geometric measurements have been added to Chou and Hannaford's models. Chou and Hannaford assumed that the PAM is perfectly cylindrical, but actually, there is a deformation at both ends of the muscle. Doumit et al. (Doumit et al., 2009) assumed the deformation to be conical in shape at both ends and the middle part a cylinder.

3.6.2 PAMs' Phenomenological Model

The axial output force of a PAM depends on the contraction ratio. Serres, Reynolds, Phillips, Rogers, and Repperger (2010) suggested that this behaviour is similar to a combination of a spring, a damper and contractile elements placed together in parallel, as shown in Figure 3.22.

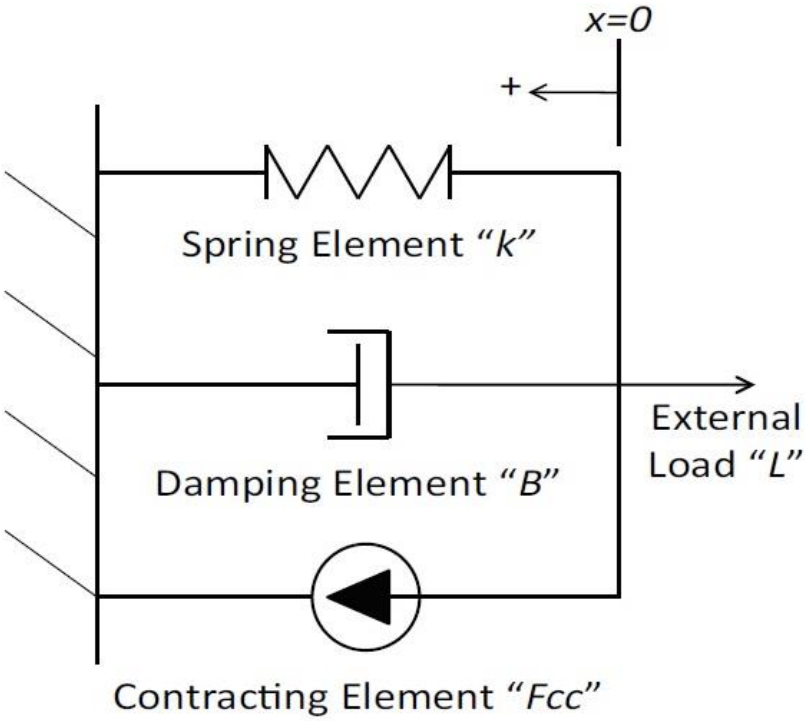

Figure 3.22: Phenomenological Model (Serres et al., 2010).

These elements each had a mathematical model and then they derived a new phenomenological PAM model based on these models. Experiment verification was conducted and this model worked efficiently with an acceptable amount of error between the mathematical model and the experimental results.

3.6.3 Curved PMA Model

There are numerous mathematical models for ordinary linear PAMs but there are no models for bending muscles. However, Zhang, Yang, Chen, Zhang, and Dong (2008) proposed two approximate models based on physics: the membrane and beam models for pneumatic muscles operating when curved around an object. These two models were used to control the joint torque of a wearable elbow exoskeleton.

3.6.4 Empirical Model of PMA

There is a functional similarity between a PAM and a mechanical spring because both produce a tensile force when attached to a load. For the spring, force is produced by the material used to create it and for a PAM, the force is a function of applied pressure (see Figure 3.23). Based on this idea, Wickramatunge and Leephakpreeda (Wickramatunge & Leephakpreeda, 2010) proposed a PAM model based on adding a new parameter to the mechanical spring model; this parameter is the gauge pressure inside the artificial muscle.

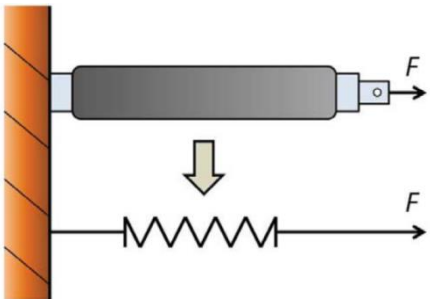

Figure 3.23: Similarity between a PAM and a mechanical spring (Wickramatunge & Leephakpreeda, 2010).

3.7 Control

There is a wide range of control strategies to control various actuators; Figure 3.24 illustrates a control strategies diagram based on the actuators' behaviour (linear or nonlinear) (Jouppila, 2014).

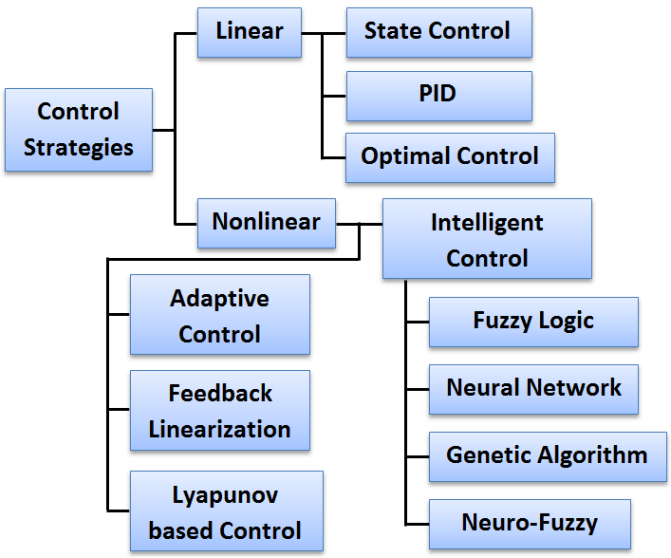

Figure 3.24: Control strategies diagram (Jouppila, 2014).

As a rule, the majority of natural physical devices are nonlinear. Nevertheless, if the range of the control operation system is limited, and if the nonlinearity of these systems is smooth, then the controller of these devices may be a set of linear controllers which serve the purpose and produce acceptable results.

The numerous advantages of PAMs push the researchers to do research into the control area of PAMs, the nonlinearity of these actuators is the major challenge in modelling and controlling them. Numerous control methods have been developed to solve this problem. D. Caldwell et al. (1993) proposed a PID controller (traditional type) with feed-forward terms to control a multi-jointed manipulator for robot fingers. After two years, the same researchers developed their work into an adaptive controller to control the elbow of a robot arm (D. G. Caldwell et al., 1995).

An efficient solution to control the nonlinear PAMs is to combine a linear controller approach with higher level controller approaches, such as fuzzy, adaptive, neural network, genetic algorithms, and so on. Nouri, Gauvert, Tondu, and Lopez (1994) proposed a generalised variable structure model reference adaptive control to control an artificial muscle actuator, and Hesselroth, Sarkar, Van Der Smagt, and Schulten (1994) also used a traditional PID with a neural network to develop a soft robot arm controller.

A Fuzzy PD+I controller was proposed by Chan, Lilly, Repperger, and Berlin (2003) to track a mass position attached to the PAM terminal. A nonlinear PID controller was used with a neural network to create an efficient controller for a two axes PAM manipulator (Thanh & Ahn, 2006). A sliding mode control based on the proxy to control a 2-DOF planar manipulator-based PPAM was developed by Van Damme et al. (2007). This method is an extension of a sliding mode and PID controller to provide more safety for human interaction with their planar manipulator. Zhu, Tao, Yao, and Cao (2008) presented an adaptive robust posture controller to manipulate the problem of controlling a parallel manipulator driven by pneumatic muscles (PMDPM). Shen (2010) presented a nonlinear model-based method of control of PAM servo devices. This technique proposed a controller method for servo systems-based PAMs to deal with the four major processes in these devices: the flow, pressure, force, and load dynamics. Based on these processes, a fully nonlinear model and efficient controller were created. A position control approach based on a sliding mode controller relay type for a robot arm manufactured by soft

pneumatic actuators was developed by (József Sárosi & Gyeviki, 2009; J Sárosi, Gyeviki, Véha, & Toman, 2009).

An adaptive controller based on a fast hybrid fuzzy technique was proposed by Hosovsky, Novak-Marcincin, Pitel, Borzikova, and Zidek (2012) as a nonlinear controller for PAM and the adaptive control was created by using genetic algorithms. Nuchkrua and Leephakpreeda (2013) presented a real time conventional self-tuning PID by using fuzzy logic to create an efficient non-linear controller for PAMs. A tracking controller for PAM was presented by Qian, Huang, and Ri (2015b), who used a combination between a conventional sliding mode control method and a fuzzy control to create a robust adaptive controller.

Finally, a fuzzy-PID self-tuning controller was also used by Sun, Yan, Han, Song, and Zhang (2016) to control a damping seat based on PAMs, used in a crawler construction vehicle. Many controller methods have been developed in this area (soft pneumatic actuators) in many industrial and medical applications because this is an interesting field for researchers to create safer robots and machines for direct human interaction.

3.8 PAMs Applications

During the last fifteen years there has been a noteworthy increase in PAMs applications, such as biorobotic, medical, industrial, and aerospace applications, because the PAMs have a wide range of advantages.

The similarity of the PAMs with organic muscles inspires researchers to use them in manufacturing robots like animals or humans. A pleated pneumatic artificial muscle has been used to construct a biped walking robot named Lucy. This robot has 6 degrees of freedom (DOFs) with two legs, manufactured using a combination of rigid and soft units as shown in Figure 3.25 (a) (Verrelst et al., 2005). Scarfe and Lindsay (2006) presented a humanoid robot hand based on PAMs; this hand has 10 DOFs for the elbow, wrist and finger joints, and is also capable of some real human hand functions, such as gripping and pinching movements (see Figure 3.25 (b)). Mowgli is a bipedal jumping and landing robot presented by (Niiyama, Nagakubo, & Kuniyoshi, 2007). This robot has six PAMs with some rigid parts to do the jumping and landing functions using only two legs, as shown in Figure 3.25 (c). Zwei-Arm-Roboter (ZAR5) is also a soft humanoid robot constructed by Boblan and Schulz (2010). ZAR5 is a fully soft actuated human-like robot with two five

finger hands, as shown in Figure 3.25 (d). Shin, Yeh, and Khatib (2014) designed a safe human interaction robot actuated by PAMs and a magnetic particle brake. This robot has a human-like body with two four finger hands, as shown in Figure 3.25 (e). An ambidextrous robot hand was presented by Mukhtar, Akyurek, Kalganova, and Lesne (2015). This was a five-finger hand actuated by contracted PAMs with most human hand functions (see Figure 3.25 (f)). Finally, Sun et al. (2016) presented a damping seat based on PAMs and used it in a crawler construction vehicle to protect the driver from violent vibration and shock.

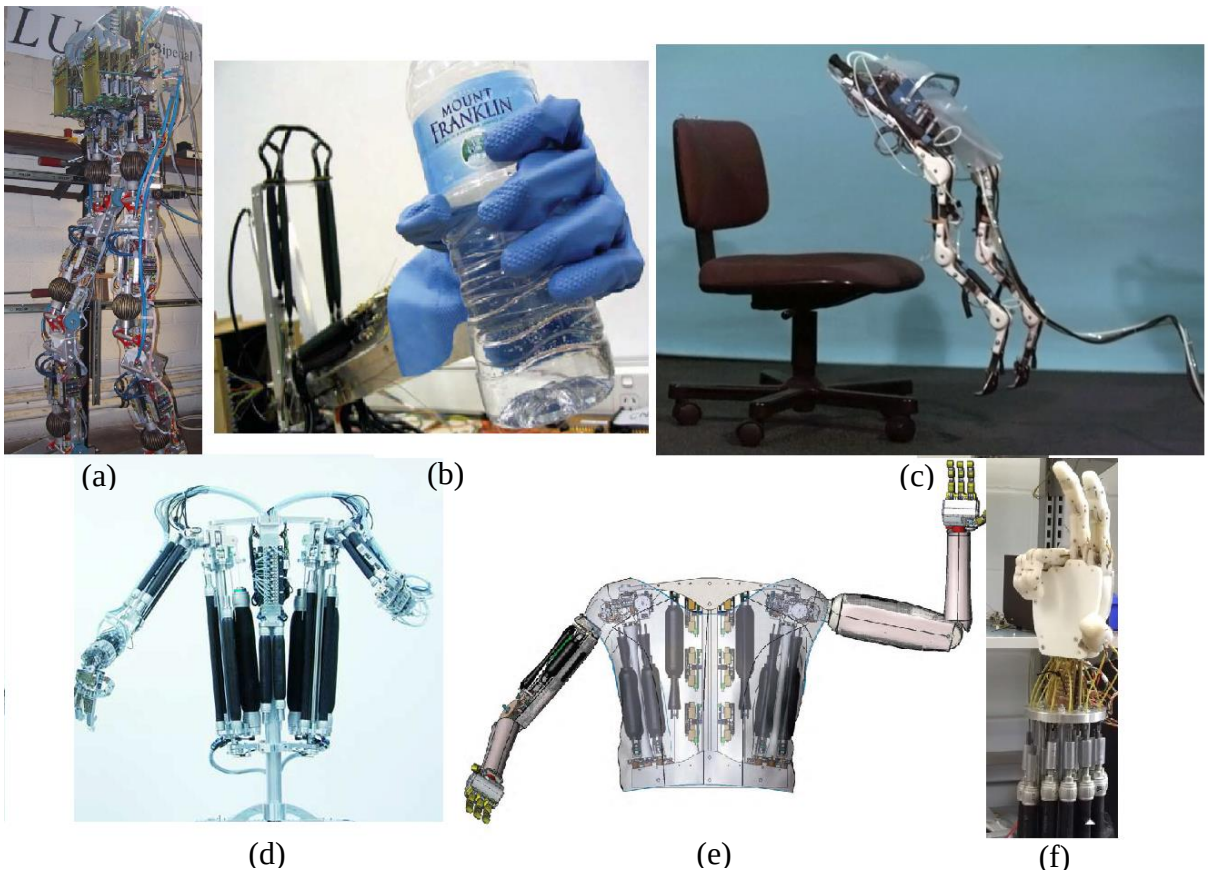

(a) (b) (c)

(d) (e) (f)

Figure 3.25: PAMs Applications: (a) Lucy (Verrelst et al., 2005), (b) a humanoid robot hand (Scarfe & Lindsay, 2006), (c) Mowgli (Niiyama et al., 2007), (d) ZAR5 (Boblan & Schulz, 2010), (e) human interaction robot (Shin et al., 2014) and (f) ambidextrous robot hand (Mukhtar et al., 2015).

3.9 Conclusion

The major inspiration for researchers to invent and use PAMs is the huge similarity between them and organic muscles. The most common PAMs design is based on McKibben's muscles. PAMs have been widely used in manufacturing as a new robot generation named ‘soft robots’. Furthermore, because the PAMs are constructed from soft

materials, they have the capability of providing much safer systems when compared to traditional rigid robots with direct human interaction. It is obvious from our literature review that there are numerous modelling types for PAMs. However, there is currently no 100% accurate mathematical model for these actuators due to their highly nonlinear behaviour and the materials they are constructed from: latex or rubber also show high hysteresis behaviour. Most previous models have been done on the contraction PAMs type and there is a lack of extensor PAMs models and bending muscles. The majority of soft continuum robots are based on contraction muscles only, ignoring other muscle behaviour types, such as extensor PAMs models and bending muscles.

On the other hand, many control methods have been used to create an efficient controller for these soft actuators, but because there are no accurate mathematical models, there are serious problems with the controllers of PAMs.

Numerous applications have been done on PAMs because of their wide range of points of interest. These applications have increased in the last decade, covering many fields, such as biorobotic, medical, industrial, and aerospace applications.

Chapter 4

The Design and Mathematical Model of a Novel Variable Stiffness Extensor-Contractor Pneumatic Artificial Muscle (ECPAM)

4.1 Introduction

Soft robotics typically have high numbers of degrees of freedom and are able to flex and bend at multiple locations rather than at discrete fixed joint locations as is the case for a traditional robot. This means soft robots can deform when they are in contact with an object, distributing contact stresses over a greater area. This combined with the fact that many soft robots are constructed from lightweight materials; means soft robots are potentially safer for human interaction than traditional robots.

Soft robots often use soft and compliant actuators and one of the most well-known soft actuator is the pneumatic artificial muscle (PAM). Pneumatic artificial muscles vary significantly from conventional pneumatic actuators and have seen application in bionic, anthropomorphic and humanoid robots, physiotherapeutic and rehabilitation robots, and also for the mechanisation of industrial processes.

This chapter reports the development of a novel Extensor-Contractor pneumatic artificial muscle. The main contributions of the new actuator are its capability to both contract and extend relative to its resting length with both contraction and extension forces

being generated. The new actuator also allows the muscle's stiffness to be varied at any specific length. The design and construction of this actuator are explained in detail below. A new output force mathematical model for the novel actuator is presented. This mathematical model has been validated experimentally. Stiffness and position control experiments have been performed to validate the main contribution of the new actuator.

4.2 Contraction Pneumatic Artificial Muscles

The new actuator developed in this work uses a combination of both contractor and extensor pneumatic muscles. The behaviour of these two muscle types will be investigated before they are combined into a single actuator.

The contractor muscles used in this research are constructed from a braided nylon sleeve with a maximum unpressurised extended length of 18.4cm and a corresponding resting diameter of 5mm; an inner bladder formed from two layers of latex rubber tube 18.4cm length and 5mm diameter and two 3D printed cap ends, one which is closed and the other with a port through which compressed air can be supplied to the muscle. A contraction muscle decreases in length when the applied pressure is increased until it reaches its minimum energy state, which occurs at a braid interweave angle of 54.7°. Figure 4.1 shows the proposed contracting muscle at different supplied pressures.

The characteristic relation between the supplied air pressure and the actuator contraction (at no load) is illustrated in Figure 4.2. The contraction occurs when increasing the supplied pressure (this experiment is done my increasing the supply pressure in steps of 50 kPa), and this results in the creation of a contractile force. The maximum contraction ratio of the actuator used is approximately 30% at 500kPa pressure. The displacement is decreased from the contraction muscle nominal length (18.4 cm) to approximately 12.8 cm as the pressure raised from 0 to 500kPa. It is clear from the graph, the relationship between the pressure and the displacement is linear between 0 and 250kPa pressures and above this range, the displacement was slightly decreased.

The stiffness of a PAM is proportional to the pneumatic pressure within it. An experiment was performed to calculate the stiffness of the contractor actuator at a range of different applied pressures. Figure 4.3 shows the experimental setup used. The actuator was positioned vertically with the muscle end cap through which air is applied secured to a fixed mounting plate.

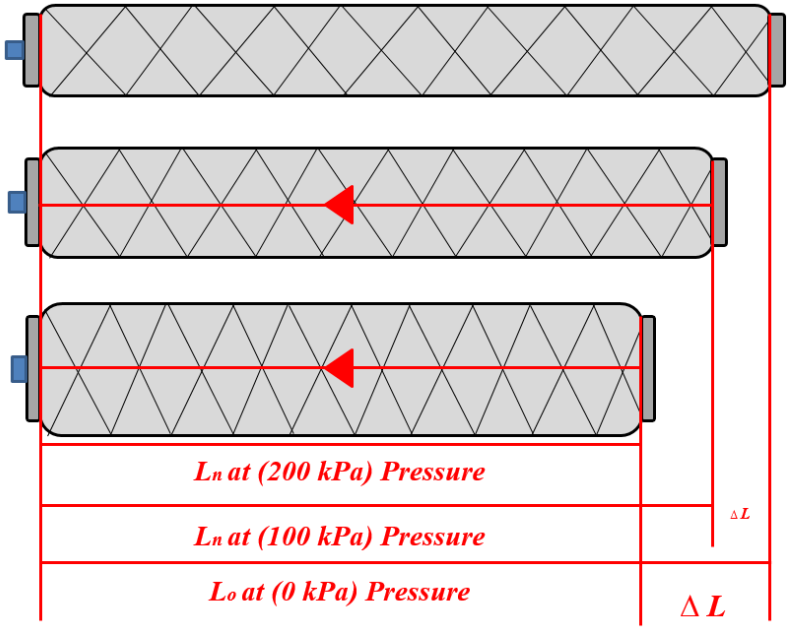

Figure 4.1: The contraction artificial muscle with no-load at different pressures.

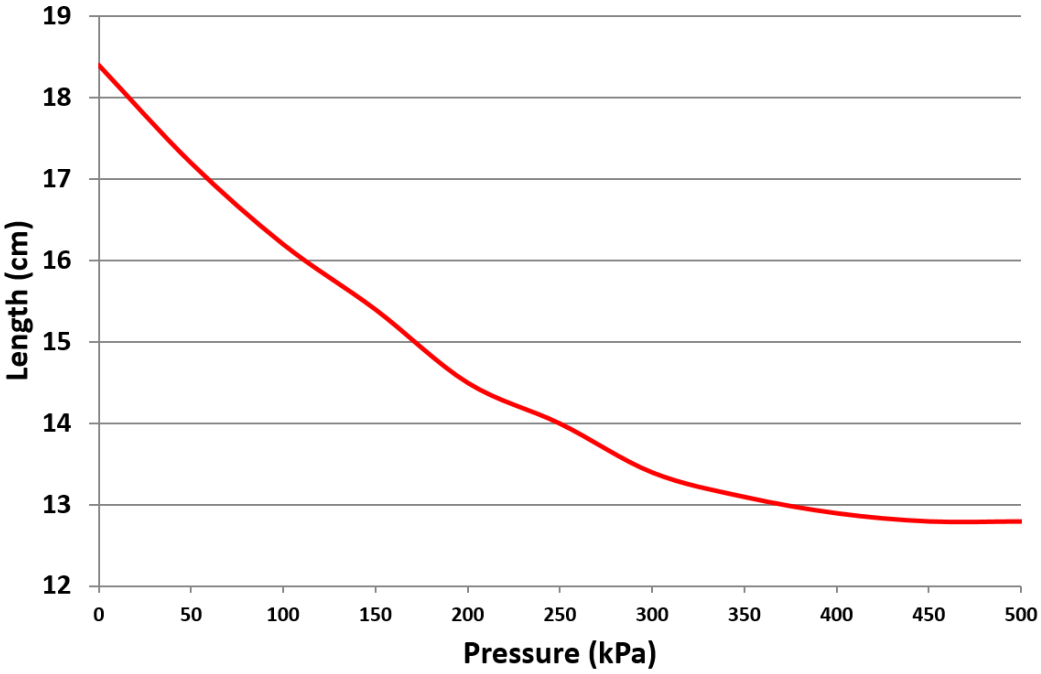

Figure 4.2: No-load displacement characteristic of the contraction muscle with increased applied pressure.

The unloaded muscle was then pressurised and its contracted length was recorded. Increasing loads where then applied to the free end of the muscle and the resulting change in length of the muscle at each load value was recorded. This experiment was repeated four times with four supplied pressures (200kPa, 300kPa, 400kPa and 500kPa). Figure 4.4

demonstrates the results of these four experiments. In each experiment, the muscle was pressurised to 200kPa, loads were attached to the free end of the actuator starting from 100g to 1600g in step of 100g. The force/displacement curves are approximately linear; the stiffness is a rational relation between the force to the displacement. The stiffness of each curve is calculated by the average stiffness of all stiffness points (point for each load) at that specific pressure. Figure 4.5 shows the behaviour of the contraction muscle stiffness as the applied pressure is increased. The stiffness is increased from 1000 N/m to 2600 N/m as pressure raised from 200 kPa to 500 kPa.

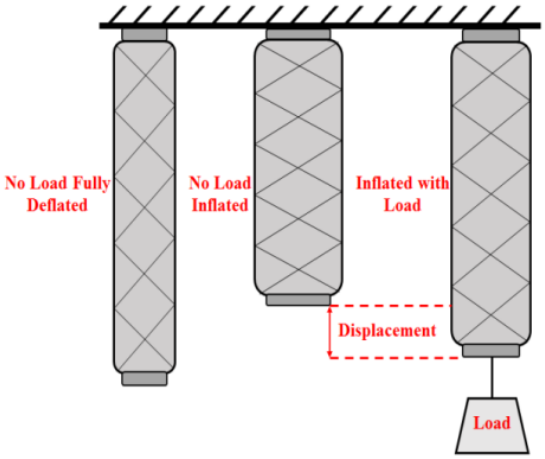

Figure 4.3: Experiment setup to calculate the stiffness of the PAM.

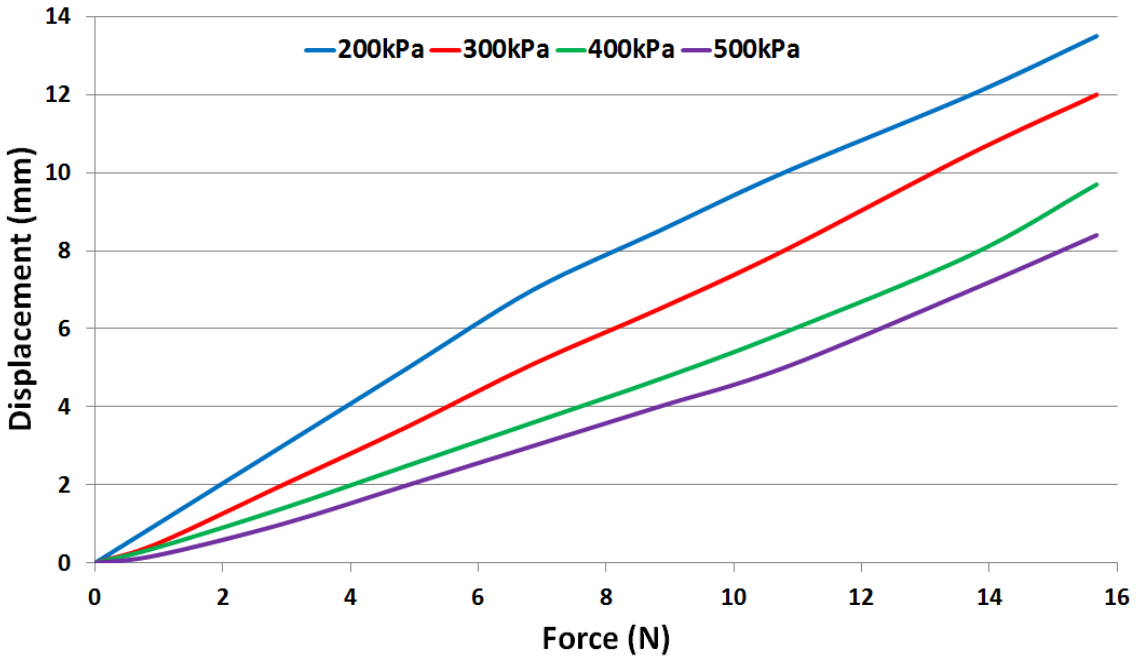

Figure 4.4: The experimental results of the contraction muscle change in length with different attached loads at specific amounts of supplied pressure.

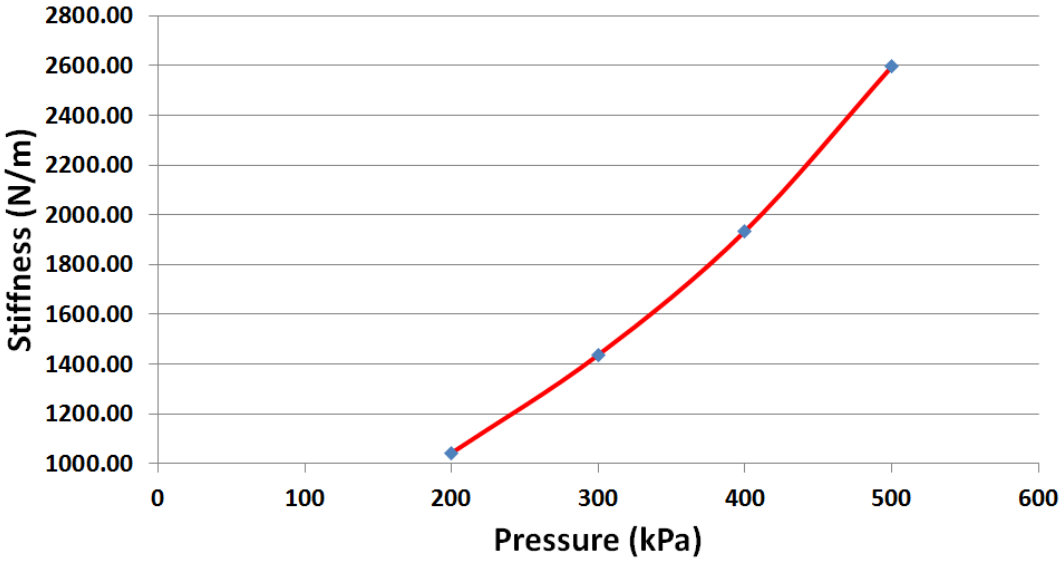

Figure 4.5: The contraction muscle stiffness in relation with increasing the supplied pressure.

4.3 Extensor Pneumatic Artificial Muscles

The extensor artificial muscle used in the development of the new actuator uses the same type of woven braid as for the contractor muscle. However, the resting diameter of the braid was double that of the contractor muscle (10mm) and its length was 32cm. The inner rubber tube of the extensor muscle also had a diameter of 10mm and was half the length of the braided sleeve (16cm). The muscle end caps were the same as those used with the contractor muscles. As the braided sleeve was considerably longer than the length of the rubber tube it needed to be compressed axially to match the length of the bladder. This meant that the muscle had a resting braid interweave angle greater than 54.7° which meant when it was pressurised the muscle would extend in length. Figure 4.6 shows the extensor artificial muscle at a range of different applied pressures and it can clearly be seen that the muscle's length increases as the pressure is raised.

Figure 4.7 shows the relationship between the pressure inside the muscle and muscle length when no load is applied (this experiment is done my increasing the supply pressure in steps of 50 kPa). It can be seen from the graph that the extensor muscle achieves a maximum length of 25.1cm at 500kPa pressure. This represents an extension from its resting, unpressurised, length of 56%. Between the pressures 50 kPa and 250 kPa there is an approximately linear relationship between the pressure and the displacement and above

this pressure range the increasing in pressure dose not lead to significant change in displacement.

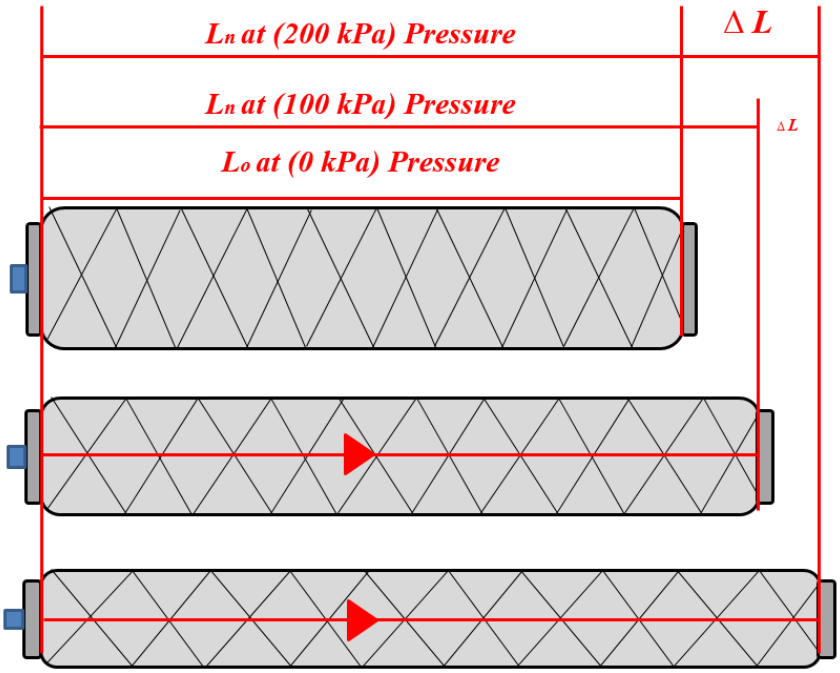

Figure 4.6: The Extensor artificial muscle with no-load at different pressures.

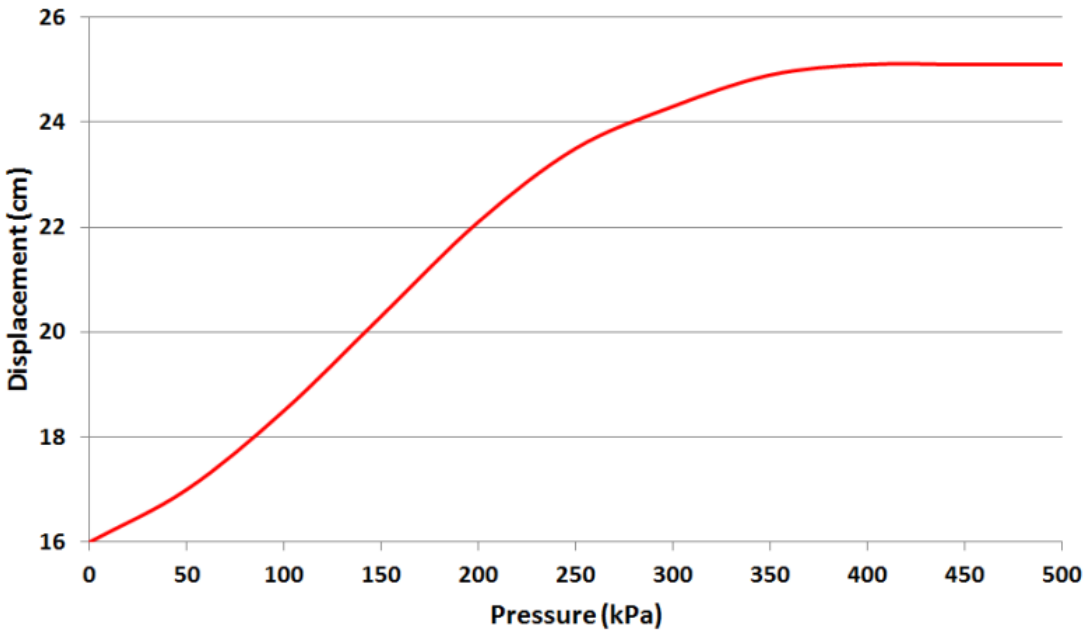

Figure 4.7: No-load displacement characteristic of the extensor muscle with increased applied pressure.

To calculate the stiffness of the extensor muscle, the same experiment used to determine the stiffness of the contraction muscle was performed. This experiment was also

repeated four times with four supplied air pressures (100kPa, 200kPa, 300kPa and 400kPa). Figure 4.8 illustrates the results of these four experiments and again the force displacement curves are approximately linear. Figure 4.9 shows the behaviour of the extensor muscle stiffness when increasing the supplied air pressure.

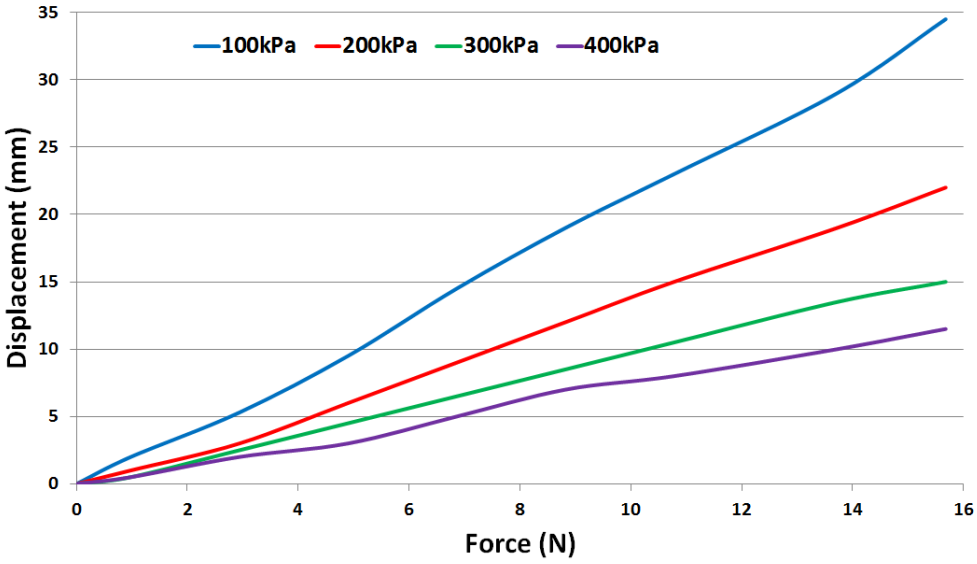

Figure 4.8: The experimental results of the contraction muscle change in length with different attached loads at specific amounts of supplied pressure. The stiffness is increased from 480 N/m to 1460 N/m as pressure raised from 100 kPa to 400 kPa.

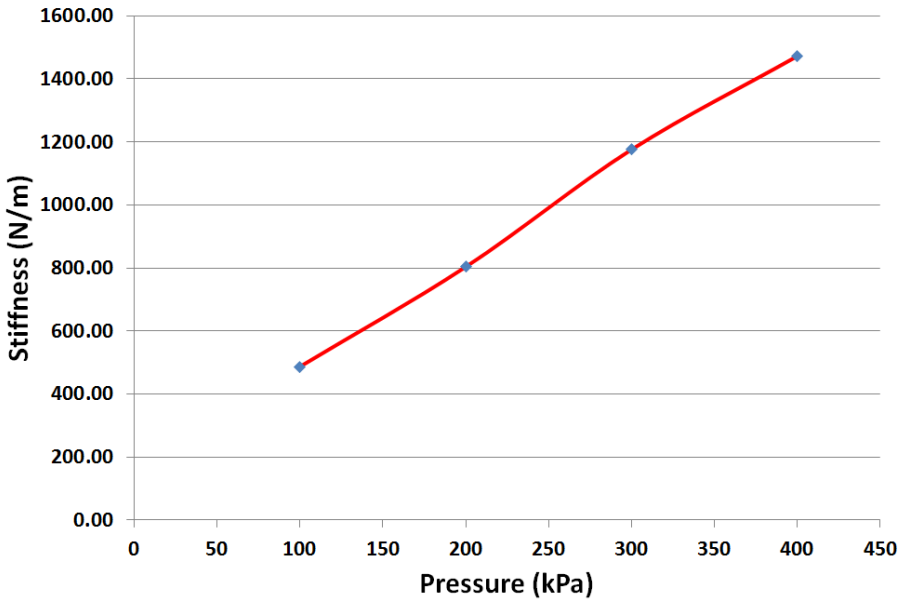

Figure 4.9: The extensor muscle stiffness in relation with increasing the supplied pressure.

It is obvious from the above plots that the contraction muscle has greater stiffness than the extensor. This is not an unexpected finding as although both actuators are

constructed from the same braid and therefore have the same force/pressure profile the extensor muscle is able to displace almost double the distance of the contractor muscle. This means the gradient of a force/displacement plot for the extensor muscle would be considerably shallower than for the contractor muscle.

4.4 Novel Extensor-Contractor Pneumatic Artificial Muscles (ECPAM)

Based on the previous research presented in the literature review and the results presented above there are limitations associated with both the contraction and extensor muscles. These limitations are summarised as follows:

- The contraction muscle only generates a contraction force in response to supplied air pressure.
- The extensor muscle only generates extension force in response to supplied air pressure.
- There is no single PAM capable of performing both contraction (decreasing in length) and extension (increasing in length) with reference to its nominal length.
- There is no single PAM able to produce bidirectional (extension and contraction) force.
- Each muscle type has a fixed stiffness at a specific length and load.
- When muscle pressure is low (e.g. when the force the muscle is generating is small) actuator stiffness will be low as stiffness increases with pressure.

These limitations inspired the design and construction of a novel Extensor-Contractor Pneumatic Artificial Muscles (ECPAM) as described in the following sections.

Several ideas of combining extensor and contractor have been already reported in the previous research such as (Suzumori, Wakimoto, Miyoshi, & Iwata, 2013) and (Giannaccini et al., 2018). These papers describe systems where the actuators are parallel to each other not one inside the other and our system is more compact and takes up less space.

In addition, the force a muscle produces is a function of the surface area of the muscle not the volume. This means that the central volume of the muscle is “dead space”

which must be pressurised but does not contribute to actuator force. Placing the contractor muscle inside the extensor muscle helps to fill this "dead space" meaning that the new actuator will use slightly less air than two muscles positioned side by side.

4.4.1 Design and Construction of the ECPAM

The Extensor-Contractor Pneumatic Artificial Muscle (ECPAM) is formed from a combination of contraction and extensor muscles. The new actuator consists of a contraction muscle placed inside an extensor muscle. The construction of the new actuator began with the creation of two end caps as shown in Figure 4.10 (a), these endcaps form the ends of both the extensor and contractor muscles. The thin central section of the endcaps is for attaching the contraction muscle and one of them has a hole in the centre for the air supply. The larger diameter section of the endcaps is for the outer extensor muscle and again one cap contains a hole in the side as shown in the Figure for the application of air.

As can be seen in Figure 4.10 (b) the contraction muscle is secured to the inner section of the two endcaps using a combination of nylon treads and a resin adhesive and then the muscle is inserted into the rubber bladder of the extensor muscle. The rubber bladder of the extension muscle is 15% shorter than the contraction muscle (this different percentage in length is default for the design of the ECPAM because the new actuator is capable of contacting and extending 15% of its nominal length and this will be clarified in the next sections). The contraction muscle is therefore compressed inside the extensor muscle's bladder so that the bladder can be secured to the second endcap. The extensor muscle's braided sleeve is then compressed and secured to the two endcap using both thread and plastic cable ties, as can be seen in Figure 4.10 (c).

Figure 4.10 (d) shows contraction of the ECPAM caused by pressurising the inner contraction muscle to 300kPa whilst the extensor muscle remains unpressurised. The extension operation of the actuator is illustrated in Figure 4.10(e) where the outer extensor muscle is pressurised to 200kPa whilst the contractor muscle remains unpressurised.

To investigate the relation between the supplied pressure and the muscle length an experiment was performed that involved inflating each muscle (the contractor and the

extensor) independently gradually from zero to 500kPa in steps of 50kPa; the results are shown in Figure 4.11. It is clear from the graph, there is no action in length of ECPAM when pressurise the contraction muscle below 100 kPa because this amount of pressure is actuated only the contraction muscle to contract approximately 15% (from 18.4 to 16 cm) until reach the same length on the ECPAM (16 cm is the ECPAM nominal length, this length has been chosen randomly as a example of the ECPAM construction) and above 100 kPa it will decrease the ECPAM length. In addition, there is no action in extension of ECPAM when pressurise the extensor muscle above 100kPa because the ECPAM was reaches its maximum length (the same contraction muscle length 18.4 cm).

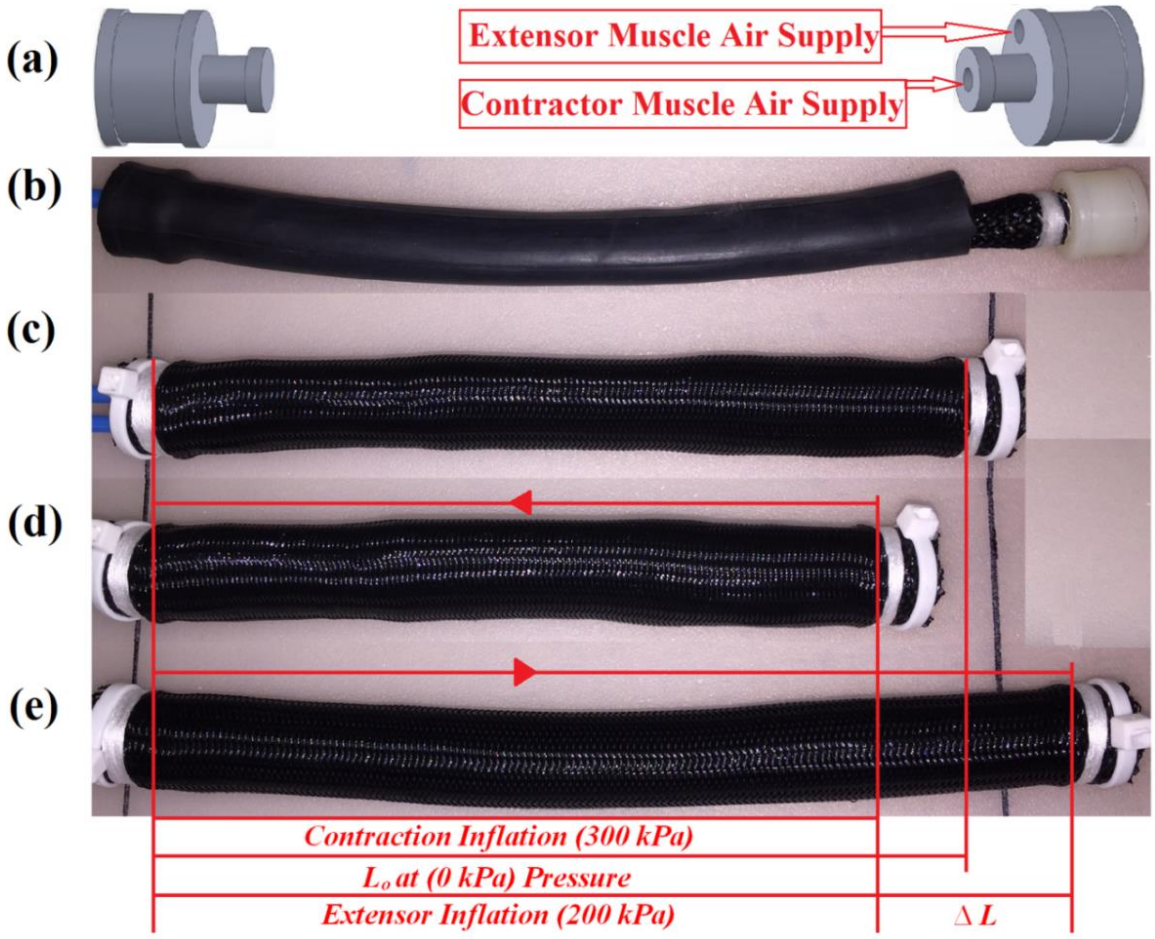

Figure 4.10: Construction and operation of the novel ECPAM; (a) Endcaps design, (b) The contraction muscle inside the extensor muscle bladder, (c) The ECPAM with no pressure, (d) The ECPAM with pressurised only the inner contraction muscle by 300kPa, and (e) The ECPAM with pressurised only the outer extensor muscle by 200kPa.

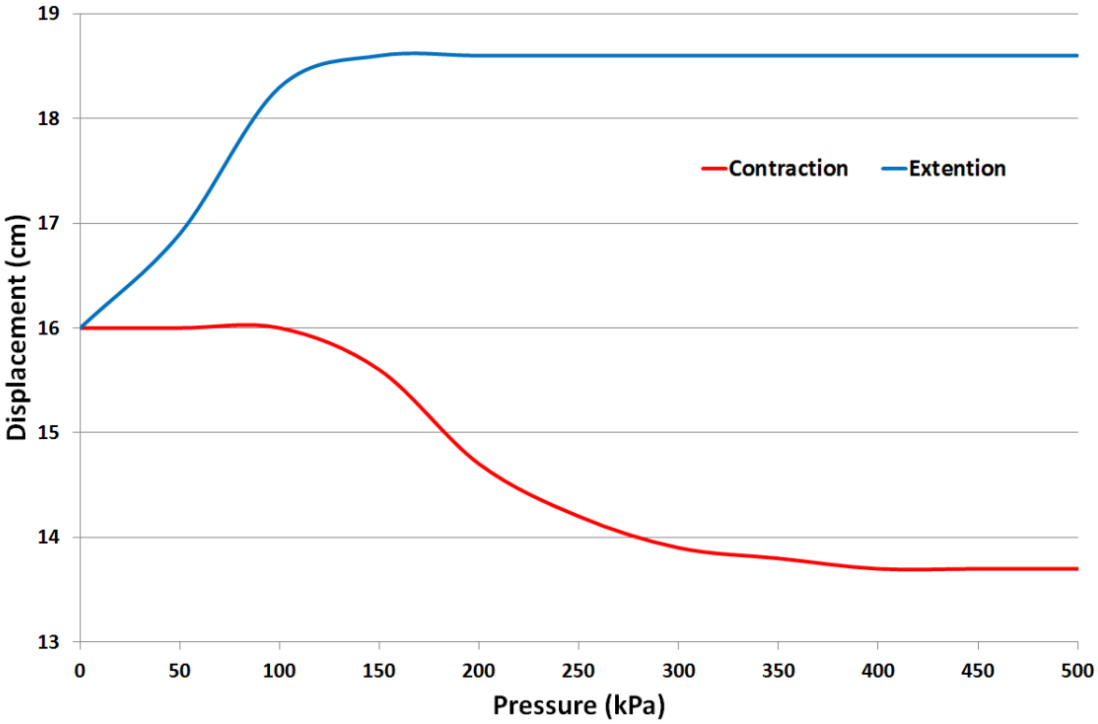

Figure 4.11: The experimental results of the relation between the ECPAM and increasing the supplied pressure for the inner and outer muscles independently.

The resting, unpressurised, length of the extensor muscle was 16cm. However, the contractor muscle was 15% longer than this which meant that when the ECPAM was unpressurised the contractor muscle would be compressed inside the bladder of the extensor muscle to a length of 16cm. As the extensor muscle was pressurised and extended the contractor muscle would become stretched until it reached its maximum length. At this point the contractor muscle would prevent the extensor muscle from being able to extend any further. From it's resting length of 16cm to the point where the contractor muscle prevented any further extension of the ECPAM it extended by approximately 15% to 18.4cm, as can be seen in Figure 4.11.

As was proven previously the contractor muscle is able to contract by approximately 30%. This means that at its minimum length the contractor muscle would be shorter than the resting (unpressurised) length of the extensor muscle and this caused the extensor muscle to become compressed. Pressurising the contractor muscle to its maximum pressure whilst the extensor muscle was unpressurised resulted in the ECPAM contracting from its resting length of 16cm to 13.6cm, a contraction of approximately 15%, as can be seen in Figure 4.11. The overall ECPAM is therefore able to extend and contract from its resting length by approximately 15%.

4.4.2 Kinematics Analysis of ECPAM

Figure 4.12 illustrates the general geometry of PAM, assuming the middle part of the actuator is perfectly cylindrical and the actuator length L, Diameter D and θ represents the braid angle between a single braided thread and the muscle central axis (Chou & Hannaford, 1996). The single thread of the sleeve b encircles the muscle n times.

The extensor actuator differs from the contractor in that the resting length of the sleeve is significantly longer than the length of the rubber tube. In other words, the sleeve must be compressed (θ increased) to reach the same length as the rubber tube.

Based on Figure 4.12 the initial length of the PAM will be:

$$L = b \cos\theta \tag{4.1}$$

And the muscle diameter:

$$D = \frac{b \sin\theta}{n\pi} \tag{4.2}$$

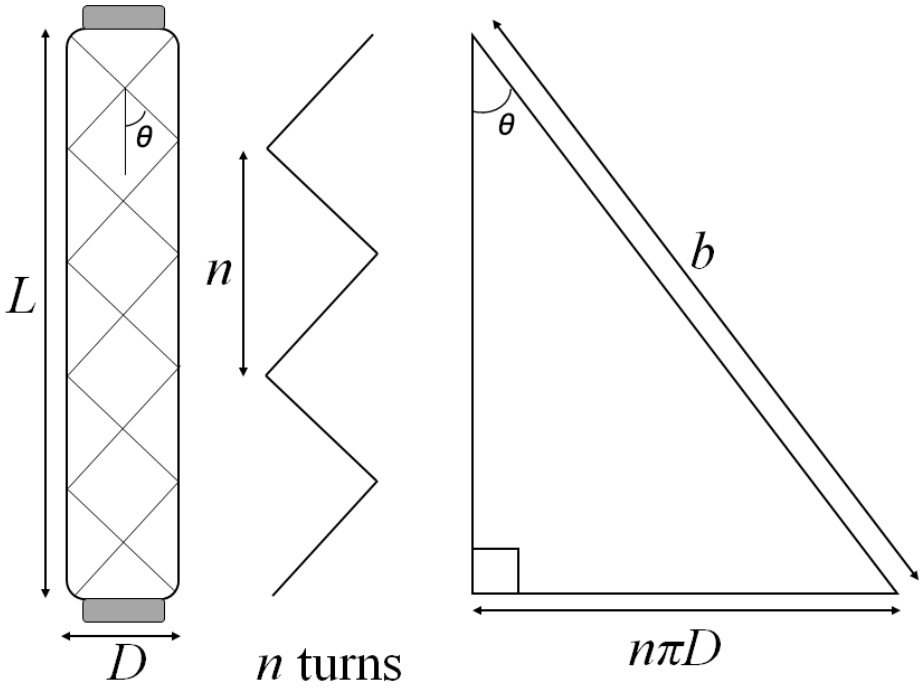

Figure 4.12: The general geometry of PAM.

Assuming the middle segment of the PAM is cylinder then the actuator volume is:

$$V = \frac{\pi D^2 L}{4} \tag{4.3}$$

The analysis of the ECPAM is based on the following assumption: there are no friction forces between the braids and the bladders, or between the nylon threads of the braid, or between the contractor muscle and the bladder of the extensor muscle, and there are no elastic forces within the bladders.

Figure 4.13 illustrates the geometrical kinematic analysis of the ECPAM.

The ECPAM is constructed using the same contraction and extensor muscles (discussed above in sections 4.2 and 4.3). There is a geometrical relationship between these two muscles as follows: the resting sleeve diameter of the contraction muscle is half of the resting sleeve diameter of the extensor (both have the same sleeve type but different braid angles). As mentioned above, the contraction muscle is longer than the extensor muscle by 15% as shown in Figure 4.13 (c). Therefore, at the resting length of the ECPAM the contraction muscle will be bent or compressed inside the extensor muscle to match the extensor muscle's length as shown in Figure 4.13 (d).

$$L_c = 1.15L_e \rightarrow L_e = \frac{1}{1.15} L_c \tag{4.4}$$

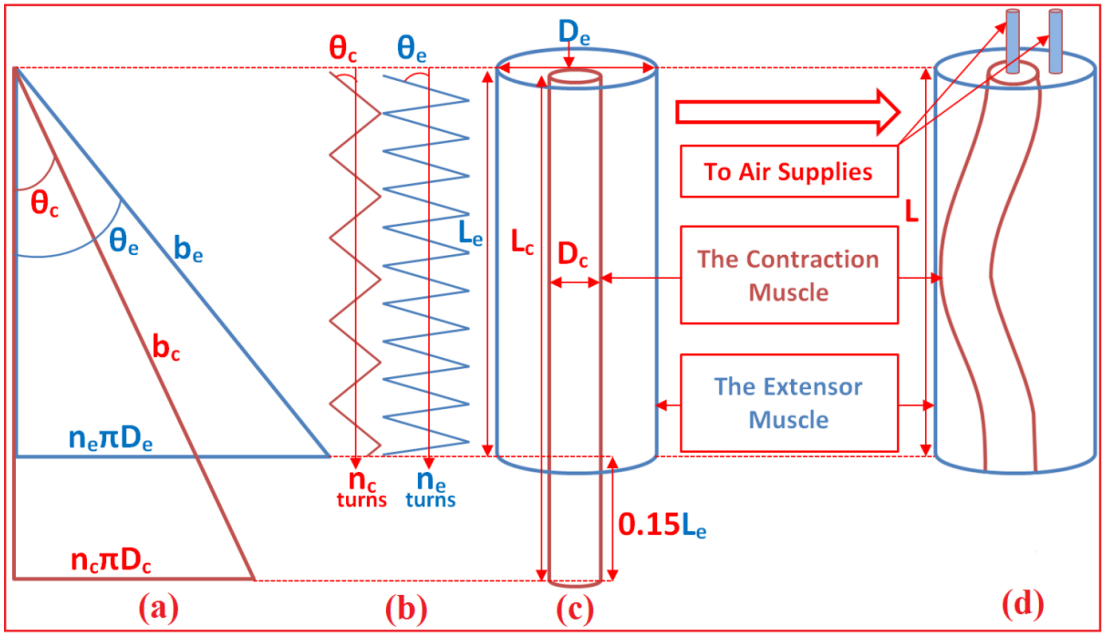

Figure 4.13: Kinematics of the ECPAM; (a) The general geometry of PAM (The contractor and the extensor muscles), (b) The braid angles and the number of turns of both muscles, (c) The lengths relation between the muscles and (c) The ECPAM design.

Where L_c is the contraction muscle length and L_e is extensor muscle length.

The sleeve length of the extensor muscle is double its bladder length (the ECPAM's resting length). Based on the relationship between the sleeve diameters (the contractor muscle's resting sleeve length is half that of the extensor one) and the relationship between the sleeve lengths (normally the length of the extensor muscle sleeve is double that of the contractor muscle; in our case the contractor muscle is longer than the extensor muscle's resting length by 15% as shown in equation 4.4. Normally, if two sleeves of the same type, with the same length, but one having double the diameter of the other are selected then the larger diameter sleeve will have half *n* of the smaller diameter sleeve whilst they have the same *b* length. From this and the sleeves resting diameter:

$$n_c = 1.15 n_e \;\rightarrow\; n_e = \frac{1}{1.15} n_c \tag{4.5}$$

$$2b_c = 1.15 b_e \;\rightarrow\; b_e = \frac{2}{1.15} b_c \tag{4.6}$$

Where n_c is the number of turns of thread in the contractor muscle, n_e is the number of turns of thread in the extensor muscle, b_c is the single thread length of the contraction muscle sleeve and b_e is the single thread length of the extensor muscle sleeve.

Based on Figure 4.13, the contraction and extensor muscles geometrical parameters will be:

$$L_c = b_c \cos\theta_c \tag{4.7}$$

$$L_e = b_e \cos\theta_e \tag{4.8}$$

$$D_c = \frac{b_c \sin\theta_c}{n_c \pi} \tag{4.9}$$

$$D_e = \frac{b_e \sin\theta_e}{n_e \pi} \tag{4.10}$$

$$V_c = \frac{\pi {D_c}^2 L_c}{4} \tag{4.11}$$

$$V_e = \frac{\pi {D_e}^2 L_e}{4} \tag{4.12}$$

Where θ_c is the angle between the braided thread and central actuator axis of the contraction muscle, θ_e is the angle between braid and central actuator axis of the extensor

muscle, D_c is the contraction muscle diameter, D_e is the extensor muscle diameter, V_c is the contraction muscle volume and V_e is the extensor muscle volume.

4.4.3 Modelling the Output Force of the ECPAM

Chou et al. (Chou & Hannaford, 1996) derived the output force mathematical model of the PAM based on its cylindrical shape as follows:

$$F = -P' \frac{dV}{dL} \tag{4.13}$$

Where P' is the relative PAM pressure.

In the case of ECPAM's contraction muscle, the relative pressure in it is affected by the pressure inside the extensor muscle (i.e. a higher pressure in the extensor muscle reduces the relative pressure in the contractor muscle), therefore:

$$P' = (P_c - P_e) \tag{4.14}$$

Where P_c is the pressure of the contraction muscle and P_e is the pressure of the extensor muscle.

Substituting equations (4.7), (4.11) and (4.14) into equation (4.13) gives the contraction muscle force F_c:

$$F_c = -(P_c - P_e) \frac{dV_c}{dL_c} \tag{4.15}$$

Differentiating equation (4.15) with respect to θ_c gives:

$$F_c = \frac{b_c^2 (P_c - P_e)}{4\pi n_c^2} (3\cos^2 \theta_c - 1) \tag{4.16}$$

The extensor muscle is affected by the volume of the contraction muscle only not by the pressure inside the contraction muscle, in effect the contractor muscle represents a hollow cylindrical section along the centre of the extensor muscle. This means the true shape of the extensor muscle is represented by a thick wall cylindrical shell, therefore the cylinder extensor muscle force F_s will be:

$$F_s = P_e \frac{dV_s}{dL_e} = P_e \frac{dV_e - dV_c}{dL_e} = P_e \left(\frac{dV_e}{dL_e} - \frac{dV_c}{dL_e} \right) \tag{4.17}$$

Where V_s is the volume of the cylinder representing the extensor muscle.

By substituting the relation between the contractor and extensor muscles lengths in equation (4.4) into equation (4.17):

$$F_s = P_e\left(\frac{dV_e}{dL_e} - 1.15\frac{dV_c}{dL_c}\right) \tag{4.18}$$

Differentiating equation (4.18) gives:

$$F_s = P_e\left(\frac{{}^{dV_e}/_{d\theta_e}}{{}^{dL_e}/_{d\theta_e}} - 1.15\frac{{}^{dV_c}/_{d\theta_c}}{{}^{dL_c}/_{d\theta_c}}\right) = P_e\left(1.15\frac{b_c^2(3\,cos^2\,\theta_c - 1)}{4\pi n_c^2} - \frac{b_e^2(3\,cos^2\,\theta_e - 1)}{4\pi n_e^2}\right) \tag{4.19}$$

Substituting equations (4.5) and (4.6) into equation (4.19) and simplifying the result gives:

$$F_s = \frac{b_c^2 P_e}{4\pi n_c^2}(1.15(3\,cos^2\,\theta_c - 1) - 4(3\,cos^2\,\theta_e - 1)) \tag{4.20}$$

The ECPAM has two opposite forces: F_c is the contraction force and F_s is the extension force.

$$F = (F_c - F_s)\begin{cases} if\ F\ is\ positive \rightarrow it\ is\ a\ Contraction\ Force \\ if\ F\ is\ negative \rightarrow it\ is\ a\ Extension\ Force \end{cases} \tag{4.21}$$

Substituting equations (4.16) and (4.20) in equation (4.21) and simplifying the result gives the ECPAM total force model *F*:

$$F = \frac{b_c^2}{4\pi n_c^2}(P_c(3\,cos^2\,\theta_c - 1) + 0.15P_e(3\,cos^2\,\theta_c - 1) - P_e(3\,cos^2\,\theta_e - 1)) \tag{4.22}$$

4.4.4 Experimental Verification of the ECPAM Output Force Model

An experimental verification of the ECPAM model has been performed using the experimental setup shown in Figure 4.14. The ECPAM was suspended vertically in a rig with the unpressurised actuator being at its resting length (16cm). The end cap through which air was supplied was secured to a mounting plate and the free end of the actuator was attached via a load cell to a second fixed point. The actuator was surrounded by a rigid cylindrical nylon tube to limit any buckling or lateral deformations of the muscle during extension force testing, as shown in Figure 4.14 (b) and (c). Figure 4.14 (a) illustrates how

the contraction force could be measured using the same rig by reversing the load cell direction and removing the cylinder tube.

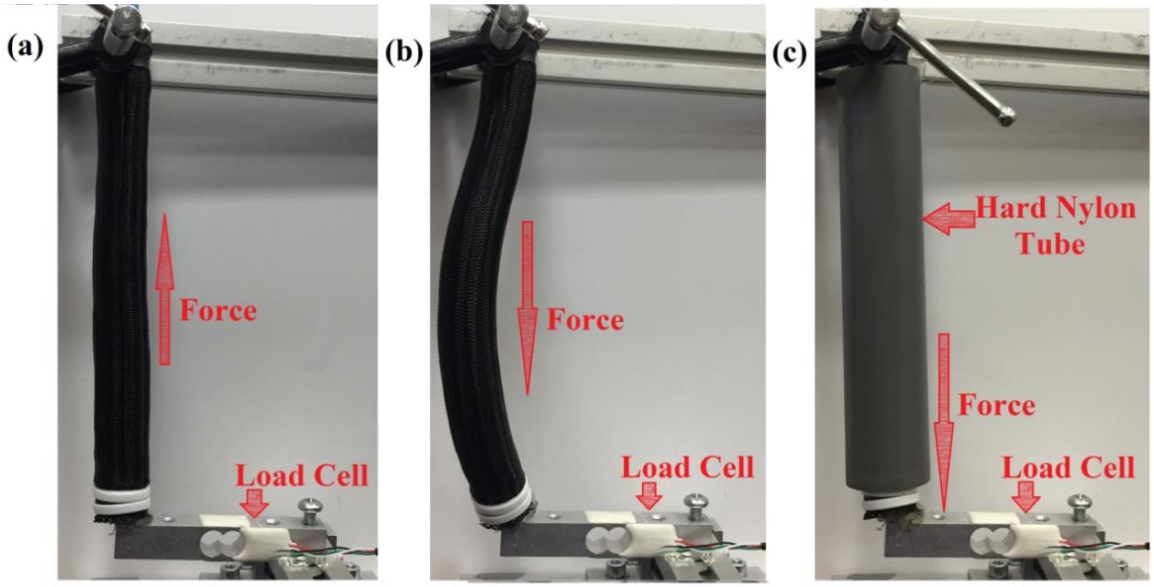

Figure 4.14: Experiment setup to calculate the extension and contraction force of the ECPAM; (a) Calculating the contraction force of the ECPAM, (b) Buckling or lateral deformations of the ECPAM at extension and (c) Calculating the extension force of the ECPAM with a rigid cylindrical nylon tube.

The experiment began by pressurising the extensor muscle to 100kPa (P_e) and recording the extension force measured by the load cell. The pressure in the contraction muscle (P_c) was then gradually increased from zero to 500kPa in 50kPa increments and the contraction force was recorded. The experiment was then repeated twice more with the extensor muscle pressure (P_e) equal to 300kPa and 500kPa. Figure 4.15 shows the experimental results of these three experiments.

The average error percentages between the mathematical model and the experimental results are 20.23%, 20.31% and 21.09% for the three experiments with extensor muscle pressures 100kPa, 300kPa and 500kPa respectively. These errors were expected because the force losses were neglected; for example, we assumed there were no frictional forces between the braids and the bladders or between the nylon threads of the braid or between the contractor muscle and the bladder of the extensor muscle and that there were no elastic forces within the bladders.

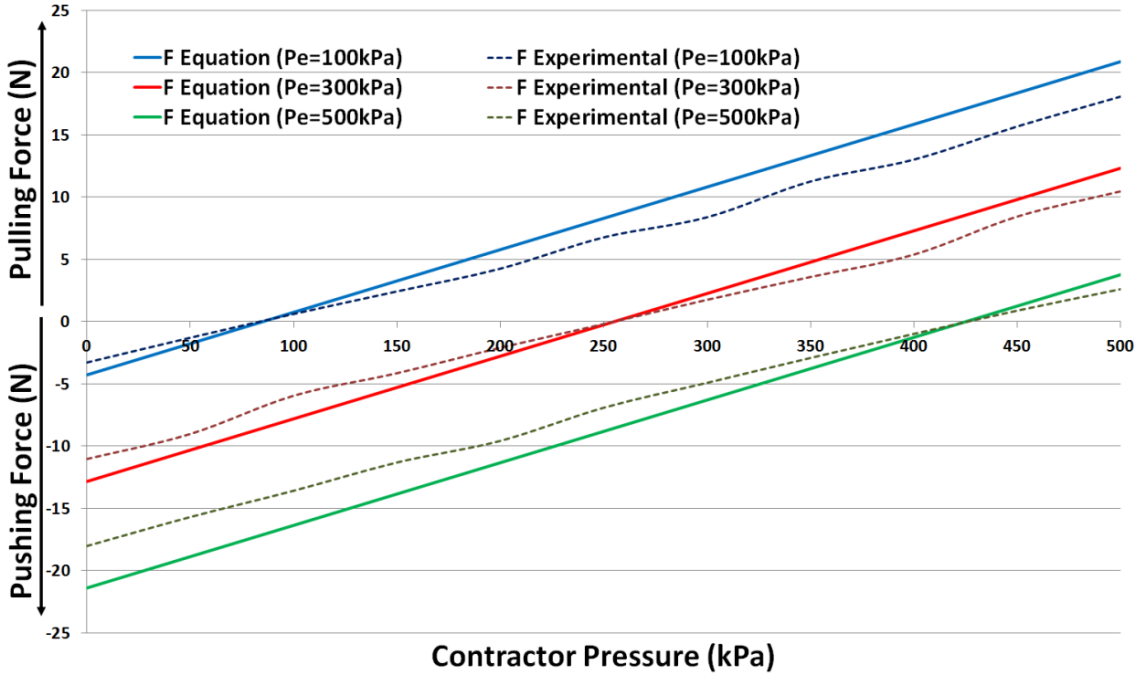

Figure 4.15: The Experimental results of the output force of the ECPAM with its mathematical model (the upper part of the graph shows the contraction forces and the lower part shows the extension forces of the ECPAM).

These losses caused these errors as an approximately fixed percentage (20%) of the total force and this increased in relation with the force. This error percentage has been calculated by the average percentage difference for all force points and each point with pressure step of 50kPa. Based on this a correction factor *C* is introduced to represent these losses and decrease the average error percentage as far as possible. A similar approach has been used by other researchers to account for frictional losses and hysteresis in the past (Giannaccini et al., 2018). The total force equation with the suggested correction factor will be:

$$F_t = F - CF \tag{4.23}$$

This correction factor was calculated experimentally and in this work was assumed to be 20%, derived from the average error percentage between the experimental results and the mathematical model. Figure 4.16 shows the new mathematical force model with consideration of the correction factor and the experimental results.

The average error percentages between the mathematical model, with the correction factor, and the experimental results are 5.32%, 5.91% and 5.14% for the three experiments

with extensor muscle pressures 100kPa, 300kPa and 500kPa respectively. The factor *CF* represents the losses and it is not a constant because it is a percentage of the optimal force *F*, therefore it must be small for low pressures and high for higher pressures in order to decrease the gap between the two curves. Clearly more advanced mathematical models of the actuator performance would reduce the need for the correction factor and more detailed modelling of the new actuator will represent future work.

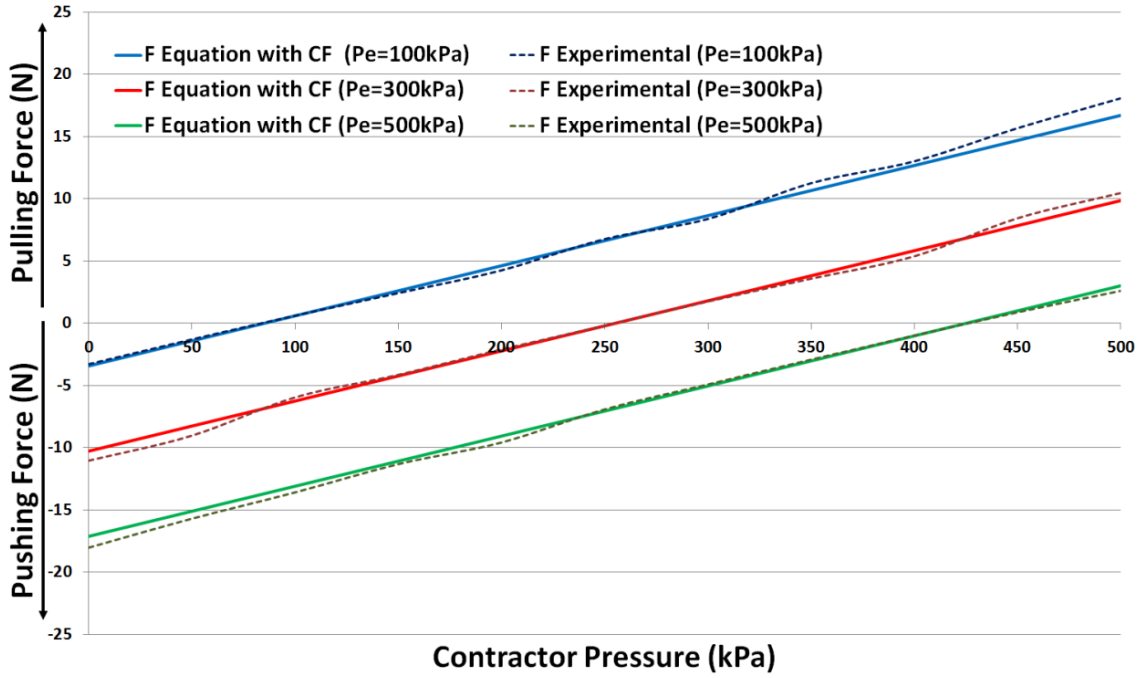

Figure 4.16: The Experimental results of the output force of the ECPAM with its mathematical model with consideration of correction factor (the upper part of the graph shows the contraction forces and the lower part shows the extension forces of the ECPAM).

As can be seen in the experimental procedure buckling of the actuator was a potential problem and a mechanical support was used to prevent it. In the new actuator both the internal contractor muscle and the external extensor can experience buckling. However, in reality buckling of contractor muscle only occurs when it is unpressurised and so has no effect on the force output of the actuator, as soon as the contractor is pressurised it will experience tension and this will force it into an straight, unbuckled configuration. Buckling of the extensor muscle is more of a problem. When the extensor muscle extends it places the contractor muscle inside it under tension, which causes it to behave like an internal tether between the two endcaps. If the extensor muscle buckles it makes contact with the taught contractor muscle which prevents it from extreme buckling, however, some

degree of buckling is still possible. This is a problem common to many types of soft extending pneumatic actuator not just the new actuator described in this chapter. There are various methods that can been used to prevent buckling of extending actuators including the addition of a rigid support structure or soft guides located on the mechanical structure being actuated which prevent buckling. Alternative methods include using the muscle as a bending actuator (i.e. intentionally creating and exploiting buckling) or as part of a continuum manipulator. These methods will be further explored as future chapters on the application of the new actuator.

4.4.5 Stiffness of the ECPAM

At a fixed load and position a traditional pneumatic muscle has a single fixed stiffness value. The reason for this is that the actuator's stiffness is a result of the pressure in the actuator, with higher pressure resulting in greater stiffness. However, pressure is proportional to muscle output force and so increasing the pressure in a muscle which is supporting a fixed load will result in contraction of the muscle and change in position. It is therefore not possible to change a pneumatic muscle's stiffness independently of its force or position. The newly developed ECPAM, however, has the ability to potentially vary its stiffness independently of its position.

Stiffness experiments were conducted to prove and validate that the novel ECPAM's stiffness can be adjusted without resulting in a change of actuator length. The ECPAM was again suspended vertically, but this time with the distal end being free. The actuator was initially at its unpressurised nominal length of 16cm. The contractor muscle was pressurised to 100kPa which resulted in a shortening with reference to the nominal length. The pressure in the extensor muscle was then increased until the actuator extended in length to again reach the nominal length. The extensor pressure required to achieve this was measured to be 75kPa. To calculate the stiffness at this combination of muscle pressures, loads of increasing mass were applied to the free end of the muscle and the axial displacement at each load was measured. It was then possible to determine the stiffness from the gradient of the resultant force/displacement plot Figure 4.17 and this was found to be 4611N/m. To prove that it was possible to achieve a different stiffness value at the same length, the contractor muscle pressure was increased to 150kPa. This again caused the ECPAM to become shorter than the nominal length and so the extensor muscle pressure was again increased until it reached its nominal length (16cm). The extensor pressure

required to achieve this was 100kPa. The stiffness was again found experimentally and calculated to be 5478N/m. The reason the stiffness increased was because both the muscle pressures were higher and as previously stated stiffness is a function of muscle pressure. For further verification that the stiffness could be varied at a fixed length (16cm), the experiment was repeated twice more at the same actuator length but with the pressure in the contractor and extensor muscles being P_c=200kPa/P_e=125kPa and P_c=250kPa/P_e=150kPa respectively. The resulting stiffness values were determined to be 6172N/m and 7788N/m respectively. The experimental results from all four experiments are shown in Figure 4.17 and it can be seen that different stiffness can be achieved at the same actuator length.

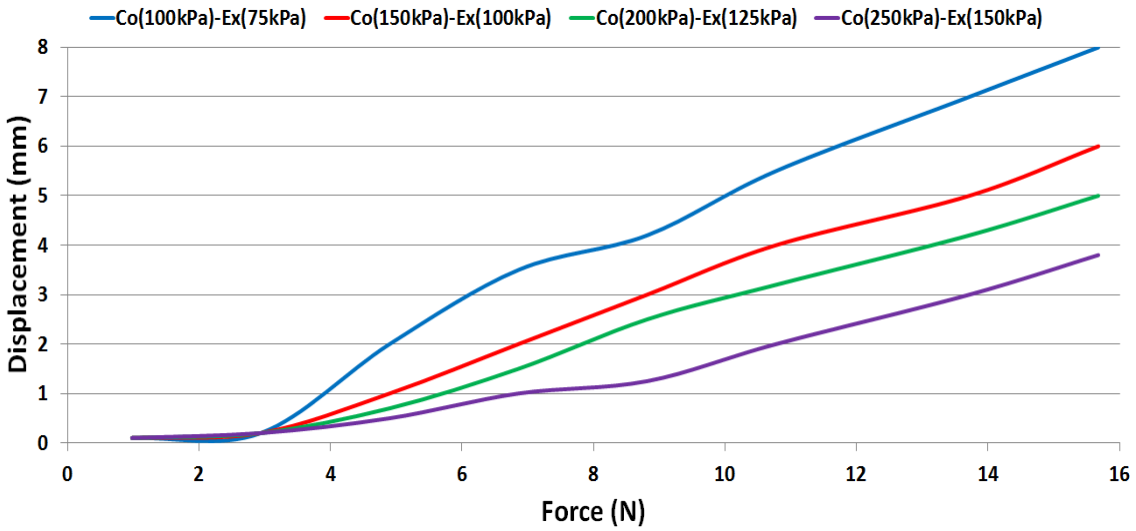

Figure 4.17: Stiffness experimental results for the ECPAM at length 16cm.

For further verification that the stiffness of the ECPAM can be adjusted whilst at a fixed length the same experiment described above was repeated twice more, once with a muscle length shorter than the nominal length (15cm) and once with it longer (17cm). All ECPAM's stiffness results are summarised in Table 4.1.

Unlike a traditional pneumatic muscle, the ECPAM can have the same stiffness at different lengths. In the table above, it can be seen that experiments 2,6 and 12 all have broadly similar stiffness values but in each the muscle length is different. This therefore proves that ECPAM's stiffness can be set independently of position (actuator length).

Table 4.1: A summary of ECPAM's stiffness results.

Experiment No.	Muscle Length	P_c	P_e	Stiffness
1	16cm	100kPa	75kPa	4611N/m
2	16cm	150kPa	100kPa	5478N/m
3	16cm	200kPa	125kPa	6172N/m
4	16cm	250kPa	150kPa	7788N/m
5	15cm	200kPa	60kPa	3550N/m
6	15cm	250kPa	90kPa	5796N/m
7	15cm	300kPa	120kPa	7492N/m
8	15cm	350kPa	150kPa	9961N/m
9	17cm	50kPa	100kPa	1634N/m
10	17cm	100kPa	125kPa	2640N/m
11	17cm	150kPa	150kPa	3077N/m
12	17cm	200kPa	175kPa	5337N/m

4.6 Stiffness and Position (length) Control of the ECPAM

Accurate control of McKibben muscles presents a major challenge, this is because of both the nonlinear behaviour of the muscles and the compressibility of air. Much of the control of pneumatic muscle has relied on classical control techniques and simple models of the actuator functionality that include many assumptions.

Based on the above experimental stiffness results a control system has been created capable of controlling both the length and the stiffness of the novel ECPAM, as shown in Figure 4.18. The first stage of the stiffness and position controller system is a neural network identifier. This stage is utilised to generate the appropriate pressures set-point for the contractor and extensor muscles, based on our stiffness experiments in Table 4.1. This neural network identifier is designed using a Matlab neural network data fitting application (one of the curve fitting techniques based on inputs and its outputs data). The experimental stiffness and lengths data for the ECPAM are used as inputs and the amount of appropriate contractor and extensor pressures are utilised as outputs to design this identifier. This neural network includes one input layer, four two layers and one output layer. A Bayesian Regularisation (Demuth, Beale, De Jess, & Hagan, 2014) training technique is used to train the proposed neural network identifier. It is a network training technique that updates the weight and bias values according to Levenberg-Marquardt optimisation; it minimises a combination of squared errors and weights, and then determines the correct combination so as to produce a network that generalises well.

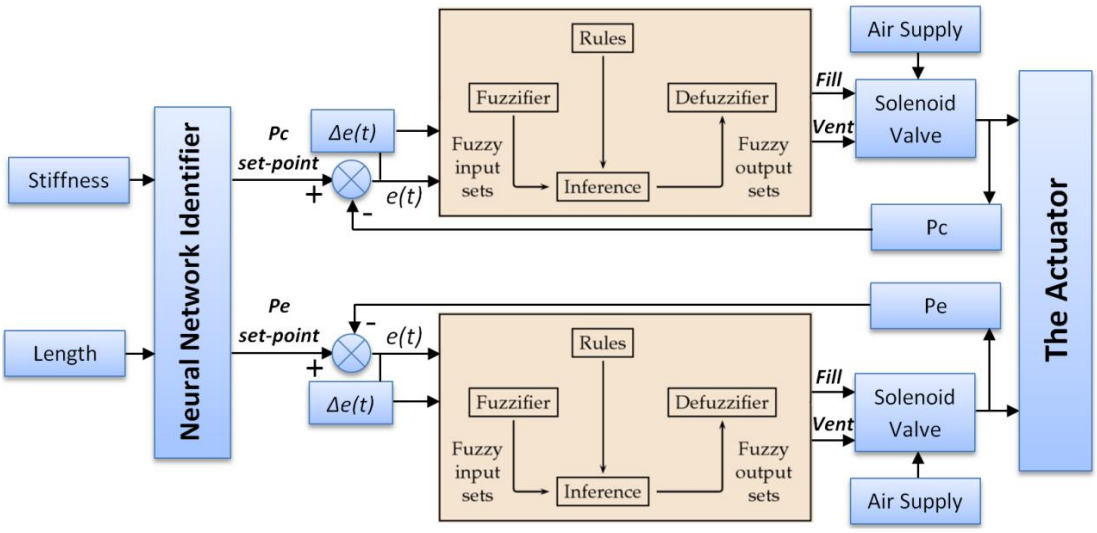

Figure 4.18: The proposed stiffness and position controller of the ECPAM.

Two Fuzzy logic controllers are utilised in the stiffness-position controller system to control the level of pressure inside the contractor and extensor muscles. The appropriate pressure set-points for each contractor and extensor muscle come from the neural network identifier. These two fuzzy controllers are identical. Each one has two inputs (error and change of error) and two outputs (Fill and Vent). MATRIX 3x3 (see Figure 4.19) solenoid valves are used to control the air flow by PWM (Pulse Width Modulation). The advantages of this valve are: (i) compact dimension, (ii) short response time, (iii) insensitivity both to frequency work and to vibrations, (iv) low absorbed power, precision, repetitiveness and (v) flexibility and long operation life. The same valve port can be used as either a fill or vent valve depending on the applied PWM signal. The ECPAM has two valves, one for the contractor muscle and the other for the extensor muscle.

The solenoid valve was controlled by Arduino Mega 2560, because of the Arduino PWM output is only 5V and the valve operate on 24V PWM, a driver circuit to transform 5V PWM to 24V PWM as shown in Figure 4.20.

The feedback pressures are calculated by MDPS002 pressure sensor (700kPa) vacuum absolute pressure sensor. The output of this type of pressure sensor is microvolt, but the Arduino analogue read pins sensitive range is 0-5 v. The INA122 precision instrumentation amplifier for accurate, low noise differential signal acquisition is used to amplify the pressure sensor signal as shown in Figure 4.21.

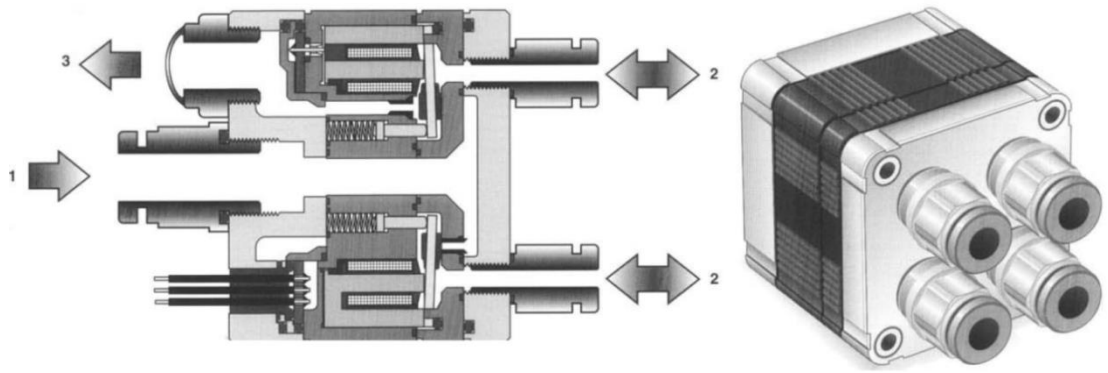

Figure 4.19: MATRIX 3/3 750 series solenoid valve.

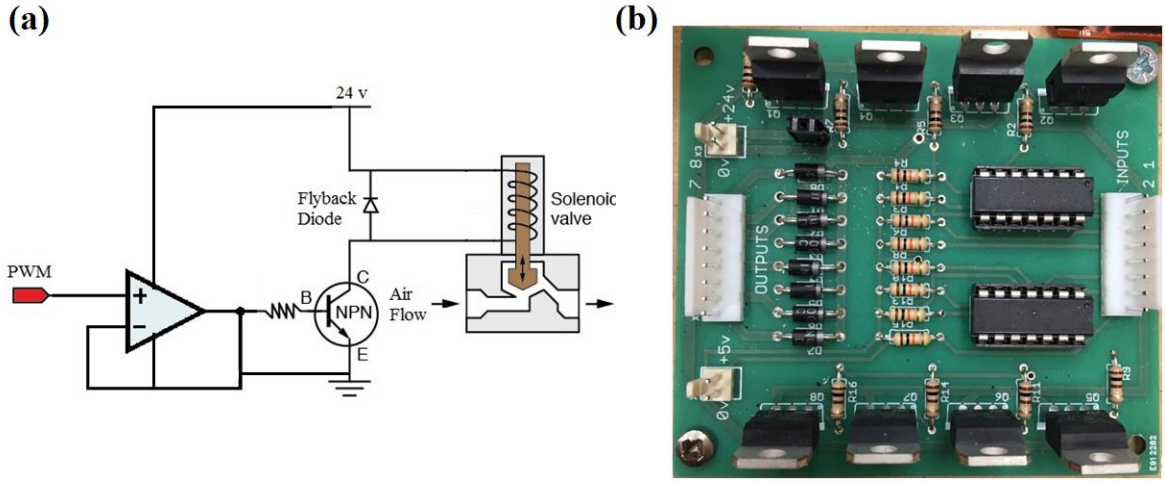

Figure 4.20: The solenoid valve driver circuit; (a) schematic diagram of single driver circuit and (b) 8-channals driver circuit.

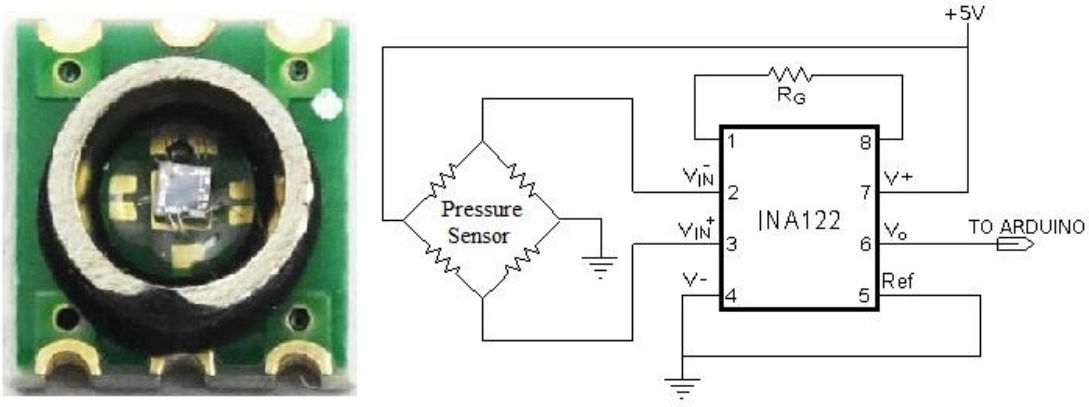

Figure 4.21: The pressure sensor circuit.

Based on this, each Fuzzy controller has two outputs to control the percentage of the PWM duty cycle for each filling and venting valve. The valve PWM frequency is

125Hz. Figure 4.22 shows the membership functions of the inputs and outputs of both Fuzzy controllers.

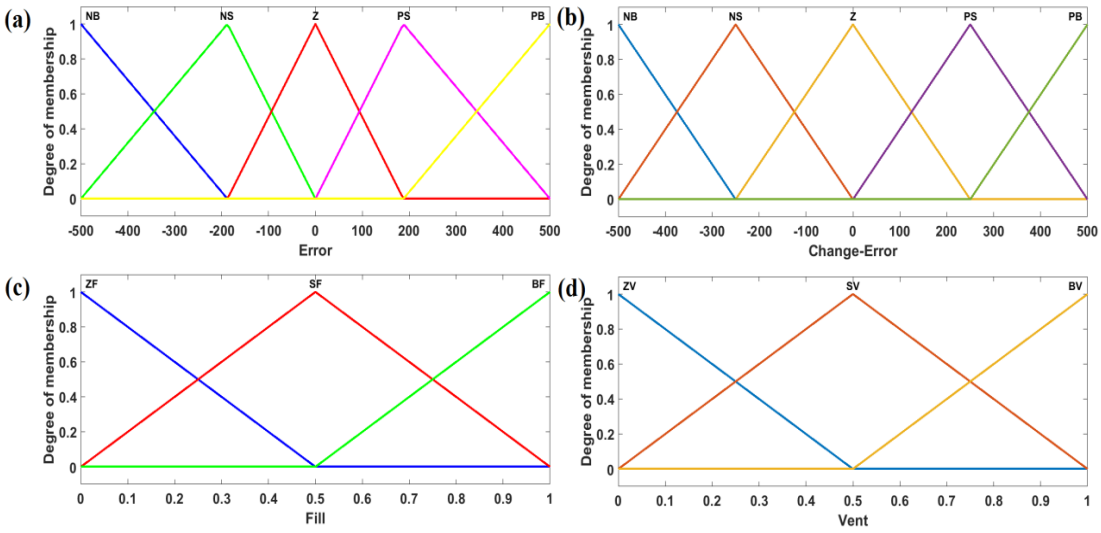

Figure 4.22: The membership functions for the inputs and outputs for the Fuzzy controllers of the proposed stiffness and position controller of the ECPAM; where NB is Negative Big, NS is Negative Small, Z is Zero, PS is Positive Small, PB is Positive Big, ZF is Zero Fill, SF is Small Fill, BF is Big Fill, ZV is Zero Vent, SV is Small Vent and BV is Big Vent; (a) The membership function of the input error, (b) The membership function of the input change in error, (c) The membership function of the Fill output and (d) The membership function of the Vent output.

There are five ranges for the input error and five ranges for the change in error, with the entire range being -500 to 500, because the contractor and the extensor muscles act in a range between zero to 500kPa; this range of pressure was chosen based on the maximum operating pressures of the valves. Likewise, there are three intervals for PWM fill output percentage and the same for vent output. All membership functions are triangle type for its straightforwardness, but the membership functions of the error input are smaller close intervals to zero. This serves to diminish the gain of the controller close to the desired set point, to achieve superior stability and to avoid excessive overshoots on the controller response. It is easy and rapid to implement this Fuzzy controller and it has been shown in the literature to successfully control pneumatic muscles with sufficient accuracy to prove the hardware developed (Nuchkrua & Leephakpreeda, 2013; Qian, Huang, & Ri, 2015a; Zhang et al., 2008). Figure 4.23 demonstrates the Fuzzy controllers' rules surface of each fill and vent output.

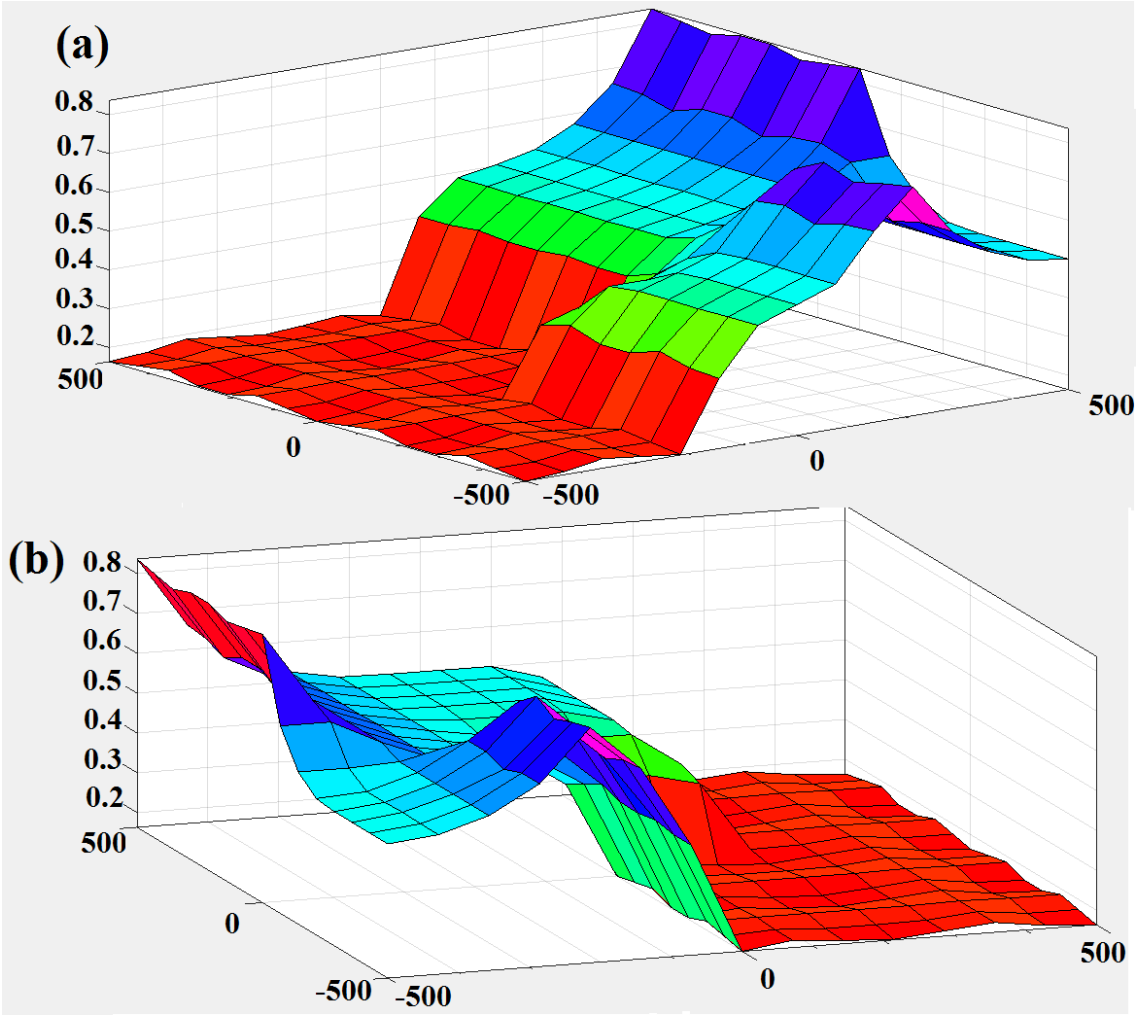

Figure 4.23: The Fuzzy controllers rules surfaces of each Fill and Vent outputs; (a) The rules surface of the Fill output and (b) The rules surface of the Vent output.

The proposed stiffness-position controller was experimentally tested. Six different experiments were conducted to examine the performance of the proposed control system, as shown in Figures 4.24, 4.25 and 4.26. Figure 4.24 illustrates two experimental results. The first experiment in Figure 4.24 (a) was with a stiffness set point of 7500N/m and an actuator length of 15cm. At these stiffness and length set points, the neural network identifier generated contractor and extensor pressures of 300.6kPa and 119.8kPa respectively. The second experiment in Figure 4.24 (b) was with a stiffness set point of 3500N/m and the same actuator length 15cm. At these stiffness and length set points, the neural network identifier generated contractor and extensor pressures of 199.1kPa and 59.78kPa respectively. These two experiments prove that we can control the stiffness of our novel actuator without changing its length.

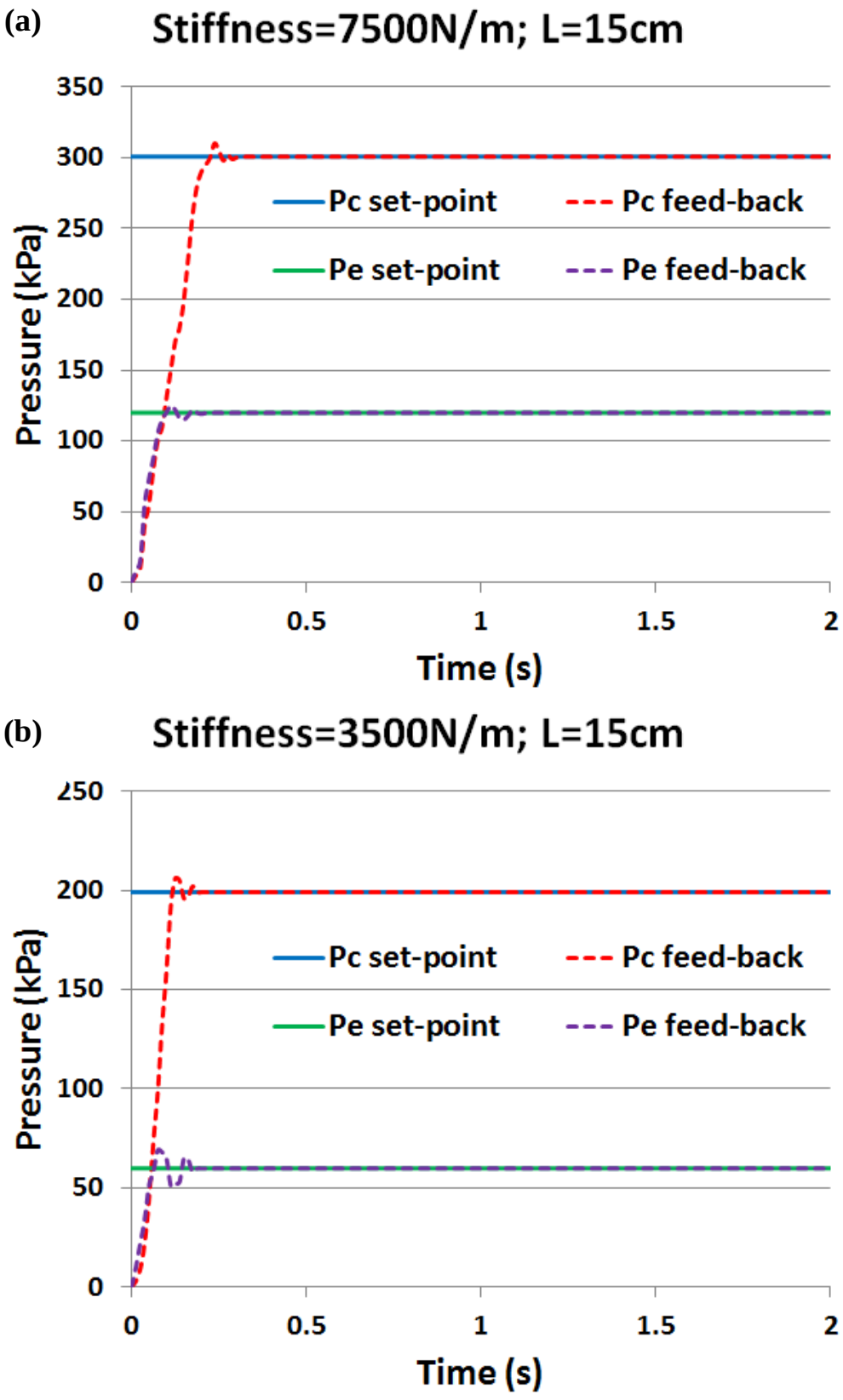

Figure 4.24: Stiffness-position controller results at actuator length 15cm and two different stiffness.

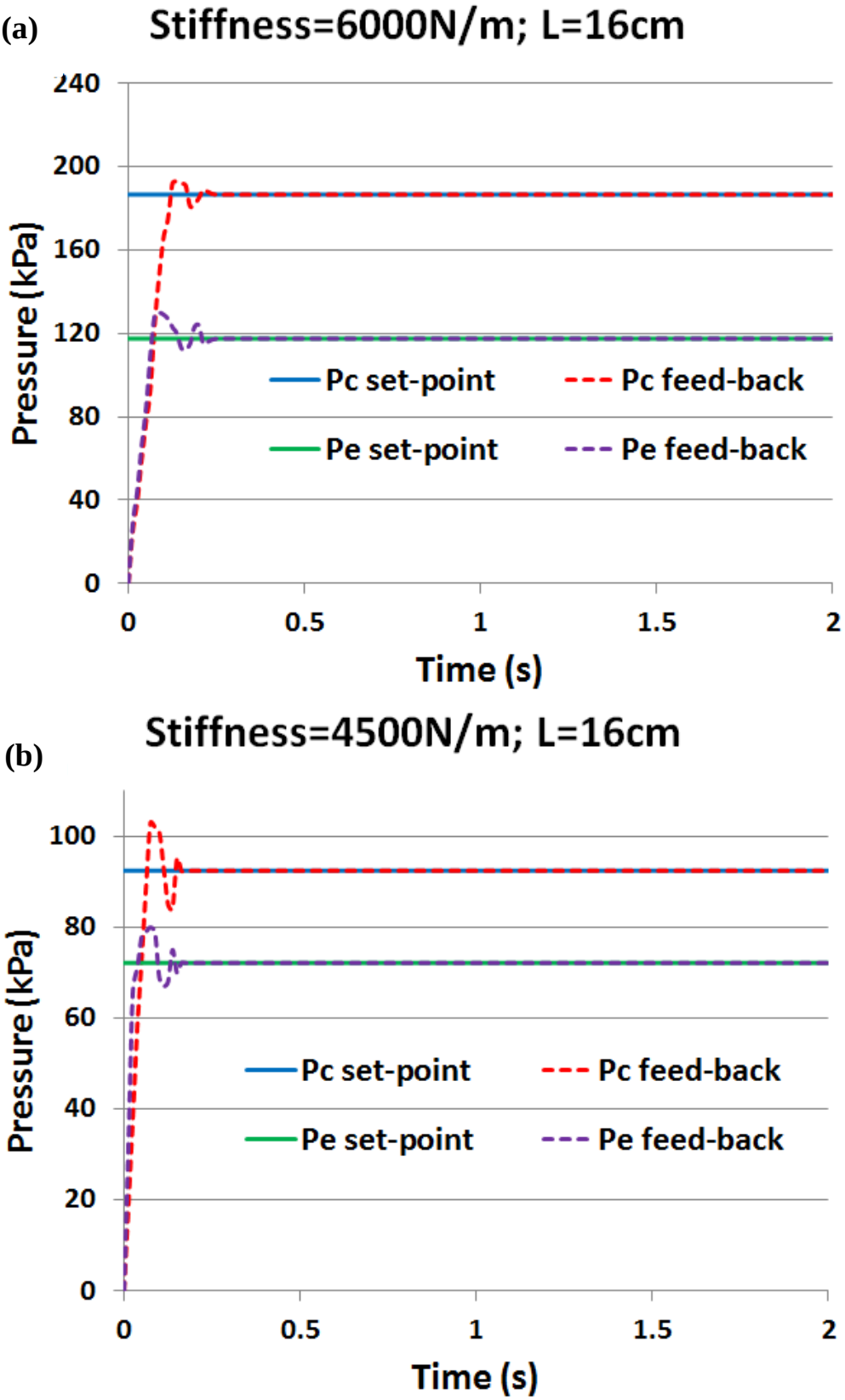

Figure 4.25: Stiffness-position controller results at actuator length 16cm and two different stiffness values.

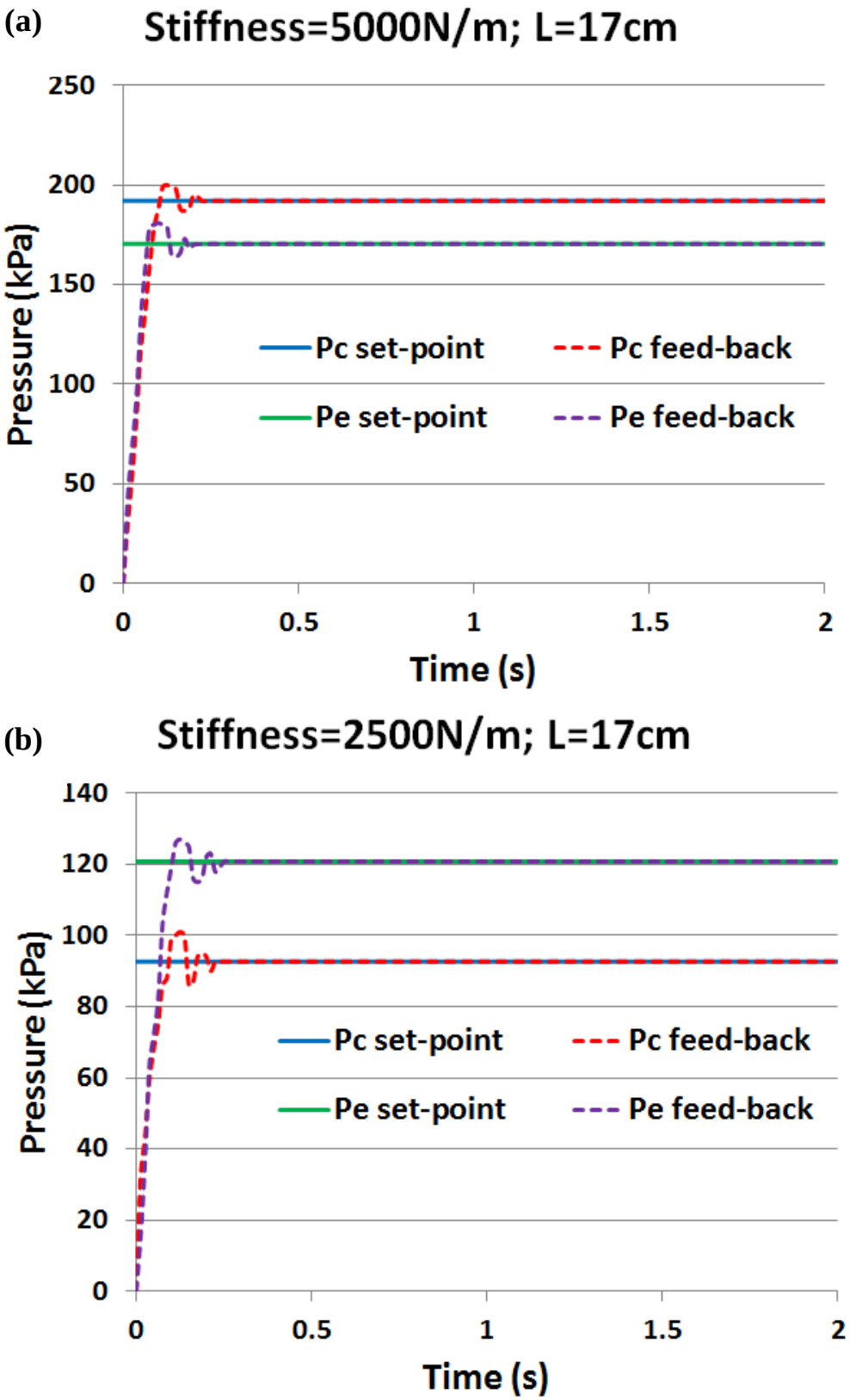

Figure 4.26: Stiffness-position controller results at actuator length 17cm and two different stiffness values.

To validate this concept, we conducted another two experiments for another actuator length as shown in Figure 4.25. The first experiment in Figure 4.25 (a) was with a stiffness set point of 6000N/m (randomly chosen) and actuator length of 16cm. The identifier in this case generated contractor and extensor pressures of 186.6kPa and 117.5kPa respectively. The second experiment in Figure 4.25 (b) was with a stiffness set point of 4500N/m and the same actuator length 16cm. At these stiffness and length set points, the neural network identifier generated contractor and extensor pressures of 92.44kPa and 72.14kPa respectively.

For further validation, we also conducted another two experiments for another actuator length as shown in Figure 4.26. The first experiment in Figure 4.26 (a) was with a stiffness set point of 5000N/m (randomly chosen) and actuator length of 17cm. The identifier in this case generated contractor and extensor pressures of 192kPa and 170.4kPa respectively. The second experiment in Figure 4.26 (b) was with a stiffness set point of 2500N/m and the same actuator length 17cm. At these stiffness and length set points, the neural network identifier generated contractor and extensor pressures of 92.66kPa and 120.8kPa respectively.

The actuator length and stiffness results of all of the above six experiments in Figures 4.24, 4.25 and 4.26 were verified manually after each experiment. The length was measured and the stiffness determined using the same experimental procedure described in section 4.4.5. The average percentage error of the ECPAM stiffness and length were determined to be 3.95% and 4.18% respectively.

4.7 Conclusion

This chapter has described the design and construction of a novel extensor-contractor pneumatic muscle. This new actuator overcomes some of the limitations associated with the use of single pneumatic muscles as well as having additional features. This new actuator has bidirectional action allowing it to both extend and contract and create force in both directions.

A mathematical model has been developed for the new novel ECPAM which describes the actuator output force. This mathematical model has been verified experimentally with the average error percentage between the mathematical model and the experimental results being less than 6%.

The stiffness of a pneumatic muscle is dependent on the pressure inside it, however, for a fixed load the length of a traditional pneumatic muscle is also a function of pressure. This means that it is not possible to change the stiffness of a pneumatic muscle (with a fixed load) without changing its length. It has been shown that the new ECPAM is able to adjust its stiffness without this resulting in a change of actuator length. Numerous stiffness and length experiments were performed to investigate the ability to vary the actuator's stiffness independently of position. A stiffness position controller has been developed to control the stiffness of the actuator at specific lengths. Verification was conducted using the controller and the average stiffness and position errors were found to be less than 5%.

Chapter 5

The Design and Mathematical Modelling of Novel Extensor-Bending Pneumatic Artificial Muscles (EBPAMs)

5.1 Introduction

As discussed in section 3.6 of chapter 3, there has been a considerable amount of research into the mathematical modeling of contraction PAMs. The purpose of modeling approaches is to create a mathematical relationship between the length of the PAM, the amount of pressure inside it, and the force it generates. These mathematical models depend on variable parameters such as applied pressure, axial force, length and diameter of the PAMs, as well as the properties of the materials used. All these variables play a considerable role in the dynamic behavior of the soft actuators. There is strong evidence of the non-linear behavior of PAMs. Thus, the major challenge is to build a robust controller for the PAM.

This Chapter proposes a novel form of pneumatic muscle which bends when activated. The Chapter first describes the construction of the new extensor bending pneumatic artificial muscle. Numerous prototypes have been developed, and their behavior has been assessed experimentally. A new mathematical model of the actuator was then developed and verified against the experimental results. Three enhancement stages were

done successfully to decrease the average error percentage between the experimental output force of the novel actuator and the new mathematical model.

5.2 Extensor-Bending Pneumatic Artificial Muscles

The proposed extensor bending pneumatic artificial muscles (EBPAMs) are based on linearly extending McKibben artificial muscles. These muscles are reinforced along one side keeping one side of the actuator at a fixed length. This means that when pressurised the new actuator does not extend in length but rather bends.

Development of the bending pneumatic muscle began with the experimental analysis of a series of extending pneumatic muscles. A prototype pneumatic muscle (M1) was produced which consisted of a rubber bladder with resting length 160 mm and diameter 10 mm. This was encased by a braided nylon sleeve whose length was double that of the rubber and had a minimum diameter of 8 mm and maximum diameter of 18 mm. The muscle had two 3D printed terminals at either end, one closed and the other containing a small hole for the supply of pressurised air. The rubber and braid were secured to the terminals using cable ties and the resulting actuator had an experimentally measured resting diameter of 18 mm; the same as the maximum diameter of the sleeve.

Due to the fact the braided sleeve was significantly longer than the rubber tube (meaning the muscle had a resting braid angle greater than 54.7°) an increase in the supplied pressure causes an increase in the muscle length i.e. the muscle is of the extending type. The length of muscle increases with increasing supplied pressure; the maximum increase in length was measured to be 68%.

Figure 5.1 illustrates the characteristic behaviour of extending pneumatic muscle relative to the supplied pressure. During operation, an axial compressive force is produced at the end of the actuator.

This experiment is done by increasing the supply pressure of the actuator by steps of 25 kPa until 500 kPa. There is no movement action before 25 kPa pressurised because this amount of lost pressure needs to inflate the bladder until be in contact with the braid.

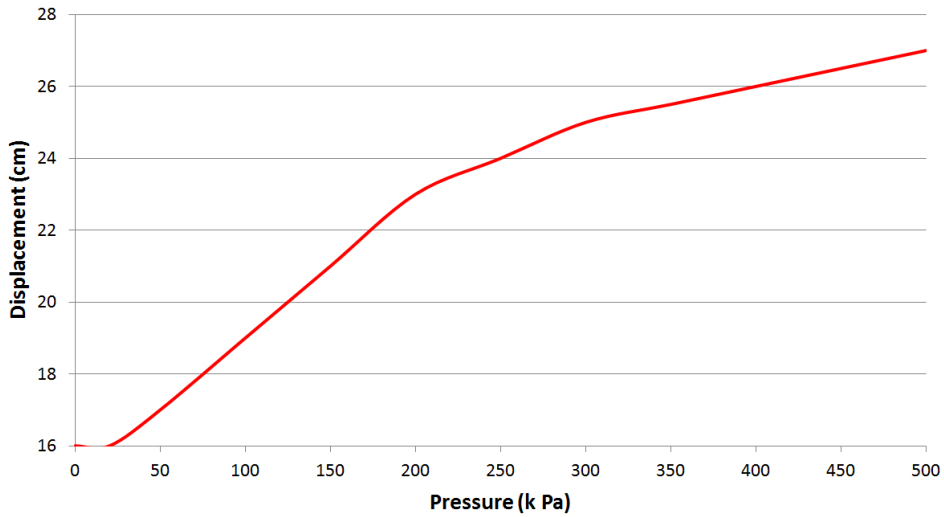

Figure 5.1: EPAM length related to the supplied pressure.

By reinforcing one side of the extending pneumatic muscle using a fixed length thread with a 500N breaking strength, as shown in Figure 5.2, the muscle is converted to a bending actuator. The thread prevents one side of the actuator from extending whilst the opposite side remains free to extend when pressurised. The resultant difference in length of the two sides of the actuator mean it bends as seen in the figure.

Figure 5.2 shows the configuration of the EBPAM at four arbitrary but increasing pressures. It can be seen that one side of the actuator remains at a fixed length whilst the over side increases in length leading to bending of the actuator.

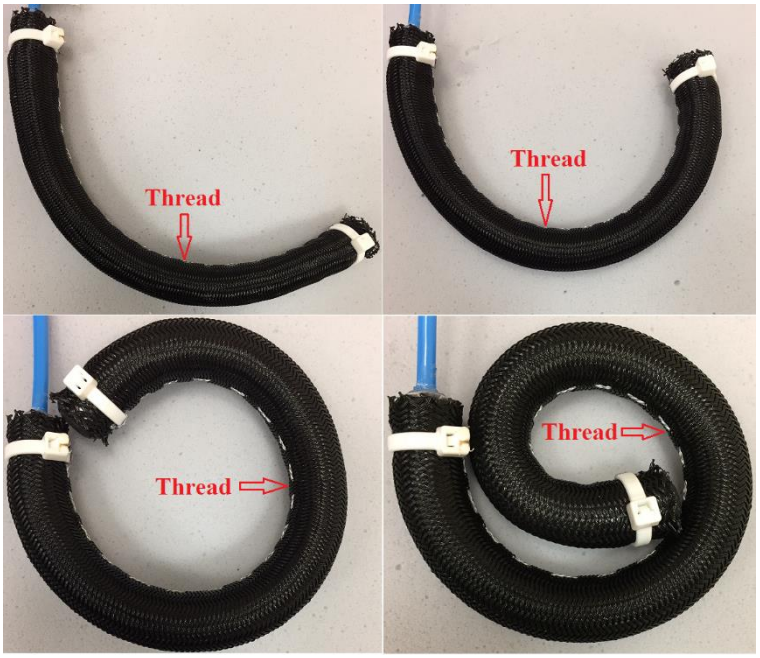

Figure 5.2: EBPAM pressurised by different amounts of pressure.

The bending angle of the proposed actuator increases with increasing supplied pressure and this relationship was explored experimentally. The pressure in the actuator was gradually increased and the angle of the remote end of the muscle relative to its initial position was measured. The angle of the actuator is measured manually by increasing the supply pressure in step of 25 kPa and measure the angle manually at each pressure from 0 to 500 kPa. Figure 5.3 illustrates the relationship between the supplied pressure and the bending angle of the proposed artificial muscle. Again, there is no bending action before 25 kPa pressurised because this amount of lost pressure needs to inflate the bladder until be in contact with the braid.

To verify these findings, two further EBPAMs, M2 and M3, were created using the same end caps and bladder as the first muscle (M1) but using a larger diameter braid, as Table 5.1 shows. The initial muscle diameters are the same as the maximum sleeve diameter because they are extensor type muscles. A larger diameter braid results in higher muscle force, so each muscle prototype generates a greater force than the previous.

Table 5.1: M1, M2 and M3 characteristics.

Muscle No.	M1	M2	M3
Muscle length	160 (mm)	160 (mm)	160 (mm)
Bladder diameter	10 (mm)	10 (mm)	10 (mm)
Sleeve diameter	8 (mm)	10 (mm)	12 (mm)
Muscle diameter	18 (mm)	23 (mm)	35 (mm)

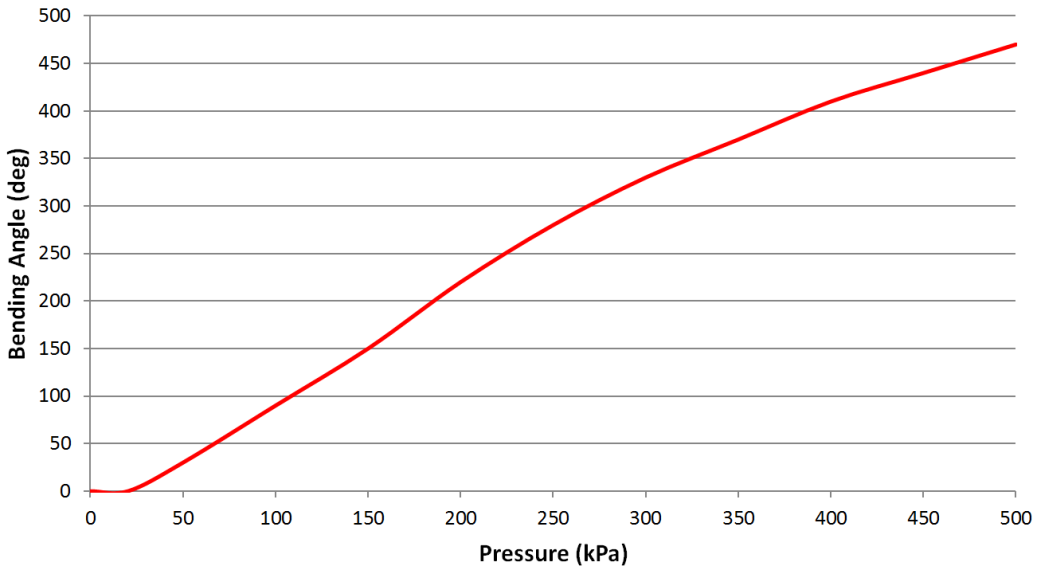

Figure 5.3: EBPAM bending angle with the supplied pressure.

Figure 5.4 (a) and Figure 5.5 (a) shows the relationship between the applied pressure and the actuator length for muscle M2 and M3, respectively, before the reinforcing thread is added.

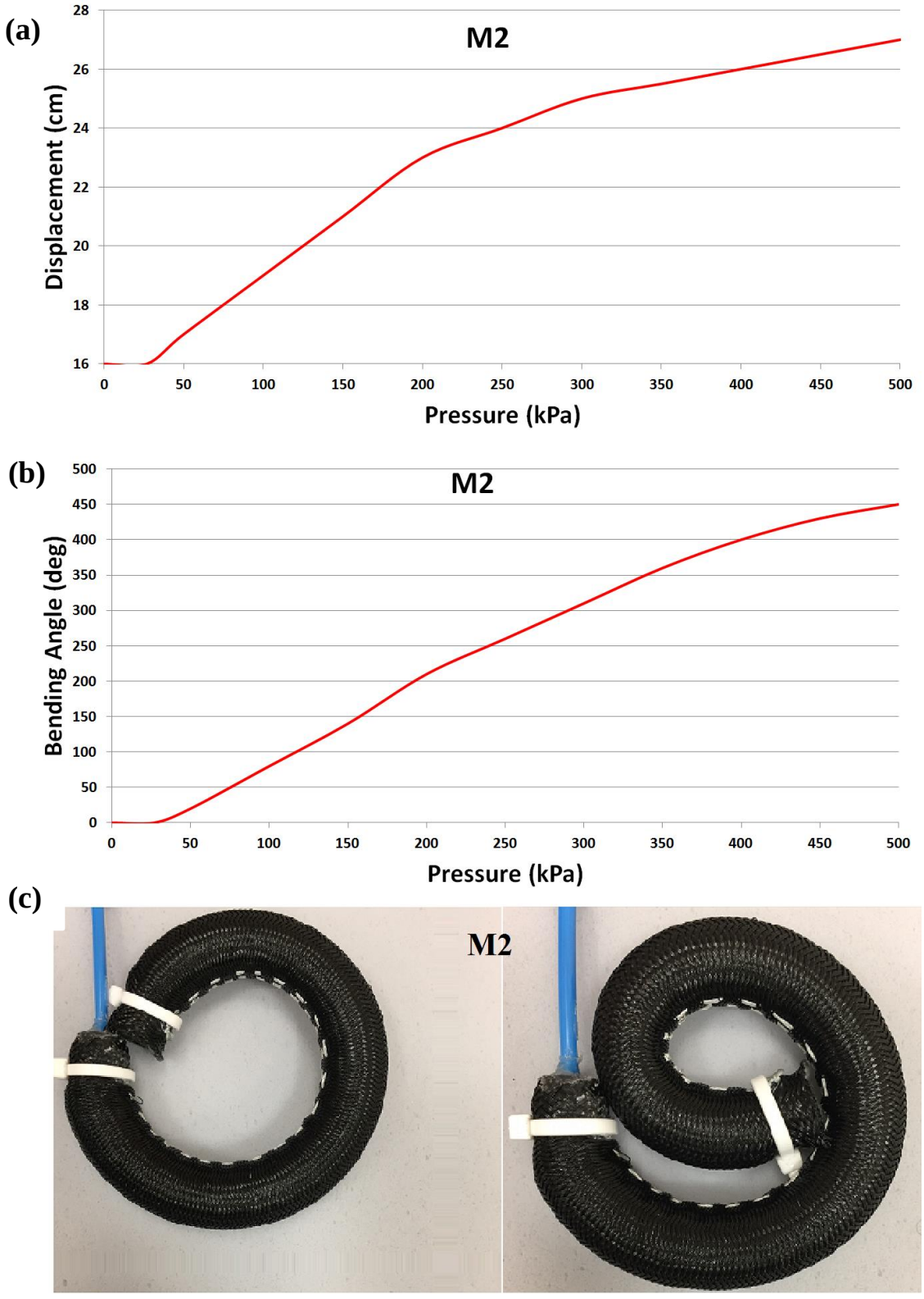

Figure 5.4: M2 with its characteristics.

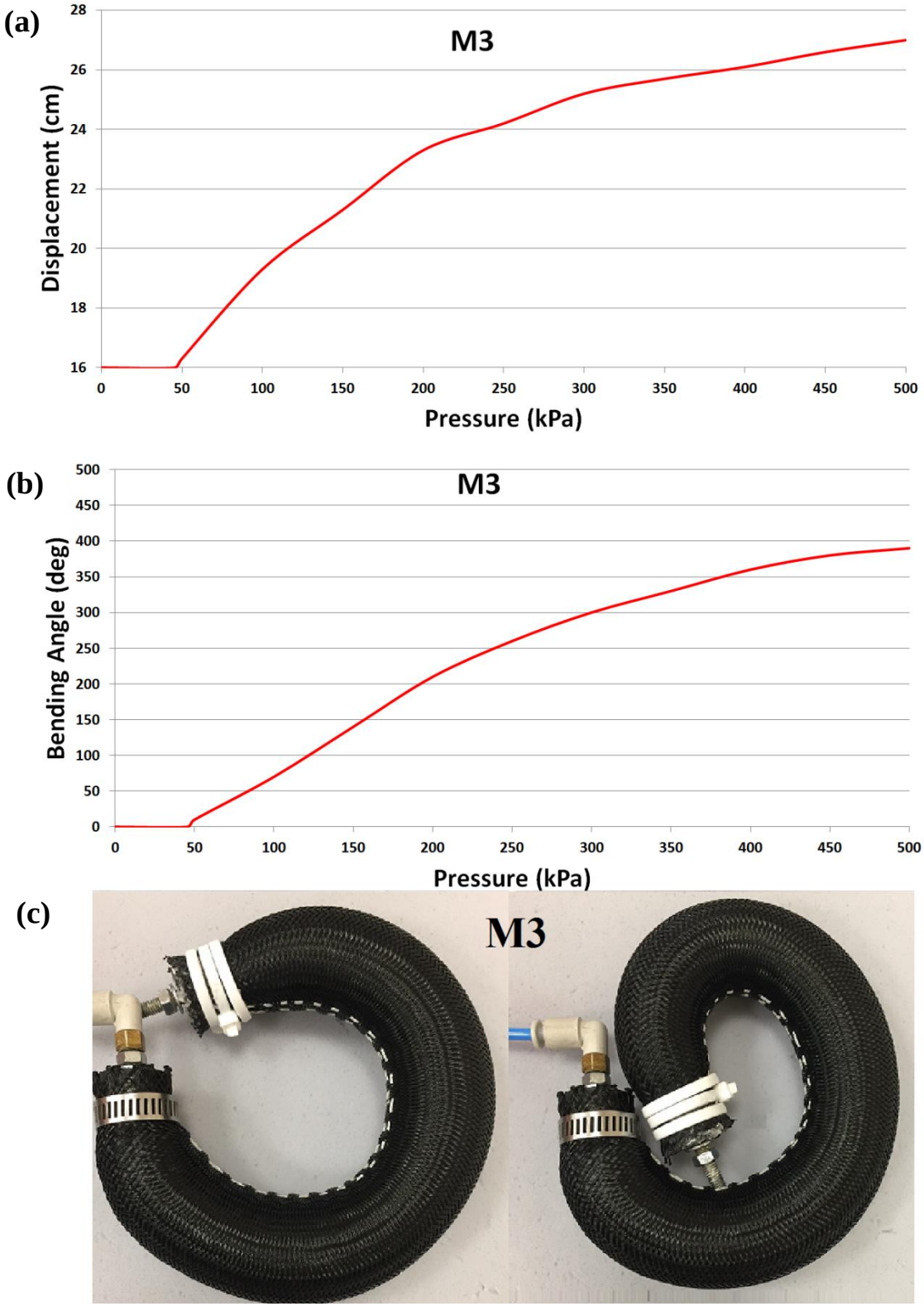

Figure 5.5: M3 with its characteristics.

In both instances, the extending ratio is 68%, which is the same as for M1. This result is not unexpected as it is the braid length, not its diameter, that determines the maximum extension of the muscles. Figure 5.4 (b) and Figure 5.5 (b) shows the

relationship between the pressure and bending angle for M2 and M3, respectively. The relationship is broadly the same for all three muscles. Again, and for the same reason, this result is not unexpected. However, at high pressure, the results for the three muscles diverge.

The reason for this can be seen in Figure 5.4 (c) and Figure 5.5 (c), as the muscle approaches maximum bending it collides with itself and the muscle becomes deformed. As can be seen, this problem is more significant for the larger diameter muscles.

This section has experimentally proven the operation of the EBPAM; the following sections will attempt to analyse its behaviour mathematically and develop a numerical model.

5.3 Kinematic Analysis of the Proposed EBPAM

The general geometry of a McKibben muscles is shown in (chapter 4 Figure 4.12. In addition, the muscle length *L*, diameter *D* and the volume *V* are mentioned previously in chapter 4 equations (4.1), (4.2) and (4.3) respectively. An extensor muscle differs from a contracting muscle in that the resting length of the braid is significantly longer than the length of the bladder. This means the braid must be compressed (braid angle increased) to make it the same length as the bladder. This means that the muscle will have an unpressurised braid angle θ greater than 54.7° (the minimum energy configuration), when pressurised the braid angle will reduce in an attempt to reach the minimum energy state and this will result in extension of the muscle. The bending muscle is derived from the extensor one by reinforcing one side of the braid. This means that one side of the braid θ is always at its maximum value and cannot increase in length. When pressurise the increase in actuator length will only occur on the free side and this results in bending.

The analysis of the EBPAM is based on the following assumption: the muscle retains a circular cross-section during bending, the threads used to form the sleeve and reinforce one side of the muscle are inextensible, there is no friction force between the sleeve and the bladder and between the threads of the sleeve and there are no elastic forces within the bladder.

Figure 5.6 shows the bending muscle geometry, where $L_o$is the muscle length on the reinforced side, L_n is the length of bending muscle on the free side, D_c is the curved

muscle diameter, α is the bend angle of the muscle, r_o is the inner radius and r_n is the outer radius. The actuator length will be the average length:

$$L_c = \frac{L_o + L_n}{2} \tag{5.1}$$

The actuator diameter in relation to the inner and outer radius is given by:

$$D_c = r_n - r_o \tag{5.2}$$

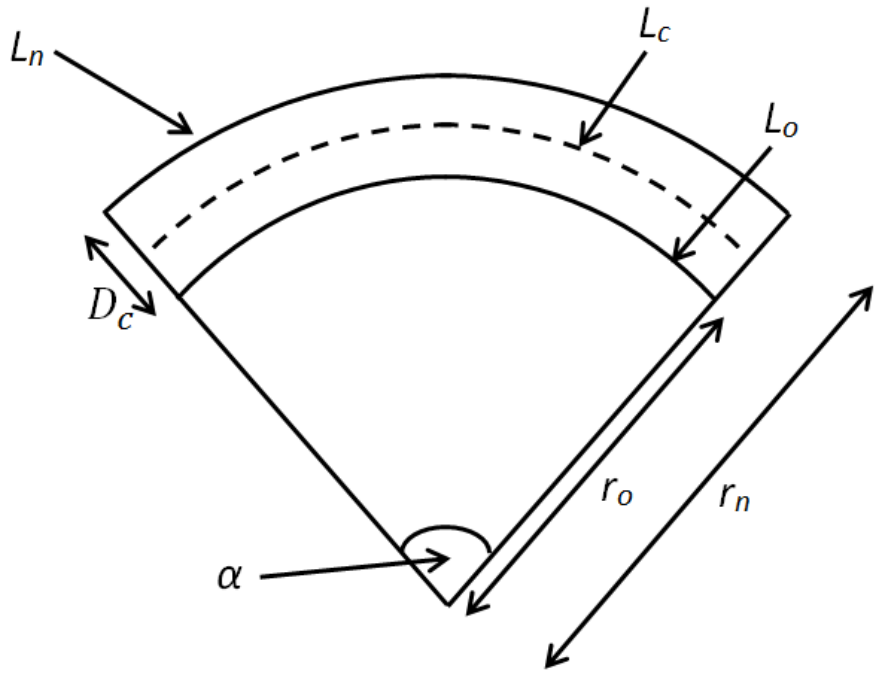

Figure 5.6: Bending muscle geometry.

Combining actuator length (4.1) with the equation for the length of an arc the following equations can be produced which describe the length of two opposite sides of the bending muscle:

$$L_o = b\ \cos\theta_{max}\ =\ r_o\alpha \tag{5.3}$$

$$L_n = b\ \cos\theta =\ r_n\alpha \tag{5.4}$$

The radius inside the curve is determined by the maximum braid angle(θ_{max}), which is fixed as a result of the reinforcing thread, and the radius outside the curve is determined by the braid angle θ, which reduces as the muscle bends.

Unlike a traditional pneumatic muscle, the braid angle around the circumference of the bending muscle is not a constant. Instead, the braid angle will decrease around the circumference from θ on the outside edge of the bend (point A in Figure 5.7) to θ_{max} at on the inner edge of the bend (point B in Figure 5.7). Each of these braid angles will have an associated muscle diameter as shown in Figure 5.7. If we assume that the muscle cross section forms a perfect circle, then the overall diameter will be the sum of the radii on the outside of the curve (r_1) and inside of the curve (r_2) as shown in Figure 5.7. Actuator diameter equation (4.2) can be used to determine the diameter of the bent muscle:

$$r_1 = \frac{D_1}{2} = \frac{b \sin\theta}{2n\pi} \tag{5.5}$$

$$r_2 = \frac{D_2}{2} = \frac{b \sin\theta_{max}}{2n\pi} \tag{5.6}$$

$$D_c = r_1 + r_2 \tag{5.7}$$

$$D_c = \frac{b \sin\theta + b \sin\theta_{max}}{2n\pi} \tag{5.8}$$

Using the above information, it is possible to develop the kinematic equations of the bending muscle which describe the bending angle α, the radius of curvature r_o and the length of the central axis of the muscle L_c as follows:

By substituting Equation (5.2) in Equation (5.4):

$$L_n = (D_c + r_o)\alpha \tag{5.9}$$

Substituting Equations (5.3) and (5.4) in Equation (5.9) gives the following equation:

$$L_n = \left(D_c + \frac{L_o}{\alpha}\right)\alpha = D_c\,\alpha + L_o = b\cos\theta \tag{5.10}$$

From Equations (5.10) and (5.3) we can derive the curvature angle as a function of θ and θ_{max} using the following equation:

$$\alpha = \frac{b\cos\theta - b\cos\theta_{max}}{D_c} \tag{5.11}$$

Also, the actuator length can be determining by substituting Equations (5.3) and (5.4) in Equation (5.1):

$$L_c = \frac{b\,cos\theta_{max} + b\,cos\theta}{2} \tag{5.12}$$

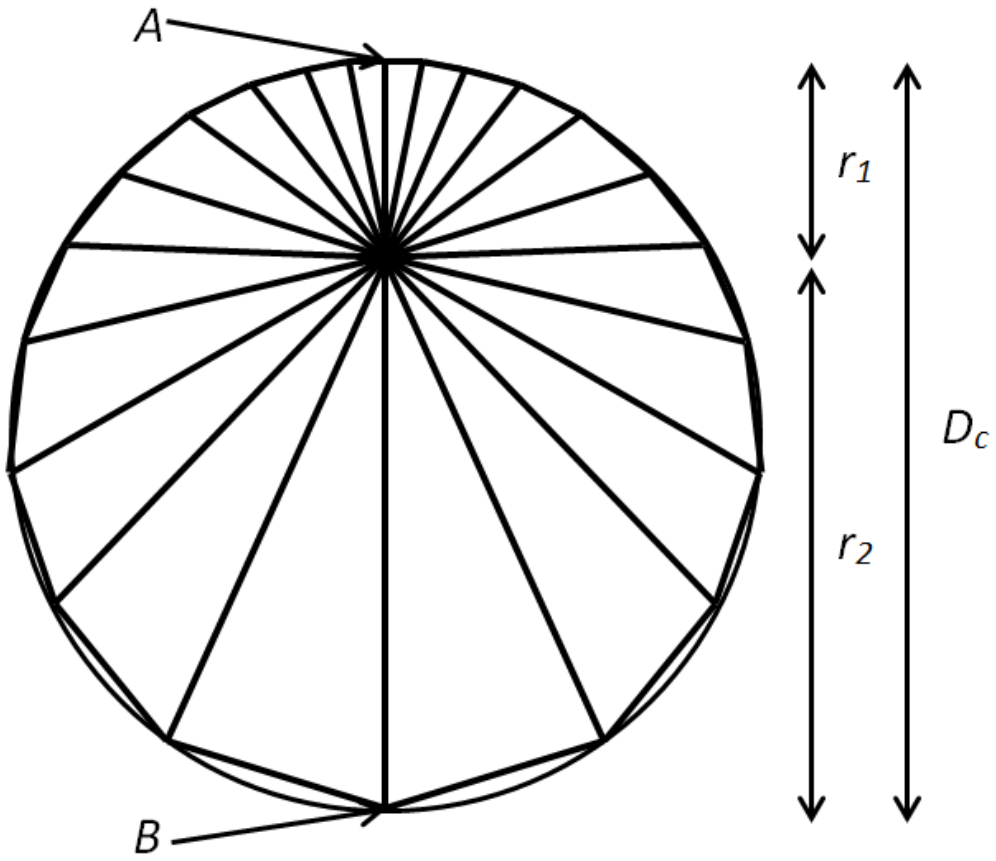

Figure 5.7: Radii inside curved muscle.

5.4 Modelling the Output Force of the Proposed EBPAM

The previous section presented a kinematic analysis of the bending muscle. However, if the bending muscle is to be used in an application, it is important that its force generating behaviour is also understood. This analysis is performed using the theory of conservation of energy as was performed by Chou et al. (Chou & Hannaford, 1996) for a contracting pneumatic muscle.

The input work W_{in} which occurs in the artificial muscle is in the form of applied air pressure which acts on the inner surface of the actuator and leads to a change in actuator volume. This can be described by the following formula:

$$dW_{in} = \int_{s_i} (P' - P_o)\, dl_i . d_{s_i} = (P' - P_o) \int_{s_i} dl_i . d_{s_i} = P . dV_c \tag{5.13}$$

Where P' is the internal absolute air pressure, $P_o$is the environment pressure (103360 Pa on the day of testing), P is the relative differential air pressure, S_i is the actuator inner surface, dl_i is the inner surface displacement vector, d_{s_i} is the area vector, and dV_c is the actuator volume change.

Based on the volume of a cylinder volume formula in equation (4.3), the curved actuator volume V_c will be:

$$V_c = \frac{\pi {D_c}^2 L_c}{4} \rightarrow$$

$$V_c = \frac{b^3(cos\,\theta + cos\,\theta_{max})(sin^2\theta + 2\,sin\,\theta_{max}\,sin\,\theta + sin^2\theta_{max})}{32\pi n^2} \tag{5.14}$$

Where D_c is the curved muscle diameter from Equation (5.8) and L_c is the central curved muscle length from Equation (5.12).

The output work W_{out} done when the EBPAM bends is associated with an increase in actuator length L_c as a result of the change in volume. This can be described by the following formula:

$$dW_{out} = F.dL_c \tag{5.15}$$

Figure 5.8 shows the EBPAM output force direction.

From the theory of energy conservation, the change in input work is equal to the change in output work:

$$dW_{in} = dW_{out} \tag{5.16}$$

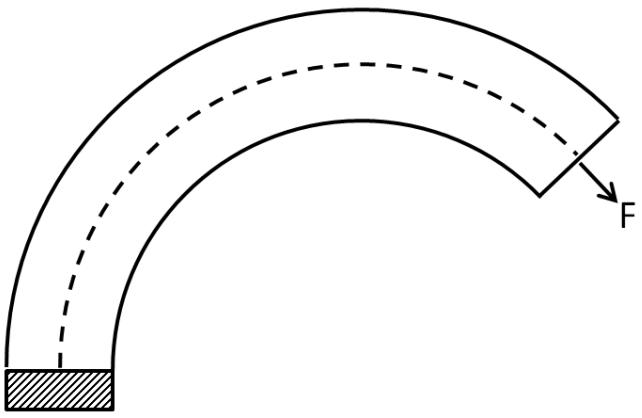

Figure 5.8: EBPAM output force direction.

The output force can therefore be determined by combining (5.13) an (5.15) as follows:

$$F = P\frac{dV_c}{dL_c} \tag{5.17}$$

Differentiating with respect to θ gives:

$$\frac{dV_c}{d\theta} = \frac{b^3}{32\pi n^2} \times$$

$$((\cos\theta + \cos\theta_{max})(2\cos\theta\sin\theta + 2\sin\theta_{max}\cos\theta) - \sin\theta(\sin\theta + \sin\theta_{max})^2) \tag{5.18}$$

and:

$$\frac{dL_c}{d\theta} = \frac{-bsin\theta}{2} \tag{5.19}$$

The final mathematical model of the proposed EBPAM output force results from substituting Equations (5.18) and (5.19) in Equation (5.17) as follows:

$$F = \frac{Pb^2}{8\pi n^2}\left(\frac{(cos\,\theta+cos\,\theta_{max})(cos\,\theta\,sin\,\theta+sin\,\theta_{max}\,cos\,\theta)}{sin\theta} - \frac{(sin\theta+sin\theta_{max})^2}{2}\right) \tag{5.20}$$

Equation (5.20) relies on values of θ which is particularly difficult to measure directly with a high degree of accuracy. However, equation (5.12) allows θ to be determined from the measured muscle length. As the length of the muscle is considerably easier to measure, in the experimental verification described in the next section the muscle length is measured and then θ calculated using (5.12).

To validate this output force mathematical model of the bending muscles the three muscles (M1, M2 and M3), previously described, were again used. These muscles were each placed in a rig, which held them in an isometric configuration at a range of known bending angles, as can be seen in Figure 5.9. A load cell was mounted to the remote end of the muscle to allow actuator force to be measured and recorded to a PC.

Each muscle to be tested was placed in the rig and then the pressure applied to it was increased from 50kPa to 500kPa in 50kPa increments and the force generated was recorded. The experiment was repeated at muscle bend angles of 90°, 135° and 45°. These bending angles have been chosen randomly to test the actuator in different positions and

the angles do not form part of the calculations of the output force. The experimental results along with the modelled data can be seen in Figures 5.10, 5.11 and 5.12.

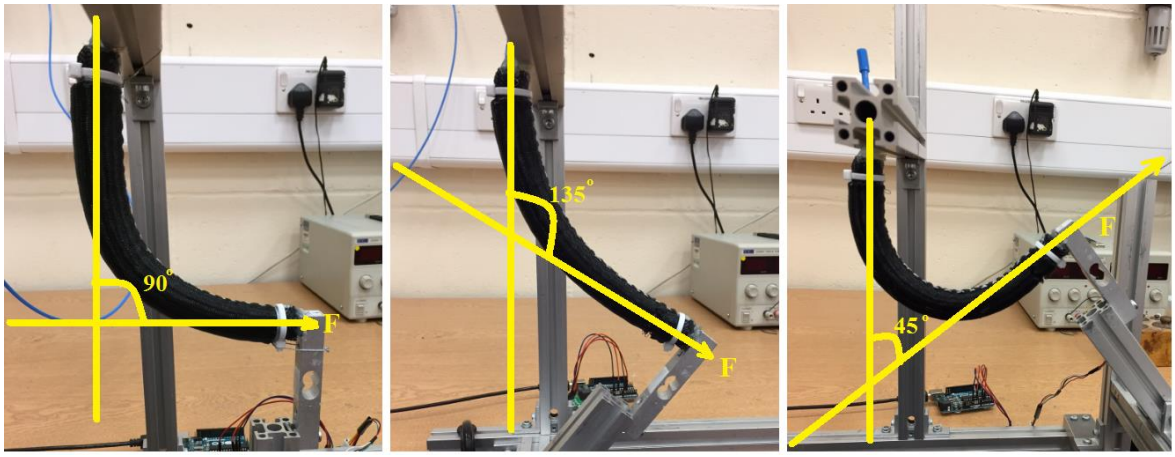

Figure 5.9: Test rig used to measure muscle force at a range of bending angles.

There is an obvious observable error between the experimental and theoretical results in the form of a relatively constant over estimation of each muscle's force output. For M1 the average error across all three bend angles was calculated to be 2.65N. This was determined by measuring the force error at each pressure value for each of the three bend angles and then taking an average of these values. This represents an error of 13.36% of the maximum force generated by the muscle. For M2 and M3 the average errors were 4.02N and 8.19N respectively. These values correspond to 14.95% and 19.13% of the maximum output force for the two muscles M2 and M3.

These errors are not unexpected as the model used is simplistic and does not consider energy losses within the muscle. However, the accuracy of the simple model is broadly similar to when the same approach has been used to model contracting pneumatic muscles (Davis et al., 2003).

5.5 Enhancements to the Mathematical Model based-on Radial Expansion Pressure

From the previous section, it is clear that there is a considerable gap between the theoretical and experimental results. There are many factors which introduce energy losses in PAMs. One of these factors is the energy spend radially expanding the rubber bladder before it makes contact with the braided sleeve.

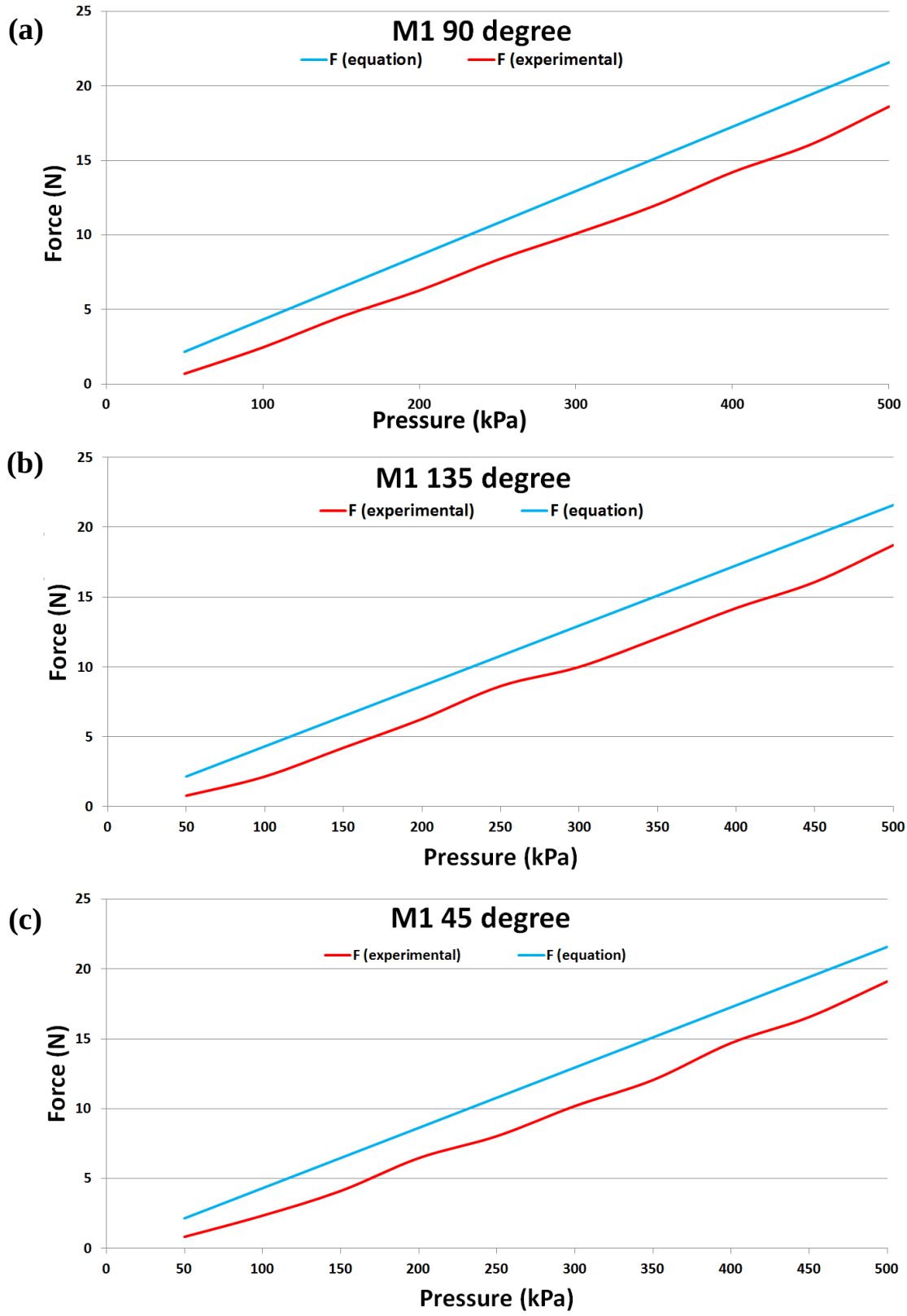

Figure 5.10: Measured and modelled force for muscle M1 at 90°, 135° and 45° bend angle.

Figure 5.13 shows there is a certain amount of pressure needed to inflate the bladder tube until it comes into contact with the sleeve, and below this pressure the

actuator output force will be zero (Al-Ibadi, Nefti-Meziani, & Davis, 2016; Tsagarakis & Caldwell, 2000).

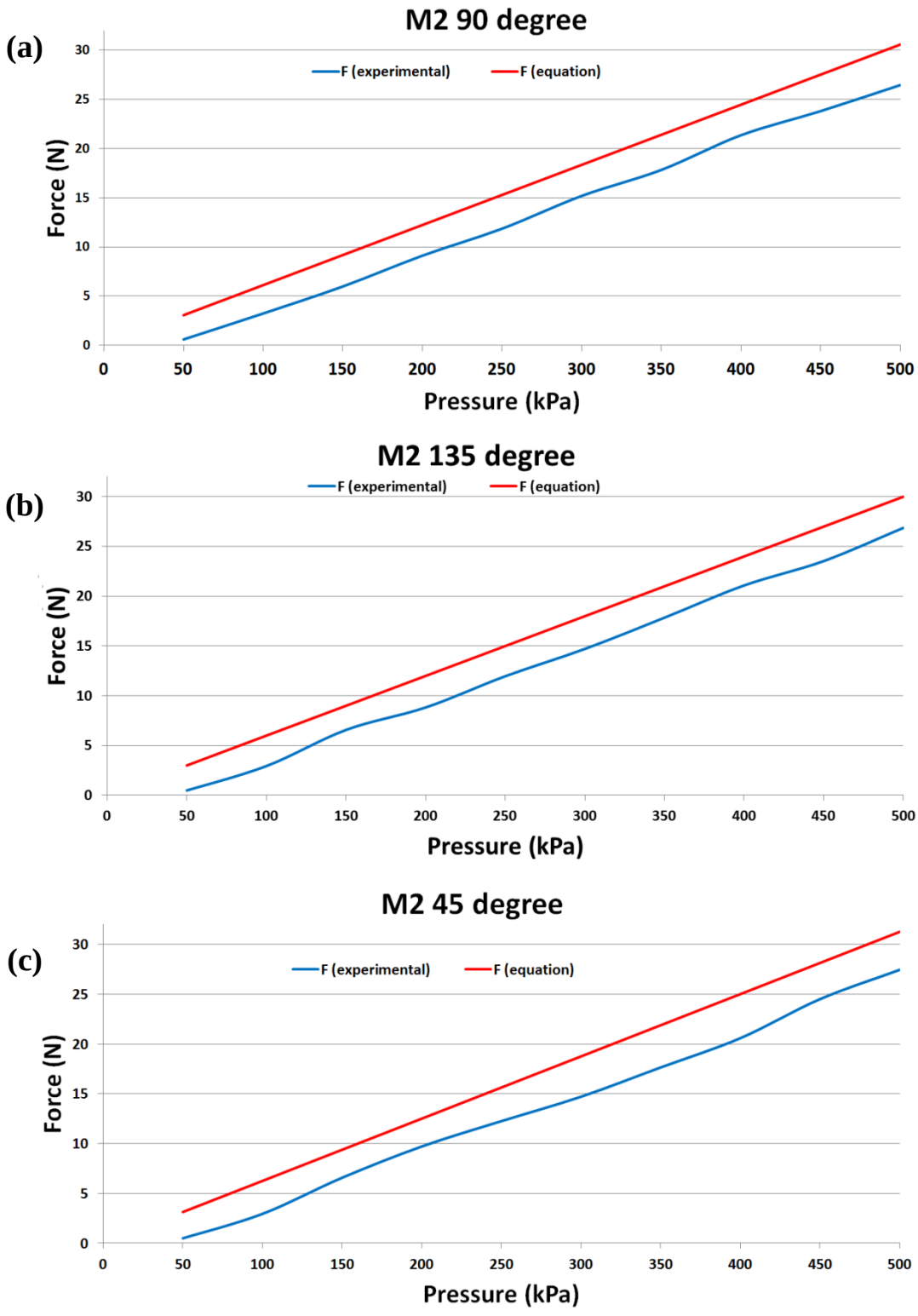

Figure 5.11: Measured and modelled force for muscle M2 at 90°, 135° and 45° bend angle.

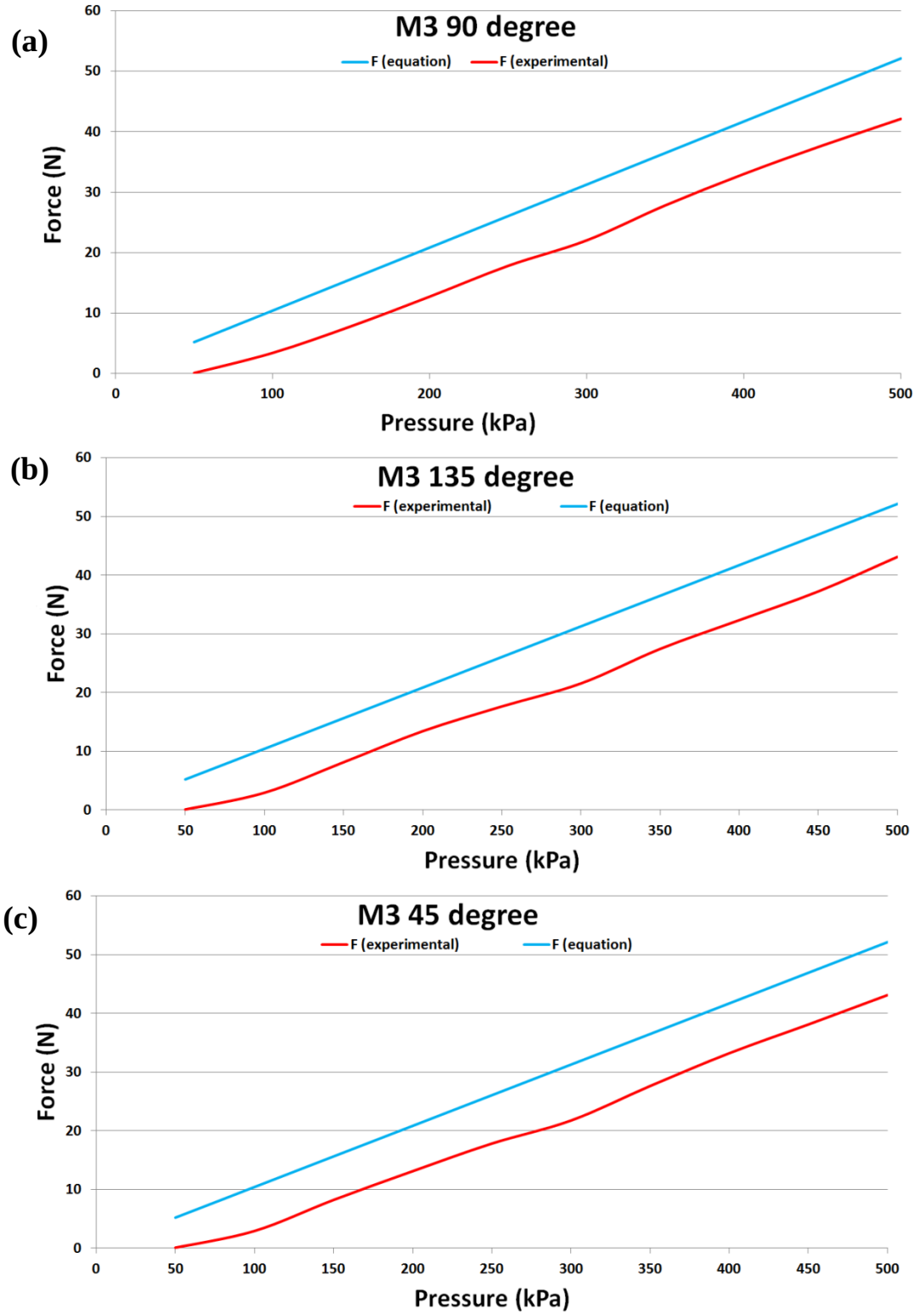

Figure 5.12: Measured and modelled force for muscle M3 at 90°, 135° and 45° bend angle.

We will call this pressure needed to radially expand the bladder to make contact with the braid P_r. To take into consideration this lost pressure effect, the active drive pressure for the actuator in the model (Equation 5.20) is replaced with the actual pressure P_a where:

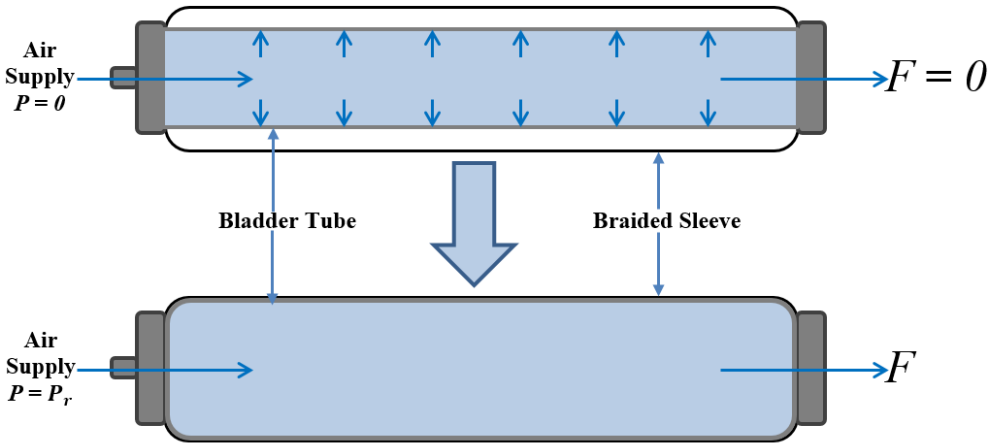

Figure 5.13: Pressure needed to inflate the bladder tube.

$$P_a = P - P_r \tag{5.21}$$

Figure 5.14 shows the experimental results obtained for P_r for the three test muscles M1, M2 and M3. The results were obtained by pressurising the bladders and measuring their diameter as the pressure increased up to the point where the diameter was equal to that of the resting braid diameter.

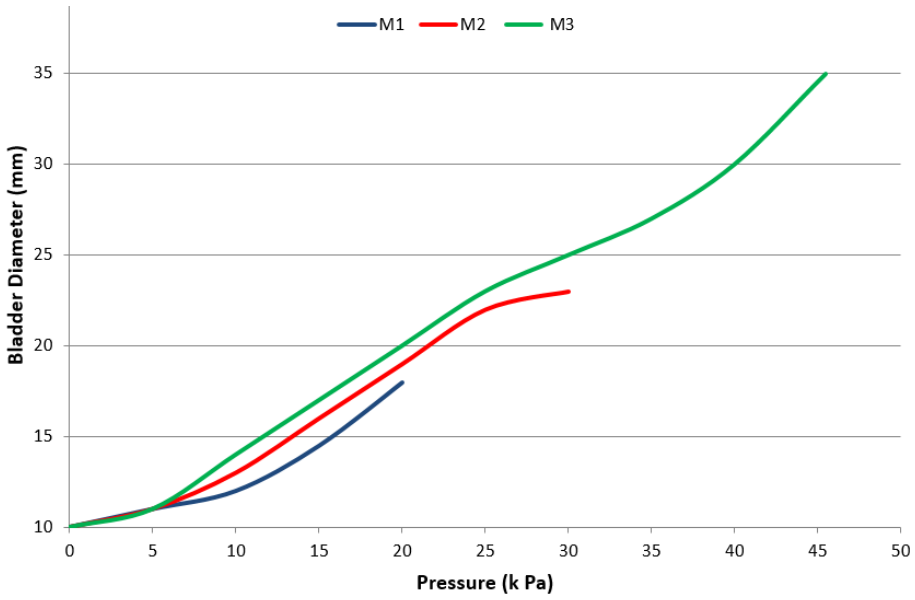

Figure 5.14: Pressure needed to inflate rubber.

Tsagarakis and Caldwell (Tsagarakis & Caldwell, 2000) modelled the radial expansion pressure for their contraction muscle. Based on this model, we derived a new model of this lost pressure experimentally.

We represent the radial expansion pressure P_r in the following equation:

$$P_r = K_r(D_o - D_c \sin\theta) \tag{5.22}$$

Where D_o is the actual bending muscle diameter and K_r is the linearised radial actuator elasticity obtained from the experiment above (Tsagarakis & Caldwell, 2000):

$$K_r = 2000\ kPa/m \text{ for } D_c \sin\theta < \frac{D_o}{2}$$

$$K_r = 500\,\frac{kPa}{m} \text{ for } D_c \sin\theta > \frac{D_o}{2}$$

The final output force model of extensor bending muscles is given by the following equation:

$$F = \frac{P_a\, b^2}{8\pi n^2}\left(\frac{(\sin\theta+\sin\theta_{max})^2}{2} - \frac{(\cos\theta+\cos\theta_{max})(\cos\theta\sin\theta+\sin\theta_{max}\cos\theta)}{sin\theta}\right) \tag{5.23}$$

Figures 5.15 shown the performance of the new model when compared to the experimental and previously modelled results.

It is clear from the graphs in Figures 5.15, 5.16 and 5.17 that the average percentage errors are decreased by a considerable amount when using the new model. Table 5.2 illustrates a comparison between the previous errors and the new errors for all proposed bending muscles at bending angles of 90^o, $135^o$and 45^o.

Across the three bending angles the average percentage error for muscles M1, M2 and M3 were found to be 8.62%, 8.59% and 8.11% respectively. The percentage reduction in modelled error when P_r was included was 35.48%, 42.54% and 57.61% for M1, M2 and M3 respectively. It is obvious, this enhancement stage reduces the error for high diameters muscles more than for the muscles with small diameters. This is because we used the same bladder diameter for all muscles, therefore the muscle with the largest maximum sleeve diameter has the maximum loss of radial expansion pressure.

Table 5.2: The average error as a percentage of the maximum actuator force with and without consideration of *Pr*.

Muscle No.	M1		M2		M3	
Bending Angle	% Error	% Error with P_r	% Error	% Error with P_r	% Error	% Error with P_r
90^o	13.70	8.98	15.29	8.79	19.47	8.20
135^o	13.68	7.88	15.32	7.77	19.21	6.75
45^o	12.71	9.01	14.25	9.21	18.71	9.37

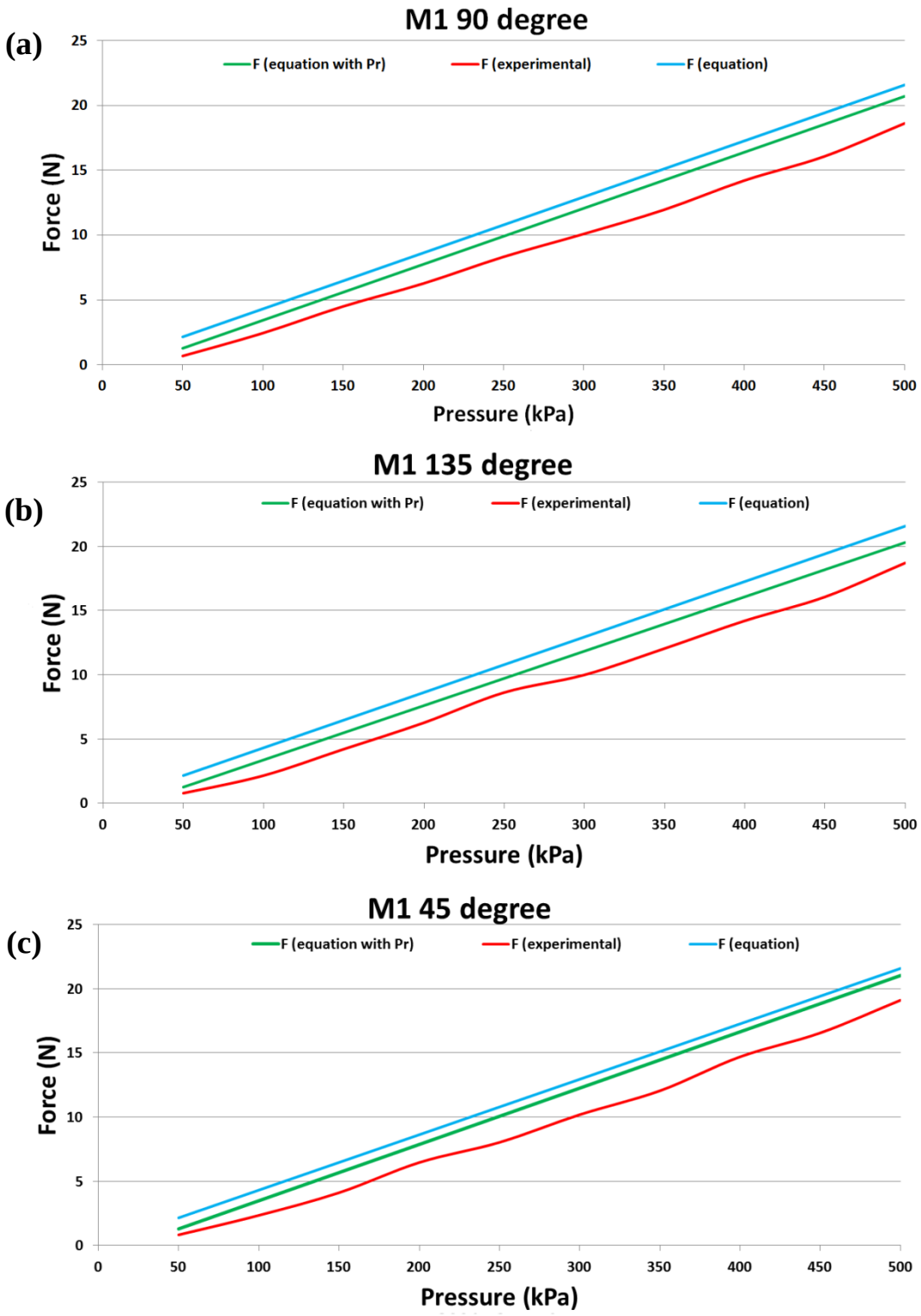

Figure 5.15: Final results of the output force for M1 in consideration with P_r.

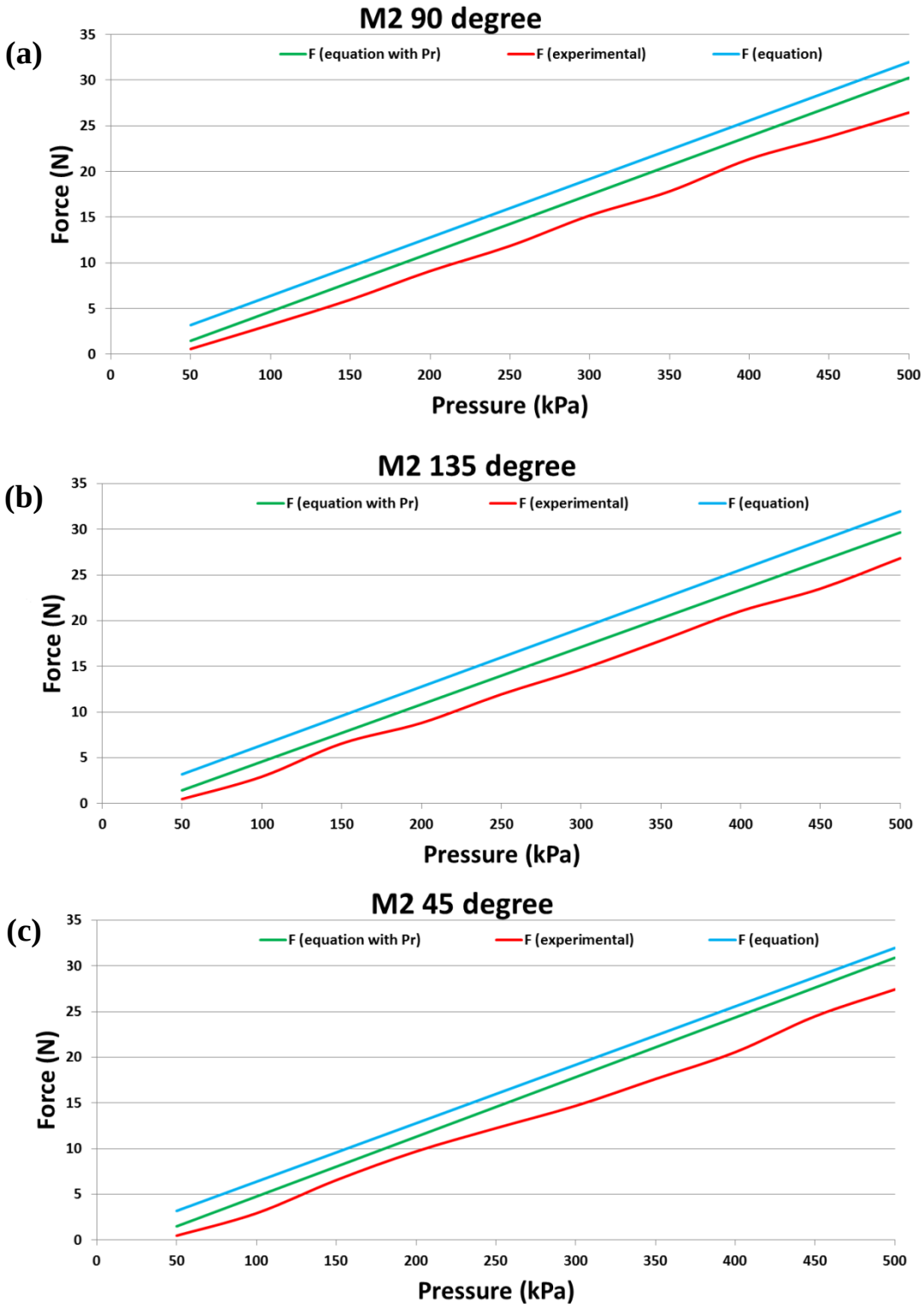

Figure 5.16: Final results of the output force for M2 in consideration with P_r.

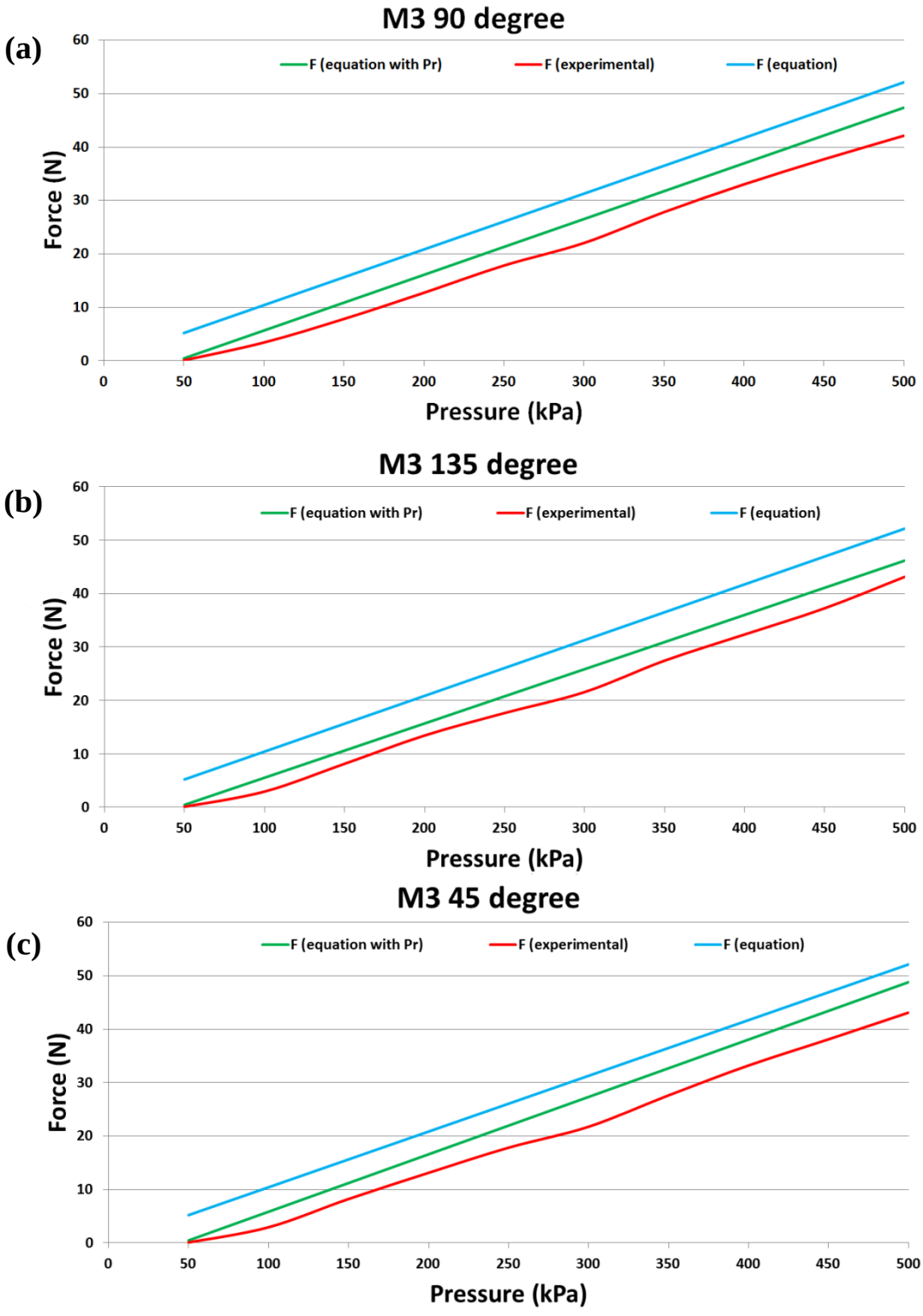

Figure 5.17: Final results of the output force for M3 in consideration with P_r.

5.6 Enhancements to the Mathematical Model based on Actual Diameter

The proposed mathematical model of the proposed actuator is based on an assumption, which is the muscle has no thickness (the thicknesses of the sleeve and the bladder is zero). This assumption simplifies the model but increases the error between the experimental results and the proposed model.

In this enhancement stage, we will take into consideration the thicknesses of the sleeve (t_s) and the bladder (t_b) then the total muscle border thickness (t_a) will be:

$$t_a = t_s + t_b \tag{5.24}$$

This thickness (t_a) effects the muscle diameter and its volume. The proposed bending actuator diameter is expressed by the following equations:

$$D_a = D_c - 2t_a \tag{5.25}$$

$$D_a = \frac{b\sin\theta + b\sin\theta_{max}}{2n\pi} - 2t_a \tag{5.26}$$

The bending muscle actual volume V_a will be:

$$V_a = \frac{\pi {D_a}^2 L_c}{4} \longrightarrow \tag{5.27}$$

$$V_a = \frac{1}{32\,n^2\,\pi} \times \left((b\cos\theta_{max} + b\cos\theta) \times (b\sin\theta + b\sin\theta_{max} - 4\,n\,\pi\,t_a)^2\right)$$

The proposed actuator output force can therefore be determined based on Equation (5.17) as follows:

$$F = P_a \frac{dV_a}{dL_c} \tag{5.28}$$

Differentiating the bending muscle actual volume with respect to θ gives:

$$\frac{dV_a}{d\theta} = \frac{1}{32n^2\pi} \times \tag{5.29}$$

$$(2b^2\cos\theta\,(\cos\theta + \cos\theta_{max})(b(\sin\theta + \sin\theta_{max}) - 4n\pi t_a) - b\sin\theta\,(b(\sin\theta + \sin\theta_{max}) - 4n\pi t_a)^2)$$

The final mathematical model of the output force of the proposed extensor bending artificial muscle results from substituting (5.29) and (5.19) in (5.28) as follows:

$$F = \frac{-2P_a}{32n^2\pi b \sin\theta} \tag{5.30}$$

$$(2b^2 \cos\theta\,(\cos\theta + \cos\theta_{max})(b(\sin\theta + \sin\theta_{max}) - 4n\pi t_a) - b\sin\theta\,(b(\sin\theta + \sin\theta_{max}) - 4n\pi t_a)^2)$$

Figures 5.18, 5.19 and 5.20 show the performance of the new model when compared to the experimental and previously modelled results.

Based on the graphs in Figures 5.18, 5.19 and 5.20 it can be seen that the average percentage errors are decreased by a considerable amount when using the new model. Table 5.3 shows a comparison between the previous errors (when including P_r) and the new errors (when including t_a) for all three proposed bending muscles at bending angles of 90^o, $135^o$and 45^o.

Table 5.3: The average error as a percentage of the maximum actuator force with and without consideration of t_a.

Muscle No.	M1		M2		M3	
Bending Angle	% Error	% Error with t_a	% Error	% Error with t_a	% Error	% Error with t_a
90^o	8.98	5.85	8.79	6.17	8.20	6.26
135^o	7.88	4.79	7.77	5.22	6.75	4.88
45^o	9.01	5.94	9.21	6.66	9.37	7.45

Across the three bending angles the average percentage error for muscles M1, M2 and M3 were found to be 5.53%, 6.02% and 6.19% respectively. The percentage reduction in modelled error when t_a was included (with the last model in section 5.5) was 35.89%, 29.92% and 23.63% for M1, M2 and M3 respectively.

5.7 Enhancements to the Mathematical Model based on Total Volume

All mathematical models in the previous sections were based on a further assumption, which is the actuator is perfectly cylinder and there are no deformations segments at the ends of the actuator. In reality, there are that deformations occurred at the actuator terminals because the ends caps of the extensor muscles have a diameter smaller than the muscle cylindrical body. These deformations are similar in shape to a frustum of a cone. Figure 5.21 shows the frustum of cone geometry with its parameters.

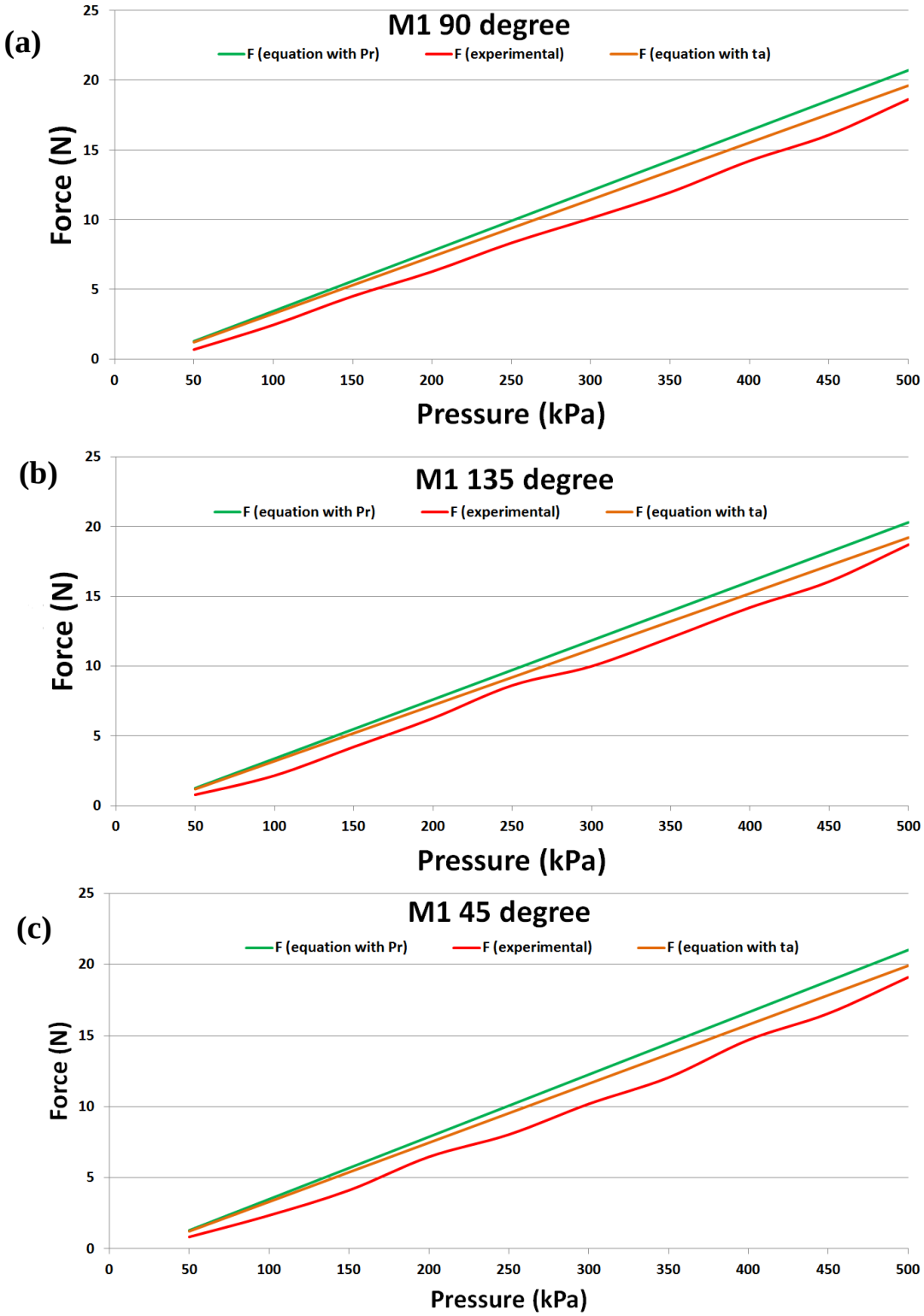

Figure 5.18: Final results of the output force for M1 in consideration with t_a.

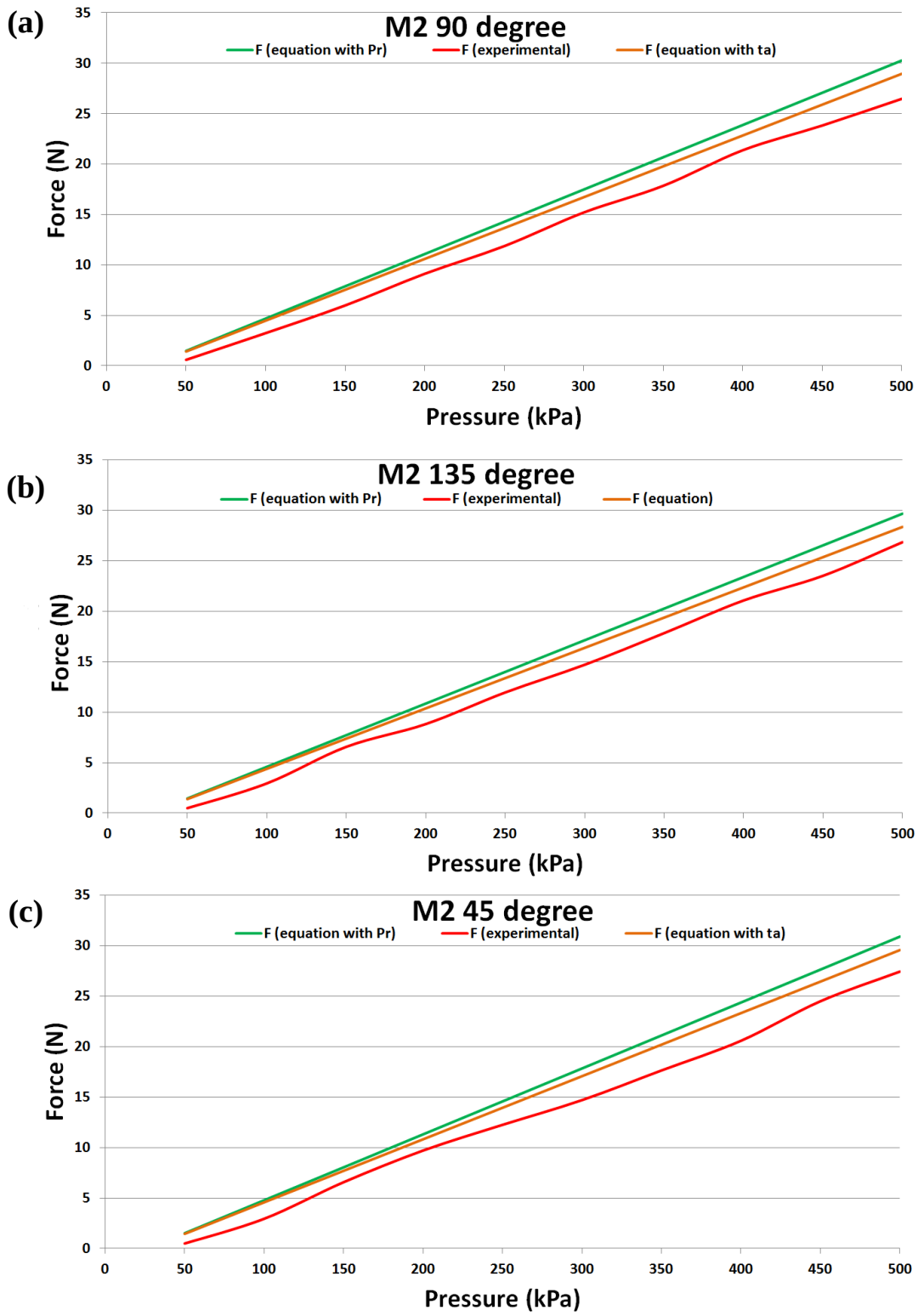

Figure 5.19: Final results of the output force for M2 in consideration with t_a.

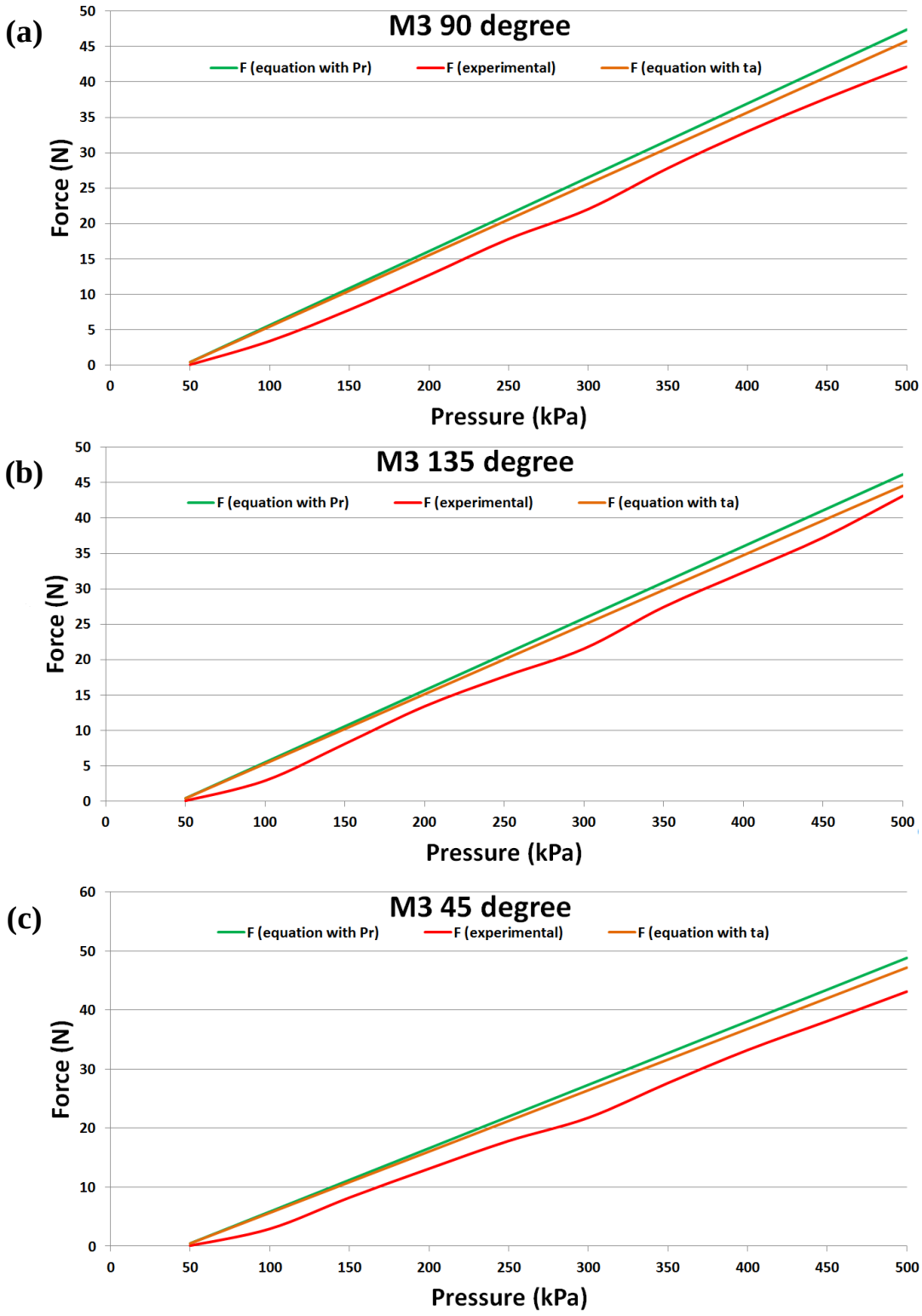

Figure 5.20: Final results of the output force for M3 in consideration with t_a.

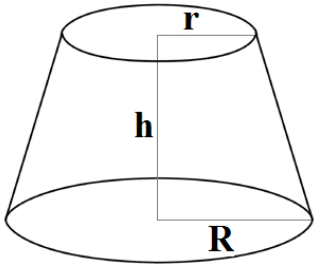

Figure 5.21: The frustum of cone geometry with its parameters.

The frustum of a cone volume is given by the following equation:

$$V = \frac{\pi h}{3}(R^2 + Rr + r^2) \tag{5.31}$$

Where h is the height of the frustum of a cone, r is the radius of the upper base and R is the radius of the lower base.

The proposed extensor bending muscle's new geometry including this deformation is shown in Figure 5.22.

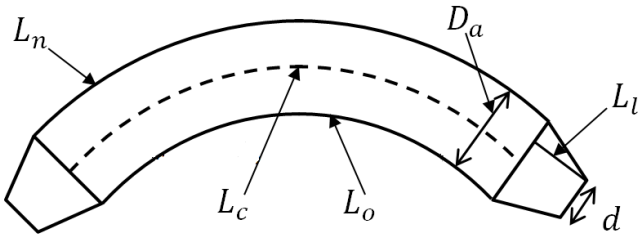

Figure 5.22: The proposed extensor bending muscle new geometry with its parameters.

Based on Figure 5.22, the volume equation of each actuator end is given by the following equation:

$$V_l = \frac{\pi L_l}{12}(D_a^2 + d^2 + D_a d) \tag{5.32}$$

Where V_l is the deformed volume, $L_l$is the deformed length and d is the actuator end cap diameter.

By substituting the body muscle diameter from equation (5.26) to equation (5.32); the volume of each deformation is given by the following equation:

$$V_l = \frac{\pi L_l}{12}\left[\left(\frac{b\sin\theta + b\sin\theta_{max}}{2n\pi} - 2t_a\right)^2 + \left(d\left(\frac{b\sin\theta + b\sin\theta_{max}}{2n\pi} - 2t_a\right)\right) + d^2\right] \tag{5.33}$$

And its derivative with respect to θ:

$$\frac{dV_l}{d\theta} = \frac{L_l}{48\pi n^2}\left(2b\cos\theta\left(b(\sin\theta + \sin\theta_{max})\right) - n\pi(4t_a - d)\right) \tag{5.34}$$

From the theory of energy conservation, the change in input work is equal to the change in output work:

$$P_a dV_t = F\ dL_t \tag{5.35}$$

$$P_a(dV_a + 2dV_l) = F(dL_c + 2dL_l) \tag{5.36}$$

$$F = P_a \left[\frac{\frac{dV_a}{d\theta}+2\frac{dV_l}{d\theta}}{\frac{dL_c}{d\theta}+2\frac{dL_l}{d\theta}}\right] \tag{5.37}$$

Assuming L_l is a constant experimentally measured for each actuator, the force equation will be:

$$F = P_a \left[\frac{\frac{dV_a}{d\theta}+2\frac{dV_l}{d\theta}}{\frac{dL_c}{d\theta}}\right] \tag{5.38}$$

Where P_a is the actual pressure from equation (5.21), $\frac{dV_a}{d\theta}$ is the change in volume of the actuator cylindrical segment from equation (5.29), $\frac{dV_l}{d\theta}$ is the change in volume of the frustum of a cone at each actuator end from equation (5.34) and $\frac{dL_c}{d\theta}$ is the change in length of the cylindrical segment of the proposed actuator from equation (5.19).

Figures 5.23, 5.24 and 5.25 show the performance of the new model when compared to the experimental and previously modelled results.

From the graphs in Figures 5.23, 5.24 and 5.25 it can be seen that the average percentage errors are decreased by a considerable amount when using the new model in equation (5.38). Table 5.4 illustrates a comparison between the previous errors (when considering t_a) and the new errors (when considering V_l) for all three proposed bending muscles at bending angles of 90^o, $135^o$and 45^o.

Table 5.4: The average error as a percentage of the maximum actuator force with and without consideration of V_l.

Muscle No.	M1		M2		M3	
Bending Angle	% Error	% Error with V_l	% Error	% Error with V_l	% Error	% Error with V_l
90^o	5.85	4.73	6.17	4.74	6.26	4.72
135^o	4.79	3.70	5.22	3.83	4.88	3.42
45^o	5.94	4.84	6.66	5.25	7.45	5.90

Across the three bending angles the average percentage error for muscles M1, M2 and M3 were found to be 4.42%, 4.61% and 4.68% respectively. The percentage reduction

in modelled error when t_a was included (with the last model in section 5.6) was 20.1%, 23.42% and 24.39% for M1, M2 and M3 respectively.

5.8 Conclusion

This chapter has described the construction of a bending pneumatic muscle based on an extending McKibben muscle. By reinforcing one side of the muscle to prevent extension, a bending motion actuator has been developed and modelled mathematically. This model relies upon the geometric parameters of the extending bending pneumatic muscle to determine the output force as a function of the input pressure. The model has been verified against experimental results for a range of actuator sizes and at a range of bending angles. The chapter has experimentally assessed the effectiveness of the novel muscle and our mathematical model.

Three enhancements to the model have been added to enhance the output force mathematical model to decrease the average error percentage to the minimum.

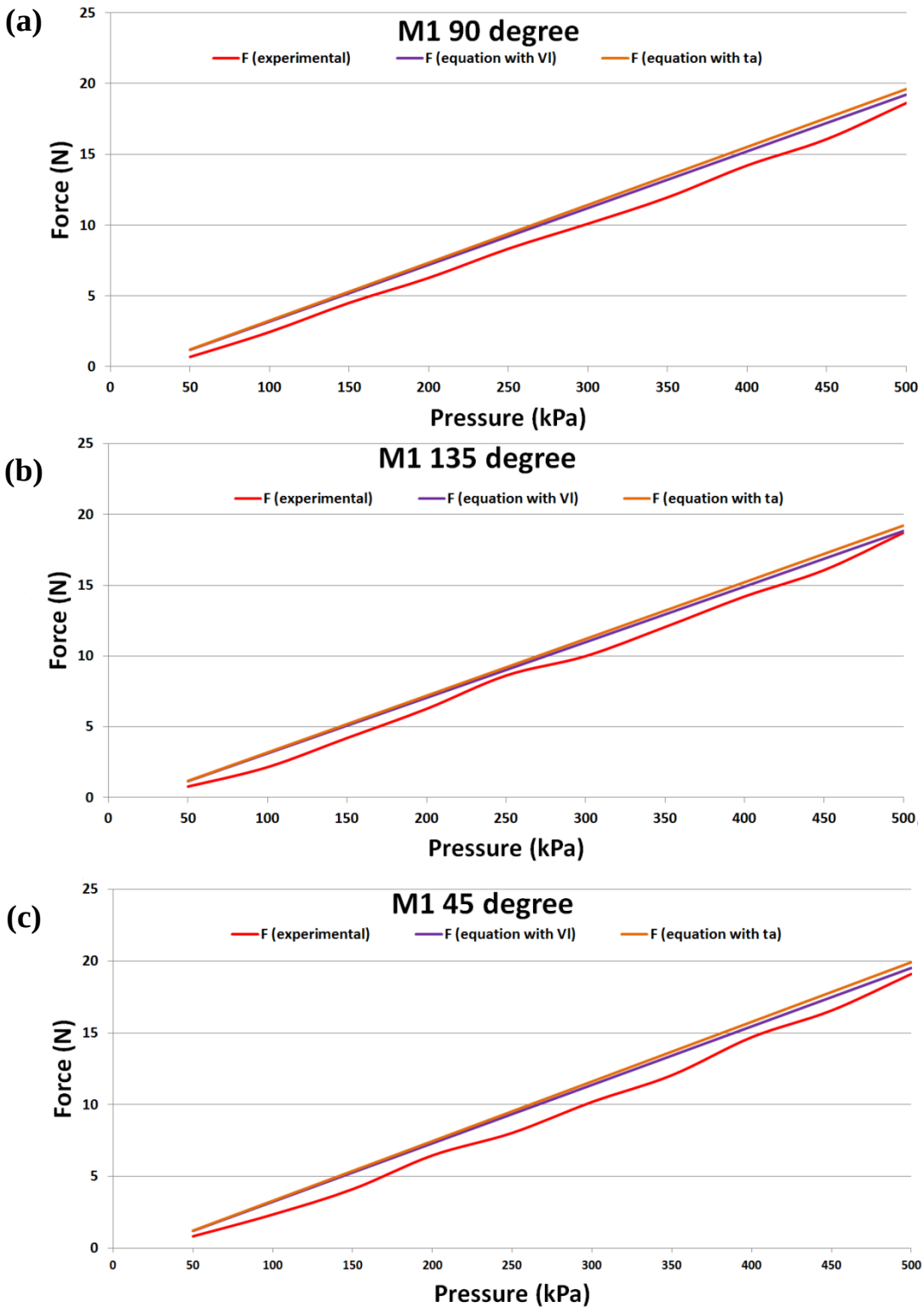

Figure 5.23: Final results of the output force for M1 in consideration with V_l.

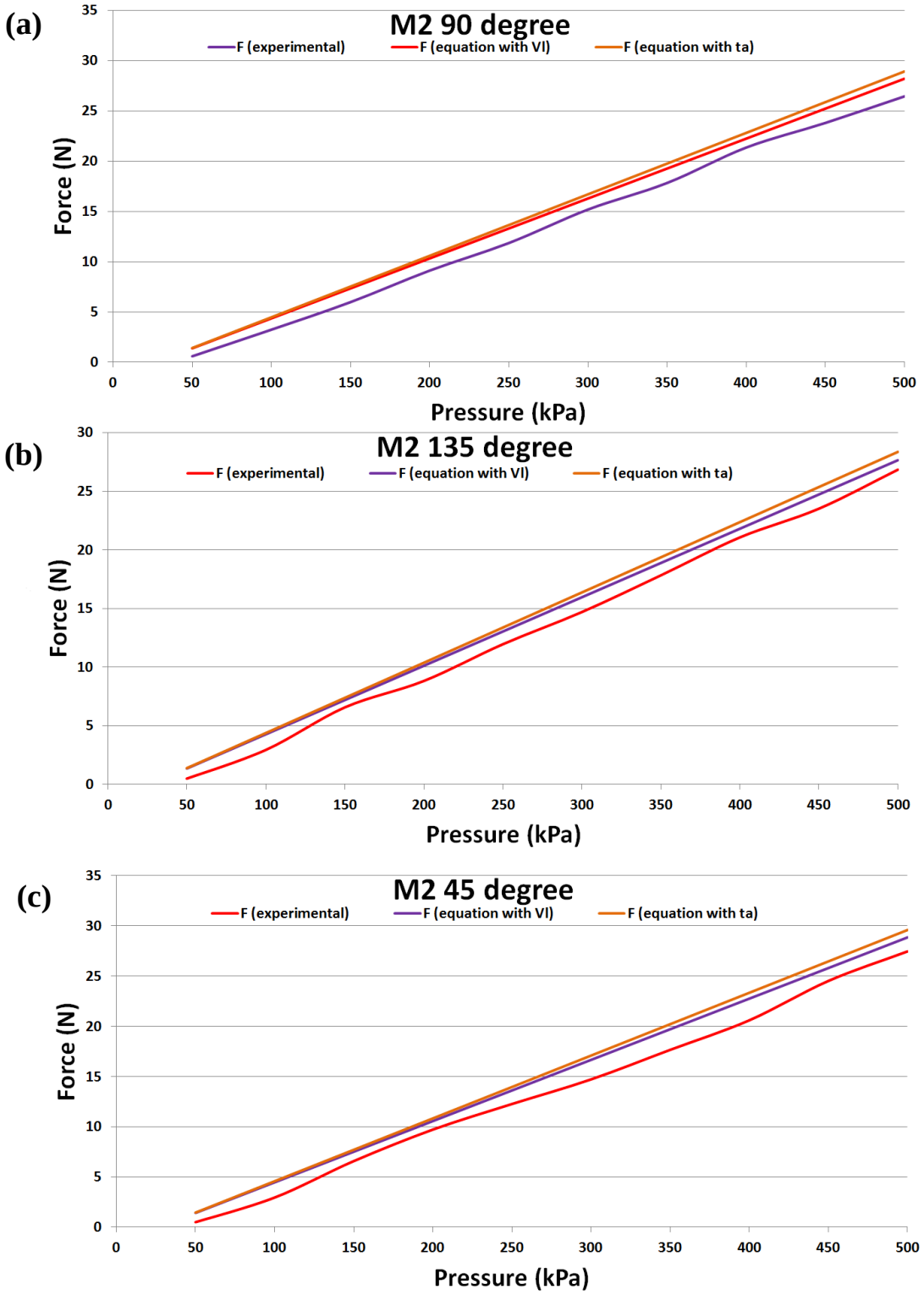

Figure 5.24: Final results of the output force for M2 in consideration with V_l.

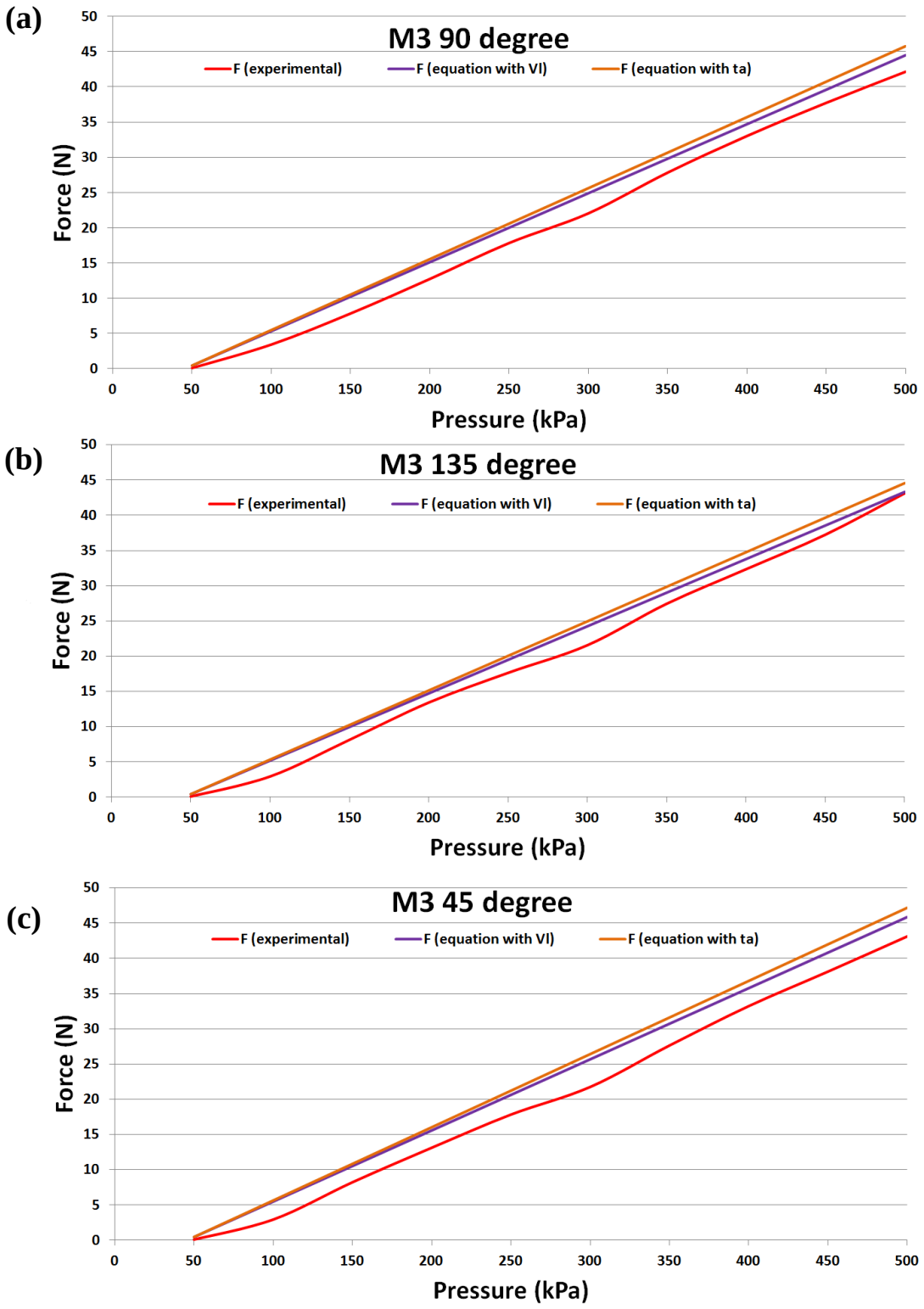

Figure 5.25: Final results of the output force for M3 in consideration with V_l.

Chapter 6

Power Assistive and Augmentation Wearable Robot Based on Soft Actuators

6.1 Introduction

In the increasingly rapid development in wearable robots of recent decades, one important area of innovation has been alleviating heavy tasks (Malcolm, 1996). Human–robot power assistance refers to the utilisation of robotics systems to increase human functionalities in various operations (Kazerooni, 1990). Generally, the power assistance of people's functionalities using robotic systems refers exclusively to augmentation in mechanical abilities, including movement control and limbs output force. This involves complex functionalities and taking advantage of perceptual abilities. There are instances of working conditions in which human–robot assistance can form a fundamental part of the operation, e.g., tasks for wreckage elimination after an earthquake in which human employees wearing such devices can move and work in a more adaptable and precise way than machines, such as excavators or cranes.

This chapter presents the developments in the design of a power assistive and/or augmentation soft glove based on our novel EBPAMs (described in chapter 5). The early version of our glove is capable of multiple gripping and pinching movements. In this glove, we used a simple control algorithm based on a bang-bang controller. A hybrid cascaded position/force intelligent control system has been developed to control the latest version of the glove. These soft exoskeletons are able to fit any adult hand size without the

need for any mechanical system changes or calibration. The potential beneficiaries of the system are post-stroke patients and the elderly who have reduced strength, with the exoskeleton allowing for increased independent daily living. There are potentially significant psychological benefits to be gained from enhanced patient independence.

6.2 Power Assistive Soft Glove

This section will describe the design of a soft wearable glove for power assisted and/or augmentation based on pneumatic soft actuators. The extensor bending type of pneumatic soft actuators was used; an examination of their characteristics proved that these actuators are appropriate. A proposed solution for a release movement is also presented and experimental results show that this solution works efficiently. Electromyography (EMG) signals are monitored to examine the proposed prototype. The proposed glove provides assistive power for multi-griping and multi-pinching movements, depending on the wearer's intention. The elderly, partially disabled and strenuous workers can use this glove. An efficient control algorithm is used which detects signals from sensors located within the glove; these capture the type of movement and bending angle to provide appropriate assistance. A wide range of rehabilitation exercises can be carried out using this soft wearable glove.

To make the glove capable of multiple gripping and pinching movements, pneumatic soft actuators are used as hand exoskeleton muscles to assist finger joints. Our system aims to fit any adult without needing to be changed mechanically. All movements are controlled by the glove's wearer, who is then provided with suitable assistance using electronic sensors to capture the movement and provide the system with enough feedback information. The main contribution of this chapter is to solve the release movement challenge whereby power assistance is active and overcomes the problems with release movements which occurred in many previous research studies. An efficient control algorithm is used to control the proposed system.

6.2.1 The Glove Characteristics

The power assistive glove is a wearable soft glove to assist in gripping and pinching movements. Movements are assisted by placing pneumatic artificial muscles on

the glove's surface. When any movement occurs, the air flow pressurises the muscles to bend to a suitable degree to amplify the hand's power.

The soft actuator proposed to actuate this glove (M1) is the same as that which is described and modelled in chapter 5.

We manufactured a power assistive glove based on the proposed actuator discussed in the previous chapter and our prototype in Figure 6.1. Four bending muscles have been sewed on the back of a standard worker's glove and the air flow is controlled by MATRIX 3/3 solenoid valves. The features of this prototype are that it is: flexible, lightweight (approximately 100g), working to assist most human hand functions, made from good quality materials for a long working life, and containing enough sensors to capture most movements (to be discussed in later sections).

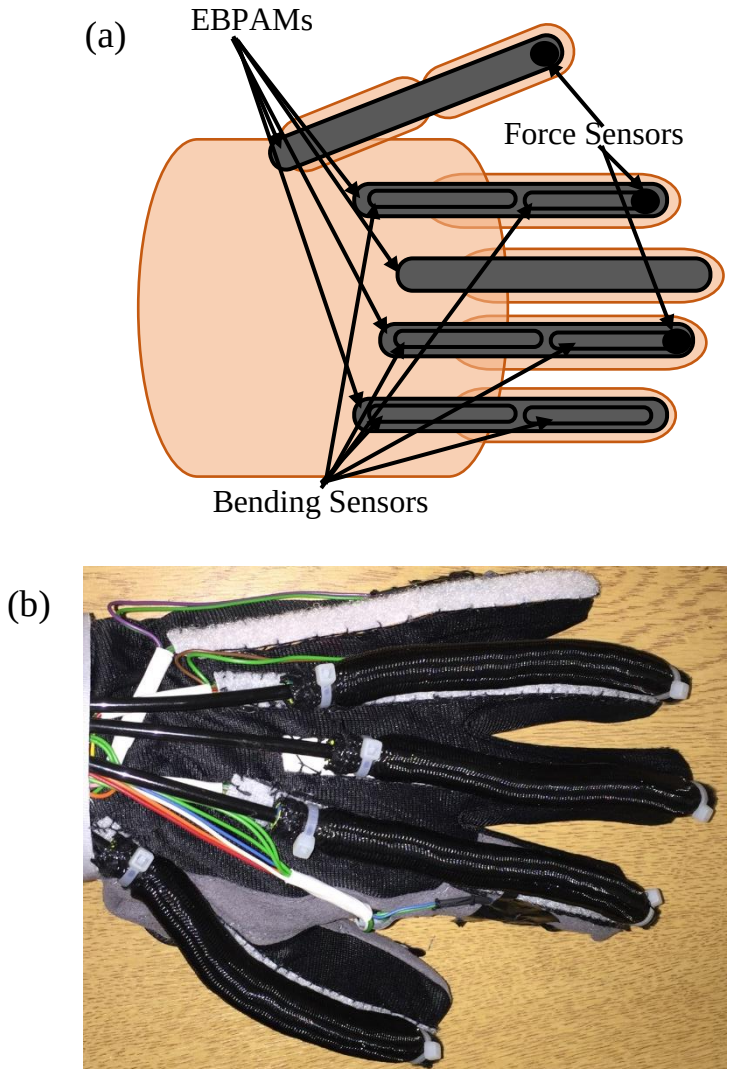

Figure 6.1: Proposed soft glove; (a) The design and (b) The real prototype.

6.2.2 Output Force of the Proposed Prototype

When our prototype was examined, the artificial muscles on the glove were found to be very flexible when no pressure exists whilst the maximum assisting force was 17N at 4bar pressurised. This compares with healthy individuals aged 50 or over who have an average pinching force (on the index finger) of 43N for men and 38N for women (Kadowaki et al., 2011).

This power assistive glove therefore amplifies the healthy person's force by up to 40% - 45% for males and females respectively, and for partially disabled or unhealthy individuals this percentage can be increased depending on the level of neurological damage.

6.2.3 Sensing

The glove sensing data is useful for capturing and collecting enough information about a movement to produce suitable assistance from the controller. There are 6 SparkFun 2.2" flex bend sensors located between the muscles and the glove, as shown in Figure 6.2, and 3 SparkFun force sensitive sensors (sensing area: 0.3") on the other side of the glove. A pressure sensor for each muscle has been placed on the air entrance.

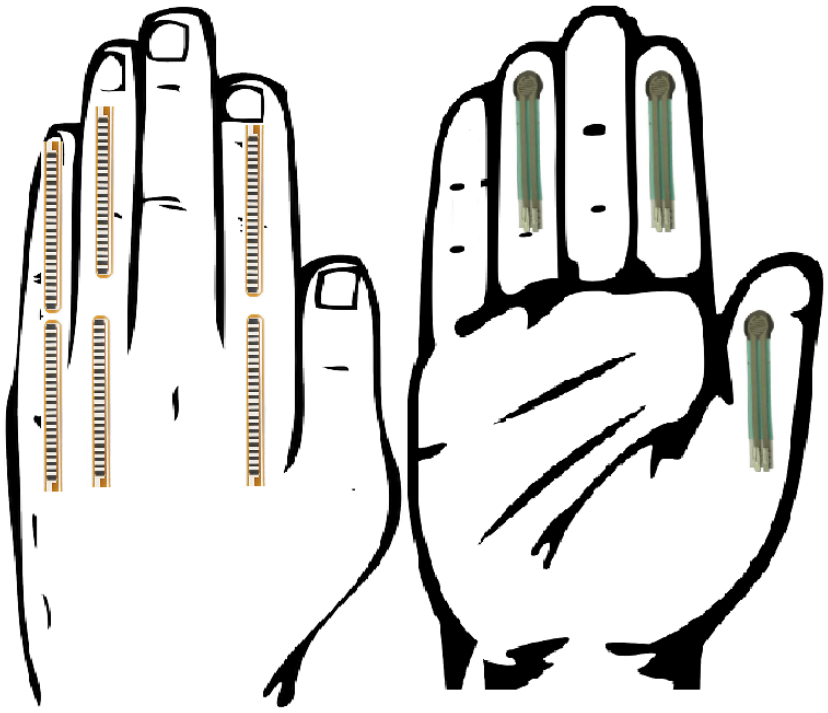

Figure 6.2: Glove sensors.

The force sensitive sensors are used as touch sensors to classify the movement as pinch or grip. If the index and thumb sensors are in contact, and no others are touching them, it is a pinch movement. The index finger's joint angle from the bend sensors is then read to produce suitable pressure. If all touch sensors are touching, the movement is a grip, so the bending data from the flex sensors on the index and ring fingers are then read to recognise the grip angle and produce suitable pressure. There are no sensors on the middle finger because in most daily activities the middle finger's movements are the same as the ring finger's, so we assume both move together in gripping movements. Figure 6.2 shows no bending sensors on the thumb because our assumption is that the thumb moves in relation to the index finger in pinching and gripping movements. We will explain the function of the sensors on the little finger in another section.

6.2.4 Proposed Solution for the Release Movement Problem

The major challenge for power assistive and rehabilitation wearable robots is the release movement, because when assistance is active (muscles are pressurised), the patient or the elderly person cannot produce enough opposite force for a release movement. In other words, if a person grasps something with the glove's assistance, he cannot release it without removing the assistance because his power is less than the assistive power.

Robots were only developed for gripping and/or pinching movements, without any mention of the release movement (Noritsugu, 2005; Noritsugu et al., 2008; Noritsugu et al., 2004; Polygerinos, Wang, et al., 2015; Tadano, Akai, Kadota, & Kawashima, 2010). Using the wearable glove was only used for rehabilitation exercises, it was not important to control the release movement because these were repetitive movements, depending on the time and movement type (Polygerinos et al., 2013; Polygerinos, Wang, et al., 2015; Yap et al., 2015b). According to Toya et al. (2011), the release movement problem was solved by estimating the average duration of the pinching or gripping movements, which was not an efficient solution because there is no fixed time for grasping something for every person, and therefore it is impossible to estimate that time for multiple people. Finally, researchers faced this problem and tried to solve it by using EMG characteristic signals, but found that this was not an efficient solution because the EMG signals of attempted release movements can conflict with other EMG signals, such as wrist movement signals (Kadowaki et al., 2011; Polygerinos, Galloway, et al., 2015; Sasaki et al., 2014).

Our proposed solution to the release movement problem is to leave the little finger without assistive muscle, as shown in Figure 6.2. The little finger is free to move because there is no opposite assisted force exerted on it. When a gripping movement is made, all fingers are bending; and when a release movement is made, only the little finger will move. The controller understands this is a release movement and orders the muscles to move in relation to the little finger, depending on the sensors in the little finger (Figure 6.2).

6.2.5 Proposed Control Algorithm

Figure 6.3 shows the block diagram of the control system.

We designed a control algorithm that works efficiently in most movement situations. It is done by using two bang-bang closed loop controllers. The algorithm for the bang-bang controllers can be written as follows (Kaitwanidvilai & Parnichkun, 2005; Verrelst et al., 2005; Zhang et al., 2008):

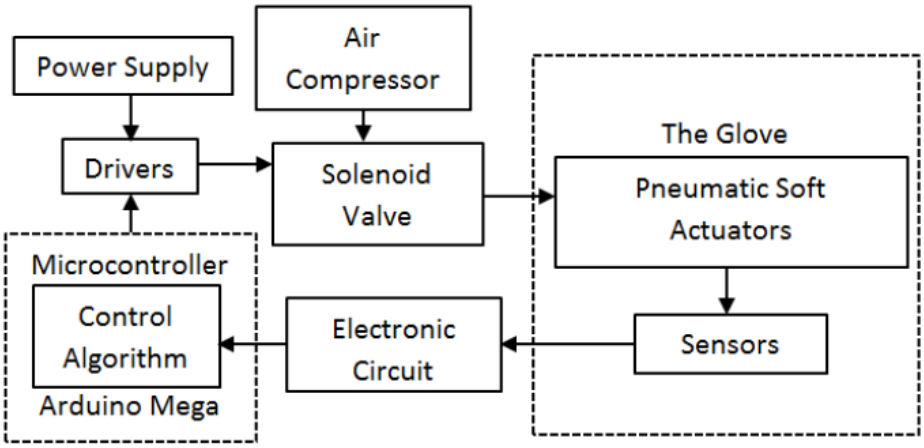

Figure 6.3: Control system.

$$y = \begin{cases} F \; if \; feedback \leq set\ point - \epsilon \\ 0 \; if \; set\ point - \epsilon < feedback < setpoint + \epsilon \\ V \; if \; feedback \geq set\ point + \epsilon \end{cases}$$

Where y is the controller output, F is a valve fill, V is a valve vent, and ϵ is a small constant. Figure 6.4 shows a flowchart of the proposed control algorithm; the initial state is all muscles unpressured. After that, whether the movement type is pinch or grip, it's

recognised by a feedback signal from the touch sensors on the thumb, index and ring fingers, respectively. The touch is recognised by a threshold force with each touch sensor.

If the movement is a pinch, then the pinch movement controller is started, the pressure point is set as the pinch movement comes from the bending angle of the index finger and the feedback signals come from the pressure sensors of the assisting muscles placed on the index and thumb fingers. The release pinching movement is made when the little finger starts to unbend. Then the system starts to check again for any further movement.

If the movement is gripping, the same pinching procedure will work, but the grip movement controller will start; the pressure set point of the controller comes from the bent angles of the ring finger, and the feedback signals come from the pressure sensors of the assisting muscles on all fingers. The grip is released when the little finger starts to unbend. Then the system starts to check again for any further movement.

EMG signals from the hand are monitored. Figure 6.5 (a) shows the experimental results of EMG signals for hand grip carrying a 0.5 kg weight. Figures 6.5 (b) and (c) show the signals of the same hand carrying a weight with all fingers assisted, and only four fingers assisted, without assistance for the little finger, respectively. These results proved that the EMG signals for full hand assistance show a decrease in muscular fatigue. Moreover, the full assistance and assistance without the little finger are almost the same, proving that our release movement solution has no effect on muscular fatigue.

6.3 Power Augmentation Hand Exoskeleton based-on Human Intention

This section presents our developed version of a soft materials power augmentation wearable robot, dependant on soft artificial muscles. The previous version (section 6.2) is used as a power assistive glove for elderly people who have hand muscle weakness, not as a power augmentation glove for healthy individuals. This soft exoskeleton has been developed as a human hand power augmentation for healthy or partially hand disabled individuals with high augmentation force. The proposed prototype serves healthy manual workers by decreasing the muscular effort for grasping objects. Furthermore, it is a power augmentation wearable robot for partially hand disabled or post-stroke patients, supporting and augmenting the fingers' grasping force with minimum muscular effort in most everyday activities.

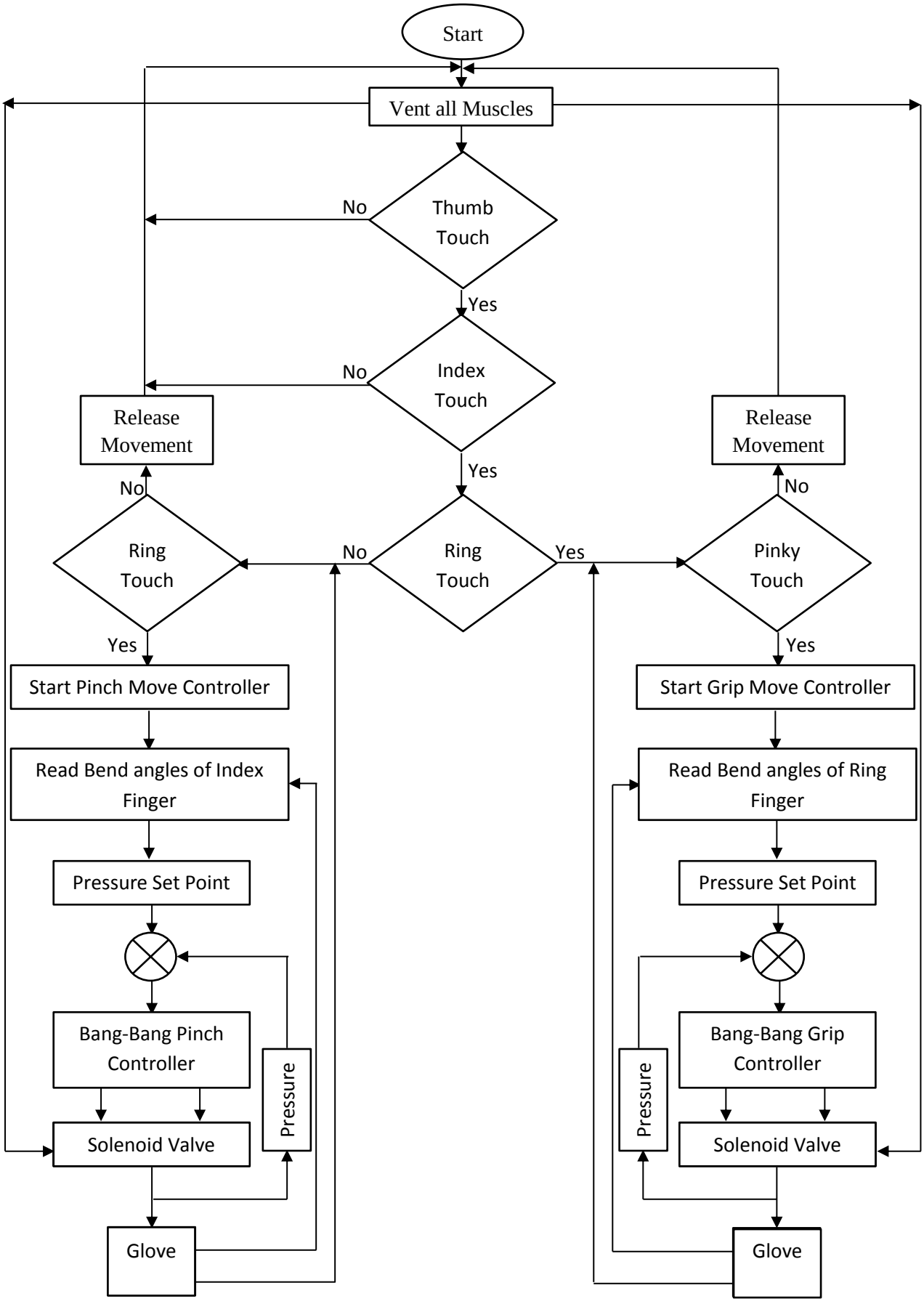

Figure 6.4: Proposed control flowchart.

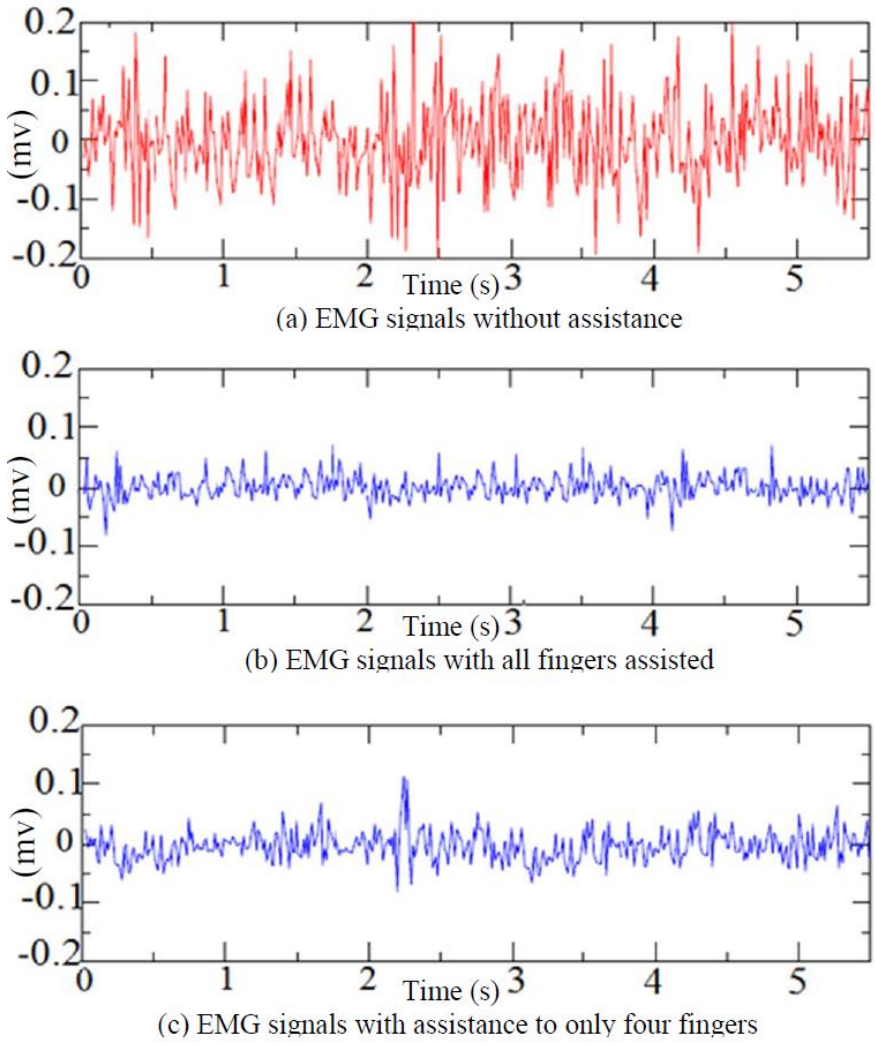

Figure 6.5: Hand EMG signals.

The control system for this exoskeleton is more accurate and more advanced than the previous version and the controller developed has been created by hybridisation between cascaded position and force closed loop intelligent controllers. The cascaded position controller is designed for the bending actuators to follow the fingers in their bending movements and the force controller is developed to control the grasping force augmentation. The operation of the controller system with the exoskeleton has been experimentally validated. EMG signals were monitored during the experiments to determine whether the proposed exoskeleton system decreased the muscular efforts of the wearer.

This glove was manufactured, and the muscles were attached, using the same method as described for the previous prototype. The soft bending actuator M2 is used to construct this prototype (see chapter 5).

The power augmentation soft glove was constructed based on the proposed bending actuator, as shown in Figure 6.6. Four bending actuators are reinforced (sewn) on the back surface of a traditional worker's leather glove; one muscle for each finger except the little finger. The air supplied for all muscles is controlled by a solenoid valve type MATRIX 3x3. The proposed soft exoskeleton glove has a weight of approximately 0.12 kg.

The proposed exoskeleton sensing data is helpful in catching and gathering enough data about a hand motion to create appropriate assistance by the controller. There are two (2.2 inch) flex bend sensors, placed between the soft actuator and the glove, on the index finger joints; one bend sensor to capture the bending angle of the root of the finger is named the MP joint (Metacarpophalangeal Joint) and the others are for the PIP middle joint (Proximal Interphalangeal Joint) and the DIP terminal joint (Distal Interphalangeal Joint). As the assumption of our controller is that all fingers bend together at the same time for a full grasping movement, the index finger flex sensors provide the feedback of the grasp movement angle of the hand. The force sensitive sensor (sensing area: 0.5") on the front side of the glove (on the index fingertip) is also reinforced. This sensor is attached to give feedback on the tactile pressure force of the index finger when grasping an object. An air pressure sensor is attached to the soft bending actuators for live feedback of the pressure inside the glove muscles.

Figure 6.6: The proposed power augmentation exoskeleton.

The proposed solution of the release movement problem is to leave the little finger without any assistance muscle (similar to the solution of the release movement problem which is discussed in section 6.2.4).

Instead of the assistive muscle, we placed a flex bend sensor (size 4.4”) on the back of the little finger to provide the controller with real-time feedback on the little finger bending angle. As usual, when grasping an object, all the fingers will bend and the controller will start working.

If we need to release the object, first we release the little finger (because it is free of assisted force) then, depending on the angle of the little finger reaching a zero-bend angle, the controller will understand that it is a release movement, then deflate all actuators.

6.3.1 The Proposed Control Algorithm with Experimental Results

In all events, the control precision and stabilisation of the pneumatic actuator (for example, pneumatic cylinder or McKibben muscle) presents a major challenge due to both the nonlinear working behaviour and the compressibility of air. The classic control techniques are regularly created via simple models of the actuator functionality that fulfil the important assumptions, and through the uncommon tuning of comparatively basic linear or nonlinear controllers.

Figure 6.7 illustrates the proposed controller system flowchart. The initial state of the control system has vented all actuators (all bending muscles with zero air pressure). The next state is reading all sensors: flex bend sensors (on the index and little fingers), the force sensitive sensor on the index fingertip, and the pressure sensor.

The first conditional block in the proposed algorithm is testing the little finger’s bending angle (if the little finger’s bending angle = 0). If there is no bend or return to the straight position, the release movement state will occur as explained in the previous section. If there is bending in the little finger, the next condition continues. The second condition is to test the force sensitive sensor whether the index fingertip is in contact with the object or not (the force > 0). If there is no force applied, the position controller starts; if there is a force, the force controller starts. In other words, when the wearer needs to grasp an object, the wearer starts to bend his/her fingers to touch the object (in this case, the position controller system actuates the muscles to follow the fingers until the fingers are in contact with the object, then the controller system stops the position controller and switches on the force controller, depending on the index fingertip press force).

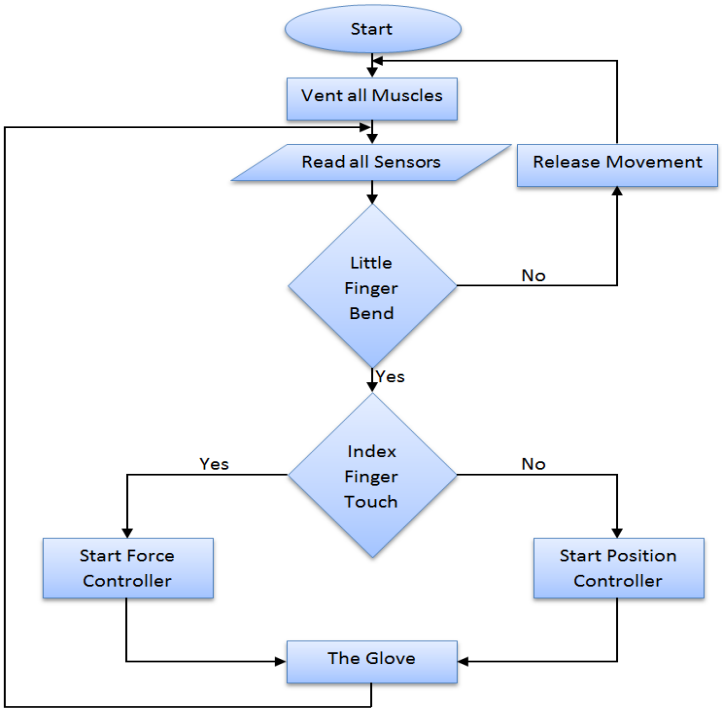

Figure 6.7: The flowchart of the proposed control algorithm.

6.3.2 The Position Controller System

An assumption is made in this work that all bending actuators follow the bending angle of the index finger (all fingers bent at the same time and their angles based on the index finger bending angle). This assumption does not limit the fingers movements when grasping cylindrical or spherical objects; when grasping other shaped objects, the force on the fingertips will vary by small amounts depending on the shape of the object grasped. It is not difficult to place flex bend sensors on all fingers and copy the proposed controller for each finger, but that will increase the cost of the proposed exoskeleton and also increase the processing controller response time. Figure 6.8 shows the proposed position control system block diagram.

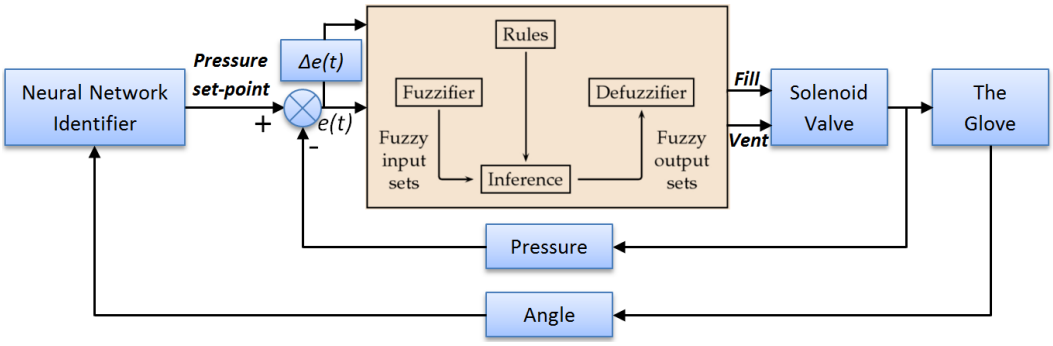

Figure 6.8: The block diagram of the proposed position controller system.

The computational burdens of the NN identifier and Fuzzy controller, from the viewpoint of real-time implementation, are acceptable because the control system is simple and the NN is already trained. The control system is implemented by Matlab and there is no noticeable delay occurring in real-time interface operations.

6.3.2.1 The Neural Network Identifier

The first block of the proposed position control system is the neural network identifier. This block is used to generate the appropriate pressure set-point for the position controller, depending on the online feedback signal of the index finger bending angle. This neural network identifier is designed by the Matlab neural network data fitting application. The experimental data, from the relationship between the actuator bending angles and the amount of supplied pressure, are used to design this identifier. The network includes one input layer, four hidden layers and one output layer. The Bayesian Regularisation (Demuth et al., 2014) training technique is used to train the proposed neural network identifier. It is a network training technique that updates the weight and bias values according to Levenberg-Marquardt optimisation. It minimises a combination of squared errors and weights and then determines the correct combination so as to produce a network that generalises well. Figure 6.9 illustrates the results of this identifier and the error between the targets and outputs.

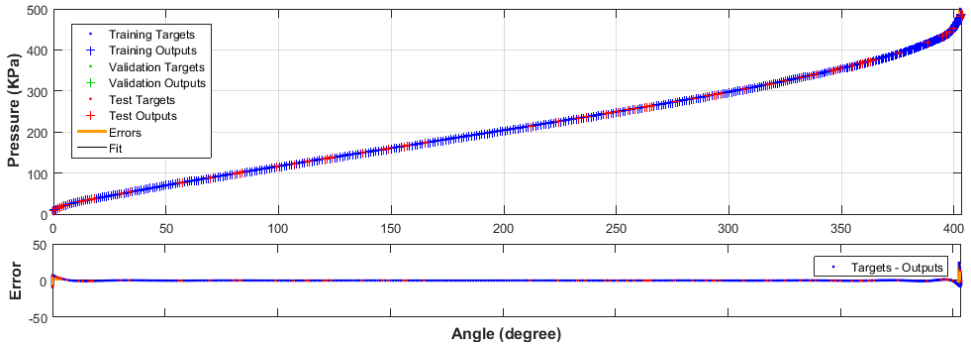

Figure 6.9: Results of the neural network identifier and the error of the targets and outputs.

6.3.2.2 The Fuzzy Logic Controller of the Position Controller

A Fuzzy logic controller is used in the proposed position control system to control the pressure amount inside the bending muscles. The desired pressure set-point for each bending angle comes from the neural network identifier (real-time feedback signal). This Fuzzy controller has two inputs (error and change of error) and two outputs (fill and vent).

As we used a MATRIX 3x3 solenoid valve to control the air flow by PWM (Pulse Width Modulation), the same valve output can fill and vent by applying two separate PWM signals. Based on this, the Fuzzy controller has two outputs to control the percentage of the PWM duty cycle for each filling and venting signal. The valves are pulse width modulated at a frequency of 125Hz and this allows the flow of air through the valve to be regulated. A 3-3 valve has three states of operations: i) regulating the filling air pressure; ii) regulating the venting air pressure and; iii) holding a specific air pressure inside the actuator when the controller is stable. These three operations are controlled by the control system. Figure 6.10 shows the membership functions of the inputs and outputs of the fuzzy controller.

There are five ranges for the input error and five ranges for the change in error, with the entire range being -200 to 200 because during experiments the proposed actuator, when placed on the index finger, reached its maximum angle at less than 200KPa pressure. Likewise, there are three intervals for the PWM fill output percentage and the same for vent output. All membership functions are the triangle type for simplicity, but the membership functions of the error input are smaller intervals, close to zero. This serves to diminish the gain of the controller close to the desired set-point, achieve superior stability, and avoid excessive overshoots on the controller response. Figure 6.11 demonstrates the Fuzzy controller rules surface of each fill and vent output.

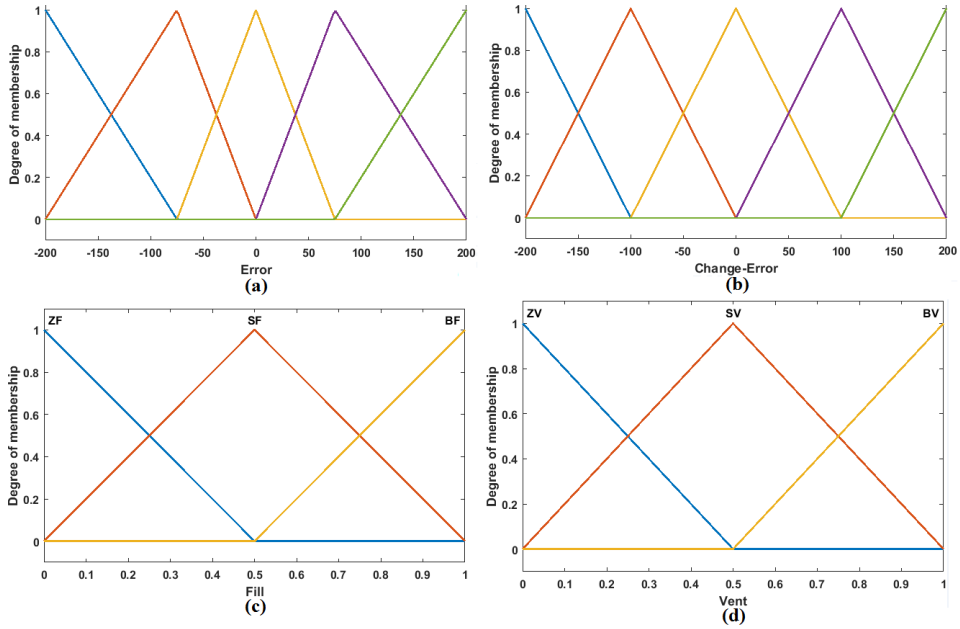

Figure 6.10: The membership functions for the inputs and outputs for the Fuzzy controller of the proposed position controller; where NB is Negative Big, NS is Negative Small, Z is Zero, PS is Positive Small, PB is Positive Big, ZF is Zero Fill, SF is Small Fill, BF is Big Fill, ZV is Zero Vent, SV is Small Vent and BV is Big Vent.

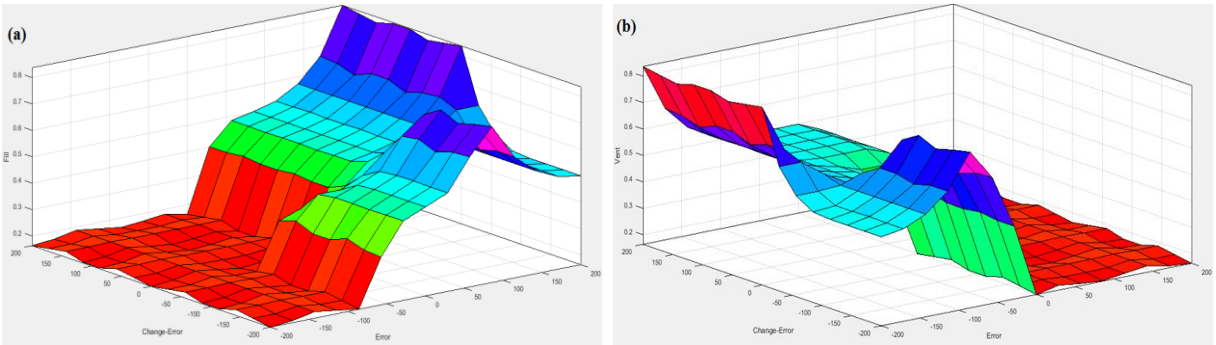

Figure 6.11: Fuzzy controller rules surface for each fill and vent output of the proposed position controller.

The proposed position controller is examined experimentally. Figure 6.12 shows the experiment results of the controller at various bending angles. These six experiments were done by grasping cylindrical shaped objects with different diameters, to reach the grasping angles of 38^{o}, 64^{o}, 90^{o}, 122^{o}, 144^{o} and 170^{o}; they are represented in Figure 6.12 (a to f), respectively.

6.3.3 The Force Controller System

The proposed force controller is based on the assumption that the applied touch force from the fingertips to the grasped object is equal for all fingers, depending on the index fingertip force (see Figure 6.13). The main purpose of the proposed controller is to decrease the muscular effort of the wearer when grasping an object. The wearer needs only to apply press force on the object with the index fingertip (the wearer estimates the amount of this press pressure) and then rests the hand. Then the controller gives feedback and calculates the maximum amount of this pressing force. This maximum press force will be added to the bent force (the bent force to reach the position at the moment of touch on the grasped object) to provide a force feedback signal to the controller system. The bent force is calculated by the kinematic analysis equations of the bending actuator. Substitute the bending angle of the actuator (it is constant when fingers are in contact with the grasped object) in these equations to calculate the sleeve strain angle θ and we have the amount of the pressure inside the actuators at the moment of touching, to calculate the bent force by using the proposed output force model in Equation 5.38. After adding the bending force to the maximum touch force, we now have the desired force of the single fingertip and the strain angle θ; then we calculate the desired pressure set-point of this pressing force, again by using Equation 5.38.

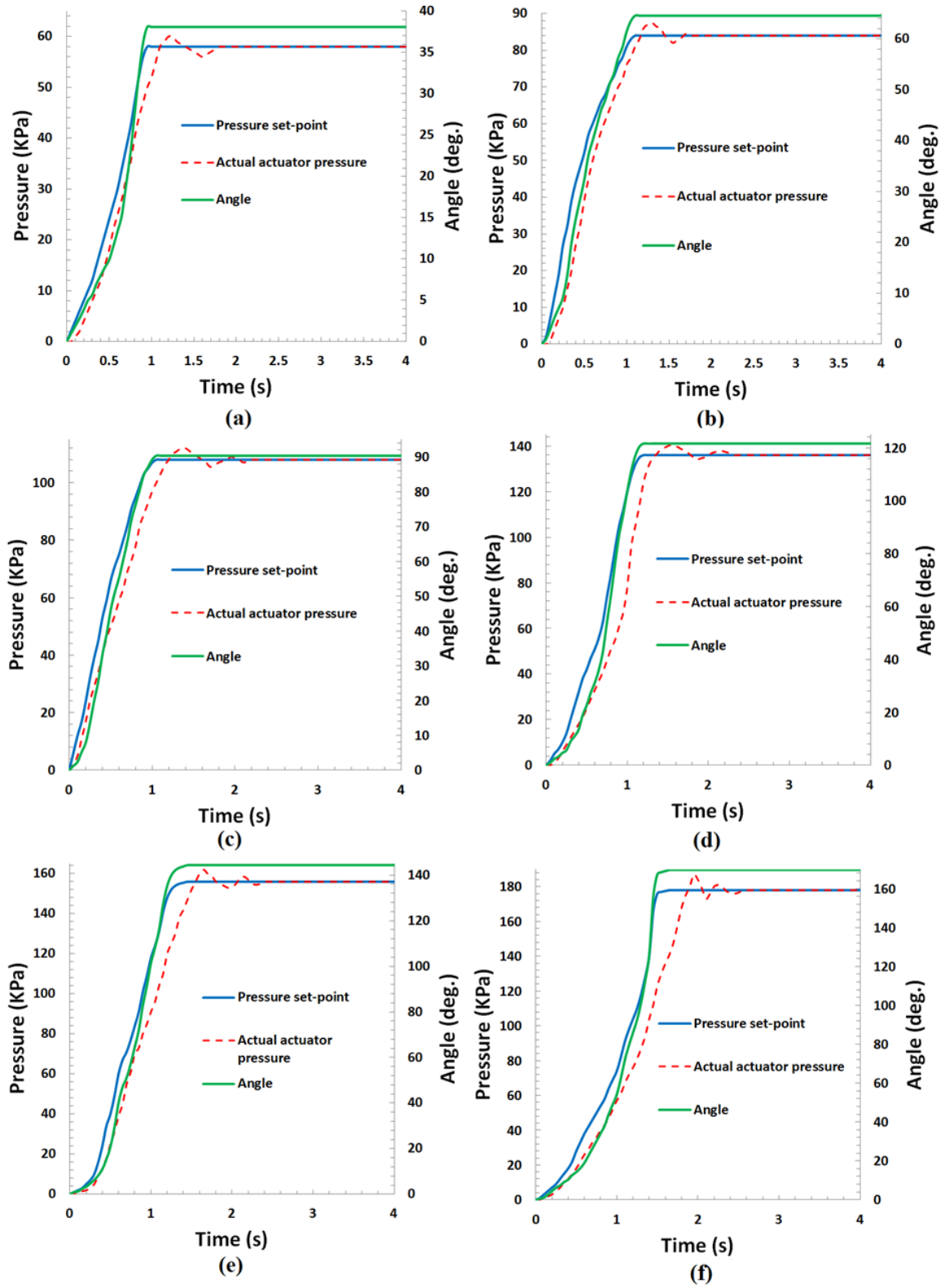

Figure 6.12: The experimental results of the position controller system.

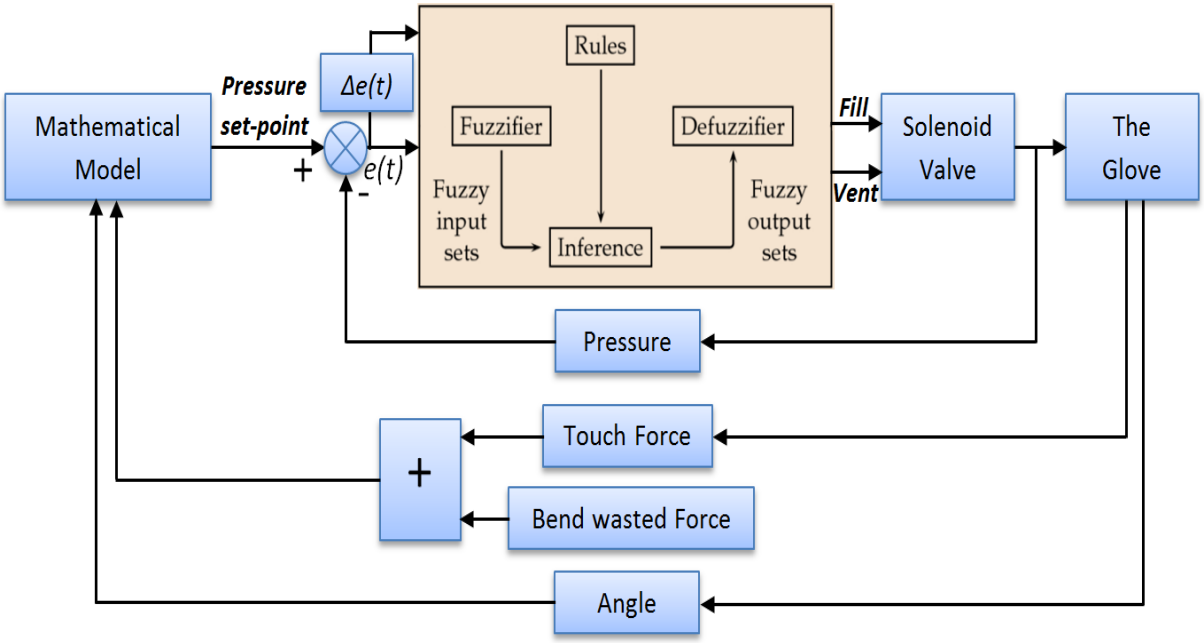

Figure 6.13: The proposed force controller.

Using the same technique as the Fuzzy controller of the position controller system, we designed the Fuzzy controller of the force controller system. This Fuzzy controller has two inputs (error and change of error) with seven membership functions of each input; and two outputs (fill and vent) with four membership functions for each output, as shown in Figure 6.14. Figure 6.15 illustrates the Fuzzy controller rules surface of each fill and vent output in this controller.

The proposed force controller has been tested using six different experiments which to examine the performance of the proposed controller system, as shown in Figure 6.16. These experiments were done by grasping three different cylindrical objects then applying a pressing force from the index fingertip to the object. Figures 6.16 (a) and (b) show the results of grasping to reach a bending angle of approximately 64°. The press index fingertip forces approximately 5.1N and 14.9N, respectively, with a bend wasted force of 5.73N (is the amount of force that needed to bend the fingers until the fingertips be in contact with the object). Other bending angles were also tested with different press forces for validation, as shown in Figures 6.16 (c) to (f).

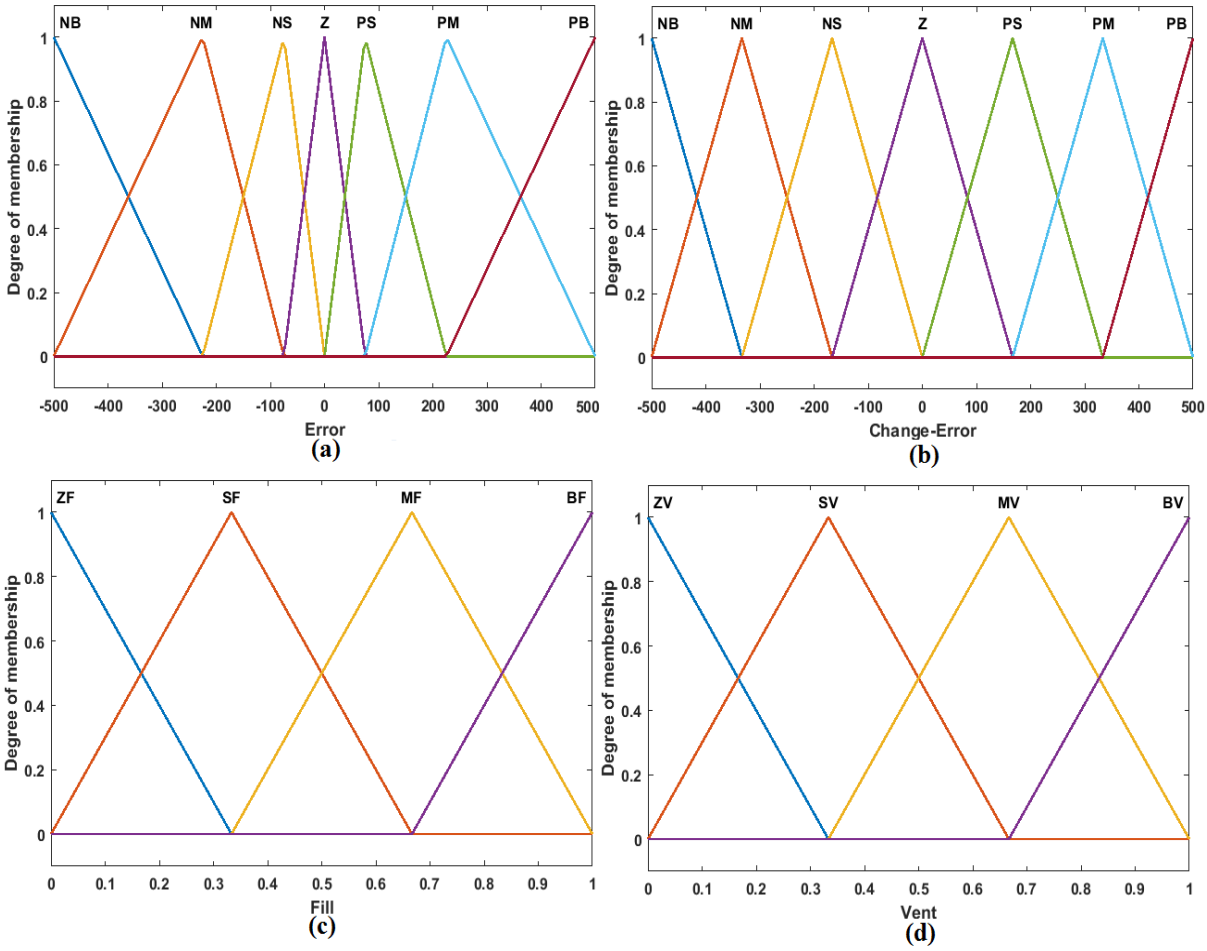

Figure 6.14: The membership functions for the inputs and outputs for the Fuzzy controller of the proposed force controller.

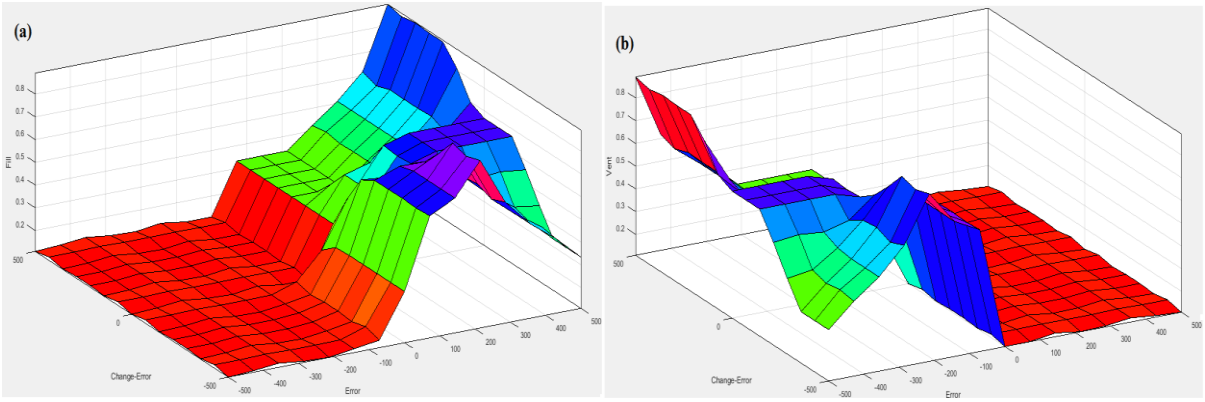

Figure 6.15: Fuzzy controller rules surface for each fill and vent output of the proposed force controller.

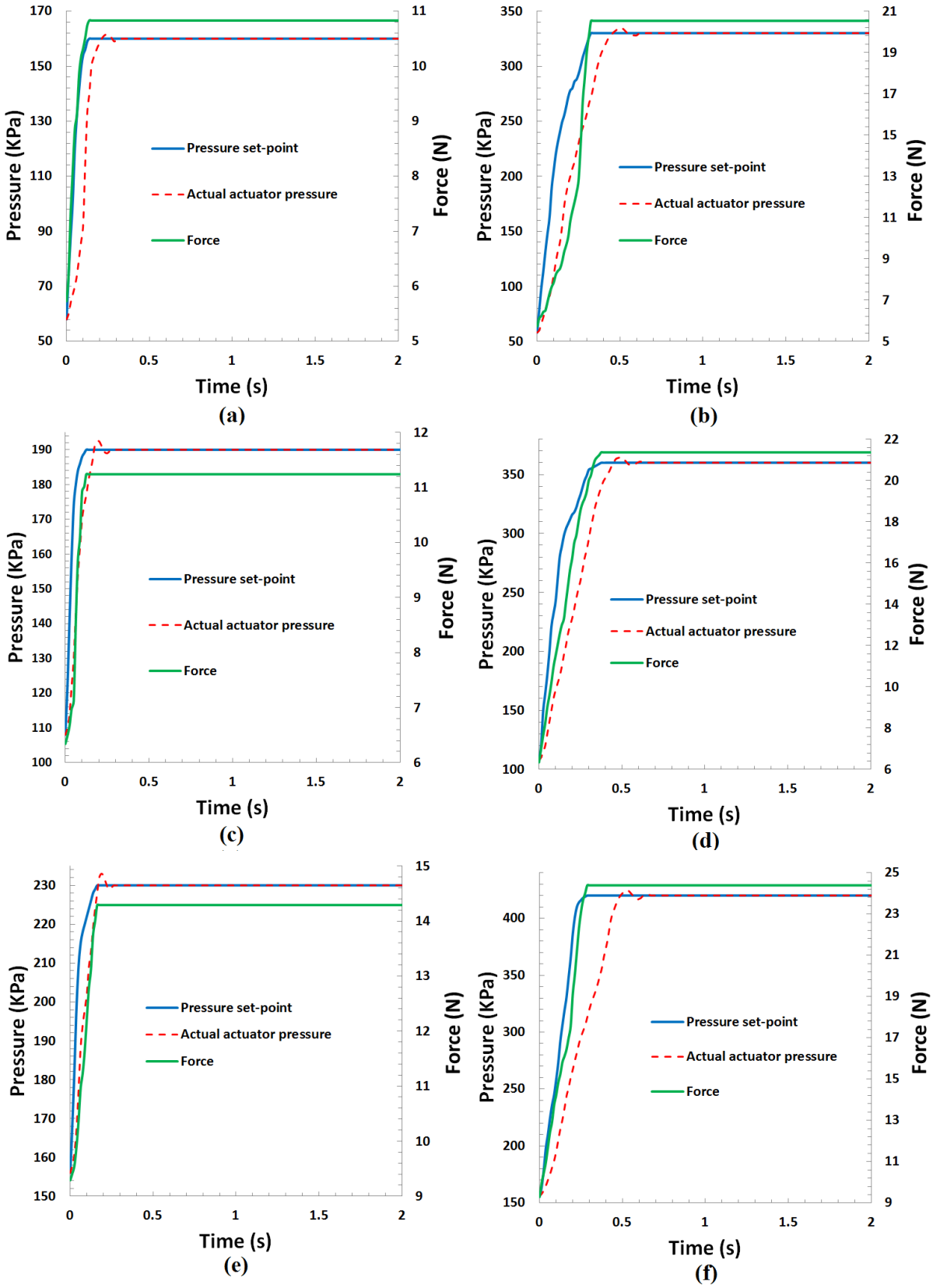

Figure 6.16: The experimental results of the force controller system.

6.3.4 The Validation of the Proposed Exoskeleton and its Controller

The validation of the proposed exoskeleton and its controller have been proven experimentally, as shown in Figures 6.17. Figure 6.17 (a) shows a human wearing the power augmentation exoskeleton and grasping to apply force on a load cell, where the hand fingers bending angle was 120^{o}. Muscular effort and fatigue cause a corresponding increase in muscle activation amplitude, measured with electromyography (EMG) (Graham, Wachowiak, & Gurd, 2015). Based on previous research, such as (Kadota et al., 2009; Noritsugu, 2005; Noritsugu et al., 2008; Polygerinos, Galloway, et al., 2015; Sasaki et al., 2005a; Tadano et al., 2010), there is a noticeable increase in EMG amplitude due to the increase in muscular efforts. EMG signals were monitored to demonstrate the muscular effort during the experiment without wearing the exoskeleton, as shown in Figure 6.17 (b), and with wearing the exoskeleton, as shown in Figure 6.17 (c). The fingers' bending angle was recorded, as shown in Figure 6.17 (d). The desired pressure set-points and the actual pressure inside the actuators are illustrated in Figure 6.17 (e). Figure 6.17 (f) shows the index fingertip press force and the total applied force on the load cell.

We divided the experiment figures into six regions (R1, R2, R3, R4, R5 and R6) to simplify what happened during the entire experiment:

- *Region R1:* the wearer wears the exoskeleton with straight fingers without any movements.

- *Region R2:* the wearer curls the fingers to touch the bar and the load cell, meanwhile the position controller is active, and the bending muscles follow the fingers until touch occurs at a bending angle of approximately 90^{o}; we can note the slightly increased muscular effort from the EMG signals because of the fingers' movement.

- *Region R3:* the wearer touches the bar and the load cell and briefly presses with the index fingertip to apply force on the force sensitive sensor. Meanwhile, the force controller is working to reach the desired force; it is obvious from Figure 6.17 (c) that in this region the muscular effort is at its maximum during the entire experiment because of the effort of the fingertip when pressing on the bar.

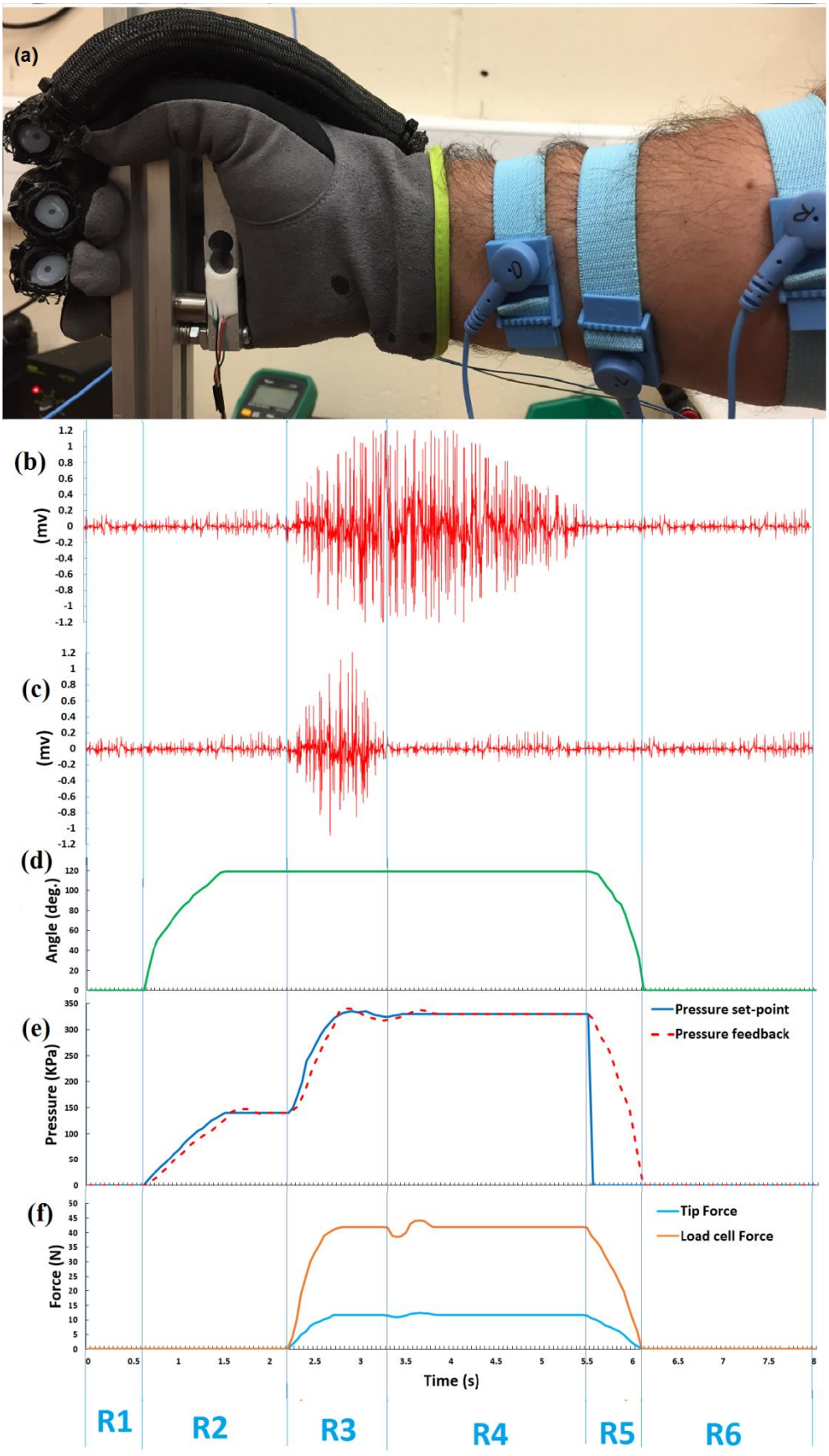

Figure 6.17: The validation experiment of the proposed prototype at grasping bending angle approximately 120^{o}.

The load cell force in Figure 6.17 (f) is higher than the applied index fingertip force (approximately four times), because the applied force on the load cell comes from four fingers (index, middle, ring and thumb), with their assistive muscles.

- *Region R4:* the wearer rests his muscles and the exoskeleton performs the grasping function with the desired force, and the proof of that is the muscular effort signals in Figure 6.17 (a) in this region.

- *Region R5:* the wearer releases his little finger to the straight bending angle, then the release movement procedure becomes active, venting all muscles to zero pressure.

- *Region R6:* the wearer's fingers are straight again without any movement (as in R1) and the controllers standby for another movement.

It is clear from Figure 6.17 (b) that the highest muscular effort occurs along grasping periods R3 and R4. However, with the glove assistance (Figure 6.17 (c)), the highest muscular effort only occurs along R3, and that proves our theory that the wearer only needs to expend considerable effort at the beginning of grasping by pressing their index fingertip on the object. The exoskeleton will then apply the appropriate assistive force and the wearer's hand can rest (the lowest muscular effort regions).

Three statistical features from the time domain are used in evaluation Daud, Yahya, Horng, Sulaima, and Sudirman (2013). Time domain features can be implemented in real-time and are usually used for detecting muscle contraction, muscle activity and onset detection. The three statistical features, based on time domain, are described as follows:

- *Maximum amplitude*: Maximum amplitude (MAX) is defined as the peak amplitude of a signal.

- *Standard deviation*: Standard deviation (SD) measures the spread of data from the mean. In signal processing, SD represents noise and other interference. It is used in comparison to the mean. This leads to the term: signal-to-noise ratio (SNR), which is equal to the mean divided by the standard deviation. Better data means a higher value for the SNR.

- *Root mean square*: Root mean square (RMS) is another feature that is popular in EMG signal analysis. RMS is defined as the square root of the mean over the time of the square of the vertical distance of the graph from the rest state, related to the constant force and non-fatiguing contraction of the muscle. In most cases, it is similar to the standard deviation method.

Figure 6.18 illustrates these three EMG features for Figures 6.17 (b) and (c). Figure 6.18 (a) shows the EMG signal analysis of the naked hand when grasping an object (experiment on Figure 6.17 (b)), to prove that the high muscular effort is during grasping periods R3 and R4. Figure 6.18 (b) shows the EMG signal analysis of a human wearing the power augmentation exoskeleton and grasping to apply force on a load cell (experiment on Figure 6.17 (c)), to prove that the high muscular effort is occurring only when pressed by the wearer's index fingertip on the load cell (R3). This analysis supports our validation of the power augmentation glove by serving the aim of augmenting or assisting the wearer's human hand whilst grasping objects.

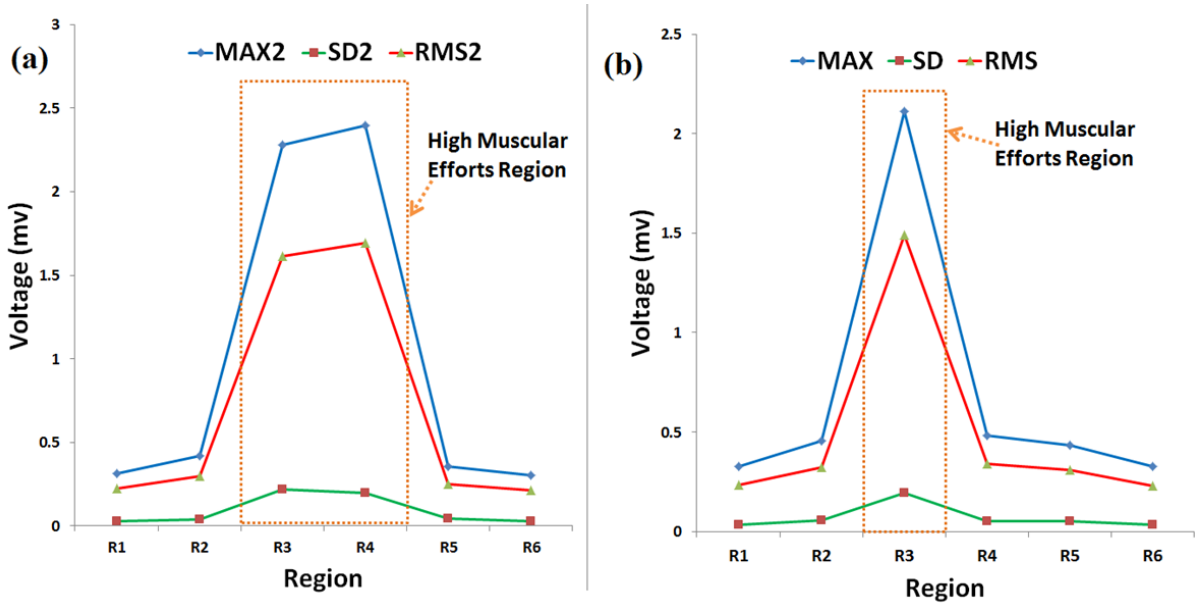

Figure 6.18: EMG signals analysis of grasping an object with a 120^{o} bending angle of the human hand.

The same experiment and analysis were repeated at the fingers bending angles of approximately 90^{o} with different index fingertip pressing force, as shown in Figure 6.19 and 6.20.

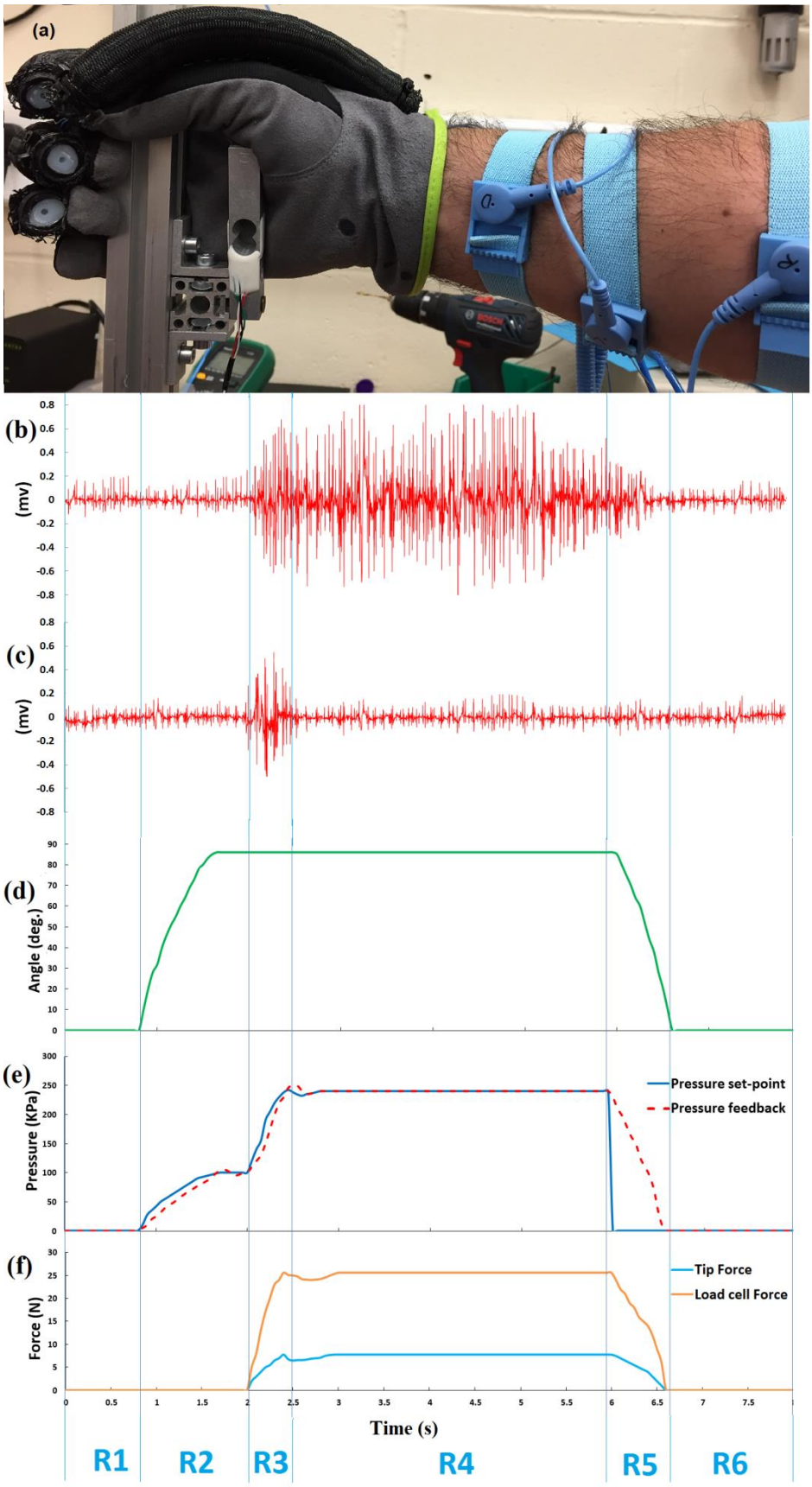

Figure 6.19: The validation experiment of the proposed prototype at grasping bending angle of approximately 90^{o}.

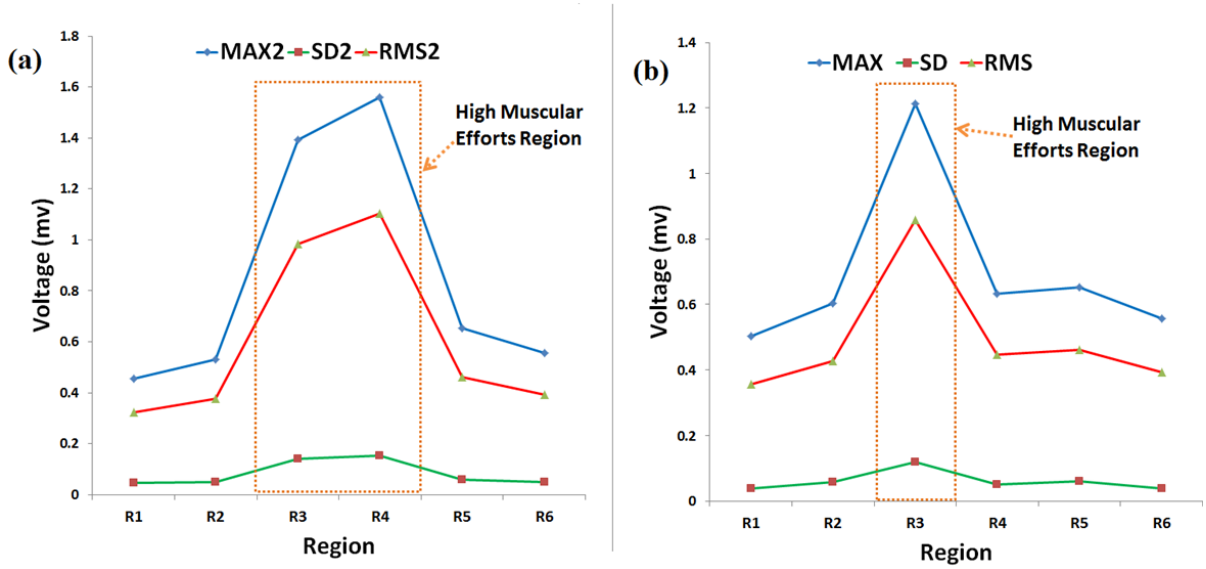

Figure 6.20: EMG signals analysis of grasping an object with a 90° bending angle of the human hand.

6.4 Conclusion

This chapter presents the preliminary stages of developing a wearable power assistive glove based on pneumatic soft actuators, where curved type artificial muscles are used. The proposed prototype outputs 17 N maximum force at the fingers for bending at 4 bar, showing that the assistive amount is up to 40% and 45% respectively for healthy men and women over 50. An efficient solution for the release movement problem is presented. EMG signals from the hand are monitored to clarify that solution. The proposed control algorithm gives a high performance of multiple gripping/pinching movements, assisted by pressure sensors as a feedback signal, and using bending joint angles as the set-points.

This chapter also demonstrates a developed version of power augmentation hand exoskeleton. The proposed bending soft actuators also actuate this exoskeleton. The control system of this exoskeleton was created by hybridisation between both the cascaded position and force closed loop intelligent controllers. The cascaded position controller is designed for the bending actuators to follow the fingers in their bending movements. The force controller was developed to control the grasping force augmentation. Validation of the controller system with the exoskeleton has been done experimentally in this research. EMG signals were monitored to validate whether the proposed exoskeleton system decreased the muscular efforts of the wearer during the experiments.

Chapter 7

Upper-Limb Rehabilitation Exoskeletons

7.1 Introduction

According to literature reviews, numerous researchers are focusing their attention on rehabilitation devices (Sarasola-Sanz et al., 2017). Wearable robots developed for physiotherapy are now being considered for various applications, for example, clinical and at-home rehabilitation (Long et al., 2017). The most common human hand disabilities which effect people are: spasticity, loss of control, muscle weaknesses as a result of a stroke, disability or muscular injuries. Cerebrovascular accidents (CVA) and spinal cord injuries (SCI) are currently the most common causes of paralysis. Stroke survivors frequently suffer impairments on their hand, wrist and paretic limbs. The complicity and versatility of the human hand tools play a major role in the individual-environment interaction. Due to the small size and numerous movement capabilities required, upper-limb wearable robots are facing numerous challenges when trying to solve rehabilitation issues and problems in other technical fields, such as bio-mechanics, neuro-physiology, rehabilitation, sensors and actuators, safety of human-robot interactions, and exoskeleton working environments.

This chapter demonstrates the upper limbs rehabilitation exoskeletons based on our novel actuators, such as the ECPAM (explained in chapter 4), EBPAM (explained in chapter 5) and other new actuators developed. Three novel versions of finger rehabilitation gloves are developed in this chapter. A novel forearm rehabilitation exoskeleton is also developed, based on the ECPAM, and two novel versions of elbow rehabilitation

exoskeletons are illustrated. Finally, two new wrist rehabilitation exoskeletons are also developed in this chapter. All exoskeletons are assessed against experimental results to validate the effectiveness of each exoskeleton.

7.2 Hand Rehabilitation Exoskeletons

The application for the new bending extensor pneumatic muscle (explained in chapter 5) is in a soft exoskeleton glove for hand rehabilitation. The main requirements of the glove are:

- Inherent safety – as it is in direct contact with a human user.
- Lightweight – to allow portability.
- Fast response – actuation speed must match that of the human user.
- High force to weight ratio – to keep weight low.
- Low/no calibration requirement – so system can easily be used by multiple people.

7.2.1 Hand Rehabilitation Exoskeletons (Version 1)

One of the disadvantages of traditional exoskeletons is that they have discrete joints which must be correctly aligned with the user's joints (Kiminori, Miyagawa, & Kubota, 2011; Noritsugu et al., 2008; Yap et al., 2015b). Incorrect alignment can lead to injury and so adjustments and calibrations are required when a different person uses the system. The main benefit of our bending muscle is that is does not have discrete joints, the entire actuator flexes instead. If the actuator is mounted to the back of a finger, it will apply force to the entire rear end of the finger when pressurised, resulting in bending at the joints. Based on this concept, a soft-force augmentation glove has been produced. The bending muscles (M1 explained in chapter 5) are sewn onto the reverse of a leather glove, as shown in Figure 7.1.

Eight muscles are used; two muscles for the thumb, index and middle finger to increase force, and single muscles on the ring and little fingers. The resultant soft glove has a weight of approximately 0.15Kg. The air supply to all the muscles is controlled by MATRIX 3-3 solenoid valves, which are pulse width modulated to allow control of the airflow. In the experiment described below, the glove is controlled in an open loop manner.

Figure 7.1: The proposed soft glove with some rehabilitation movements.

In order to demonstrate the effectiveness of the glove in simple force assistive applications, two grasping experiments were conducted, both with and without the use of the glove. The experiments involved a user grasping a 0.5kg mass using a pinch grasp and a 1kg mass using a whole hand grasp.

During experimentation, the human test subject was fitted with EMG (electromyography) sensors on their forearm. These were used to record the total muscle activity required to perform the grasping tasks. The results for the two grasps when the glove was not used can be seen in Figures 7.2 (a) and 7.3 (a). The subject then repeated the two tasks whilst using the glove. For the pinch grasp test, the thumb and index finger actuators were pressurised to 300kPa and for the full hand grasp, all actuators were pressurised to 300kPa. The user's muscle activity was again recorded using EMG and the results can be seen in Figures 7.2 (b) and 7.3 (b).

7.2.2 Hand Rehabilitation Exoskeletons (Version 2)

Most post-stroke patients (with fingers functionality disabled) have curved fingers at a zero position, as shown in Figure 7.4. When those patients wear the soft exoskeletons, their fingers will force the muscles to bend because the muscle has very low stiffness without pressure. It is then difficult to make their fingers move into a straight position to start the rehabilitation exercises by using the rehabilitation glove. This issue inspired us to develop a novel bending actuator capable of controlling its stiffness at any bending angle in order to gain a straight position.

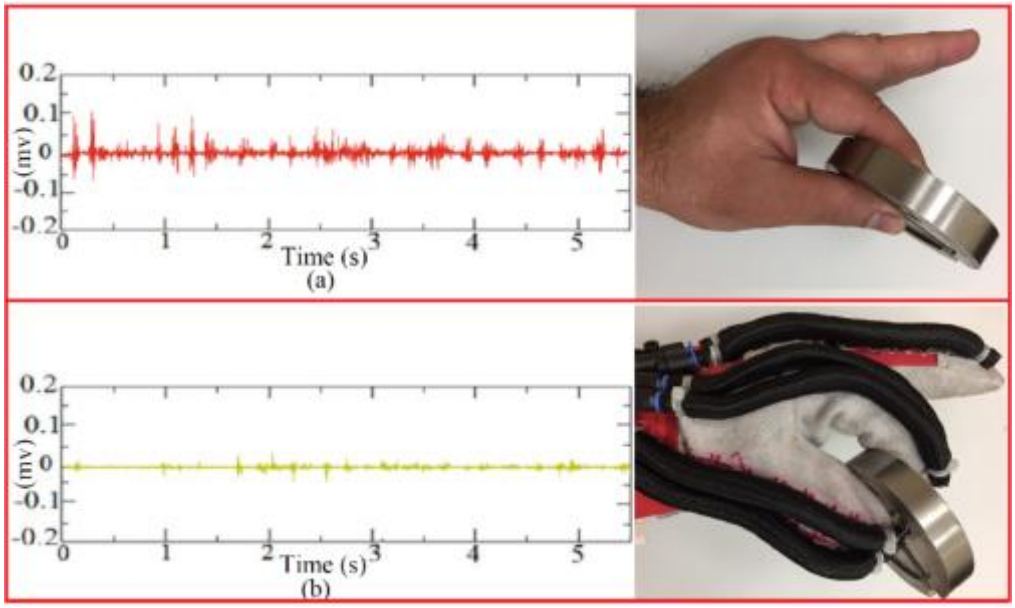

Figure 7.2: EMG signals of pinching load.

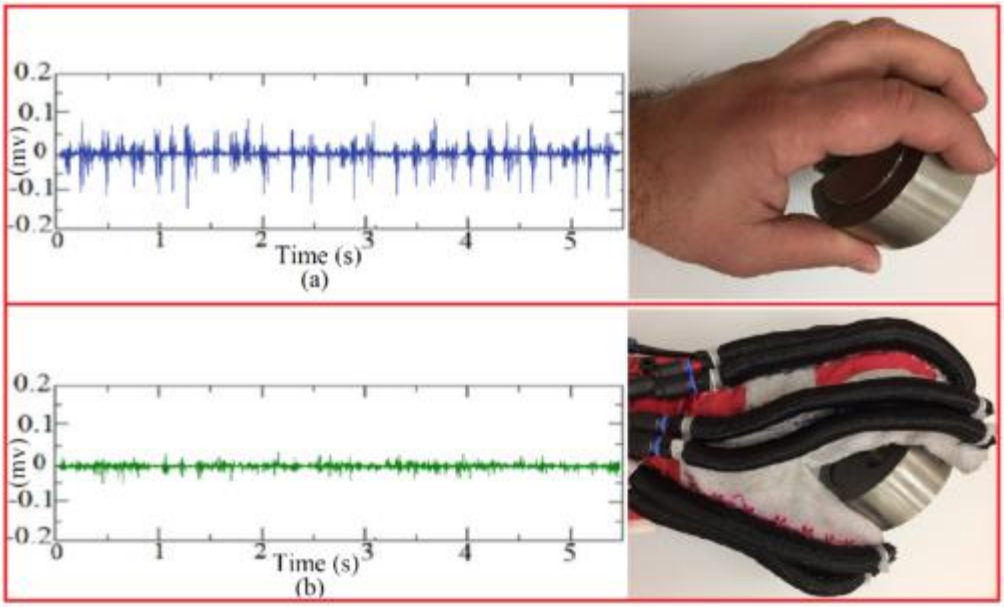

Figure 7.3: EMG signals of grasping load.

Figure 7.4: Patients with finger functionality disabled.

7.2.2.1 The Novel Controllable Stiffness Bending Actuators

Based-on the controllable stiffness extensor-contractor muscle in chapter 4 and the bending muscle in chapter 5's design techniques, we developed a novel controllable stiffness bending muscle. At first, by using the same technique for the extensor-contractor muscle, the controllable stiffness extensor muscle was developed. The controllable stiffness extensor muscle has the same construction as the ECPAM, but in this case, the inner contraction muscle is longer than the outer extensor muscle by 30% instead of 15%. When the inner contraction muscle is fully pressurised, it will contract at approximately 30% to reach the outer extensor muscles nominal length so that, when applying pressure on the outer extensor muscle, it will extend 30% to reach the inner contraction muscles nominal length.

The controllable stiffness extensor muscle has controllable stiffness by controlling both the pressures of the inner contraction muscle and the outer extensor muscle at the same time (the same concept as the controllable ECPAM in chapter 4). Finally, based on the technique of the bending muscle in chapter 5, the controllable stiffness extensor muscle has been reinforced on one side by a non-stretchable fixed-length thread to make this side of the novel muscle have a fixed-length and the other side free to bend when pressurised, as shown in Figure 7.5.

Figure 7.5: The novel controllable stiffness bending actuator.

7.2.2.2 The Proposed Exoskeleton Glove

Five controllable stiffness bending muscles are sewn on the back of a left-hand worker glove, as shown in Figure 7.6.

Figure 7.6: Rehabilitation glove based on controllable stiffness bending muscles.

To overcome the problem of bent fingers at a zero position, we can pressurise only the inner contraction muscles to keep the fingers straight. In addition, with this prototype it is possible for the muscles with high fixed stiffness at all bending angles to overcome the patients' finger resistance.

7.2.2.3 The Proposed Controller System

Hand rehabilitation exercises involve the fingers repeating several movements with help from a therapist. The patients attend a clinic in order to have a therapist help them do the rehabilitation exercises. The therapist moves the patients' fingers manually with repetitive movements for a long time. Our prototype and controller system aim to make this process easier.

To make the hand rehabilitation easier for the patients and the therapists, we made two soft gloves with flex bend sensors only, as shown in Figure 7.7.

Figure 7.7: Soft controller gloves.

For each glove, a flex bend sensor (4.4'') is placed on the top surface of the thumb, index and middle fingers. For most finger movements in daily activities, the middle, ring and little fingers move together and, based on this assumption, the ring and little fingers are without sensors because they move simultaneously with the ring fingers at the same bending angle. The patient wears the soft left-hand glove and afterwards wears the exoskeleton glove on the same hand (the exoskeleton glove above the soft glove on the same hand) and the therapist wears the right-hand soft glove as a controller glove. The idea is that when the therapist moves his fingers, the patient does the same movements at the same time with the same bending angles, without any contact between the therapist and the patient. This technique will make the rehabilitation process easier and more comfortable for both the patient and the therapist. The therapist's glove acts as a controller set point and the patient's soft glove acts as signals feedback. Each controllable stiffness bending muscle has two inputs, one for the inner contractor muscle and the other one for the outer extensor muscle. Each muscle input was connected to a solenoid valve; we used six valves, two for the thumb, two for the index finger and two for the middle fingers (the ring and little fingers are connected with the middle finger actuator). Figure 7.8 shows the hardware controller system.

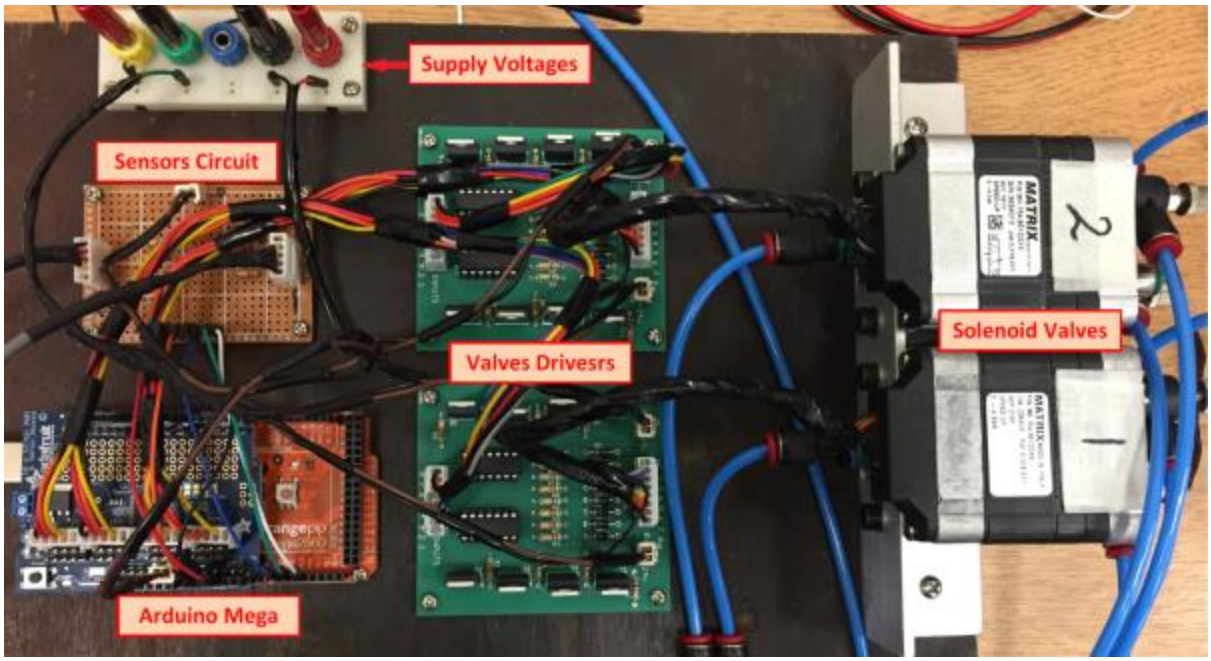

Figure 7.8: The hardware controller system.

A single fuzzy controller is used for each actuator, as shown in Figure 7.9. This fuzzy controller is repeated three times for the thumb, index and middle finger. The controller has two outputs; the bend output is to control the outer extensor bending muscle and the unbend output is to control the inner contraction muscle. Figure 7.10 shows the membership functions of the inputs and outputs of the fuzzy controller and Figure 7.11 shows its fuzzy surface.

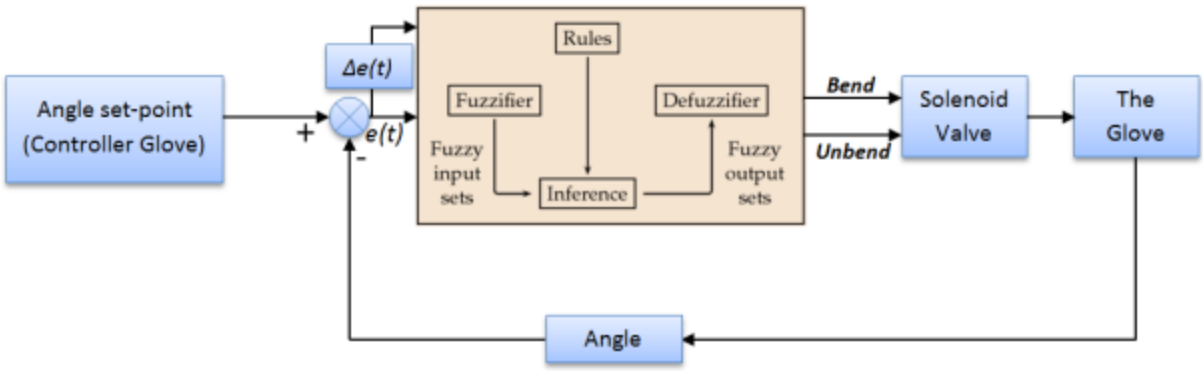

Figure 7.9: The fuzzy controller system for each actuator.

The zero position of the controller system fully inflates all the inner contraction muscles and fully deflates the outer bending muscles to make all the fingers be in a straight position, as shown in Figure 7.12 (a). A thumb rehabilitation exercise is illustrated in Figure 7.12 (b). When the thumb in the controller glove starts bending, the patients glove

responds in real-time to do the same movement by decreasing the pressure in the inner contraction muscle and increasing the pressure of the outer bending muscle of the thumb actuator at the same time. The actuator has approximately high stable stiffness at all ranges of bending angles of the finger joints. The index finger rehabilitation exercise is demonstrated in Figure 7.12 (c).

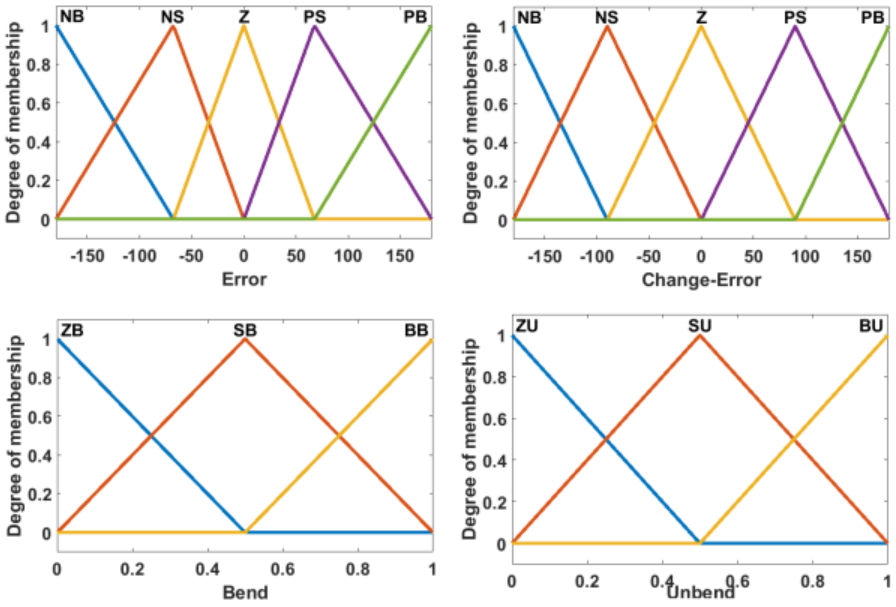

Figure 7.10: Membership function of the fuzzy controller.

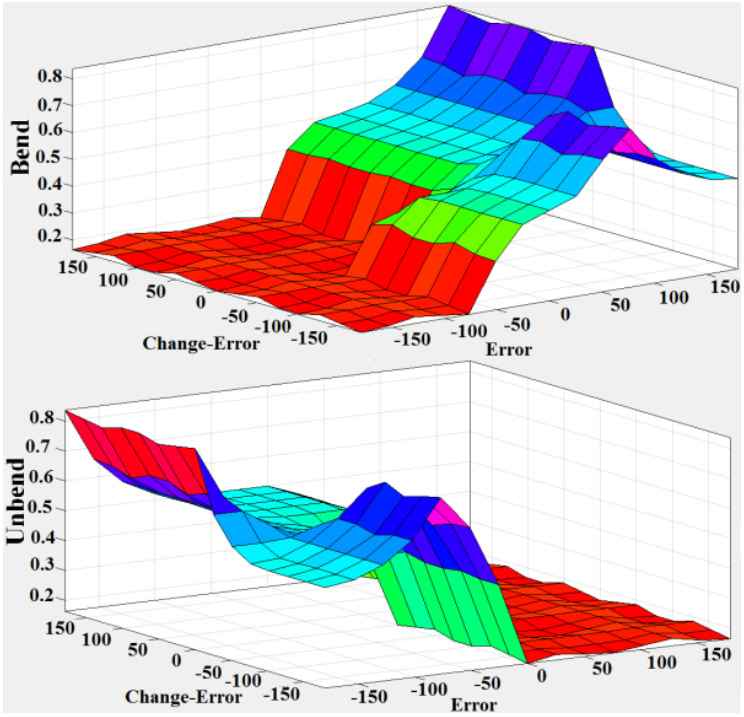

Figure 7.12: The surface of the fuzzy controller.

The same controller for the thumb is repeated for the index finger to do the index finger rehabilitation movements with other fingers in a straight position. The same controller has been repeated again for the middle finger, but in this case, all middle, ring and little fingers are moving together based on the bending angle of the middle finger, as shown in Figure 7.12 (d). Figure 7.12 (e) shows the rehabilitation exercise of all the fingers except the thumb and Figure 7.12 (f) shows all fingers rehabilitation exercises. One, two, or all three controllers can be activated to make a high range of hand rehabilitation movements based on the therapist's hand movements.

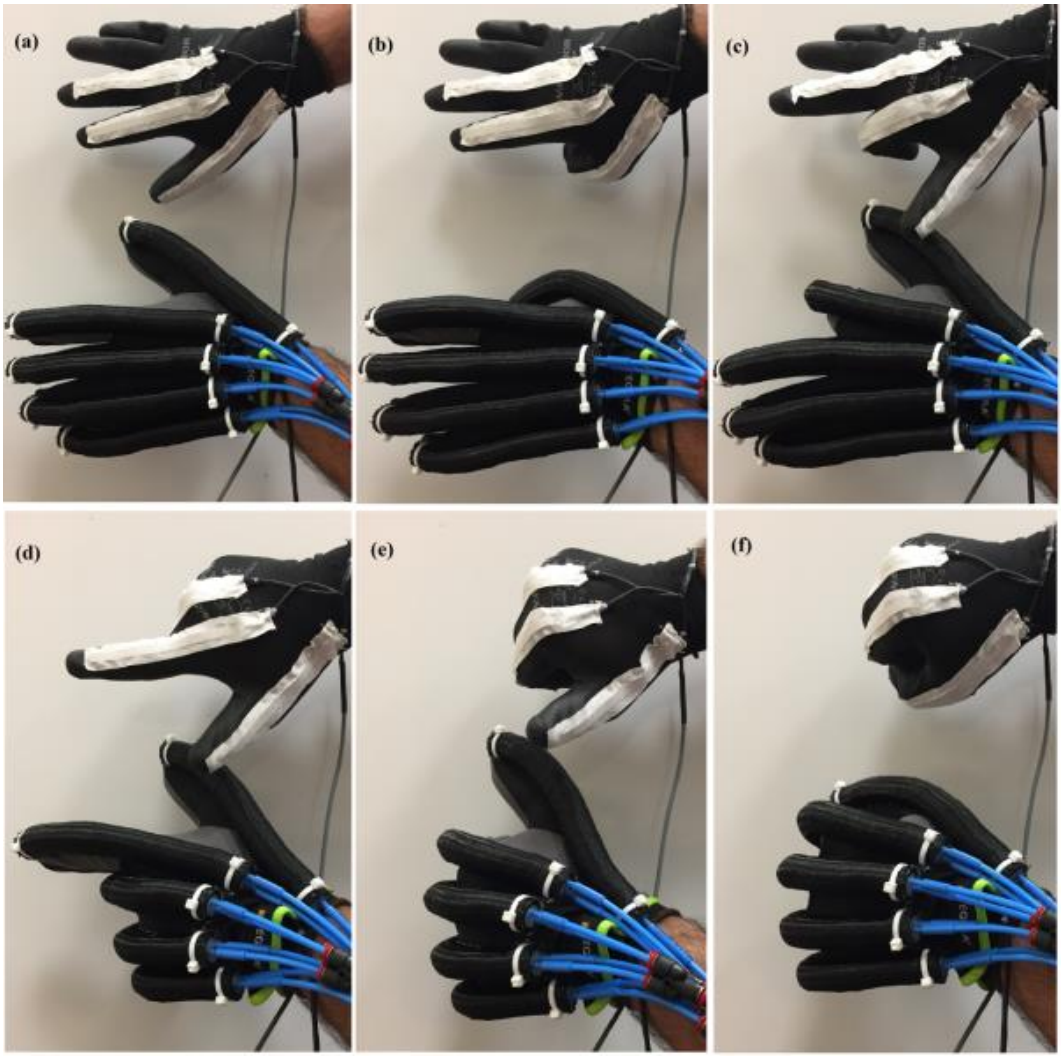

Figure 7.12: Hand rehabilitation movements controlled by a therapist's hand.

Using this controller system, it is easy to make an online controller (remotely) via the internet. In other words, the therapist at the clinic and the patient at home have the controller glove commands transferred online via internet protocol (they are dynamic set-point numbers) to the patients glove to perform the rehabilitation exercises at home

without needing to go to the clinic. In this case, the therapist can do the rehabilitation exercises remotely for more than one patient at a time if they need the same exercise. Figure 7.13 shows the controller system results.

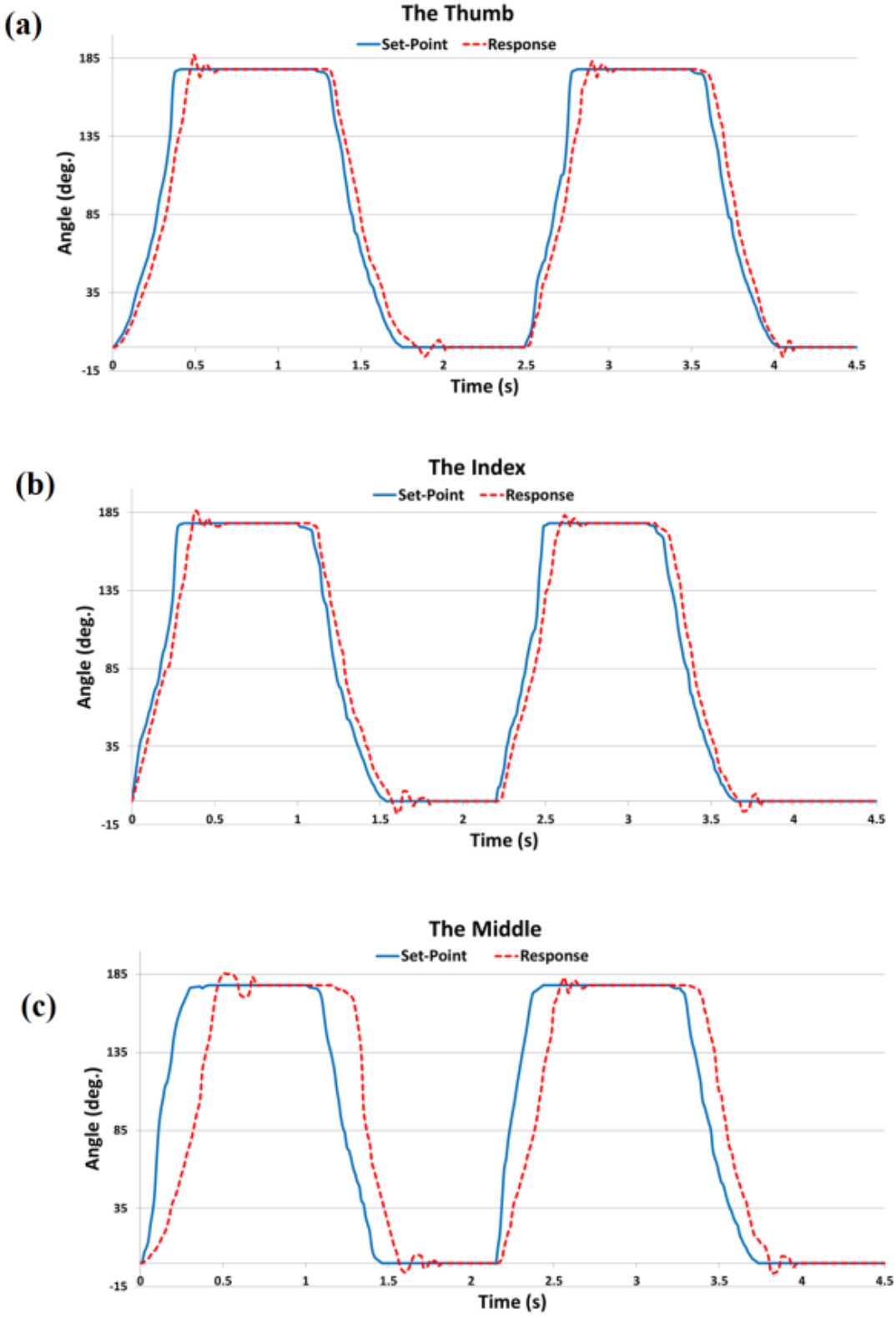

Figure 7.13: Hand rehabilitation controller results.

The thumb controller is illustrated in Figure 7.13 (a) and the index finger controller is in Figure 7.13 (b). Figure 7.13 (c) shows the middle finger controller results. The middle finger controller results are slightly different from the other fingers results because the middle, ring and little fingers all move together, and their muscles inflate/deflate using the same valve (as previously mentioned) then the air flow amount divides into three muscles. This causes a bigger delay between the set-point and the controller response.

For offline rehabilitation exercises, we designed a Matlab application to help the patients use the rehabilitation exoskeleton at home independently and do their rehabilitation exercises without involving the therapist. Figure 7.14 shows the Matlab application foreground for six hand rehabilitation exercises.

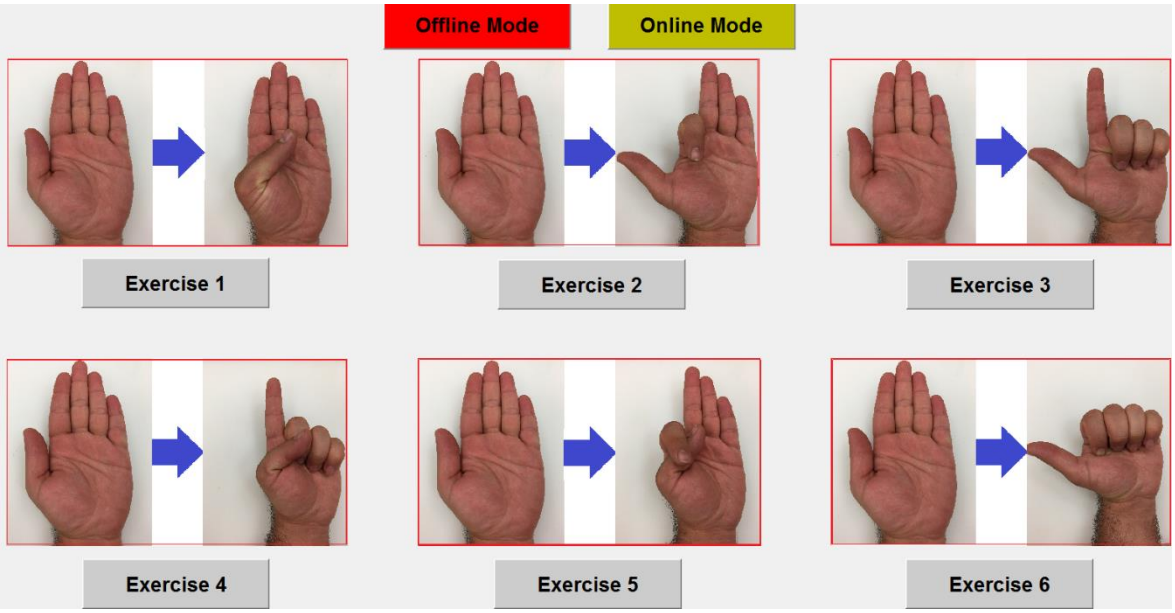

Figure 7.14: The Matlab application foreground.

The patient only has to activate the offline mode with the red button and choose the exercise number to start the exercise repeatedly. Figure 7.15 shows the offline controllers results of the thumb, index and middle fingers. The same previous controllers are used, but in this case, the controllers set-points come from the Matlab application at full bending angles for each finger, with repeated 3 second periods. The exercise buttons in Figure 7.14 is only to activate which controller will be active (thumb, index and/or middle finger controller) to start the chosen rehabilitation exercise.

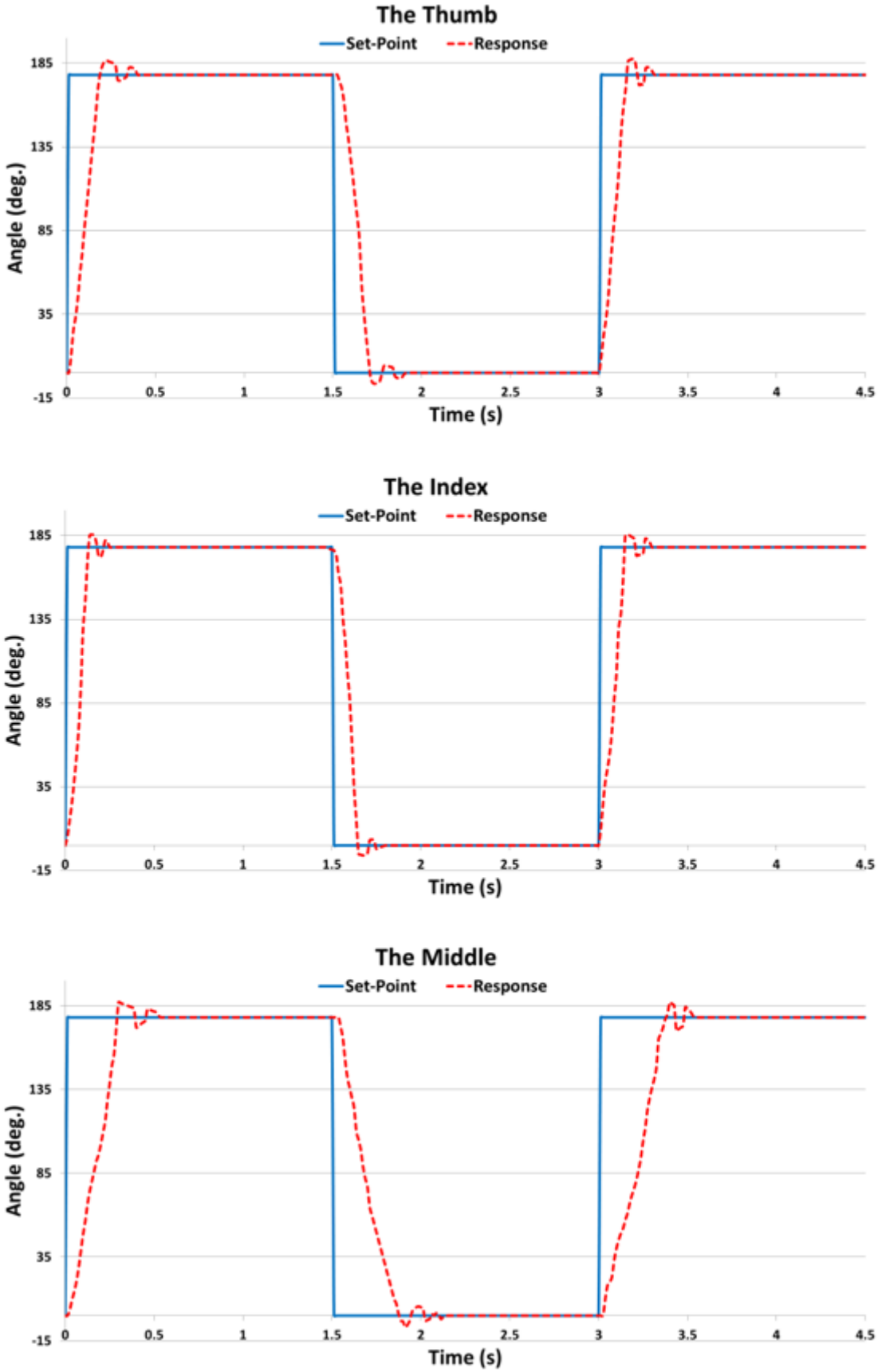

Figure 7.15: Offline controllers results.

To validate this exoskeleton system a 3D printed hand was produced and placed inside the glove. This hand contained all the joints found within the human hand, however, as it was unactuated so it allowed the glove to apply forces to the hand and to flex and extend the joints. This allowed the glove to apply repetitive movements to the hand to evaluate the system's performance and Root Mean Square Error (RMSE) values. Firstly the Thumb muscle with its controller was tested by generating a step setpoint to the system with value of 135^{o} as the bending angle setpoint. The experiment was repeated 20 times and the results are shown in Figure 7.16.

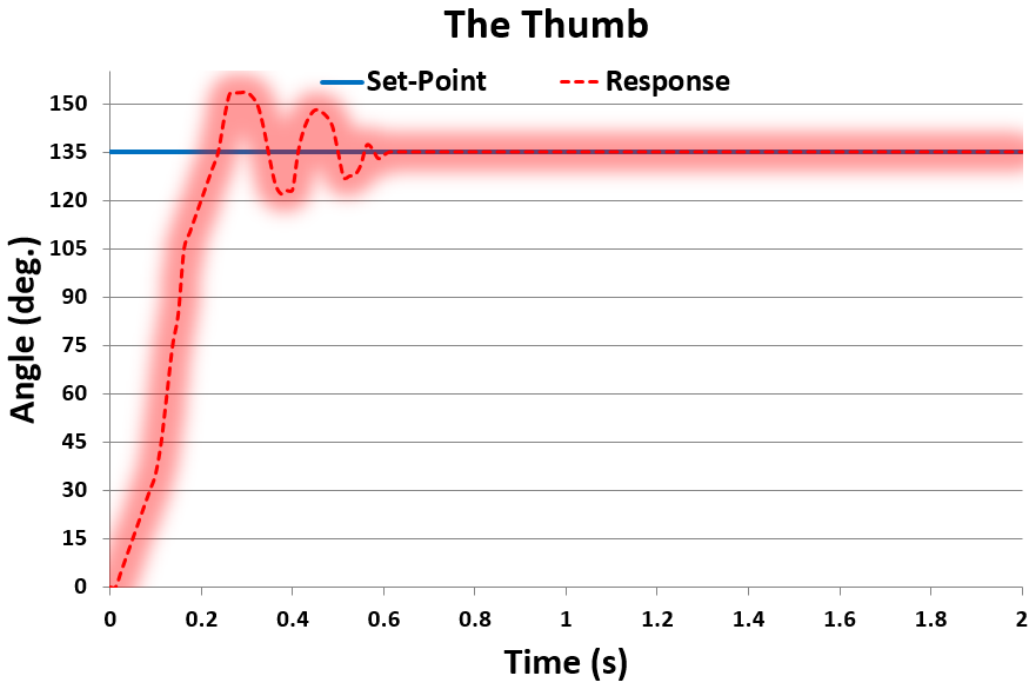

Figure 7.16: The glove validation (Thumb finger) with step setpoint.

In Figure 7.16, the blue line represents the step setpoint input from 0 to 135^{o}, the foggy red area represents the range of motions from the 20 experiments and the middle bold dashed red line is the average response of the 20 time experiments. The RMSE value between the average response and the setpoint was recorded as 13.99. this value of RMSE is not unexpected because of the recorded error between the average response and the setpoint during the start movement until the response reaches the setpoint with some overshoots until stability. This experiment has been repeated with a sinusoidal setpoint with amplitude of 178^{o} bending angle (the assumed maximum bending angle for each finger). Figure 7.17 shows the results, again the experiment was repeated 20 times using the same procedure as the experiment in Figure 7.16 and the recoded RMSE value between

the average response and the setpoint was found to be 7.04. It is clear, the second experiment has significantly less value of RMSE because the experiment in Figure 7.16, the setpoint started from the 135^{o} directly and the system started from zero bending angle and the experiments in Figure 7.17, both setpoint and the response started from zero.

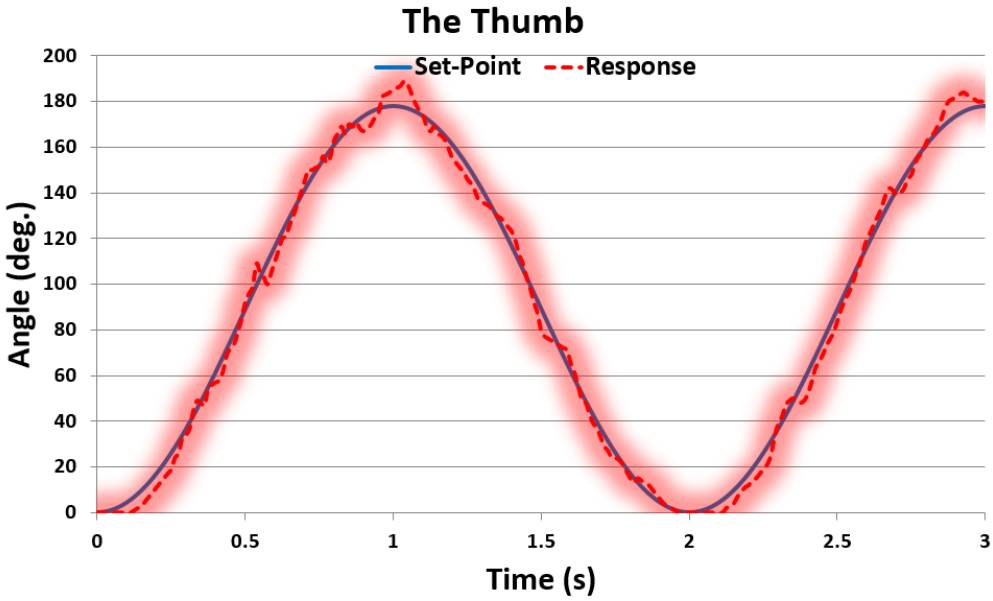

Figure 7.17: The glove validation (Thumb finger) with sinusoidal setpoint.

The above two experiments in Figures 7.16 and 7.17 were repeated for the index finger with its controller as shown in Figures 7.18 and 7.19 with RMSE 14.97 and 8.17 respectively.

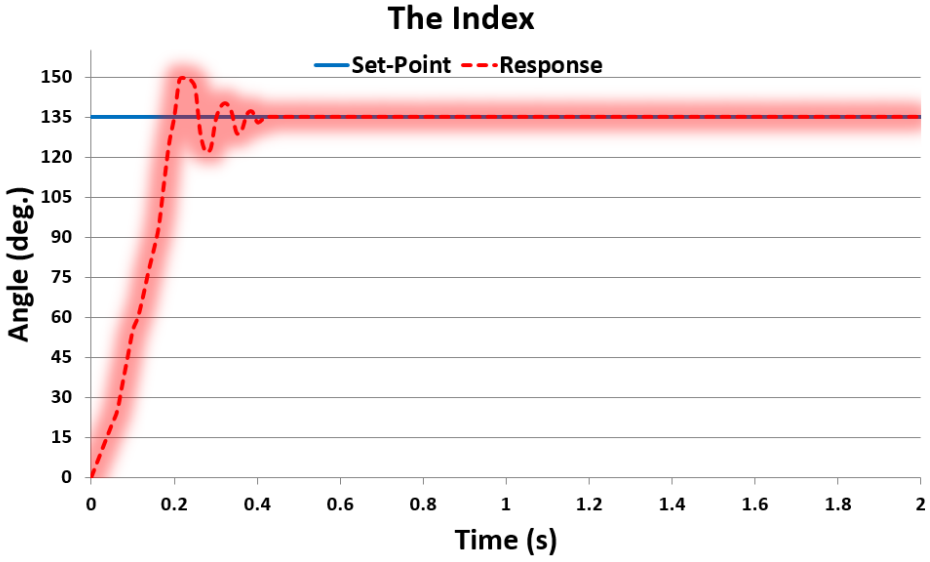

Figure 7.18: The glove validation (Index finger) with step setpoint.

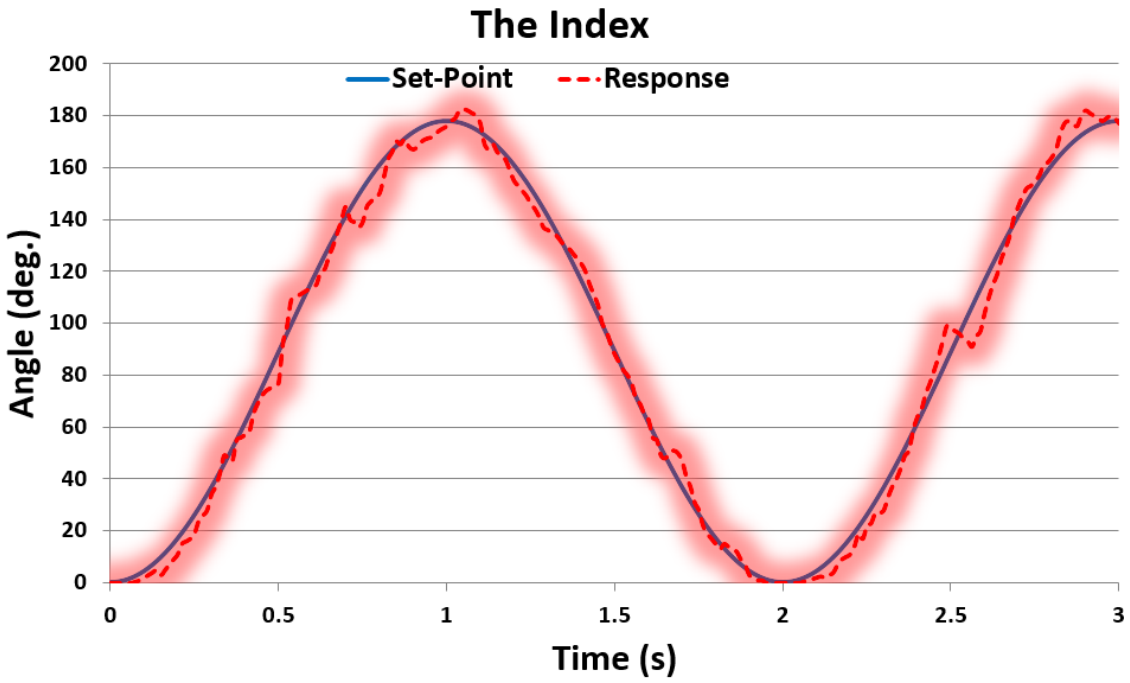

Figure 7.19: The glove validation (Index finger) with sinusoidal setpoint.

The same two experiments were repeated for the middle finger (with ring and little fingers as explained previously) with its controller as shown in Figures 7.20 and 7.21, the RMSEs were found to be 18.38 and 10.73 respectively.

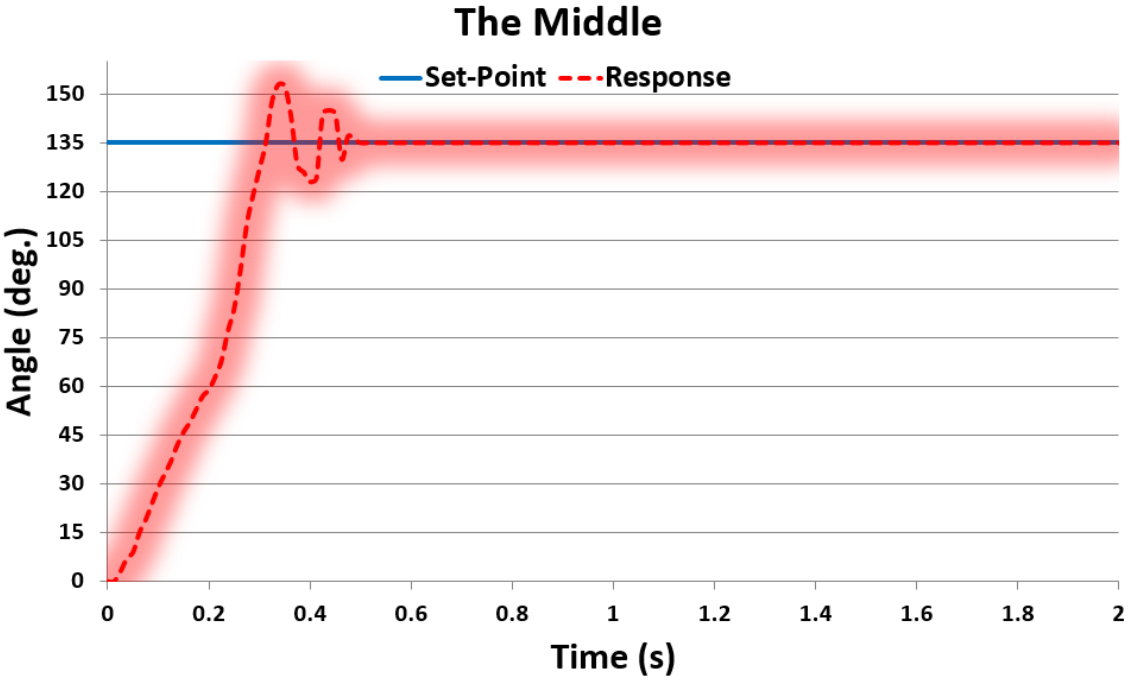

Figure 7.20: The glove validation (Middle finger) with step setpoint.

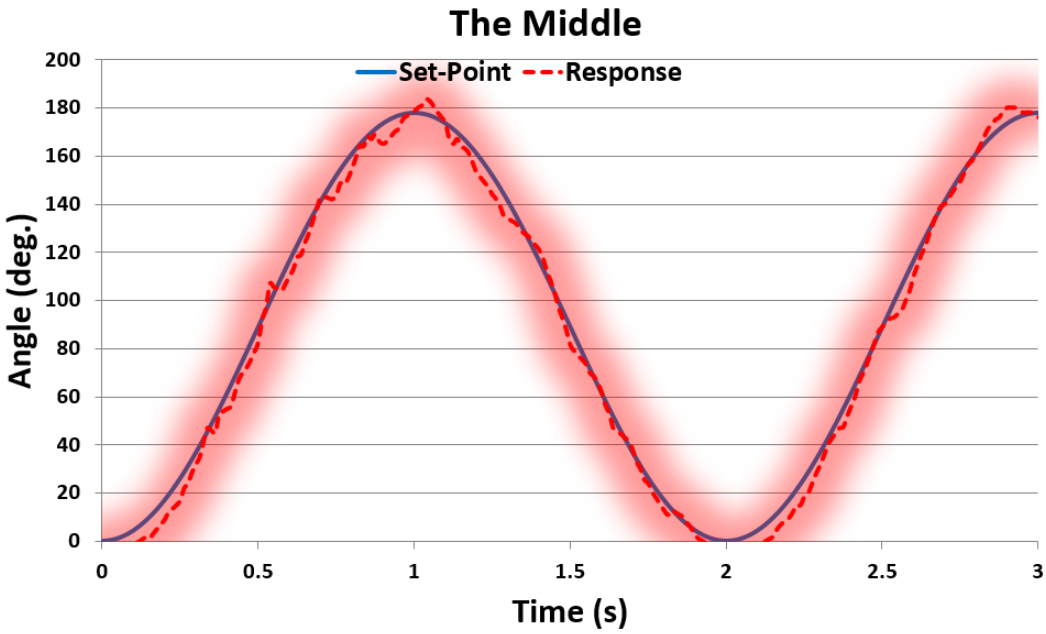

Figure 7.21: The glove validation (Middle finger) with sinusoidal setpoint.

7.2.3 Hand Rehabilitation Exoskeletons (Version 3)

The hand rehabilitation exoskeleton version 2 (see section 7.2.2) can perform a wide range of rehabilitation movements by bending the finger joints (root, middle and terminal) together at the same time. Figure 7.22 shows the general hand movements; our prototype version 3 cannot perform table top and hook movements because it cannot control the finger joints separately. Inspired by this issue, we created the hand exoskeleton version 3 with the ability to perform all the movements of prototypes versions 1 and 2 with additional movements, such as table top and hook movements.

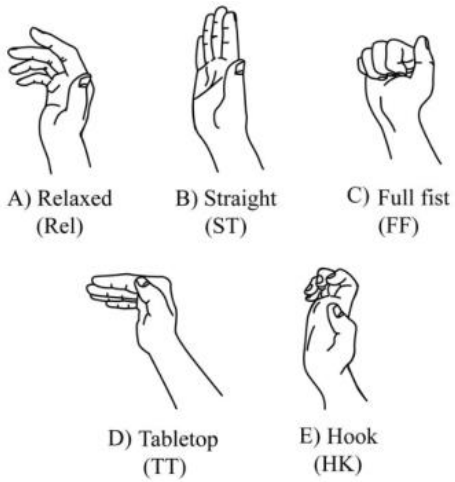

Figure 7.22: Hand movements.

7.2.3.1 The Proposed Variable Stiffness Soft Actuators

Human bodies, with their flexible limb joints, have the capability of performing numerous movements in a very effective and precise manner under different conditions, in different environments, with high flexibility.

Inspired by the human body, researchers have presented many kinds of actuators (Albu-Schäffer & Bicchi, 2016; Galloway, Clark, & Koditschek, 2013; Jiang, Xynogalas, Dasgupta, Althoefer, & Nanayakkara, 2012; Ketelaar, Visser, Stramigioli, & Carloni, 2013; S. Kim, Laschi, & Trimmer, 2013; Kuder, Arrieta, Raither, & Ermanni, 2013; Vanderborght et al., 2013; Wolf et al., 2015; Yang & Chen, 2016; Yap, Lim, Nasrallah, Goh, & Yeow, 2015a). Variable stiffness actuation is one of the most promising areas. Generally, they operate by motorising the actuator compliance and their equilibrium positions independently. Hence, many human-like motions can be achieved using a small amount of energy at the input of the actuator.

- *Partially Variable Stiffness Soft Actuator*: A novel variable stiffness soft actuator has been developed. We've combined the proposed contraction and bending artificial muscles together, as shown in Figure 7.23 (a). The contraction artificial muscle is reinforced on the free side of the bending muscle. Figure 7.23 (b) shows the partially variable stiffness soft actuator by actuating both muscles. The root part of the bending muscle is not bent because the pulling force of the contraction muscle is greater than the bending force of the bending muscle. The bending occurs only on the terminal part because it is free on one side. Figure 7.23 (c) shows the proposed actuator actuating only the bending muscle. The whole actuator is bent, but the root part bending angle is less than the terminal part because of the limitation coming from the length and the friction of the contraction muscle.

- *Fully Variable Stiffness Soft Actuator*: The partially variable stiffness soft actuator is developed to a fully variable stiffness by adding another contraction muscle on the terminal part of the bending muscle, as shown in Figure 7.24 (a). The second contraction muscle is to control the stiffness of the second part of the bending muscle. Figure 7.24 (b) illustrates the bending angle of the fully variable stiffness actuator when actuating only the bending artificial muscle. To increase the bending muscle stiffness at no bending angle (straight), we actuated only the two

contraction muscles, as shown in Figure 7.24 (c). The stiffness amount is controlled by the pressure amount inside the contraction muscles. Figure 7.24 (d & e) demonstrates the bending of the terminal and the root part of the proposed actuator by actuating the bending muscle with the root (for terminal part bending) and terminal (for root section bending) contraction muscles. As a result of controlling the pressures of all the muscles together, the stiffness of the bending actuator is controllable.

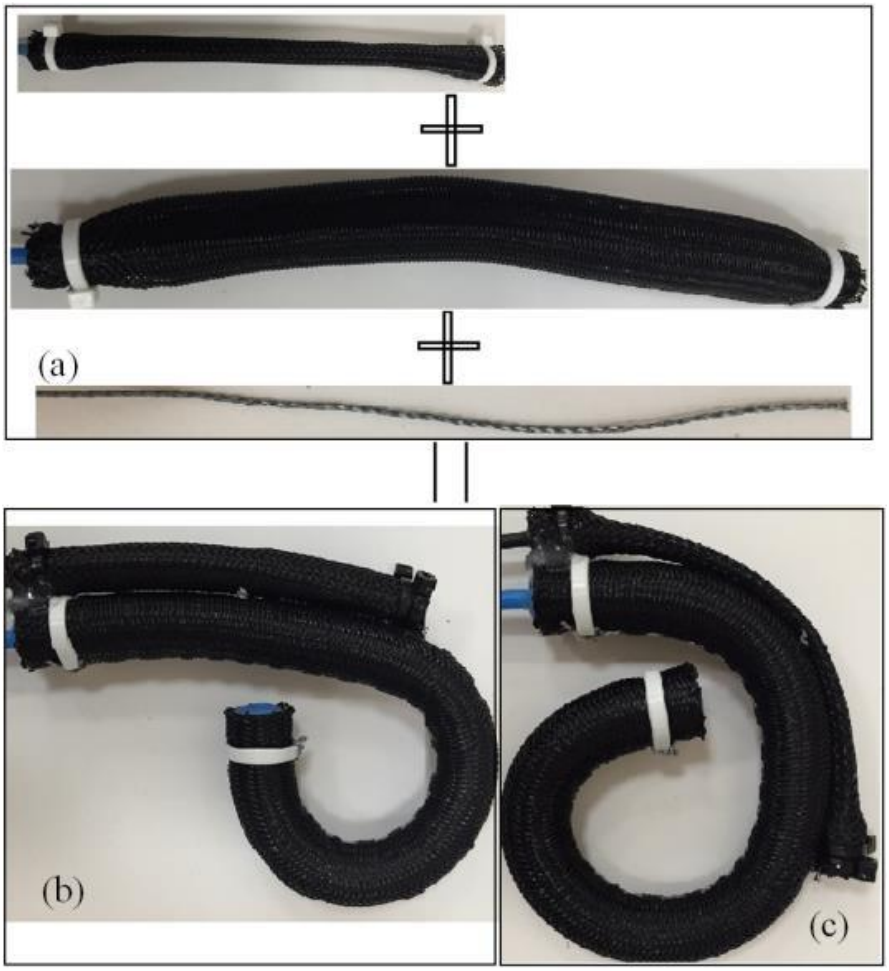

Figure 7.23: Partially variable stiffness soft actuator.

7.2.3.2 The Proposed Exoskeleton Glove

We constructed an exoskeleton glove based on the proposed fully variable stiffness actuator discussed in the section above, as shown in Figure 7.25. Four fully variable stiffness actuators were sewn on to a traditional worker gloves dorsal side. These four actuators are placed on the back side of the glove for the index, middle, ring and little fingers. The thumb finger is assisted by a bending extensor artificial muscle.

The airflow of all the muscles are controlled by MATRIX 3×3 solenoid valves. Each muscle is controlled separately by its filling/venting solenoid valve. Air can be supplied via a compressor or a miniature diaphragm pump for actuation.

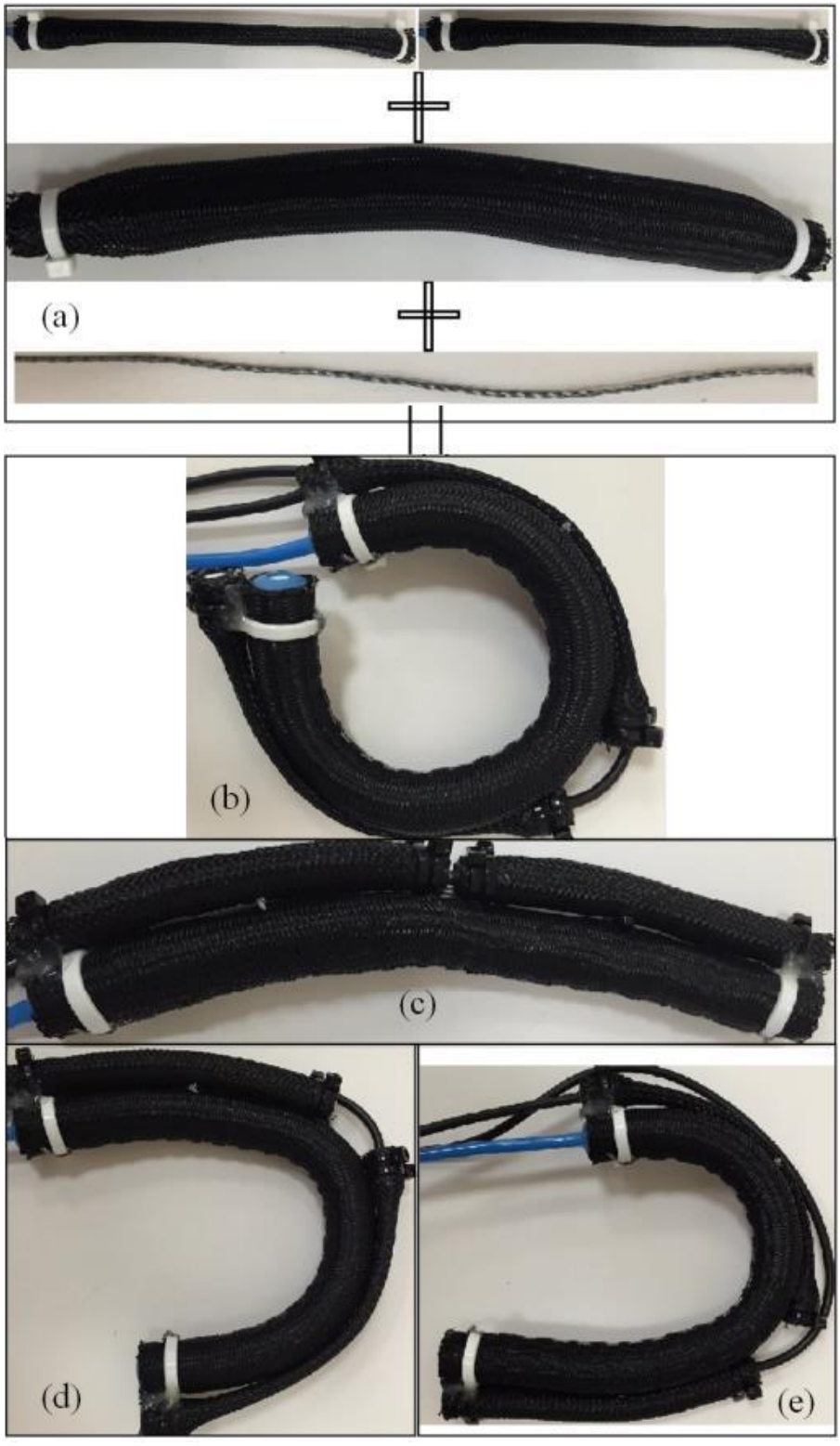

Figure 7.24: Fully variable stiffness soft actuator.

The properties of this exoskeleton glove are: flexibility (at no pressure); lightweight because it is fully soft (approximately 150g); supports most human hand rehabilitation movements, including hook and table top fist movements; safe due to no rigid parts or electricity; fast response actuation to reach the healthy human hand speed motion; small in size in order to be flexible in daily usage; and fits any adult hand size.

Figure 7.25: The proposed exoskeleton glove version 3.

There are an extensive variety of hand rehabilitation movements. The significant challenge is to accomplish most of these movements using a single rehabilitation exoskeleton without any assistance from a rehabilitation proficient.

A lightweight, small, and easy to utilise wearable robot that provides the capability to perform most rehabilitation exercises at home or anywhere rather than in the healing centre has been developed.

Figure 7.26 demonstrates most rehabilitation movements of the proposed prototype with the fully variable stiffness actuators, such as full grasp, straight grasp, hook grasp, and table top. Depending on the rehabilitation exercise type, we can program our prototype to perform many exercise modes by controlling the pressure amount inside each actuator separately.

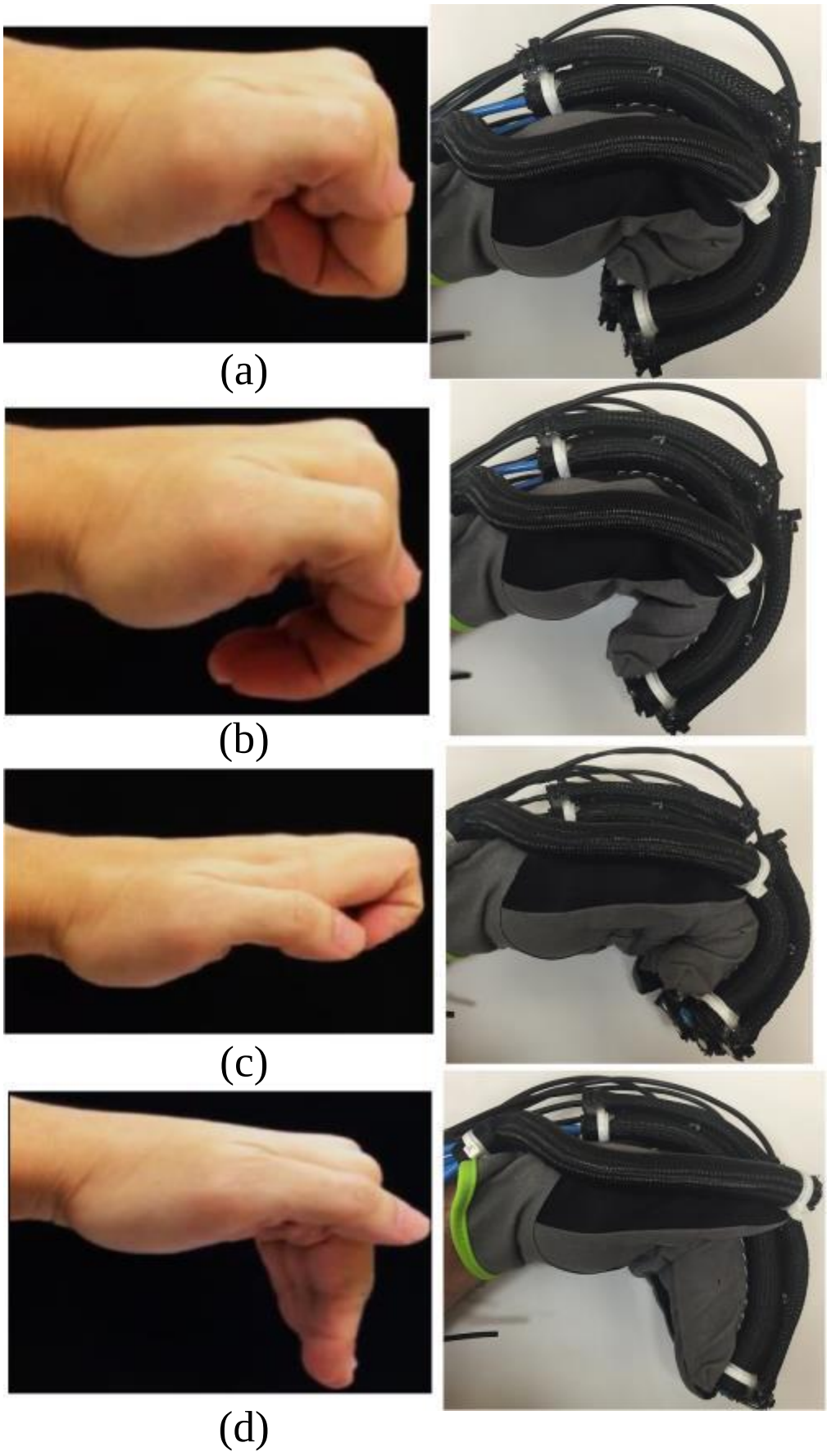

Figure 7.26: Typical hand rehabilitation exercises; a) Full Grasp, b) Straight Grasp, c) Hook Grasp, and d) Table Top.

7.3 Forearm Rehabilitation Exoskeleton

This section describes an application for the novel Extensor-Contractor Pneumatic Artificial Muscle developed in chapter 4. The ECPAM in this prototype has the same characteristics as those explained in chapter 4 but this muscle is bigger in length and diameter. The application chosen was a soft exoskeleton to be used in the rehabilitation of the forearm. There are only two movements of the forearm: pronation and supination. The challenge is to achieve both forearm movements using a single actuator without the need for any assistance from a rehabilitation therapist.

A lightweight, soft, and easy to use exoskeleton for performing forearm rehabilitation motions has been created utilising our new soft extensor-contractor actuator, as shown in Figure 7.27.

The soft actuator is secured to the forearm at the terminals and the middle section using adjustable elasticated straps. The total weight of the exoskeleton is 0.18Kg. As the proposed rehabilitation device is low in weight and created using soft materials, it is safe for direct human interaction. The system can also fit any individual patients' hand without the requirement for adjustments or mechanical changes. This potentially makes the system suited to use in a home environment without the need of a rehabilitation specialist present.

Open loop control experiments were performed to demonstrate that the actuator could be used to generate motion in the user's forearm. Figure 7.28 shows supination of the forearm achieved by actuation of the inner contraction muscle which pulls on the palm as shown. Figure 7.29 shows pronation achieved by actuating the extensor muscle to push the palm. The range of pronation and supination the exoskeleton was able to generate was approximately 90° and 75°, respectively.

Figure 7.27: The proposed forearm soft exoskeleton.

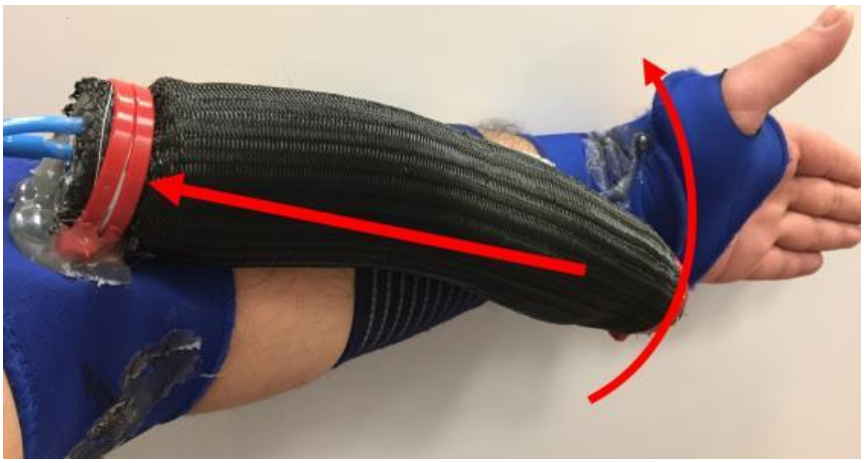

Figure 7.28: The forearm supination using the soft exoskeleton.

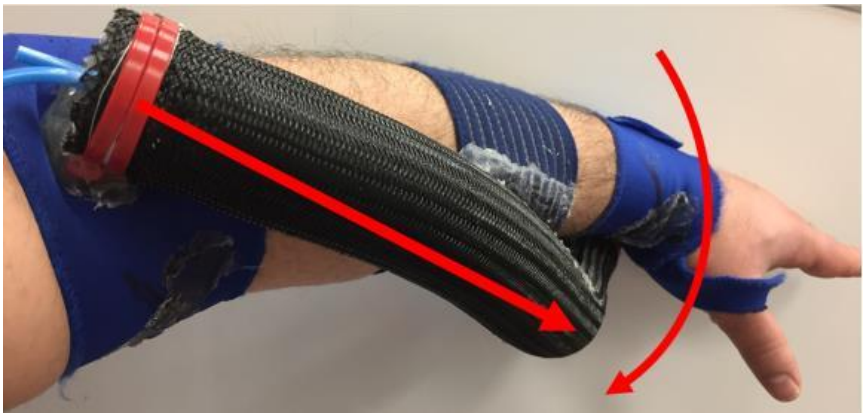

Figure 7.29: The forearm pronation using the soft exoskeleton.

7.4 Elbow Rehabilitation Exoskeleton

Flexion and extension movements of the elbow joint are an important way in which to recover from injuries and prevent them from reoccurring. Working with your physical therapist is a good idea after an elbow injury. An elbow rehabilitation exoskeleton has been developed based on EBPAM with an M3 bending muscle (see chapter 5), but the length of the muscle in this prototype is 30cm. Two bending muscles are used in this exoskeleton, as shown in Figure 7.30. Plastic handles with Velcro are used to reinforce the exoskeleton to the wearers hand and a bending muscle for each side. Both muscles have been pressurised at the same time with the same amount of pressure to produce the desired bending angle to the elbow joint of the wearer. The maximum output force for each bending actuator is 43N at 5bar pressure (approximately the same output force of M3 in chapter 5). The elbow exoskeleton has two bending actuators, then the maximum output force of the prototype is

the sum of both actuators (86N) because they have parallel forces and the maximum torque achieved by the exoskeleton is 14 Nm.

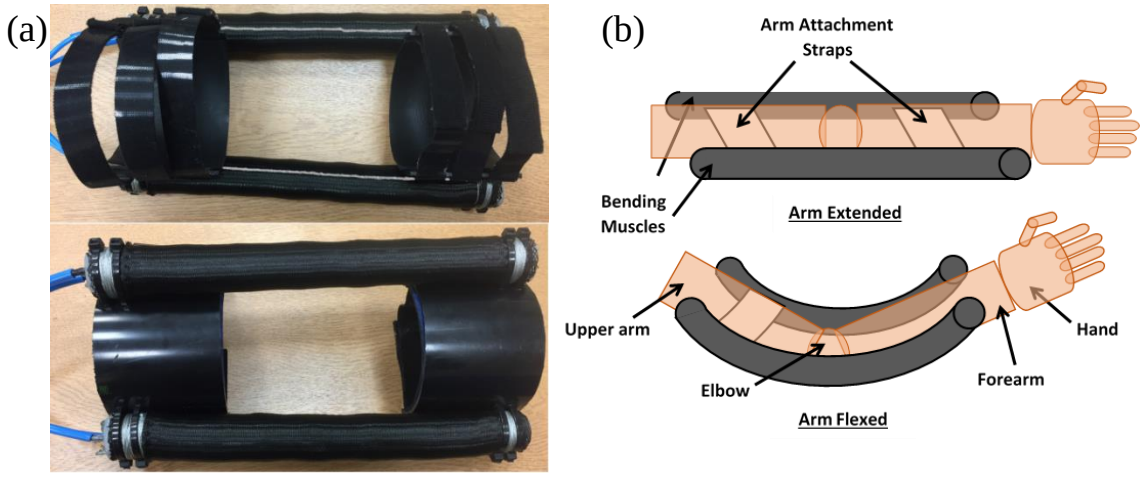

Figure 7.30: Elbow exoskeleton.

The same controller, explained in section 7.2.2.3, is used in this prototype. Two elbow medical bands are used and a 4.4'' flex bend sensor is placed on each one, as shown in Figure 7.31. To perform the online controller, as explained in section 7.2.2.3, the patient has to first wear the medical band and position the flex bend sensor to the back centre of his elbow joint, after which the patient should wear the exoskeleton. The therapist wears the other band to produce the desired elbow joint angle as a set-point to the controller during the rehabilitation exercises, as shown in Figure7.32.

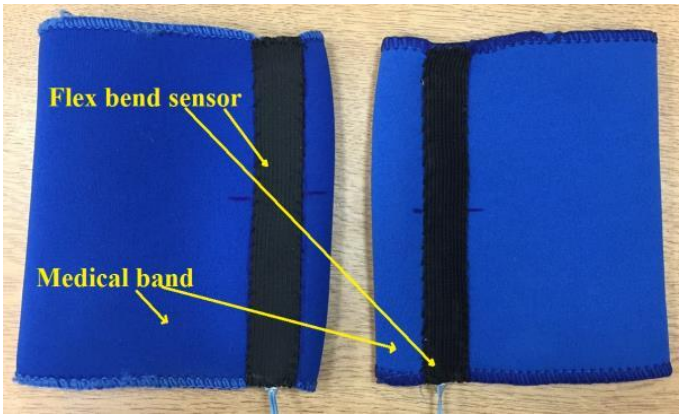

Figure 7.31: Elbow medical bands with flex bend sensors.

When the therapist bends his elbow, the patient's exoskeleton responds at the same time, bending the patient's elbow by the same angle. Figure 2.27 demonstrates the online controller results of the elbow exoskeleton.

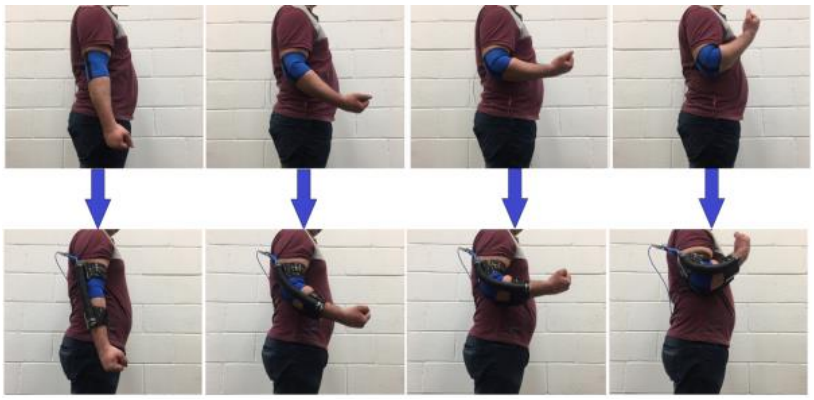

Figure7.32: Online controller for the elbow exoskeleton.

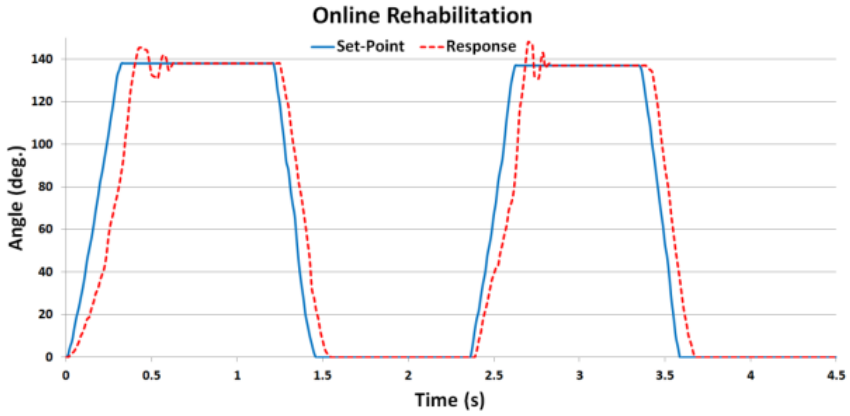

Figure 7.33: The online controller results of the elbow exoskeleton.

An offline rehabilitation application has been developed using Matlab, as shown in Figure 7.34. Three rehabilitation exercises are placed in this application; to choose a specific exercise, push its button to run the exercise repeatedly. Exercise number (1) generates a 45^{o} bending set-point to the controller system repeatedly within a period of 4 seconds, exercise number (2) uses the same controller and technique but in this case the bending angle set-point is 90^{o} and finally, exercise number (3) is with a full bending angle set-point at 135^{o}. Figure 7.35 shows the elbow offline rehabilitation controller results.

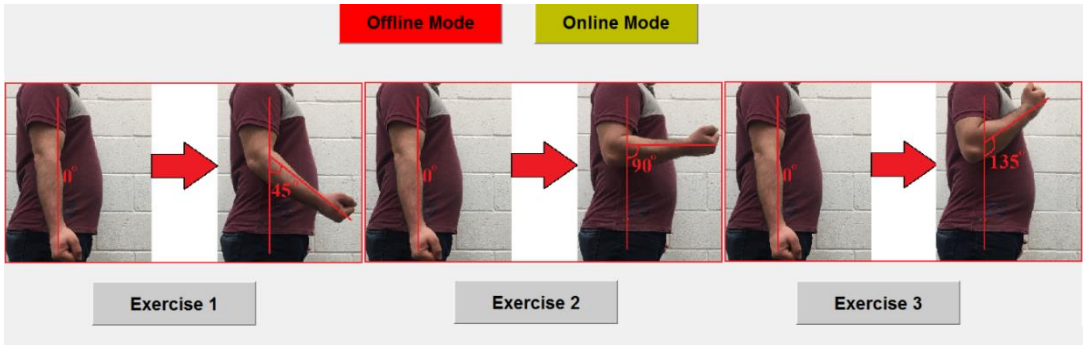

Figure 7.34: Offline elbow rehabilitation application.

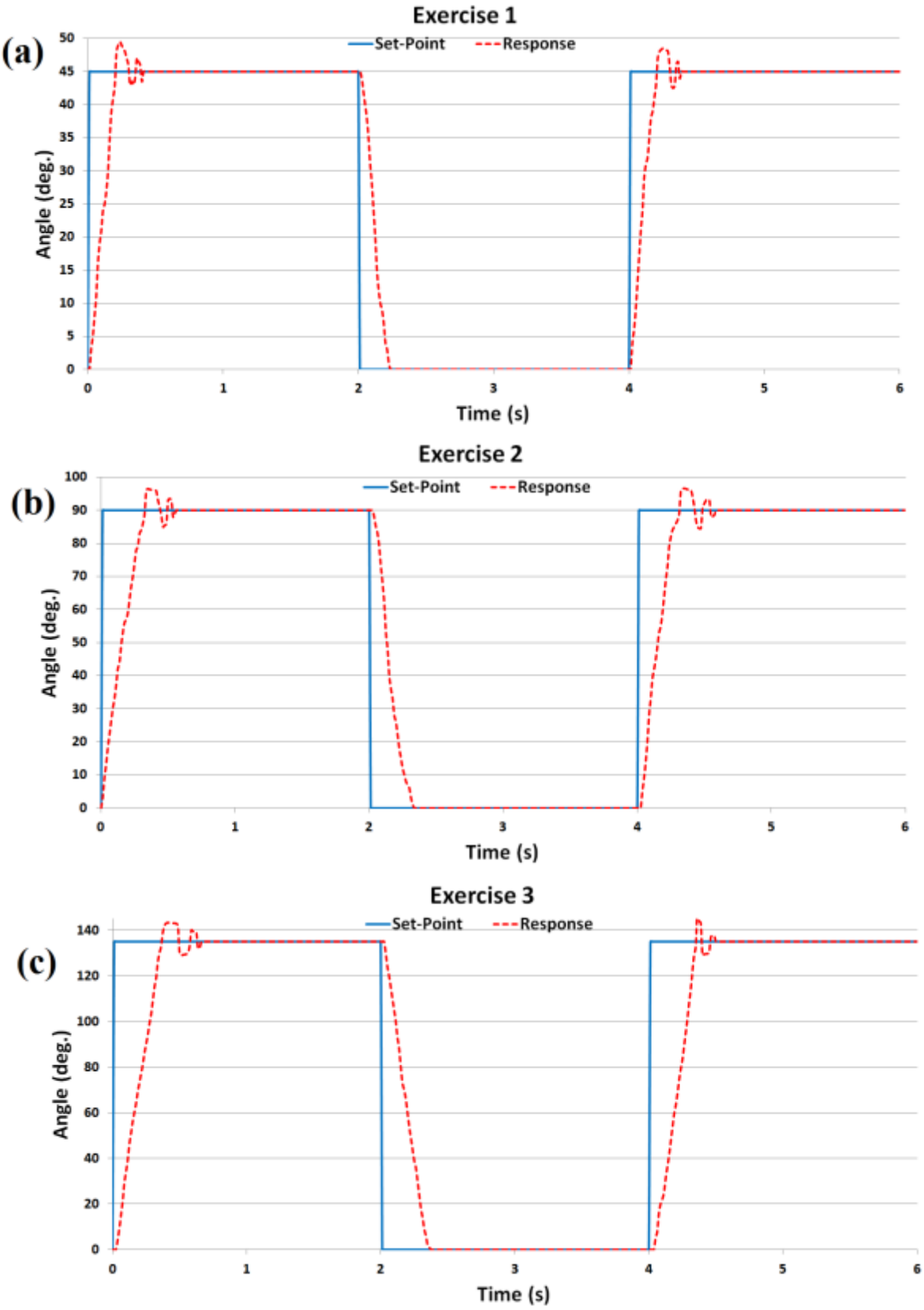

Figure 7.35: The elbow offline rehabilitation controller results.

To validate this Elbow exoskeleton system, some repetitive movement with a predefined bending angles on the system have been tested with a mechanical 3D printed Elbow to evaluate the system performance and RMSE values. The same procedure as used to validate the exoskeleton glove described in section 7.2.2.3 was again used. The elbow was tested with step responses with three bending angles 45º, 90º and 135º. The experiment was performed 20 times and an average determined for each of the three bending angles 45º, 90º and 135º. The experimental results are shown in Figures 7.36 (with RMES = 12.52), 7.37 (with RMES = 14.66) and 7.38 (with RMES = 17.27) respectively.

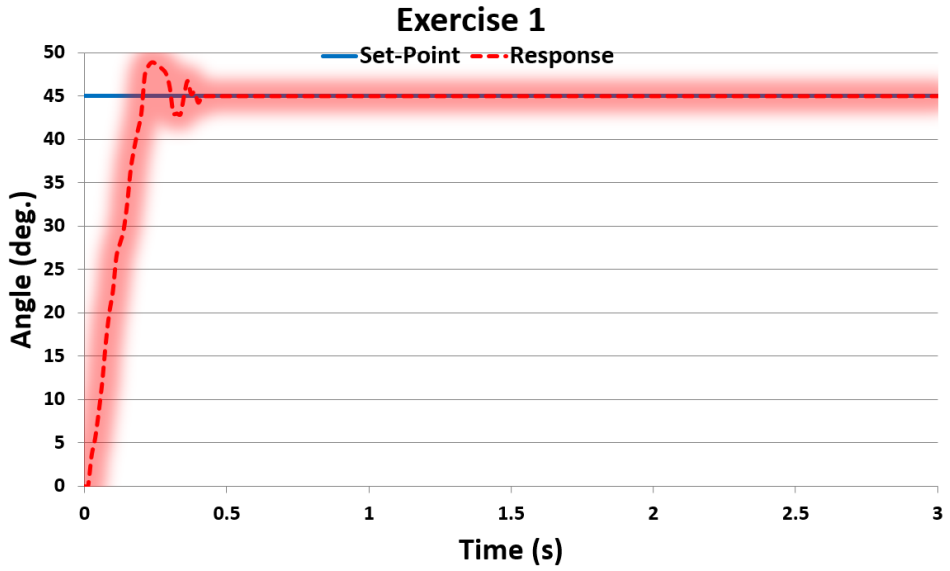

Figure 7.36: The Elbow exoskeleton validation (45º bending angle) with step setpoint.

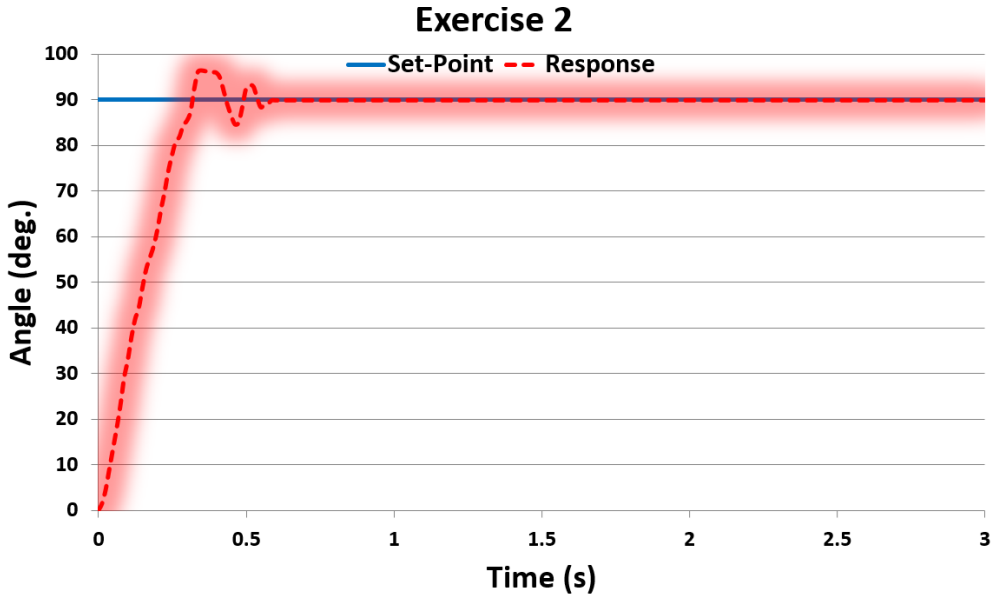

Figure 7.37: The Elbow exoskeleton validation (90º bending angle) with step setpoint.

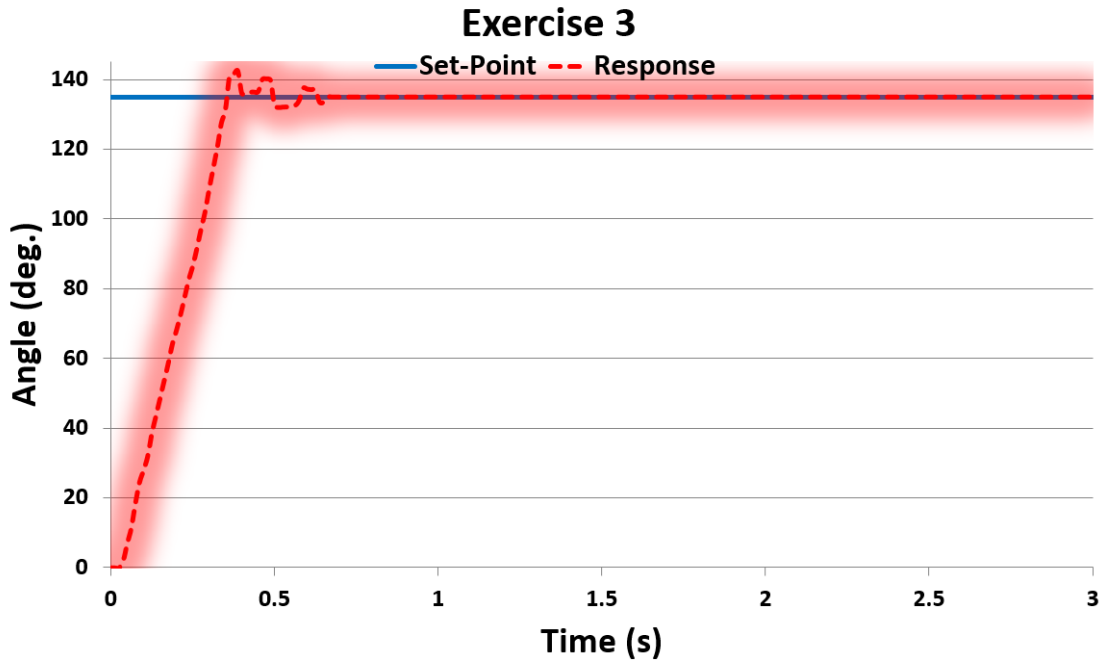

Figure 7.38: The Elbow exoskeleton validation (135^{o} bending angle) with step setpoint.

The experiment was repeated with a sinusoidal setpoint with amplitude of 138^{o} bending angle (the assumed maximum bending angle for the Elbow). Figure 7.39 shows the results which were repeated 20 times using the same procedure as the experiment shown in Figure 7.36 and the recoded RMSE value between the average response and the setpoint was found to be 9.19.

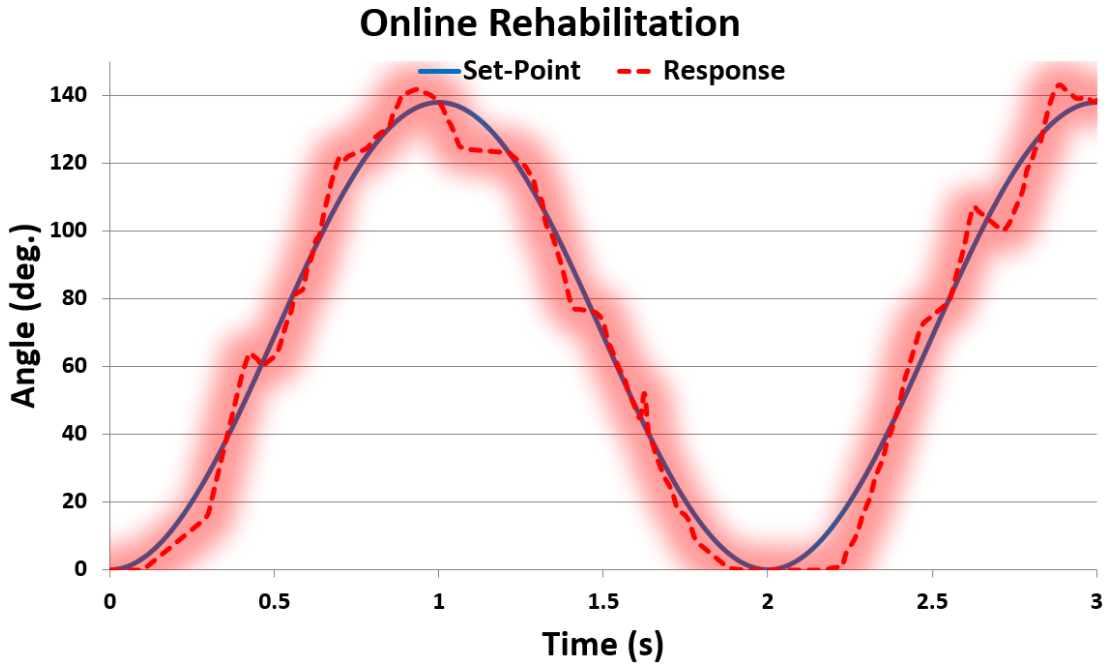

Figure 7.39: The glove validation (Thumb finger) with sinusoidal setpoint.

7.4.1 Modifications to the Elbow Rehabilitation Exoskeleton Actuation System

This elbow exoskeleton bends the wearer's arm when pressurised and, by deflating the actuators, the wearer's arm becomes unbent because of the vertical arm mass. The arm mass produces a vertical force directed to the ground. However, if the elbow rehabilitation exercise is done with the wearer's arm being horizontal, then the exoskeleton doesn't have the pulling force to make the wearer's arm straight after the bending occurs. The exoskeleton depends on the arm mass to return the arm to zero position; then the exoskeleton can perform the vertical exercises, as shown in Figures 7.30 (a), (b) and (c), but cannot perform the exercises in Figures 7.30 (d), (e) and (f).

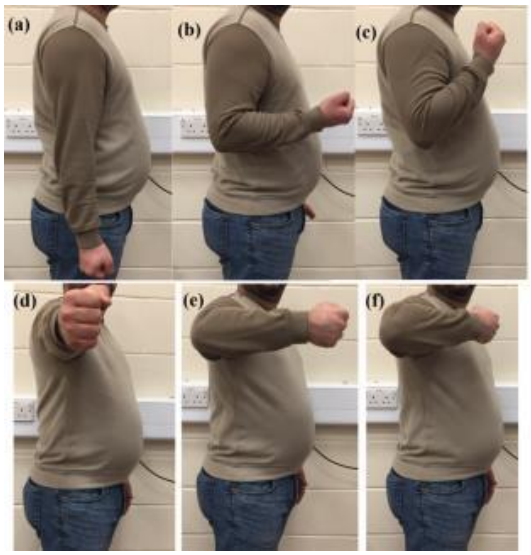

Figure 7.30: Vertical and horizontal elbow rehabilitation exercises.

Inspired by this issue, a new bidirectional bending PAM (BBPAM) has been developed to use in elbow exoskeletons and overcome this problem. To manufacture the novel BBPAM, moulding a novel elastic bladder has been made by mixing liquid elastic materials. The full bladder manufacturing process is described in detail in Appendix A1. Figures 7.31 (b) and (c) show the operation of the BBPAM by actuating each part separately to produce bidirectional bending movements. The new version of the elbow exoskeleton replaces the EBPAMs with BBPAMs. Now the new version of the elbow rehabilitation device is capable of bending in two directions in order to perform vertical and horizontal elbow rehabilitation exercises. In addition, this novel BBPAM has controllable stiffness due to the relationship between the two-part pressures. The maximum output force of BBPAM is approximately the same as the bending actuator (M3 in chapter

5); 39N in 5bars pressurised in a single direction. The output force is slightly less than the EBPAM because of the impedance applied from the deflated half of the bladder. The new elbow exoskeleton with the BBPAMs has double the force of a no load of a single one at 78N.

Figure 7.31: The BBPAM operation.

7.5 Wrist Rehabilitation Exoskeletons

There are a limited number of wrist rehabilitation movements, such as flexion, extension, radial deviation (abduction) and ulnar deviation (adduction). The challenge is to accomplish all wrist motions using a single exoskeleton without any assistance from a rehabilitation therapist.

The biomechanics of the wrist joint are more complex than the resulting movements of the wrist would suggest. The wrist movements of interest are illustrated in Figure 7.32. The Flexion/Extension, Radial/Ulnar deviation bending angles (Celestino, 2003) are:

- Extension: 0 to 70 degrees
- Flexion: 0 to 90 degrees
- Radial Deviation: 0 to 20 degrees

- Ulnar Deviation: 0 to 50 degrees

A lightweight, small and simple to utilise wearable robot, capable of performing wrist rehabilitation movements, has been developed using a combination of contracting and bending pneumatic muscles, as shown in Figure 7.33. The air pressure supply to each actuator is controlled by MATRIX 3/3 solenoid valves, which control the air flow by pulse width modulation.

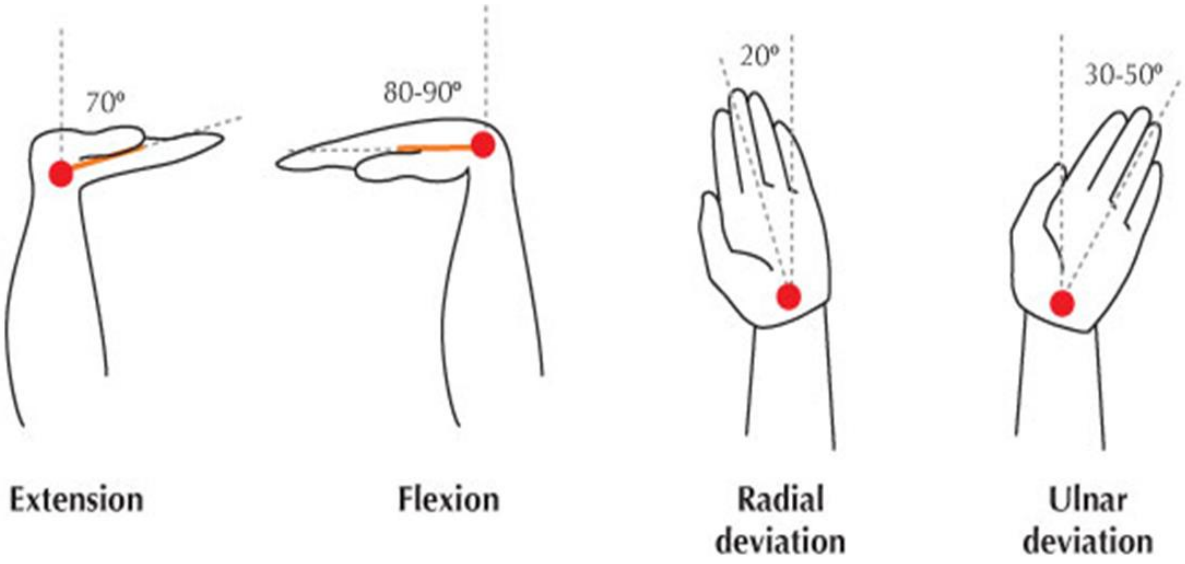

Figure 7.32: Kinematics of Wrist Motion (Medlej, 2014).

Figure 7.33 shows the prototype wrist force assist and rehabilitation wearable robot. The wrist flexion motion is generated by two (to increase power) extensor bending actuators (M2 in chapter 5) sewn onto the top face of a leather glove, as shown in Figure 7.34 (a). The extension movement is generated by a single contracting actuator located between the two bending muscles on the top of the glove, as shown in Figure 7.34 (b). Ulnar and radial deviation motions are produced by two contractor actuators placed along the sides of the leather glove which, when activated, cause the hand to move in either abduction or adduction, as shown in Figures 7.34 (c) and (d).

The overall weight of the proposed exoskeleton prototype is 0.15Kg. As the proposed exoskeleton is low in weight and made from flexible materials, it is safe for direct human interaction and is portable. It will also fit any adult hand size without the need for calibration or mechanical changes, making it suitable to use in the home and without the need of a therapist.

The performance of this soft rehabilitation exoskeleton was assessed through some basic practical experiments. The pressure in the muscles was controlled in an open loop manner and it was evident that the system was capable of moving a user's wrist joint through flexion, extension, radial deviation and ulnar deviation motions. The wrist rehabilitation exoskeleton can achieve the maximum bending angles (see Figure 7.32) for each wrist's movement side. The maximum amount of pressure needed for each movement varies from person to person because it depends on the hand size and mass.

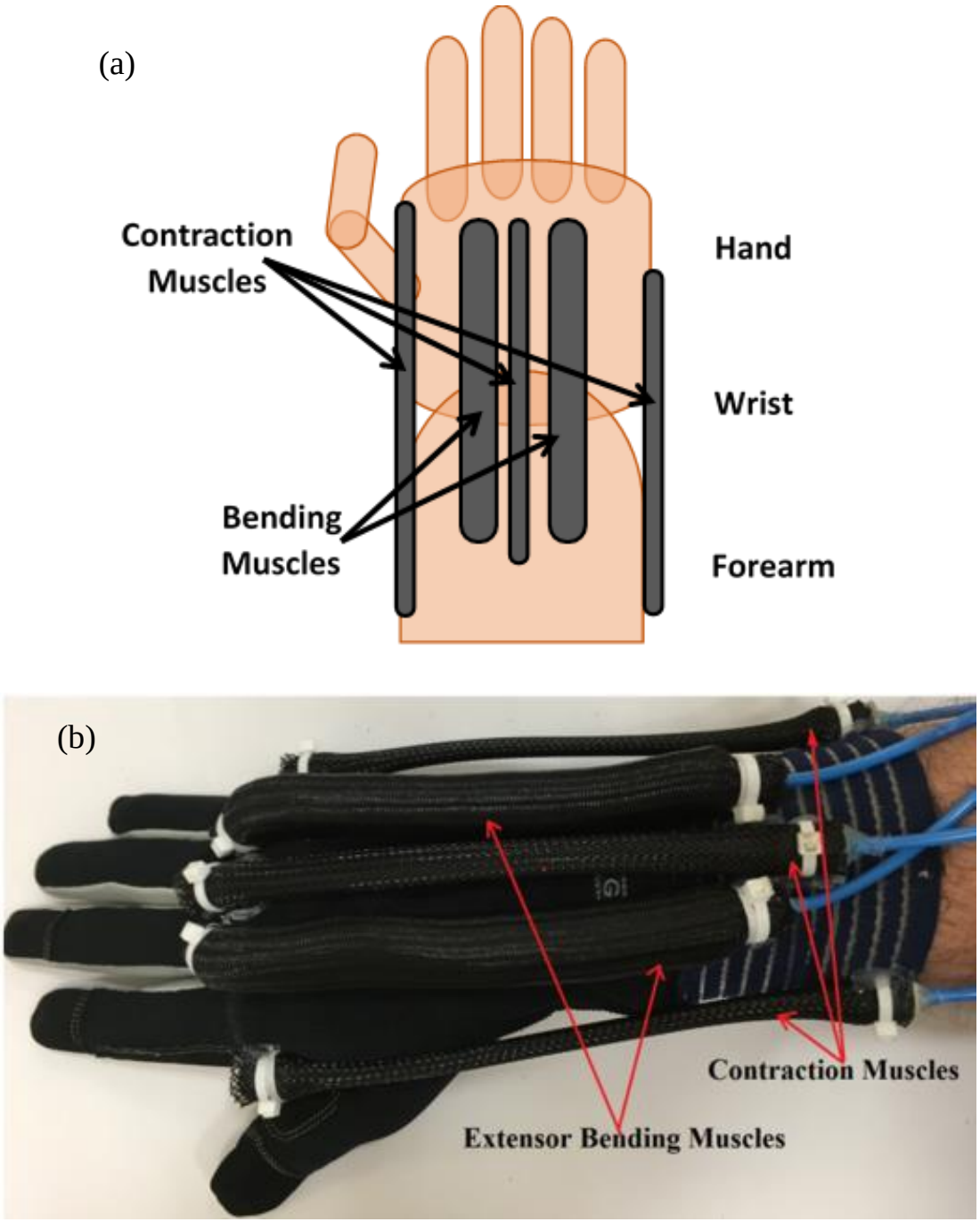

Figure 7.33: The proposed wrist soft exoskeleton.

7.5.1 Modifications to the Wrist Rehabilitation Exoskeleton Actuation System

Five actuators have been used in the wrist exoskeletons. To reduce the number of actuators to a single muscle capable of performing all wrist rehabilitation exercises, a new actuator has been developed based on the moulded bladder that was explained in section 7.4. All directional bending PAM (ABPAM) has been made by using the moulding bladder technique. The full bladder manufacturing process is described in detail in Appendix A2. The maximum output force of ABPAM is approximately the same as the bending actuator (M3 in chapter 5); 37N in 5bars pressurised in a single direction. The output force is slightly less than the EBPAM because of the impedance applied from the other three deflated bladders.

Figure 7.34: The rehabilitation movements of the proposed wrist soft exoskeleton: (a) Wrist flexion movement, (b) Wrist extension movement, (c) Wrist ulnar deviation movement (d) Wrist radial deviation movement.

Figure 7.35 shows the ABPAM operation using pressurised bladder lines altogether to have a stiff actuator for a straight zero position (Figure 7.35 (a)). Figures 7.35 (b to e) illustrates that by pressurising a single line of the bladder each time, it will have a different binding direction each time also. This actuator has controllable stiffness by controlling the amount of pressure in each line of the bladder. The new version of the wrist rehabilitation only places one ABPAM on the middle top of the leather glove with three bits of Velcro to keep the actuator alignment on the top of the hand, as shown in Figure 7.36. The wrist rehabilitation exercises using the new prototype is shown in Figure 7.37.

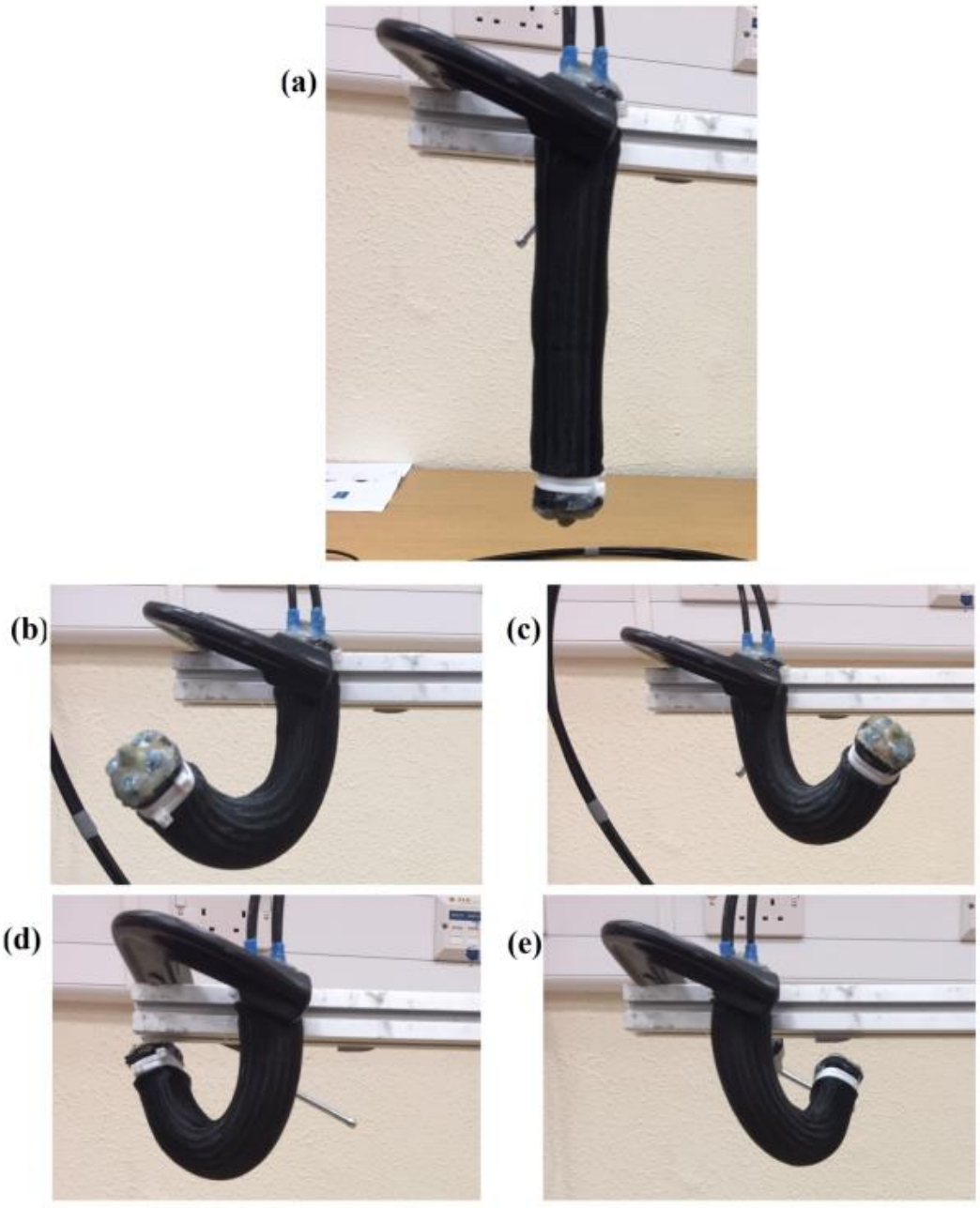

Figure 7.35: The ABPAM operation.

The range of motions with the new wrist prototype is the same as the previous prototype, with the only difference being the applied pressure in each directional movement. The maximum output force in each direction of the new prototype depends on the supplied pressure. The previous prototype had greater maximum force in each direction because the flection movement was actuated by two bending muscles and the other movements were actuated by contraction muscles (the contraction muscles have a higher force-to-weight ratio than the bending muscles).

Figure 7.36: Wrist rehabilitation exoskeleton based on ABPAM.

Figure 7.37: Wrist rehabilitation exercises based on the new version of the wrist rehabilitation prototype.

7.6 Conclusion

Human assistance innovation is essential in an increasingly aged society and one technology that may be applicable is exoskeletons. However, traditional rigid exoskeletons have many drawbacks. Upper-limb rehabilitation devices have been developed in this chapter; hand, wrist, forearm and elbow exoskeletons are developed to serve the rehabilitation issues.

Fingers rehabilitation glove has been developed to bend the fingers (full bending) by using our novel bending muscles. To solve the zero position (straight fingers) problem for post-stroke patients, a new controllable stiffness bending actuator has been developed with a novel prototype. Online and offline controller systems have been designed for the hand exoskeleton and the results have been assessed experimentally. A new design of variable stiffness actuators to control the bending segment have been developed to create a new version of hand exoskeletons to achieve more rehabilitation movements in the same single glove, such as hook and table fists.

A forearm rehabilitation exoskeleton has been developed for pronation and supination movements. This exoskeleton is based on our novel ECPAM and is actuated by an open loop controller to evaluate the performance of the exoskeleton.

The elbow rehabilitation exoskeleton is designed based on our novel bending actuators with online and offline feedback controllers. A novel two-directional bending actuator has been developed based on moulding a bladder from elastic liquid materials. This bending actuator has been used to enhance the elbow exoskeleton to make it capable of performing the rehabilitation exercises vertically and horizontally with a controllable stiffness.

A wrist exoskeleton has been developed to perform the wrist rehabilitation movements. This prototype is based on five actuators (two bending and three contraction actuators) and is operated using an open loop controller to examine the performance of the device. The novel all-directional bending actuator is developed based on the moulding bladder technique. This actuator is used to develop the wrist rehabilitation exoskeleton by reducing the five actuators to a single all-directional bending muscle.

Chapter 8

Parallel Processing based on On-Chip Controllers for a Totally Portable Exoskeleton

8.1 Introduction

In the last few decades there have been huge developments in the control systems. Control systems are used in numerous applications, such as robotics, computer control, space technology and power systems, as well as a lot of other applications. Due to the fast development in control systems, many types of controllers have been developed. Each control system has advantages and disadvantages, and the researcher must choose the best controller for his system based on many factors, such as the nature of the prototype (size, nonlinearity, time varying and complexity), specifications, control objective, and cost. On-Chip Controller (OCC) is a co-processor that is embedded directly onto the main processor die. The OCC is used for embedded and portable systems which don't need a computer to build a controller on its application, such as Matlab. These systems generally contain a central processing unit (CPU), memory and input/output ports, all on a single board. It might include analogue, digital, mixed signal, and digital signal processing, depending on the board properties. Parallel processing is a technique for concurrently processing functions and executing the program parts in parallel on multiple microprocessors to reduce the execution time and have several programs active in parallel. This can be done by a single computer with a multi-processor or by a network for more than one computer. Using Field-Programmable Gate Array (FPGA) is the best choice if you want to switch

between the OCC and parallel processing programming to have parallel processing controllers on one board without needing a PC.

This chapter includes a procedure for designing and implementing a totally portable rehabilitation system based on parallel processing controllers on-chip. A portable, small and lightweight air compressor is designed as an air pressure supply for the pneumatic rehabilitation system. A rehabilitation glove is used to perform the finger rehabilitation exercises. Rehabilitation exercises are activated by manual switches to perform the desired hand rehabilitation exercise. Three controllers for the thumb, index and middle fingers are programmed concurrently to work in parallel by using the Field-Programmable Gate Array board. The whole system is put in a small bag on the back with a total weight of approximately 4 kg. The system performance was assessed experimentally with successful results.

8.2 Field-Programmable Gate Array (FPGA)

FPGA is a device that includes a reconfigurable gate array logic circuitry matrix. To implement a software for a specific application, the FPGAs internal logic gates are connected to describe the software program in hardware circuitry. In contrast to processors, FPGAs utilise dedicated hardware circuits for logic processing and don't have any operating system. FPGAs are genuinely parallel in nature and various processing tasks don't need to compete for similar resources. Thus, the execution of one part of the application isn't influenced when other processing parts are included. Additionally, multiple control loops can run on a single FPGA device at different rates and all of the controllers can be activated in parallel. FPGA-based control systems can enforce critical interlocking logic and can be designed to prevent I/O forcing by an operator. FPGA boards deliver the performance and reliability of dedicated hardware circuitry (Palchaudhuri & Chakraborty, 2016).

Thousands of discrete components can be replaced by a single FPGA board by incorporating several logic circuits in a single integrated chip. The internal parts of an FPGA device consist of a matrix of configurable logic blocks surrounded by a periphery of input/output blocks, demonstrated in Figure 8.1 (Chine, Mellit, & Bouhedir, 2017).

The process of creating digital logic is not unlike the embedded software development process. A description of the hardware's structure and behaviour is written in a high-level

hardware description language (usually VHDL or Verilog) and that code is then compiled and downloaded prior to execution.

There are many types of FPGA types, such as Xilinx and Altera, and each type has numerous versions. In this research we will use the Altera type version DE0-NANO BOARD.

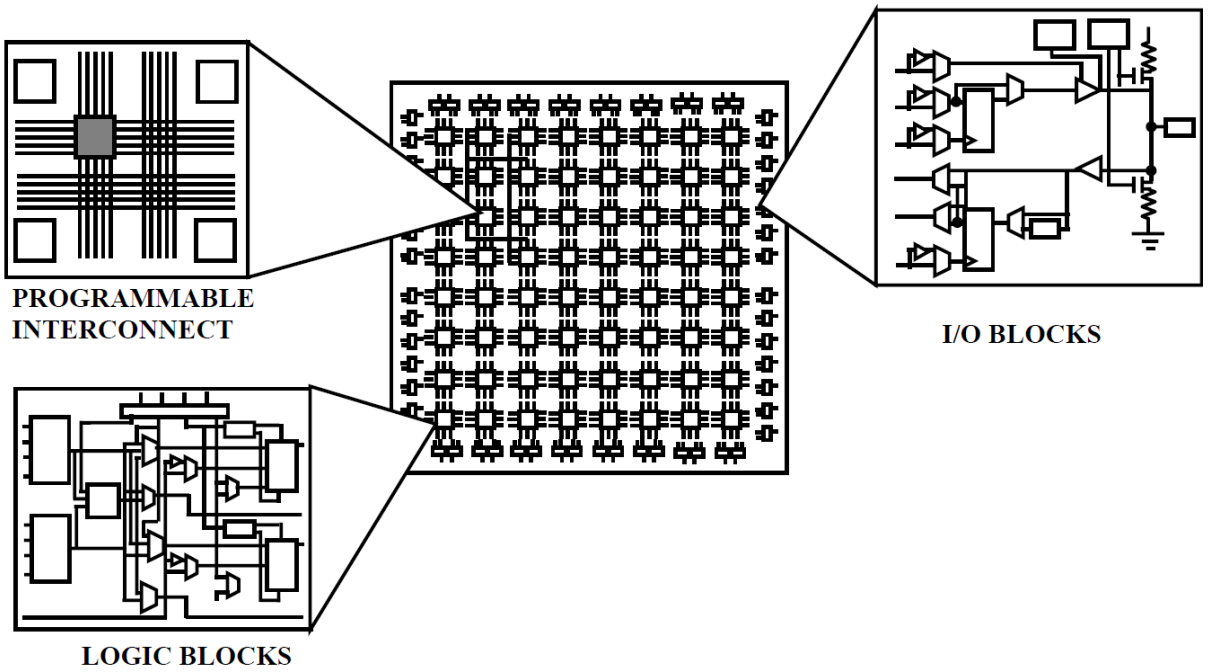

Figure 8.1: FPGA chip.

8.2.1 FPGA DE0-NANO

The DE0-Nano is ideal for use with embedded soft processors, it features a powerful Altera Cyclone IV FPGA (with 22,320 logic elements), 32 MB of SDRAM, 2 Kb EEPROM, and a 64 MB serial configuration memory device (Manual, 2012). For connecting to real-world sensors, the DE0-Nano includes a National Semiconductor 8-channel 12-bit A/D converter and it also features an Analog Devices 13-bit, 3-axis accelerometer device. Figure 8.2 shows the board component diagram and Figure 8.3 shows the board block diagram.

8.2.2 Fuzzy logic controller on FPGA DE0-NANO

A Fuzzy logic controller (FLC) system is demonstrated in Figure 8.4 (Gdaim, Mtibaa, & Mimouni, 2015). The knowledge base is the core of the FLC, including the rule

base which illustrates the controller's behaviour, and the inference engine, which integrates the rule base according to the controller entries. The rule base and the inference engine utilises fuzzy logic sets by transferring the fuzzy logic sets to real measures to have a fuzzification stage. The defuzzification stage is to calculate the controller outputs based on fuzzification and linguistic strategy stages.

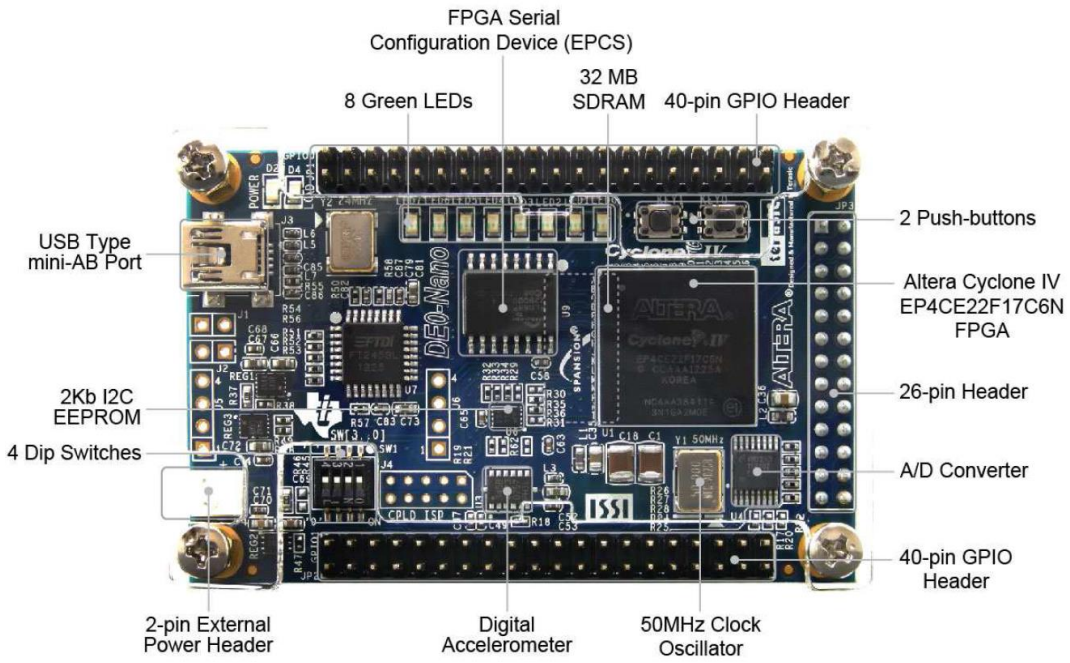

Figure 8.2: The DE0-Nano Board.

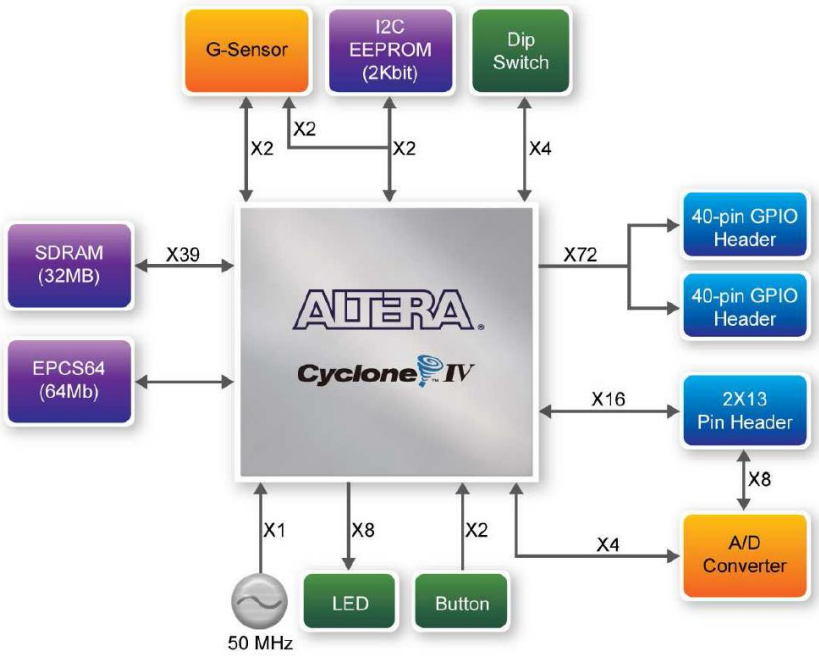

Figure 8.3: Block diagram of DE0-Nano Board.

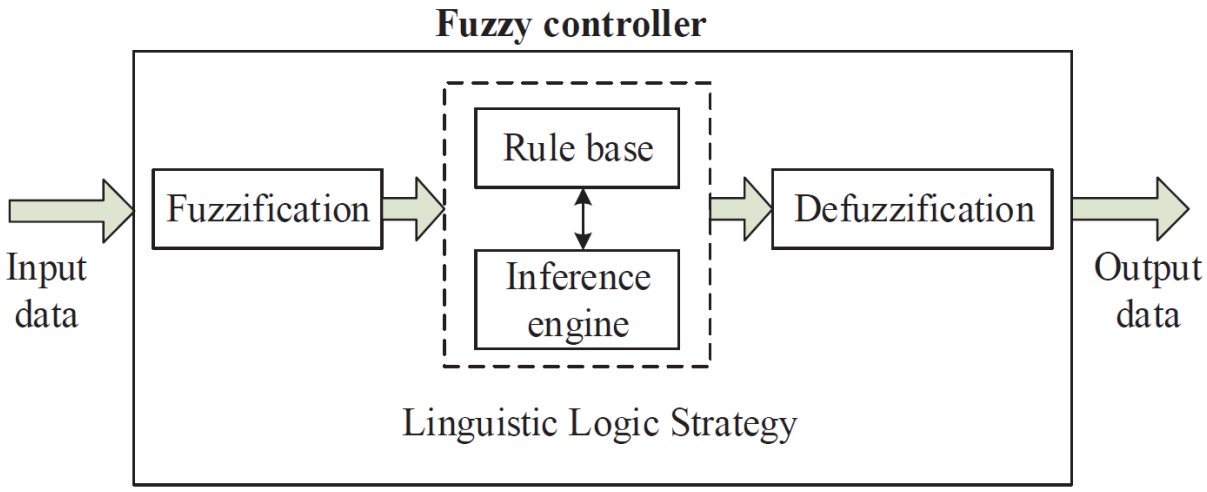

Figure 8.4: Fuzzy logic controller (FLC) system.

8.2.2.1 Fuzzification Stage

Generally, there are two inputs to the Fuzzy logic controller: error (e) and change of error (Δe). Figure 8.5 demonstrates the design of the FPGA implementation. The input values (crisp values (e) and (Δe)) are converted to an interval of $[0, 1]$ for Fuzzy values in the fuzzification block.

The fuzzification block is responsible for converting the crisp input values (error, change of error) to equivalent fuzzy values in the interval [0,1]. Triangle membership-functions are used in this controller. These triangle membership-functions are expressed in VHDL code as a trapezoidal shape presented by two slopes (slope1 and slope2) and two points (point1 and point2), as shown in Figure (8.6). The following code shows the VHDL code for a single membership degree function (Youssef, El Telbany, & Zekry, 2018). The VHDL code is written in a way that the numbers for error and change of error membership degree functions is generic, assuming symmetric membership degree functions. The system designer needs only to specify the number, points and slopes of membership functions. Membership Functions algorithm as the following:

Algorithm 1 Membership Functions

1: ***type error membership functions is array*** $(natural\ range <>)\ of\ error\ member-ship;$

2: ***constant error mfs: error membership functions***: $= ((term => NBf, point1 => x\text{“}00\text{”}, slope1 => x\text{“}FF\text{”}, point2 => x\text{“}2A\text{”}, slope2 => x\text{“}06\text{”});$

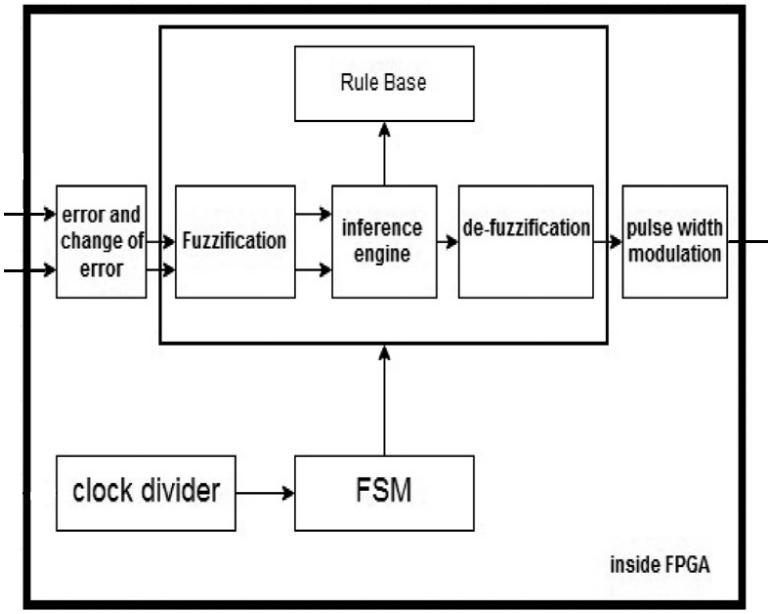

Figure 8.5: Complete VHDL design.

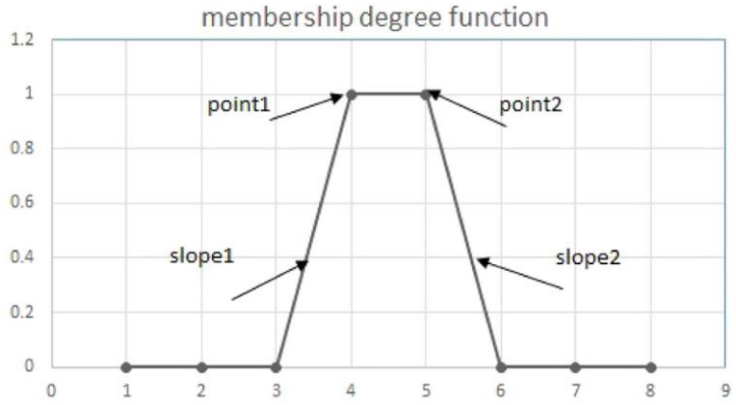

Figure 8.6: Trapezoidal membership-degree.

Figure 8.7 shows the flowchart of the fuzzification process.

Fuzzification algorithm as the following:

Algorithm 2 Fuzzification ();

1: ***Set*** $n = number\ of\ membership\ function$

2: $\boldsymbol{\mu} = array\ of\ degree\ of\ membership\ function\ m = array\ of\ membership$

3: ***function*** *start*

4: ***loop*** *for i= 1 to n*

5: ***if*** *input value<m[i].point1 then μ[i]=0; else if input value<m [i].point2then*

6: ***μ[i]****=(input value -m[i].point1)*m[i].slope1; else μ[i]= 255 - (input value - m[i].point2)*m[i].slope2;*

7: ***end*** *if;* ***end*** *loop;*

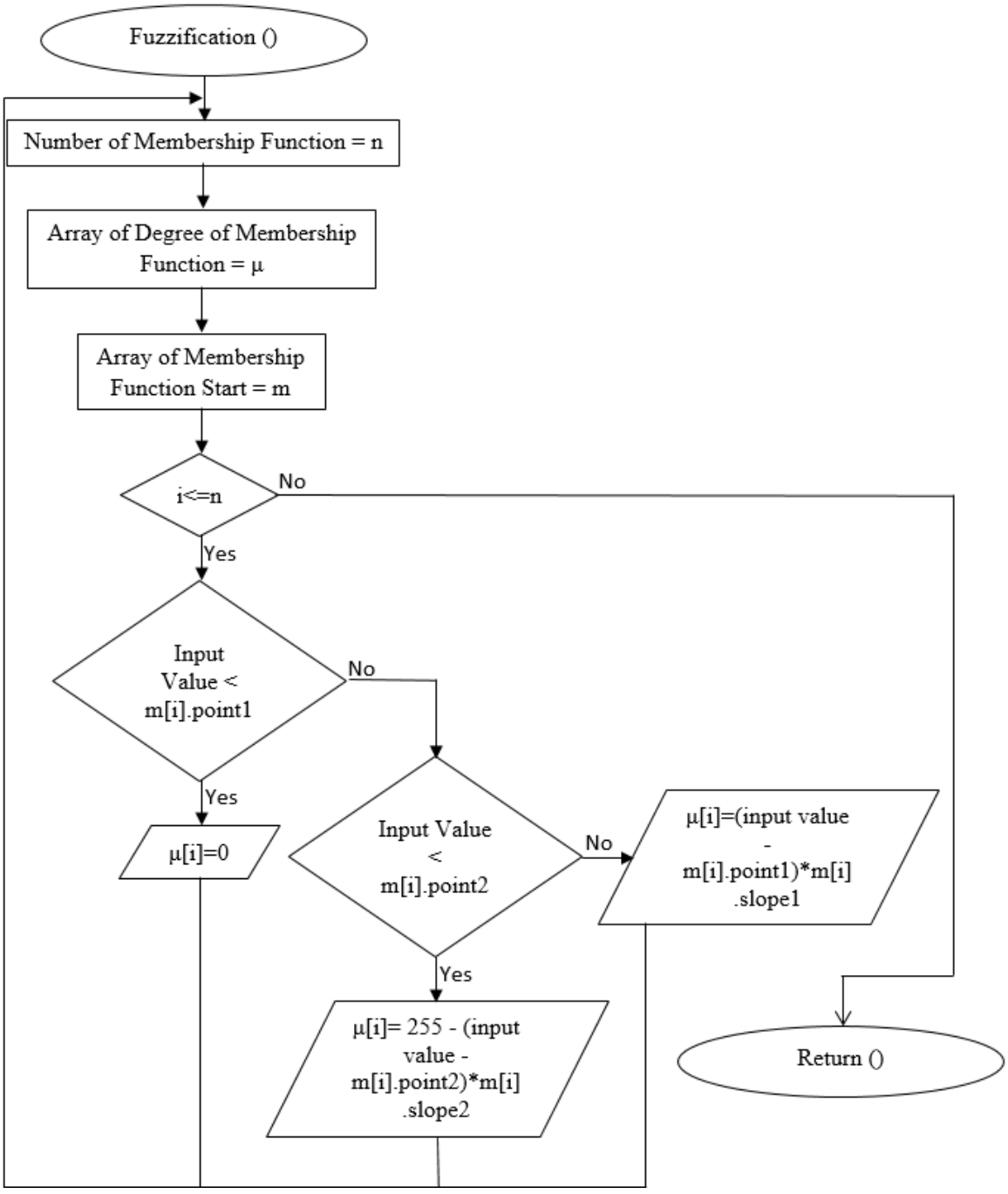

Figure 8.7: Flowchart of the fuzzification process.

8.2.2.2 Inference-Engine Stage

Maximum and minimum VHDL internal functions are used to express the inference-engine process. Two-dimensional arrays are used to implement the rule base table. Inference algorithm as the following:

Algorithm 3 Inference

1: $\boldsymbol{for}\ j\ in\ 0\ to\ noutputmemb\ loop$

2: $\boldsymbol{for}\ k\ in\ 0\ to\ mcount(j)-1\ loop\ tsignal(k):=minimum(membdegree(m1(j,k)),membdegree1(m2(j,k)));$

3: ***end*** *loop;*

4: *MDvaluesn(j): =maximum(tsignal,mcount(j));*

5: ***end*** *loop;*

Maximum function algorithm as the following:

Algorithm 4 Maximum Function

1: $\boldsymbol{function}\ maximum\ (dizi: mytype;\ par: integer)$

2: $\boldsymbol{return}\ stdlogicvector$

3: ***variable*** *maxnumber: stdlogicvector(7 downto 0) for integer i in 0 to 10*

4: ***if****(maxarray: = dizi(i))* ***then***

5: *maxnumber: = dizi(i);* ***end*** *if;*

6: ***end*** *loop;*

7: ***return*** *maxnumber;*

8: ***end*** *maximum;*

8.2.2.3 Defuzzification Stage

By assuming that the output membership-functions are a single shape which will overcome the VHDL code complexity, the centroid defuzzification technique has been used. The defuzzification output is for generating the duty cycle of the PWM block and is calculated with the following equation:

$$Duty = \frac{\sum Fuzzy\_Output \times Singlton}{Fuzzy\_Output} \tag{8.1}$$

The defuzzification algorithm as the following:

Algorithm 5 Defuzzification

1: ***For*** *i = 1 to n do begin product = (s(i) f(i))+* $product$;

2: *sum = f[i] + sum;*

8.2.2.4 Sum Block

The sum block generates the output duty cycle from the duty step size generated by the defuzzification block using the following equation:

$$Dutycycle\ D\ =\ dD(k)\ +\ D(k\ -\ 1) \tag{8.2}$$

where $dD(k)$ is the change in the duty cycle output at the instant K and $D(k\ -\ 1)$ is the duty cycle at a previous instant.

8.2.2.5 Pulse width modulation generator

This stage generates the PWM signal depending on the duty cycle value coming from the fuzzy controller.

8.2.2.6 Finite State Machine (FSM)

This block controls all the blocks of the design. It has three states: s1, s2 and s3. The first state (s1) is reading the input error (e) and change of error (Δe). This state takes four clock cycles. The second state (s2) is the fuzzy controller with one clock cycle. The third state (s3) is loading the duty cycle to the pulse width modulation block by one clock cycle.

8.2.2.7 Clock Divider

A clock divider block is built in VHDL. The block is needed to divide the input clock frequency to the desired clock frequency. Generic code that takes the output frequency as a parameter is written and tested.

8.3 Portable Air Supply

Air supply is the major obstacle to creating a totally portable exoskeleton system based on pneumatic muscles. It must be lightweight and small in size to be easily carried by the wearer. Figure 8.8 shows our design of the portable air compressor. This air compressor has no difference in function to other commercial compressors but it is small in size, low cost, lightweight and easy to makeportable.

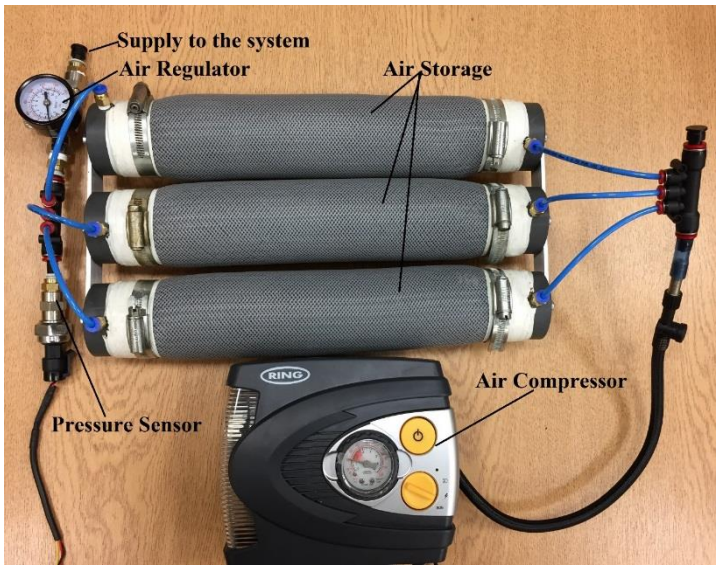

Figure 8.8: Air compressor design.

The air storage unit of the portable compressor contains three soft pneumatic muscles. These muscles are not designed to be extensors or contractors (has a fixed length when inflation or deflation) but by using a specific sleeve length with a braid angle of 54.7^{o}, with this braid angle the force will be zero. The length of each muscle is 32 cm with a 6.5 cm diameter. Traditional tyre inflators with a maximum pressure of 15 bars have been used as an air pressure supply. A manual air regulator is used to regulate the desired pressure for the exoskeleton system. An electronic pressure sensor is used as a limit for the air pressure in the storage unit. Figure 8.9 shows the portable air compressor electronic circuit. Two 18 V 5000mAh rechargeable batteries are used as a voltage supply. The batteries are connected in parallel to increase the electric current for the system. Two 12 V voltage regulators are used to regulate the Tyre Inflator voltage. One 5 V voltage regulator is used to regulate the Arduino voltage. The Arduino is used with a 16 channel servo motor shield to regulate the frequency of the solenoid valve. The driver is used to receive the controlling 5 V PWM signals from the Arduino and transfer them to 18 V PWM.

All the parts of the portable air compressor, such as storage unit, tyre inflator and the electronic circuit, are assembled in a small back-bag with the total weight of approximately 4 kg.

8.4 Totally Portable Rehabilitation System

The proposed portable rehabilitation system block-diagram is illustrated in Figure 8.10.

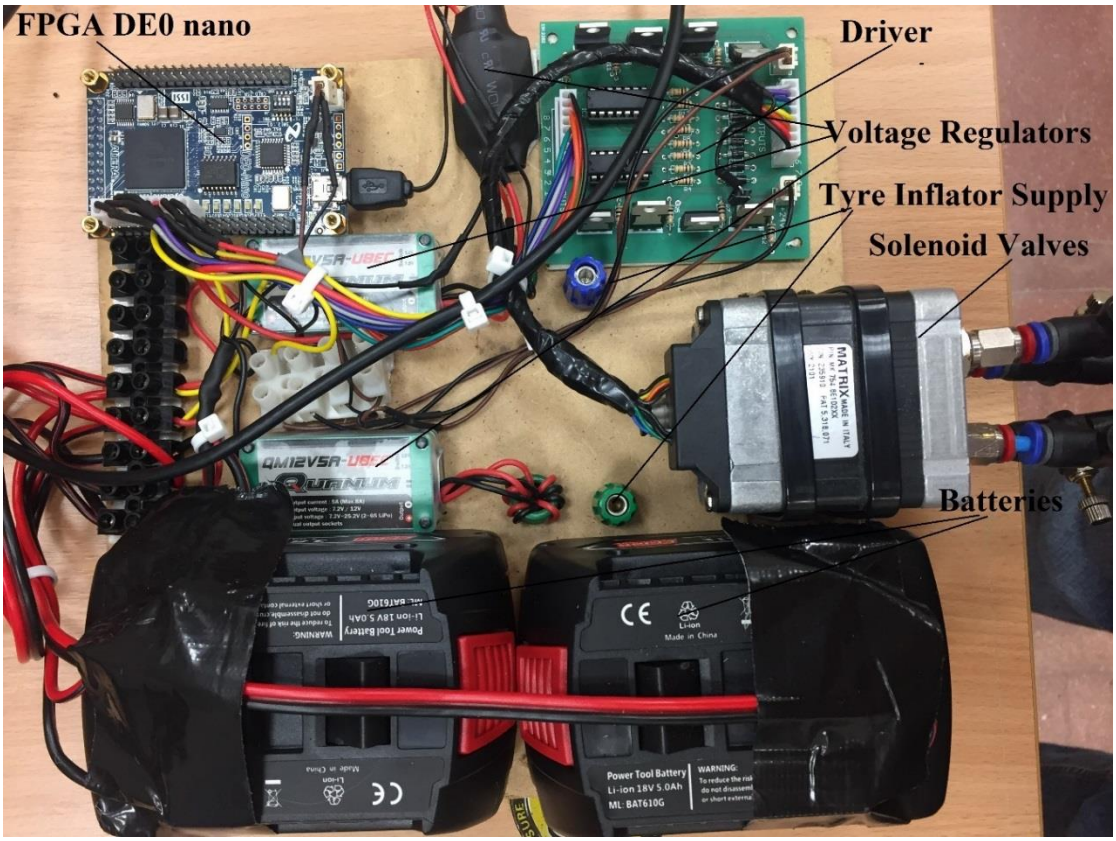

Figure 8.9: Air compressor electronic circuit.

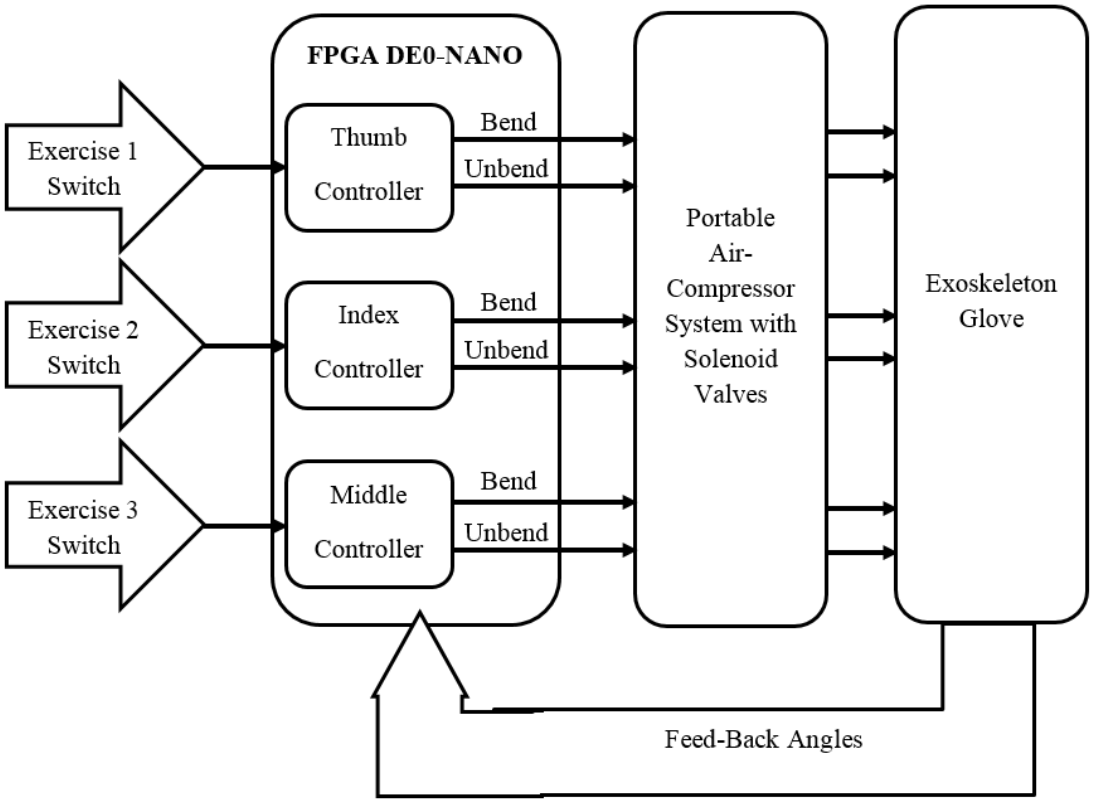

Figure 8.10: The proposed block-diagram portable rehabilitation system.

We used the same rehabilitation glove in section (7.2.2.2) with the same off-line controller in section (7.2.2.3). Three switches are used to select the desired exercise. Switch number one is used to operate a thumb finger rehabilitation exercise which is a repetitive movement that bends the thumb finger by the set-point bending angle, e.g. 150^{o}. Switch number two is used to activate the index finger controller for an index finger rehabilitation exercise. Switch number three activates the middle, ring and little fingers rehabilitation exercise together, as we explained in chapter 7.

Three Fuzzy logic controllers (the same controller in 7.2.2.3) are programmed as parallel controllers on-chip in a FPGA DE0-NANO kit. These controllers are programmed by using concurrent techniques to operate in parallel independently. Each controller is programmed by the same procedure in section 8.2.2. The thumb controller controls the thumb fingers bending angle with a procedure of repetitive movements when switch number one is active and receiving the feed-back signal from the celebrated flex bend sensor allocated between the thumb and the bending muscle. The index controller controls the index finger movements when switch number two is activated and also receives the bending angle feed-back signal from a flex bend sensor placed on the top of the index finger. Finally, the middle controller is activated when switch number three is active to control the middle, ring and little fingers together by receiving a feed-back signal from a bending sensor allocated on the middle finger. Due to the three controllers being programmed in parallel, more than one controller can be activated at the same time to discover the most commonly used hand rehabilitation exercises, as shown in chapter 7 Figure 7.15. Figure 8.11 shows the wearer wears the rehabilitation system.

8.5 Conclusion

The rehabilitation system should be lightweight and easily portable so that the rehabilitation exercises can be done anywhere, not only in the rehabilitation clinic. It should also be easy for the patient to use without needing rehabilitation supervision.

The controller system is designed to be an on-chip controller and not need any PC to be connected. A FPGA DE0-Nano Board is used as a controller system, PC free. A parallel processing controller technique is used to implement the controller system, to overcome the complexity and signals conflict, and to also reduce the processing time.

A portable air pressure supply is designed so as to supply the air pressure to the rehabilitation system. It is a rechargeable system, lightweight and small in size.

A rehabilitation glove is used as a rehabilitation exoskeleton based on our novel bending muscles. The rehabilitation exercises can be activated by three manual switches to choose the desired exercise.

Figure 8.11: The wearer wears the rehabilitation system.

Chapter 9

Conclusion and Future Work

9.1 Conclusion

Wearable exoskeleton devices are a combination of human intelligence and machine power. The strength of the human is improved when they wear the device. During recent decades, inventors have been persistently working towards increasing their knowledge of wearable exoskeletons. Exoskeleton robots are expected to play a critical part in the rehabilitation fields, mechanical assistance technology and the augmentation of human force. A limited number of upper-limb wearable robots have been created for different purposes with particular benefits and drawbacks. Power assistive and rehabilitation wearable robots have to be safe, lightweight, small and soft. All these features are found in pneumatic soft muscles and, therefore, many researchers depend on these soft actuators to manufacture power assistive and rehabilitative wearable robots.

The significant motivation for researchers to create and utilise PAMs is the remarkable closeness between them and natural muscles. The most widely recognised PAMs configuration depends on McKibben's muscles. PAMs have generally been utilised as a component when assembling another type of robot, known as ‘soft robots’ or ‘continuum robots’. Moreover, since the PAMs are developed from soft materials, they have the ability to provide safer devices when contrasted with conventional inflexible robots with direct human interaction. Numerous applications have been done based on PAMs because of their wide range of points of interest. These applications have increased

in the last decade, covering many fields, such as biorobotics, medical, industrial, and aerospace applications.

The conclusion of the work done in this research has been listed in the following points:

1- The design and implementation of a novel extensor contractor pneumatic artificial muscle. The Extensor-Contractor Pneumatic Artificial Muscle (ECPAM) is formed from a combination of contraction and extensor muscles. The new actuator consists of a contraction muscle placed inside an extensor muscle. This new actuator overcomes some of the limitations associated with the use of single pneumatic muscles as well as having additional features. This new actuator has bidirectional action allowing it to both extend and contract and create force in both directions.
    a. This muscle is capable of extending and contracting in reference to its nominal length by controlling the amount of the pressure inside both extensor and contractor muscles.
    b. This muscle has higher stiffness in contrast to traditional extensor and contractor muscles and this has been assessed experimentally to prove this novelty point.
    c. A kinematics analysis has been done of the new actuator based on its geometrical parameters.
    d. A pushing/pulling force mathematical model has been developed for this actuator to understand the behaviour of this new actuator and describe it mathematically.
    e. Experimental verification has been done for the new mathematical model. The average error percentages between the mathematical model and the experimental results are approximately 20%.
    f. Mathematical model enhancement has been made and it is assessed experimentally. This enhancement process decreased the average error percentages between the mathematical model and the experimental results by approximately 70%.
    g. At a fixed load and position a traditional pneumatic muscle has a single fixed stiffness value. The reason for this is that the actuator's stiffness is a result of the pressure in the actuator, with higher pressure resulting in greater stiffness. However, pressure is proportional to muscle output force

and so increasing the pressure in a muscle which is supporting a fixed load will result in contraction of the muscle and change in position. It is therefore not possible to change a pneumatic muscle's stiffness independently of its force or position. The newly developed ECPAM, however, has the ability to potentially vary its stiffness independently of its position. A controllable stiffness experimental verification has been made to prove the novelty of the new actuator.

h. Accurate control of McKibben muscles presents a major challenge, this is because of both the nonlinear behaviour of the muscles and the compressibility of air. Much of the control of pneumatic muscle has relied on classical control techniques and simple models of the actuator functionality that include many assumptions. A Stiffness and Position (length) Control has been created for the new actuator to validate the stiffness novelty.

2- Design and implementation of a novel extensor bending soft actuator. The proposed extensor bending pneumatic artificial muscles (EBPAMs) are based on linearly extending McKibben artificial muscles. These muscles are reinforced along one side keeping one side of the actuator at a fixed length. This means that when pressurised the new actuator does not extend in length but rather bends.

a. A kinematic analysis of this actuator has been created. The analysis of the EBPAM is based on the following assumption: the muscle retains a circular cross-section during bending, the threads used to form the sleeve and reinforce one side of the muscle are inextensible, there is no friction force between the sleeve and the bladder and between the threads of the sleeve and there are no elastic forces within the bladder.

b. A mathematical output force model for this actuator is developed. However, if the bending muscle is to be used in an application, it is important that its force generating behaviour is also understood. The average error percentage between the force mathematical model and the experimental results is approximately 15%. This error is not unexpected as the model used is simplistic and does not consider energy losses within the muscle.

c. Three stages for enhancing this model has been done. The first enhancement stage is based on the energy spent radially expanding the rubber bladder before it makes contact with the braided sleeve. This enhancement stage

reduces the error percentage by approximately 45%. The second enhancement stage takes into consideration the thicknesses of the sleeve and the bladder to reduces the error percentage (error after first stage enhancement) by approximately 30%. The third stage of the model enhancement is based on the total actuator volume by eliminate the assumption of the actuator is perfectly cylinder and there are no deformations segments at the ends of the actuator. In reality, deformations occur at the actuator terminals because the ends caps of the extensor muscles have a diameter smaller than the muscle cylindrical body. These deformations are similar in shape to a frustum of a cone, taking this in consideration to reduces the error percentage (error after second stage enhancement) by approximately 22%.

3- A novel design for a power assistive glove has been developed to overcome the release movements problem with a simple controller for validation has been created. The proposed prototype outputs 17 N maximum force at the fingers for bending at 4 bar, showing that the assistive amount is up to 40% and 45% respectively for healthy men and women over 50. An efficient solution for the release movement problem is presented. EMG signals from the hand are monitored to clarify that solution. The proposed control algorithm gives a high performance of multiple gripping/pinching movements, assisted by pressure sensors as a feedback signal, and using bending joint angles as the set-points.

4- A novel power augmentation hand exoskeleton has been developed. The proposed bending soft actuators also actuate this exoskeleton. The control system of this exoskeleton was created by hybridization between both the cascaded position and force closed loop intelligent controllers. The cascaded position controller is designed for the bending actuators to follow the fingers in their bending movements. The force controller was developed to control the grasping force augmentation. Validation of the controller system with the exoskeleton has been done experimentally in this research. EMG signals were monitored to validate whether the proposed exoskeleton system decreased the muscular efforts of the wearer during the experiments.

5- A rehabilitation glove for the fingers has been developed to bend the fingers (full bending) by using the novel bending muscles designed. To solve the zero position (straight fingers) problem for post-stroke patients, a new controllable stiffness

bending actuator has been developed with a novel prototype. Online and offline controller systems have been designed for the hand exoskeleton and the results have been assessed experimentally. A new design of variable stiffness actuators to control the bending segment have been developed to create a new version of hand exoskeletons to achieve more rehabilitation movements in the same single glove, such as hook and table fists.

6- A new design for a forearm rehabilitation exoskeleton based on the novel extensor contractor actuator has been created in this research.

7- The elbow rehabilitation exoskeleton is designed based on the novel bending actuators with online and offline feedback controllers. A novel two-directional bending actuator has been developed based on moulding a bladder from elastic liquid materials. This bending actuator has been used to enhance the elbow exoskeleton to make it capable of performing the rehabilitation exercises vertically and horizontally with a controllable stiffness.

8- A novel bidirectional bending actuator based on a moulded bladder has been developed in this research and it is used to create a new version for an elbow rehabilitation exoskeleton.

9- A novel design for a wrist rehabilitation device based on the traditional contraction muscles and the novel bending actuator has been developed in this research.

10- A novel all-directional bending actuator based on a moulded bladder has also been developed and it is used to create a new version of a wrist rehabilitation exoskeleton based on a single actuator.

11- The design and implementation of a totally portable rehabilitation system based on parallel processing controllers on-chip has been developed in this research.

9.2 Future Work

Soft robotics draws heavily from the way in which living organisms move and adapt to their surroundings. In contrast to robots built from rigid materials, soft robots allow for increased flexibility and adaptability for accomplishing tasks, as well as improved safety when working around humans. These characteristics allow for its potential use in the fields of medicine and manufacturing.

The plan for future work on this Ph.D. research is to design, construct and control lower-limb exoskeleton segments based on PAMs for power assistive and rehabilitation

purposes. The problems with previous designs of exoskeletons will be taken into consideration, then as many of these problems as possible will be addressed. During this work, all the planned aims and research objectives were successfully accomplished. However, there were some of limitations and possibilities for future work in the proposed design it will illustrated in the following points:

1- Enhance the output force mathematical model of ECPAM by taking into consideration new factors such as the frictional forces between the braids and the bladders or between the nylon threads of the braid or between the contractor muscle and the bladder of the extensor muscle and that there were no elastic forces within the bladders.
2- More enhancement stages for the EBPAM mathematical model by taking in consideration the energy losses within the muscle.
3- Develop the power assistive and augmentation gloves to be more accurate by taking in consecration the real time EMG signals from the wearer as a feedback signal to the controller system.
4- Test out rehabilitation prototypes with real patients and monitor the recovery effectiveness of the exoskeletons to the wearers to enhance the future prototypes by taking into consideration the real patients comments.

The new actuators and exoskeletons developed in this work will be of interest to researchers working in sectors other than in healthcare, the main focus of this research. The ability to use the system for force augmentation has application other sectors, for example in manufacturing or assembly tasks operators could use the systems developed to give them additional strength or to reduce fatigue by removing strain from the user's own muscles. The low material cost and the fact that the system does not need to be custom designed for individual users means it potentially offers a low cost solution in industrial settings.

Another area where the technology could be applied is in future astronaut suits. The pressure difference between the inside of an astronaut's suit and the vacuum of space combined with the multiple layers of protective fabric means it is difficult and often hard work for an astronaut to perform delicate and repetitive motions and grasps. The soft actuators developed in this research could be incorporated into a spacesuit to allow the user greater dexterity and reduce their fatigue during spacewalks.

Bibliography

Akbari, S., Rosset, S., & Shea, H. R. (2013). Improved electromechanical behavior in castable dielectric elastomer actuators. *Applied Physics Letters, 102*(7), 071906.

Al-Ibadi, A., Nefti-Meziani, S., & Davis, S. (2016). *Valuable experimental model of contraction pneumatic muscle actuator.* Paper presented at the 21st International Conference on Methods and Models in Automation and Robotics (MMAR), 2016

Albu-Schäffer, A., & Bicchi, A. (2016). Actuators for Soft Robotics *Springer Handbook of Robotics* (pp. 499-530): Springer.

Andrikopoulos, G., Nikolakopoulos, G., & Manesis, S. (2011). *A survey on applications of pneumatic artificial muscles.* Paper presented at the Control & Automation (MED), 2011 19th Mediterranean Conference on Control and Automation(MED), Aquis Corfu Holiday Palace, Corfu, Greece.

Araromi, O. A., Gavrilovich, I., Shintake, J., Rosset, S., Richard, M., Gass, V., & Shea, H. R. (2015). Rollable multisegment dielectric elastomer minimum energy structures for a deployable microsatellite gripper. *IEEE/ASME Transactions on mechatronics, 20*(1), 438-446.

Arena, P., Bonomo, C., Fortuna, L., Frasca, M., & Graziani, S. (2006). Design and control of an IPMC wormlike robot. *IEEE Transactions on Systems, Man, and Cybernetics, Part B (Cybernetics), 36*(5), 1044-1052.

Aureli, M., Prince, C., Porfiri, M., & Peterson, S. D. (2009). Energy harvesting from base excitation of ionic polymer metal composites in fluid environments. *Smart Materials and Structures, 19*(1), 015003.

Ayers, J., & Witting, J. (2007). Biomimetic approaches to the control of underwater walking machines. *Philosophical Transactions of the Royal Society of London A: Mathematical, Physical and Engineering Sciences, 365*(1850), 273-295.

Ball, S. J., Brown, I. E., & Scott, S. H. (2007). *MEDARM: a rehabilitation robot with 5DOF at the shoulder complex.* Paper presented at the Advanced intelligent mechatronics, 2007 IEEE/ASME international conference on.

Barramba, J., Silva, J., & Branco, P. C. (2007). Evaluation of dielectric gel coating for encapsulation of ionic polymer–metal composite (IPMC) actuators. *Sensors and Actuators A: physical, 140*(2), 232-238.

Beullens, T. (1989). Hydraulic or pneumatic drive device. United States: Google Patents.

Boblan, I., & Schulz, A. (2010). *A humanoid muscle robot torso with biologically inspired construction.* Paper presented at the Robotics (ISR), 2010 41st International Symposium on and 2010 6th German Conference on Robotics (ROBOTIK), Munich, Germany.

Caldwell, D., Medrano-Cerda, G., & Goodwin, M. (1993). *Braided pneumatic actuator control of a multi-jointed manipulator.* Paper presented at the International Conference on Systems, Man and Cybernetics, Le Touquet, Paris.

Caldwell, D. G., Medrano-Cerda, G. A., & Goodwin, M. (1995). Control of pneumatic muscle actuators. *Control Systems, IEEE, 15*(1), 40-48.

Carpi, F., De Rossi, D., Kornbluh, R., Pelrine, R. E., & Sommer-Larsen, P. (2011). *Dielectric elastomers as electromechanical transducers: Fundamentals, materials, devices, models and applications of an emerging electroactive polymer technology*: Elsevier.

Celestino, J. R. (2003). *Characterization and control of a robot for wrist rehabilitation.* Massachusetts Institute of Technology.

Chan, S., Lilly, J. H., Repperger, D. W., & Berlin, J. E. (2003). *Fuzzy PD+ I learning control for a pneumatic muscle.* Paper presented at the Fuzzy Systems, 2003. FUZZ'03. The 12th IEEE International Conference on Fuzzy Systems.

Chen, S., Lien, W., Wang, W., Lee, G., Hsu, L., Lee, K., . . . Lai, J. (2016). Assistive Control System for Upper Limb Rehabilitation Robot.

Chen, Z., Shatara, S., & Tan, X. (2010). Modeling of biomimetic robotic fish propelled by an ionic polymer–metal composite caudal fin. *IEEE/ASME Transactions on mechatronics, 15*(3), 448-459.

Chen, Z., Um, T. I., & Bart-Smith, H. (2011). A novel fabrication of ionic polymer–metal composite membrane actuator capable of 3-dimensional kinematic motions. *Sensors and Actuators A: physical, 168*(1), 131-139.

Chine, W., Mellit, A., & Bouhedir, R. (2017). *FPGA-Based Implementation of an Intelligent Fault Diagnosis Method for Photovoltaic Arrays.* Paper presented at the International Conference in Artificial Intelligence in Renewable Energetic Systems.

Cho, K.-J., Hawkes, E., Quinn, C., & Wood, R. J. (2008). *Design, fabrication and analysis of a body-caudal fin propulsion system for a microrobotic fish.* Paper presented at the Robotics and Automation, 2008. ICRA 2008. IEEE International Conference on.

Chopade, S. S., Kauthalkar, S. P., & Bhandari, C. B. (2013). But We Have Made the Robots Lighter. *International Journal of Modern Engineering Research (IJMER), 3*(5), 2742-2748.

Chou, C.-P., & Hannaford, B. (1996). Measurement and modeling of McKibben pneumatic artificial muscles. *IEEE Transactions on robotics and automation, 12*(1), 90-102.

Colorado, J., Barrientos, A., Rossi, C., & Breuer, K. S. (2012). Biomechanics of smart wings in a bat robot: morphing wings using SMA actuators. *Bioinspiration & biomimetics, 7*(3), 036006.

Conn, A. T., Hinitt, A. D., & Wang, P. (2014). *Soft segmented inchworm robot with dielectric elastomer muscles.* Paper presented at the Electroactive Polymer Actuators and Devices (EAPAD) 2014.

Daerden, F. (1999). Conception and realization of pleated pneumatic artificial muscles and their use as compliant actuation elements. *Vrije Universiteit Brussel, Belgium*.

Daerden, F., & Lefeber, D. (2001). The concept and design of pleated pneumatic artificial muscles. *International Journal of Fluid Power, 2*(3), 41-50.

Daerden, F., & Lefeber, D. (2002). Pneumatic artificial muscles: actuators for robotics and automation. *European journal of mechanical and environmental engineering, 47*(1), 11-21.

Daud, W. M. B. W., Yahya, A. B., Horng, C. S., Sulaima, M. F., & Sudirman, R. (2013). Features extraction of electromyography signals in time domain on biceps Brachii muscle. *International Journal of Modeling and Optimization, 3*(6), 515.

Davis, S., & Caldwell, D. G. (2011). Biologically inspired damage tolerance in braided pneumatic muscle actuators. *Journal of intelligent material systems and structures, 23*(3), 313–325.

Davis, S., Tsagarakis, N., Canderle, J., & Caldwell, D. G. (2003). Enhanced modelling and performance in braided pneumatic muscle actuators. *The International Journal of Robotics Research, 22*(3-4), 213-227.

Deimel, R., & Brock, O. (2016). A novel type of compliant and underactuated robotic hand for dexterous grasping. *The International Journal of Robotics Research, 35*(1-3), 161-185.

Demuth, H. B., Beale, M. H., De Jess, O., & Hagan, M. T. (2014). *Neural network design*: Martin Hagan.

Doumit, M., Fahim, A., & Munro, M. (2009). Analytical modeling and experimental validation of the braided pneumatic muscle. *IEEE Transactions on Robotics, 25*(6), 1282-1291.

Ergin, M. A., & Patoglu, V. (2012). *ASSISTON-SE: A self-aligning shoulder-elbow exoskeleton.* Paper presented at the Robotics and Automation (ICRA), 2012 IEEE International Conference on.

Faudzi, A. A. M., Razif, M. R. M., Nordin, I. N. A. M., Suzumori, K., Wakimoto, S., & Hirooka, D. (2012). *Development of bending soft actuator with different braided angles.* Paper presented at the 2012 IEEE/ASME International Conference on Advanced Intelligent Mechatronics (AIM).

Firouzeh, A., Ozmaeian, M., & Alasty, A. (2012). An IPMC-made deformable-ring-like robot. *Smart Materials and Structures, 21*(6), 065011.

Firouzeh, A., & Paik, J. (2015). Robogami: A fully integrated low-profile robotic origami. *Journal of Mechanisms and Robotics, 7*(2), 021009.

Frisoli, A., Rocchi, F., Marcheschi, S., Dettori, A., Salsedo, F., & Bergamasco, M. (2005). *A new force-feedback arm exoskeleton for haptic interaction in virtual environments.* Paper presented at the Eurohaptics Conference, 2005 and Symposium on Haptic Interfaces for Virtual Environment and Teleoperator Systems, 2005. World Haptics 2005. First Joint.

Galloway, K. C., Clark, J. E., & Koditschek, D. E. (2013). Variable stiffness legs for robust, efficient, and stable dynamic running. *Journal of Mechanisms and Robotics, 5*(1), 011009.

Galloway, K. C., Polygerinos, P., Walsh, C. J., & Wood, R. J. (2013). *Mechanically programmable bend radius for fiber-reinforced soft actuators.* Paper presented at the Advanced Robotics (ICAR), 2013 16th International Conference on.

Gdaim, S., Mtibaa, A., & Mimouni, M. F. (2015). Design and experimental implementation of DTC of an induction machine based on fuzzy logic control on FPGA. *IEEE Transactions on Fuzzy Systems, 23*(3), 644-655.

Giannaccini, M. E., Xiang, C., Atyabi, A., Theodoridis, T., Nefti-Meziani, S., & Davis, S. (2018). Novel design of a soft lightweight pneumatic continuum robot arm with decoupled variable stiffness and positioning. *Soft robotics, 5*(1), 54-70.

Gisby, T. A., Calius, E. P., Xie, S., & Anderson, I. A. (2008). *An adaptive control method for dielectric elastomer devices.* Paper presented at the Electroactive Polymer Actuators and Devices (EAPAD) 2008.

Godaba, H., Ng, W., & Zhu, J. (2014). *Development of a soft jellyfish robot based on dielectric elastomer actuators.* Paper presented at the IEEE International Conference on Robotics and Automation, Workshop on Soft Robots.

Gopura, R., Bandara, D., Kiguchi, K., & Mann, G. (2016a). Developments in hardware systems of active upper-limb exoskeleton robots: A review. *Robotics and Autonomous Systems, 75*, 203-220.

Gopura, R., Bandara, D., Kiguchi, K., & Mann, G. K. (2016b). Developments in hardware systems of active upper-limb exoskeleton robots: A review. *Robotics and Autonomous Systems, 75*, 203-220.

Graham, R. B., Wachowiak, M. P., & Gurd, B. J. (2015). The assessment of muscular effort, fatigue, and physiological adaptation using EMG and wavelet analysis. *PloS one, 10*(8), e0135069.

Hesselroth, T., Sarkar, K., Van Der Smagt, P. P., & Schulten, K. (1994). Neural network control of a pneumatic robot arm. *Systems, Man and Cybernetics, IEEE Transactions on, 24*(1), 28-38.

Hodgson, D. E., Ming, W., & Biermann, R. J. (1990). Shape memory alloys. *ASM International, Metals Handbook, Tenth Edition., 2*, 897-902.

Hoover, A. M., & Fearing, R. S. (2008). *Fast scale prototyping for folded millirobots.* Paper presented at the Robotics and Automation, 2008. ICRA 2008. IEEE International Conference on.

Hosovsky, A., Novak-Marcincin, J., Pitel, J., Borzikova, J., & Zidek, K. (2012). Model-based evolution of a fast hybrid fuzzy adaptive controller for a pneumatic muscle actuator. *International Journal of Advanced Robotic Systems, 9*(3), 673-681.

Hunt, S., McKay, T. G., & Anderson, I. A. (2014). A self-healing dielectric elastomer actuator. *Applied Physics Letters, 104*(11), 113701.

Hunter, I. W., Lafontaine, S., Hollerbach, J. M., & Hunter, P. J. (1991). *Fast reversible NiTi fibers for use in microrobotics.* Paper presented at the Micro Electro Mechanical Systems, 1991, MEMS'91, Proceedings. An Investigation of Micro Structures, Sensors, Actuators, Machines and Robots. IEEE.

Ikuta, K., Tsukamoto, M., & Hirose, S. (1988). *Shape memory alloy servo actuator system with electric resistance feedback and application for active endoscope.* Paper presented at the Robotics and Automation, 1988. Proceedings., 1988 IEEE International Conference on.

Ilievski, F., Mazzeo, A. D., Shepherd, R. F., Chen, X., & Whitesides, G. M. (2011). Soft robotics for chemists. *Angewandte Chemie, 123*(8), 1930-1935.

Immega, G. B. (1986). *ROMAC muscle powered robots MS86–777*: Society of Manufacturing Engineers.

Ivanova, G., Bulavintsev, S., Ryu, J.-H., & Poduraev, J. (2011). *Development of an exoskeleton system for elderly and disabled people.* Paper presented at the Information Science and Applications (ICISA), 2011 International Conference on.

Jain, R. K., Majumder, S., & Dutta, A. (2013). SCARA based peg-in-hole assembly using compliant IPMC micro gripper. *Robotics and Autonomous Systems, 61*(3), 297-311.

Jani, J. M., Leary, M., Subic, A., & Gibson, M. A. (2014). A review of shape memory alloy research, applications and opportunities. *Materials & Design (1980-2015), 56*, 1078-1113.

Jiang, A., Xynogalas, G., Dasgupta, P., Althoefer, K., & Nanayakkara, T. (2012). *Design of a variable stiffness flexible manipulator with composite granular jamming and membrane coupling.* Paper presented at the 2012 IEEE/RSJ International Conference on Intelligent Robots and Systems.

Jo, C., Pugal, D., Oh, I.-K., Kim, K. J., & Asaka, K. (2013). Recent advances in ionic polymer–metal composite actuators and their modeling and applications. *Progress in Polymer Science, 38*(7), 1037-1066.

Jouppila, V. (2014). Modeling and Control of a Pneumatic Muscle Actuator. *Tampereen teknillinen yliopisto. Julkaisu-Tampere University of Technology. Publication; 1199*.

Jung, K., Koo, J. C., Lee, Y. K., & Choi, H. R. (2007). Artificial annelid robot driven by soft actuators. *Bioinspiration & biomimetics, 2*(2), S42.

Kadota, K., Akai, M., Kawashima, K., & Kagawa, T. (2009). *Development of Power-Assist Robot Arm using pneumatic rubbermuscles with a balloon sensor.* Paper presented at the Robot and Human Interactive Communication, 2009. RO-MAN 2009. The 18th IEEE International Symposium on.

Kadowaki, Y., Noritsugu, T., Takaiwa, M., Sasaki, D., & Kato, M. (2011). Development of soft power-assist glove and control based on human intent. *Journal of Robotics and Mechatronics, 23*(2), 281.

Kaitwanidvilai, S., & Parnichkun, M. (2005). Force control in a pneumatic system using hybrid adaptive neuro-fuzzy model reference control. *Mechatronics, 15*(1), 23-41.

Kamamichi, N., Yamakita, M., Asaka, K., & Luo, Z.-W. (2006). *A snake-like swimming robot using IPMC actuator/sensor.* Paper presented at the Robotics and Automation, 2006. ICRA 2006. Proceedings 2006 IEEE International Conference on.

Kazerooni, H. (1990). Human-robot interaction via the transfer of power and information signals. *IEEE Transactions on systems, Man, and Cybernetics, 20*(2), 450-463.

Kelasidi, E., Andrikopoulos, G., Nikolakopoulos, G., & Manesis, S. (2012). *A survey on pneumatic muscle actuators modeling*.

Ketelaar, J., Visser, L. C., Stramigioli, S., & Carloni, R. (2013). *Controller design for a bipedal walking robot using variable stiffness actuators.* Paper presented at the Robotics and Automation (ICRA), 2013 IEEE International Conference on.

Khan, A., Jain, R., & Naushad, M. (2015). Development of sulfonated poly (vinyl alcohol)/polpyrrole based ionic polymer metal composite (IPMC) actuator and its characterization. *Smart Materials and Structures, 24*(9), 095003.

Kim, H.-J., Song, S.-H., & Ahn, S.-H. (2012). A turtle-like swimming robot using a smart soft composite (SSC) structure. *Smart Materials and Structures, 22*(1), 014007.

Kim, S., Hawkes, E., Choy, K., Joldaz, M., Foleyz, J., & Wood, R. (2009). *Micro artificial muscle fiber using NiTi spring for soft robotics.* Paper presented at the Intelligent Robots and Systems, 2009. IROS 2009. IEEE/RSJ International Conference on.

Kim, S., Laschi, C., & Trimmer, B. (2013). Soft robotics: a bioinspired evolution in robotics. *Trends in biotechnology, 31*(5), 287-294.

Kiminori, T., Miyagawa, T., & Kubota, Y. (2011). Power-assist glove operated by predicting the grasping mode. *Journal of System Design and Dynamics, 5*(1), 94-108.

Kobayashi, H., Suzuki, H., Nozaki, H., & Tsuji, T. (2007). *Development of Power Assist System for Manual Worker by Muscle Suit.* Paper presented at the Robot and Human interactive Communication, 2007. RO-MAN 2007. The 16th IEEE International Symposium on.

Koh, J.-S., Yang, E., Jung, G.-P., Jung, S.-P., Son, J. H., Lee, S.-I., . . . Cho, K.-J. (2015). Jumping on water: Surface tension–dominated jumping of water striders and robotic insects. *Science, 349*(6247), 517-521.

Koh, S. J. A., Keplinger, C., Li, T., Bauer, S., & Suo, Z. (2011). Dielectric elastomer generators: How much energy can be converted? *IEEE/ASME Transactions on mechatronics, 16*(1), 33-41.

Kovac, M., Guignard, A., Nicoud, J.-D., Zufferey, J.-C., & Floreano, D. (2007). *A 1.5 g sma-actuated microglider looking for the light.* Paper presented at the Robotics and Automation, 2007 IEEE International Conference on.

Kuder, I. K., Arrieta, A. F., Raither, W. E., & Ermanni, P. (2013). Variable stiffness material and structural concepts for morphing applications. *Progress in Aerospace Sciences, 63*, 33-55.

Kukolj, M. (1988). Axially contractible actuator. *US Patent*.

Lan, C.-C., & Fan, C.-H. (2010). An accurate self-sensing method for the control of shape memory alloy actuated flexures. *Sensors and Actuators A: physical, 163*(1), 323-332.

Laschi, C., Cianchetti, M., Mazzolai, B., Margheri, L., Follador, M., & Dario, P. (2012). Soft robot arm inspired by the octopus. *Advanced Robotics, 26*(7), 709-727.

Lin, H.-T., Leisk, G. G., & Trimmer, B. (2011). GoQBot: a caterpillar-inspired soft-bodied rolling robot. *Bioinspiration & biomimetics, 6*(2), 026007.

Long, Y., Du, Z., Cong, L., Wang, W., Zhang, Z., & Dong, W. (2017). Active disturbance rejection control based human gait tracking for lower extremity rehabilitation exoskeleton. *ISA transactions, 67*, 389-397.

Madden, J. D., Vandesteeg, N. A., Anquetil, P. A., Madden, P. G., Takshi, A., Pytel, R. Z., . . . Hunter, I. W. (2004). Artificial muscle technology: physical principles and naval prospects. *IEEE Journal of oceanic engineering, 29*(3), 706-728.

Maffli, L., Rosset, S., Ghilardi, M., Carpi, F., & Shea, H. (2015). Ultrafast All-Polymer Electrically Tunable Silicone Lenses. *Advanced Functional Materials, 25*(11), 1656-1665.

Malcolm, M. (1996). Abstracting Craft: The Practiced Digital Hand: The MIT Press, Cambridge, Massachusetts.

Manual, D.-N. U. (2012, October 2012). DE0-Nano User Manual. *Terasic Technologies.*

Marchese, A. D., Komorowski, K., Onal, C. D., & Rus, D. (2014). Design and control of a soft and continuously deformable 2d robotic manipulation system.

Marchese, A. D., Onal, C. D., & Rus, D. (2014). Autonomous soft robotic fish capable of escape maneuvers using fluidic elastomer actuators. *Soft robotics, 1*(1), 75-87.

Martinez, J. A., Ng, P., Lu, S., Campagna, M. S., & Celik, O. (2013). *Design of Wrist Gimbal: A forearm and wrist exoskeleton for stroke rehabilitation.* Paper presented at the Rehabilitation Robotics (ICORR), 2013 IEEE International Conference on.

Martinez, R. V., Branch, J. L., Fish, C. R., Jin, L., Shepherd, R. F., Nunes, R. M., . . . Whitesides, G. M. (2013). Robotic tentacles with three-dimensional mobility based on flexible elastomers. *Advanced Materials, 25*(2), 205-212.

Martinez, R. V., Fish, C. R., Chen, X., & Whitesides, G. M. (2012). Elastomeric origami: programmable paper-elastomer composites as pneumatic actuators. *Advanced functional materials, 22*(7), 1376-1384.

Matsuyama, Y., & Hirai, S. (2007). *Analysis of circular robot jumping by body deformation.* Paper presented at the Robotics and Automation, 2007 IEEE International Conference on.

Medlej, J. (2014). Human anatomy fundamentals: Flexibility and joint limitations. *Design & Illustration Tutorials*.

Michel, S., Zhang, X. Q., Wissler, M., Löwe, C., & Kovacs, G. (2010). A comparison between silicone and acrylic elastomers as dielectric materials in electroactive polymer actuators. *Polymer international, 59*(3), 391-399.

Mistry, M., Mohajerian, P., & Schaal, S. (2005). *An exoskeleton robot for human arm movement study.* Paper presented at the Intelligent Robots and Systems, 2005.(IROS 2005). 2005 IEEE/RSJ International Conference on.

Morin, S. A., Shepherd, R. F., Kwok, S. W., Stokes, A. A., Nemiroski, A., & Whitesides, G. M. (2012). Camouflage and display for soft machines. *Science, 337*(6096), 828-832.

Mosadegh, B., Polygerinos, P., Keplinger, C., Wennstedt, S., Shepherd, R. F., Gupta, U., . . . Whitesides, G. M. (2014). Pneumatic networks for soft robotics that actuate rapidly. *Advanced functional materials, 24*(15), 2163-2170.

Mukhtar, M., Akyurek, E., Kalganova, T., & Lesne, N. (2015). *Control of 3D printed ambidextrous robot hand actuated by pneumatic artificial muscles.* Paper presented at the SAI Intelligent Systems Conference (IntelliSys), 2015.

Najem, J., Sarles, S. A., Akle, B., & Leo, D. J. (2012). Biomimetic jellyfish-inspired underwater vehicle actuated by ionic polymer metal composite actuators. *Smart Materials and Structures, 21*(9), 094026.

Nef, T., Mihelj, M., Colombo, G., & Riener, R. (2006). *ARMin-robot for rehabilitation of the upper extremities.* Paper presented at the Robotics and Automation, 2006. ICRA 2006. Proceedings 2006 IEEE International Conference on.

Nemat-Nasser, S., & Wu, Y. (2003). Comparative experimental study of ionic polymer–metal composites with different backbone ionomers and in various cation forms. *Journal of Applied Physics, 93*(9), 5255-5267.

Nguyen, C. T., Phung, H., Nguyen, T. D., Lee, C., Kim, U., Lee, D., . . . Choi, H. R. (2014). A small biomimetic quadruped robot driven by multistacked dielectric elastomer actuators. *Smart materials and structures, 23*(6), 065005.

Niiyama, R., Nagakubo, A., & Kuniyoshi, Y. (2007). *Mowgli: A bipedal jumping and landing robot with an artificial musculoskeletal system.* Paper presented at the IEEE International Conference onRobotics and Automation (ICRA 2007)

Noritsugu, T. (2005). *Pneumatic soft actuator for human assist technology.* Paper presented at the Symposium on Fluid Power.

Noritsugu, T., Takaiwa, M., & Sasaki, D. (2008). *Power assist wear driven with pneumatic rubber artificial muscles.* Paper presented at the Mechatronics and Machine Vision in Practice, 2008. M2VIP 2008. 15th International Conference on.

Noritsugu, T., Yamamoto, H., Sasaki, D., & Takaiwa, M. (2004). *Wearable power assist device for hand grasping using pneumatic artificial rubber muscle.* Paper presented at the SICE-ANNUAL CONFERENCE-.

Nouri, A., Gauvert, C., Tondu, B., & Lopez, P. (1994). *Generalized variable structure model reference adaptive control of one-link artificial muscle manipulator in two operating modes.* Paper presented at the IEEE International Conference onSystems, Man, and Cybernetics, 1994.

Nuchkrua, T., & Leephakpreeda, T. (2013). Fuzzy self-tuning PID control of hydrogen-driven pneumatic artificial muscle actuator. *Journal of bionic engineering, 10*(3), 329-340.

O'Brien, B. M., Calius, E. P., Inamura, T., Xie, S. Q., & Anderson, I. A. (2010). Dielectric elastomer switches for smart artificial muscles. *Applied Physics A, 100*(2), 385-389.

Onal, C. D., Chen, X., Whitesides, G. M., & Rus, D. (2017). Soft mobile robots with on-board chemical pressure generation *Robotics Research* (pp. 525-540): Springer.

Otten, A., Voort, C., Stienen, A., Aarts, R., van Asseldonk, E., & van der Kooij, H. (2015). LIMPACT: A Hydraulically Powered Self-Aligning Upper Limb Exoskeleton. *Mechatronics, IEEE/ASME Transactions on, 20*(5), 2285-2298.

Palchaudhuri, A., & Chakraborty, R. S. (2016). Architecture of Target FPGA Platform *High Performance Integer Arithmetic Circuit Design on FPGA* (pp. 11-17): Springer.

Paynter, H. M. (1996). *Thermodynamic treatment of tug-&-twist technology: Part 1. Thermodynamic tugger design.* Paper presented at the Proceedings, Japan-USA Symposium on Flexible Automation, Boston, MA.

Pei, Q., Rosenthal, M., Stanford, S., Prahlad, H., & Pelrine, R. (2004). Multiple-degrees-of-freedom electroelastomer roll actuators. *Smart materials and structures, 13*(5), N86.

Petralia, M. T., & Wood, R. J. (2010). *Fabrication and analysis of dielectric-elastomer minimum-energy structures for highly-deformable soft robotic systems.* Paper presented at the Intelligent Robots and Systems (IROS), 2010 IEEE/RSJ International Conference on.

Polygerinos, P., Galloway, K. C., Sanan, S., Herman, M., & Walsh, C. J. (2015). *EMG controlled soft robotic glove for assistance during activities of daily living.* Paper presented at the Rehabilitation Robotics (ICORR), 2015 IEEE International Conference on.

Polygerinos, P., Lyne, S., Wang, Z., Nicolini, L. F., Mosadegh, B., Whitesides, G. M., & Walsh, C. J. (2013). *Towards a soft pneumatic glove for hand rehabilitation.* Paper presented at the Intelligent Robots and Systems (IROS), 2013 IEEE/RSJ International Conference on.

Polygerinos, P., Wang, Z., Galloway, K. C., Wood, R. J., & Walsh, C. J. (2015). Soft robotic glove for combined assistance and at-home rehabilitation. *Robotics and Autonomous Systems, 73*, 135-143.

Price, A., Jnifene, A., & Naguib, H. (2007). Design and control of a shape memory alloy based dexterous robot hand. *Smart Materials and Structures, 16*(4), 1401.

Punning, A., Kruusmaa, M., & Aabloo, A. (2007). A self-sensing ion conducting polymer metal composite (IPMC) actuator. *Sensors and Actuators A: physical, 136*(2), 656-664.

Pylatiuk, C., Kargov, A., Gaiser, I., Werner, T., Schulz, S., & Bretthauer, G. (2009). *Design of a flexible fluidic actuation system for a hybrid elbow orthosis.* Paper presented at the Rehabilitation Robotics, 2009. ICORR 2009. IEEE International Conference on.

Qian, J., Huang, J., & Ri, S. (2015a). *Adaptive fuzzy sliding mode control for pneumatic muscle actuator.* Paper presented at the 2015 Chinese Automation Congress (CAC).

Qian, J., Huang, J., & Ri, S. (2015b). *Adaptive fuzzy sliding mode control for pneumatic muscle actuator.* Paper presented at the Chinese Automation Congress (CAC), 2015.

Rahman, M., Ouimet, T., Saad, M., Kenne, J., & Archambault, P. (2010). *Development and control of a wearable robot for rehabilitation of elbow and shoulder joint movements.* Paper presented at the IECON 2010-36th Annual Conference on IEEE Industrial Electronics Society.

Ranjan, R., Upadhyay, P., Kumar, A., & Dhyani, P. (2012). Theoretical and Experimental Modeling of Air Muscle. *International Journal of Emerging Technology and Advanced Engineering, 2*(4).

Ren, Y., Park, H.-S., & Zhang Sr, L.-Q. (2009). *Developing a whole-arm exoskeleton robot with hand opening and closing mechanism for upper limb stroke rehabilitation.* Paper presented at the Rehabilitation Robotics, 2009. ICORR 2009. IEEE International Conference on.

Retolaza, I., Pujana-Arrese, A., Cenitagoya, A., Basurko, J., & Landaluze, J. (2008). *Design of a five actuated DoF upper limb exoskeleton oriented to workplace help.* Paper presented at the Biomedical Robotics and Biomechatronics, 2008. BioRob 2008. 2nd IEEE RAS & EMBS International Conference on.

Rocon, E., & Pons, J. L. (2011). *Exoskeletons in Rehabilitation Robotics: Tremor Suppression* (Vol. 69): Springer.

Sarasola-Sanz, A., López-Larraz, E., Irastorza-Landa, N., Klein, J., Valencia, D., Belloso, A., . . . Ramos-Murguialday, A. (2017). An EEG-Based Brain-Machine Interface to Control a 7-Degrees of Freedom Exoskeleton for Stroke Rehabilitation *Converging Clinical and Engineering Research on Neurorehabilitation II* (pp. 1127-1131): Springer.

Sárosi, J., & Gyeviki, J. (2009). EXPERIMENTAL SETUP FOR THE POSITIONING OF HUMANOID UPPER ARM. *Computer methods in biomechanics and biomedical engineering, 13*(1), 11–18. doi:10.1080/10255840902948017

Sárosi, J., Gyeviki, J., Véha, A., & Toman, P. (2009). *Accurate position control of PAM actuator in Lab VIEW environment.* Paper presented at the 7th International Symposium on Intelligent Systems and Informatics, 2009. SISY'09. .

Sasaki, D., Noritsugu, T., & Takaiwa, M. (2005a). *Development of active support splint driven by pneumatic soft actuator (ASSIST).* Paper presented at the Robotics and Automation, 2005. ICRA 2005. Proceedings of the 2005 IEEE International Conference on.

Sasaki, D., Noritsugu, T., & Takaiwa, M. (2005b). Development of Pneumatic Power Assist Splint" ASSIST" Operated by Human Intention. *Journal of Robotics and Mechatronics, 17*(5), 568.

Sasaki, D., Noritsugu, T., Takaiwa, M., & Konishi, H. (2014). Control Method Based on EMG for Power Assist Glove Using Self-Organizing Maps. *Journal ref: International Journal of Automation Technology, 8*(2), 177-185.

Scarfe, P., & Lindsay, E. (2006). Air muscle actuated low cost humanoid hand. *International Journal of Advanced Robotic Systems, 3*(1), 139-146.

Schubert, B. E. (2011). *Design, fabrication and testing of angled fiber suspension for electrostatic actuators.* UC Berkeley.

Seok, S., Onal, C. D., Cho, K.-J., Wood, R. J., Rus, D., & Kim, S. (2013). Meshworm: a peristaltic soft robot with antagonistic nickel titanium coil actuators. *IEEE/ASME Transactions on mechatronics, 18*(5), 1485-1497.

Serres, J., Reynolds, D., Phillips, C., Rogers, D., & Repperger, D. (2010). Characterisation of a pneumatic muscle test station with two dynamic plants in cascade. *Computer methods in biomechanics and biomedical engineering, 13*(1), 11-18.

Shen, X. (2010). Nonlinear model-based control of pneumatic artificial muscle servo systems. *Control Engineering Practice, 18*(3), 311-317.

Shepherd, R. F., Ilievski, F., Choi, W., Morin, S. A., Stokes, A. A., Mazzeo, A. D., . . . Whitesides, G. M. (2011). Multigait soft robot. *Proceedings of the national academy of sciences, 108*(51), 20400-20403.

Shepherd, R. F., Stokes, A. A., Nunes, R. M., & Whitesides, G. M. (2013). Soft machines that are resistant to puncture and that self seal. *Advanced Materials, 25*(46), 6709-6713.

Shi, L., Guo, S., Mao, S., Yue, C., Li, M., & Asaka, K. (2013). Development of an amphibious turtle-inspired spherical mother robot. *Journal of Bionic Engineering, 10*(4), 446-455.

Shin, D., Yeh, X., & Khatib, O. (2014). A new hybrid actuation scheme with artificial pneumatic muscles and a magnetic particle brake for safe human–robot collaboration. *The International Journal of Robotics Research, 33*(4), 507-518.

Sun, D., Yan, B., Han, B., Song, Y., & Zhang, X. (2016). Vibration characteristic simulation of a pneumatic artificial muscle damping seat. *Journal of Low Frequency Noise, Vibration and Active Control, 35*(1), 39-51.

Suzumori, K., Endo, S., Kanda, T., Kato, N., & Suzuki, H. (2007). *A bending pneumatic rubber actuator realizing soft-bodied manta swimming robot.* Paper presented at the Proceedings 2007 IEEE International Conference on Robotics and Automation.

Suzumori, K., Wakimoto, S., Miyoshi, K., & Iwata, K. (2013). *Long bending rubber mechanism combined contracting and extending tluidic actuators.* Paper presented at the Intelligent Robots and Systems (IROS), 2013 IEEE/RSJ International Conference on.

Tadano, K., Akai, M., Kadota, K., & Kawashima, K. (2010). *Development of grip amplified glove using bi-articular mechanism with pneumatic artificial rubber muscle.* Paper presented at the Robotics and Automation (ICRA), 2010 IEEE International Conference on.

Thanh, T. D. C., & Ahn, K. K. (2006). Nonlinear PID control to improve the control performance of 2 axes pneumatic artificial muscle manipulator using neural network. *Mechatronics, 16*(9), 577-587.

Tolley, M. T., Shepherd, R. F., Mosadegh, B., Galloway, K. C., Wehner, M., Karpelson, M., . . . Whitesides, G. M. (2014). A resilient, untethered soft robot. *Soft robotics, 1*(3), 213-223.

Tondu, B., & Lopez, P. (2000). Modeling and control of McKibben artificial muscle robot actuators. *IEEE control systems, 20*(2), 15-38.

Toya, K., Miyagawa, T., & Kubota, Y. (2011). Power-assist glove operated by predicting the grasping mode. *Journal of System Design and Dynamics, 5*(1), 94-108.

Trivedi, D., Rahn, C. D., Kier, W. M., & Walker, I. D. (2008). Soft robotics: Biological inspiration, state of the art, and future research. *Applied bionics and biomechanics, 5*(3), 99-117.

Tsagarakis, N., & Caldwell, D. G. (2000). *Improved modelling and assessment of pneumatic muscle actuators.* Paper presented at the IEEE International Conference on Robotics and Automation, 2000. Proceedings. ICRA'00. .

Van Damme, M., Vanderborght, B., Van Ham, R., Verrelst, B., Daerden, F., & Lefeber, D. (2007). *Proxy-based sliding mode control of a manipulator actuated by pleated pneumatic artificial muscles.* Paper presented at the IEEE International Conference on Robotics and Automation, 2007, Autom., Rome, Italy.

Vanderborght, B., Albu-Schäffer, A., Bicchi, A., Burdet, E., Caldwell, D. G., Carloni, R., . . . Ganesh, G. (2013). Variable impedance actuators: A review. *Robotics and Autonomous Systems, 61*(12), 1601-1614.

Verrelst, B., Van Ham, R., Vanderborght, B., Daerden, F., Lefeber, D., & Vermeulen, J. (2005). The pneumatic biped "Lucy" actuated with pleated pneumatic artificial muscles. *Autonomous Robots, 18*(2), 201-213.

Villanueva, A., Smith, C., & Priya, S. (2011). A biomimetic robotic jellyfish (Robojelly) actuated by shape memory alloy composite actuators. *Bioinspiration & biomimetics, 6*(3), 036004.

Vitiello, N., Lenzi, T., Roccella, S., De Rossi, S. M., Cattin, E., Giovacchini, F., . . . Carrozza, M. (2013). NEUROExos: A powered elbow exoskeleton for physical rehabilitation. *Robotics, IEEE Transactions on, 29*(1), 220-235.

Wang, Z., Wang, Y., Li, J., & Hang, G. (2009). *A micro biomimetic manta ray robot fish actuated by SMA.* Paper presented at the Robotics and Biomimetics (ROBIO), 2009 IEEE International Conference on.

Wickramatunge, K. C., & Leephakpreeda, T. (2010). Study on mechanical behaviors of pneumatic artificial muscle. *International Journal of Engineering Science, 48*(2), 188-198.

Wolf, S., Bahls, T., Chalon, M., Friedl, W., Grebenstein, M., Höppner, H., . . . Özparpucu, M. C. (2015). Soft robotics with variable stiffness actuators: Tough robots for soft human robot interaction *Soft Robotics* (pp. 231-254): Springer.

Xiang, K. K., Hua, P. C. J., Rahman, H. A., Fai, Y. C., Narayanan, A. L. T., & Ming, E. S. L. (2015). Development of Reconfigurable Rehabilitation Robot for Post-stroke Forearm and Wrist Training. *Jurnal Teknologi, 72*(2).

Yamamoto, I., Inagawa, N., Matsui, M., Hachisuka, K., Wada, F., & Hachisuka, A. (2014). Research and development of compact wrist rehabilitation robot system. *Bio-medical materials and engineering, 24*(1), 123-128.

Yang, Y., & Chen, Y. (2016). *Novel design and 3D printing of variable stiffness robotic fingers based on shape memory polymer.* Paper presented at the 2016 6th IEEE International Conference on Biomedical Robotics and Biomechatronics (BioRob).

Yap, H. K., Lim, J. H., Nasrallah, F., Goh, J. C., & Yeow, R. C. (2015a). *A soft exoskeleton for hand assistive and rehabilitation application using pneumatic actuators with variable stiffness.* Paper presented at the 2015 IEEE International Conference on Robotics and Automation (ICRA).

Yap, H. K., Lim, J. H., Nasrallah, F., Goh, J. C., & Yeow, R. C. (2015b). *A soft exoskeleton for hand assistive and rehabilitation application using pneumatic actuators with variable stiffness.* Paper presented at the Robotics and Automation (ICRA), 2015 IEEE International Conference on.

Yarlott, J. M. (1972). Fluid actuator. US Patent: Google Patents.

Youssef, A., El Telbany, M., & Zekry, A. (2018). Reconfigurable generic FPGA implementation of fuzzy logic controller for MPPT of PV systems. *Renewable and Sustainable Energy Reviews, 82*, 1313-1319.

Zhang, J.-F., Yang, C.-J., Chen, Y., Zhang, Y., & Dong, Y.-M. (2008). Modeling and control of a curved pneumatic muscle actuator for wearable elbow exoskeleton. *Mechatronics, 18*(8), 448-457.

Zhu, X., Tao, G., Yao, B., & Cao, J. (2008). Adaptive robust posture control of a parallel manipulator driven by pneumatic muscles. *Automatica, 44*(9), 2248-2257.

APPENDIXES

A1. BBPAM Bladder Manufacturing Process

Natural latex and thickener have been mixed using 95% and 5%, respectively, as shown in Figure A1.1 (a). A 3D printed template has been used to mould this bladder, as shown in Figure A1.1 (b). This template has four parts with a hole in the middle to place parallel fixed length threads. These threads are used so that the middle of the bladder has a fixed length. After the threads have been placed in the middle, the mould is painted with layers under heating until it has a desirable thickness, as shown in Figure A1.1 (c). Figure A1.1 (d) shows the novel bladder after it's dried. Finally, the bladder is encapsulated by a netted sleeve, using the same technique as the extensor muscle, and the end cap is placed on each hole (one terminal has fully solid endcaps and the other terminal has two endcaps with a hole for each airflow)

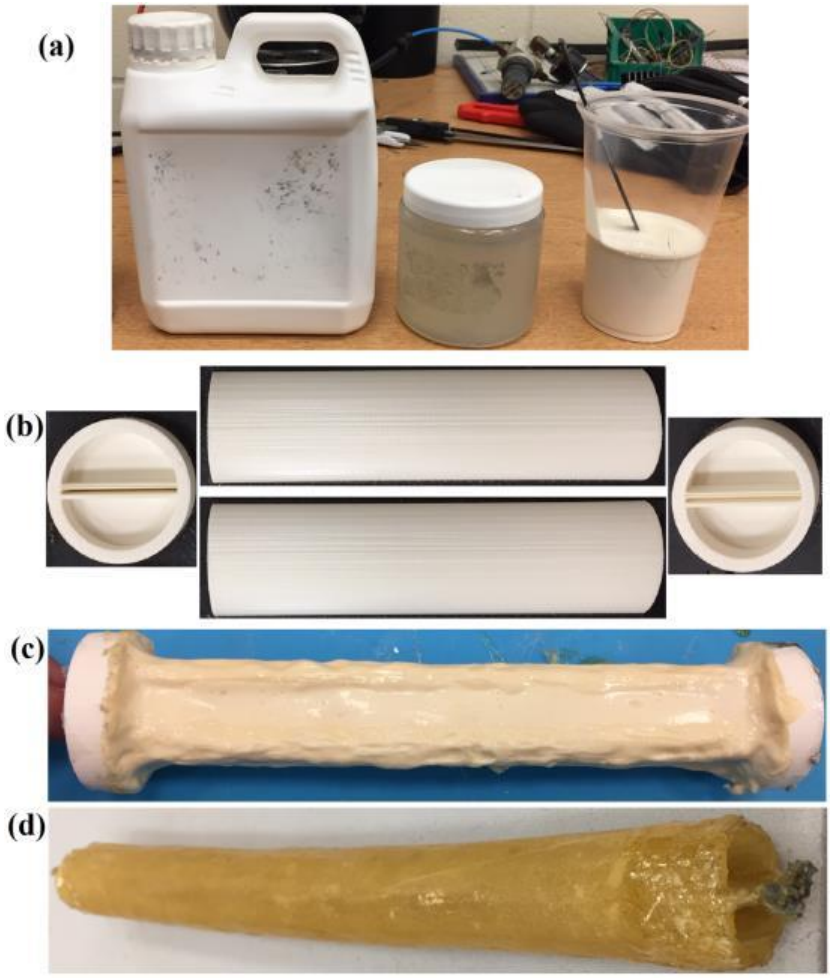

Figure A1.1: Moulding the novel bladder for BBPAM.

A2. ABPAM Bladder Manufacturing Process

Figure A2.1 (a) shows the 3D printed template, it contains four bars and two ends. Parallel fixed length threads are placed in the middle of the template (see Figure A2.1 (b)) to make the centre of the muscle always have a fixed length. The elastic liquid was painted on the template under heating (see Figure A2.1 (c)) until it reached the desired bladder thickness. Figure A2.1 (d) shows the new bladder after it's completely dried. The bladder is encapsulated by a netting sleeve as an extensor muscle and end caps are connected to each terminal. One end cap is completely closed and the other one has four holes for the airflow, as shown in Figure A2.1 (e).

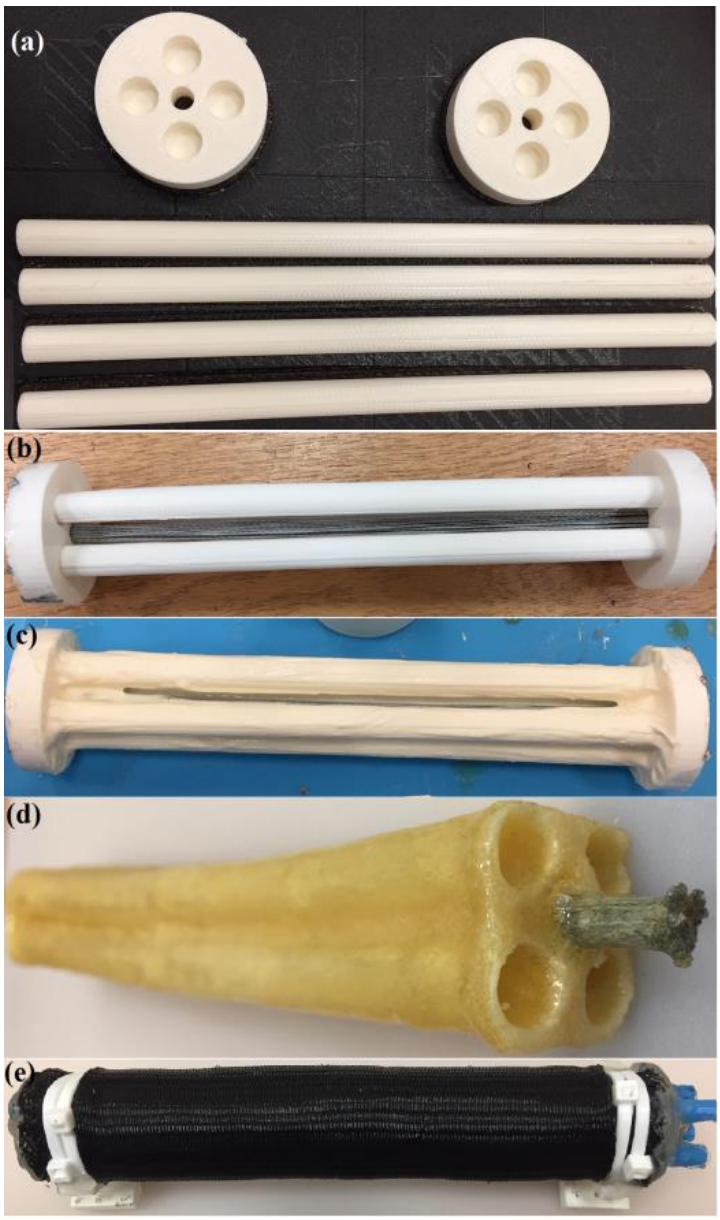

Figure A2.1: The ABPAM fabrication stages.